Creation of a gridded time series of hydrological variables for Canada

by

Frank Robert Seglenieks

A thesis

presented to the University of Waterloo

in fulfillment of the

thesis requirement for the degree of

Doctor of Philosophy

in

Civil Engineering

Waterloo, Ontario, Canada, 2009

AUTHOR'S DECLARATION

I hereby declare that I am the sole author of this thesis. This is a true copy of the thesis, including any required final revisions, as accepted by my examiners.

I understand that my thesis may be made electronically available to the public.

Abstract

There is a lack of measured, long-term, reliable, and well-distributed hydrological variables in Canada. These hydrological variables include, but are not limited to: temperature, precipitation, ground runoff, evapotranspiration, soil moisture, and snow water equivalent. Knowledge of these variables is important in many different fields, such as: land-use planning, design of engineering structures, agricultural production, flood forecasting, hydro power generation, and especially for any study of climate change. The objective of this thesis was to establish the best possible distributed estimates of these hydrological variables for Canada over the period of 1961-2000.

The first step in the creation of these datasets was to interpolate the monthly average of temperature and precipitation measured at Environment Canada stations across the country. Although the spatial density of measurement stations for these quantities in the southern parts of the country was high, for the rest of the country the spatial density was so low that traditional interpolation methods do not perform well. As a result, a method for the interpolation of these data was developed that used physiographic parameters to perform a regression on the available measured data.

These interpolated values of temperature and precipitation were then used to calculate the other hydrological variables using the Waterloo Flood Forecasting Model (WATFLOOD). In order to use WATFLOOD, it was necessary to properly segment the watershed into grids, each with its own topographic characteristics such as river elevation, slope, and drainage direction; these and other characteristics are referred to as the drainage database. The Waterloo Mapping technique (WATMAP) was developed to use topographic and land cover databases to automatically and systematically derive the information needed to create the drainage database. This technique takes data from the very fine resolutions of Digital Elevation Models and upscales them to the coarser resolutions typically used by mesoscale hydrological models. The drainage database for Canada was created using WATMAP on a polar stereographic grid with a resolution of 51 km. WATFLOOD was then run using the WATMAP-derived drainage database with the interpolated temperature and precipitation as the input data.

As with most hydrological models, there was a need to calibrate many of the parameters in WATFLOOD that govern how water moves through the modeled landscape. WATFLOOD was calibrated with the Dynamically Dimensioned Search (DDS) algorithm using the difference between the measured and simulated streamflow as the objective function. Calibrations were performed using objective functions based on both the volume difference between the measured and simulated flow and also the timing differences of the flows.

After a final calibration of 100 separate DDS runs, distributed time series for runoff, evapotranspiration, soil moisture, and snow water equivalent were created for the country. The monthly values for these parameters were examined in different climatic regions of Canada. The

areas of highest runoff, snow water equivalent, and soil moisture were generally seen along the west coast, the western mountains, and along the east coast. The Arctic showed much less evapotranspiration and a delayed runoff peak.

The calculation of distributed runoff also allowed for the creation of products that could be used in engineering design or watershed planning, such as simulated streamflow records and flow frequency diagrams for any point in the country regardless of whether they were gauged or ungauged.

A simple assessment was made for the predictive uncertainty in the simulated streamflow results based on the results of the final calibration. As well, the implications of various climate change scenarios were examined in the context of how they would change the hydrological parameters.

Among the major conclusions from the study were that the WATMAP technique performed much better than using a method based on the average elevation of the grid squares and that it was important to consider diagonal flow in the creation of the drainage database.

With regard to the interpolation technique that was developed, it performed better than the inverse weighted distance technique in terms of both root mean squared error and mean error. In order to properly implement this regression-based interpolation technique, the country had to be split into six regions for the precipitation data and three regions for the temperature data.

During the calibration, it was found that when an objective function was used that was based on the annual difference in the simulated and measured total runoff, the most important parameters to optimize were those related to the calculation of evapotranspiration. When using an objective function that took into account the timing of the differences in the measured and simulated flow, more parameters were now needed in the calibration, including those that dealt with snow melt, flow through the soil, and river channel roughness.

The recommendations for future study included: finding other gridded datasets that could be used to verify the ones that were created in this study, examining the datasets for trends to see if they reveal any indications of climate change in different regions of the country, and examining further the magnitudes of the different kinds of predictive uncertainty (data, model, and parameter).

Also recommended was that in the future, despite the reliability of the WATFLOOD model in its ability to predict streamflow, other models should be used that have more a more sophisticated treatment of the energy balance and the sub-surface soil layers. These types of models will make it possible to fully utilize the results from finer resolution regional climate models that are currently being run for different climate-change scenarios.

The results of this thesis fit in well with the goals of the International Association of Hydrological Sciences (IAHS) study on Predictions in Ungauged Basins (PUB). This is an international effort to increase skill in understanding key hydrological processes within ungauged basins and thus allow for

better predictions of hydrological processes within these basins. The objectives of PUB were advanced by the research done in this thesis, and in particular, it focused in on some of the unique challenges of working with ungauged basins in the Canadian environment.

This thesis was organized along the principle of "design the process, not the product". As such, although a set of final products are presented at the end, the most important part of the thesis was the process that achieved these products. The thesis laid out a series of techniques and procedures that could be used in many different studies for predictions in ungauged basins. Thus it is not assumed that every technique designed in this thesis will be applicable to every other researcher, but it hoped that most researchers in the field will be able to use at least some parts of the techniques developed here to help improve their own research goals.

Acknowledgements

I would like to thank everybody who helped me in the creation of this thesis; this includes my supervisors, fellow graduate students in the Waterloo Hydrology Lab, the technical staff of Civil and Environmental Engineering, and everybody who gave me advice during the preparation of this thesis.

Dedication

To my father: Imants Seglenieks (1914-1999) and

my best friend: Derek Weiler (1968-2009)

Table of Contents

List of Figures

List of Tables

Chapter 1
Introduction

1.1 Background and motivation

There is a lack of measured, long-term, reliable, and well-distributed hydrological variables in Canada. These hydrological variables include, but are not limited to: temperature, precipitation, ground runoff, actual evapotranspiration, soil moisture, and snow water equivalent.

Knowledge of these variables is important in many different fields, such as: land-use planning, design of engineering structures, agricultural production, flood forecasting, hydro power generation and especially for any study of climate change. For example, a set of gridded hydrological data produced by the Climate Research Unit has been used in such diverse studies as: the transmission of malaria, carbon sinks, and the demography of the holly-leaf miner (Mitchell and Jones, 2005).

All of these types of studies (and others not listed here) would benefit from having well-distributed (both spatially and temporally) and reliable estimates of these hydrological variables. Unfortunately, in Canada for a majority of these variables such information either does not exist, or exists at such a poor resolution (both spatially and temporally) that it has limited use. This is both a result of the lack of resources to measure these variables over such a large area and the fact that many of these variables are difficult to accurately and reliably measure.

As an example of the difficulties involved with the field measurement of some of these hydrological variables, consider runoff. A true measurement of runoff would involve devising a method to measure the amount of water that passes through a plane extending from the ground surface to below the water table. Of course, this would also have to done without disturbing the soil matrix in order to get a true measurement. This type of measurement has been achieved on small test sites; however, large-scale implementation would be all but impossible. As a result of the difficultly in measuring runoff, estimates of runoff are often made using measurements taken at streamflow gauges. However, this type of analysis only gives the overall average amount of runoff of a watershed and gives no information on its distribution throughout the watershed. Thus the spatial distribution of the estimate of runoff calculated with this method is dependent on the distribution of streamflow measurement stations.

Given that they are measured at most meteorological stations, it could be reasoned that there should not be any difficulty in creating distributed maps of temperature and precipitation. Unfortunately, even with the relatively high density of meteorological stations in some parts of the country, there are other parts with very few measurement stations. For example, in the Canadian Arctic, there can easily be hundreds of kilometres between measurement stations, and in fact, the density of stations is on par with those found in developing nations of the world (Lammers et al., 2001). This was shown graphically by New *et al.* (1999), as the density of the station locations where

they were able to find precipitation normals in northern Canada, was similar to the densities seen in parts of South America, Africa, and northern Russia (Figure 1.1).

The arctic regions of Canada are expected to be particularly severely impacted by the effects of climate change. From various future climate scenarios, the rise in temperature over these areas is forecasted to rise significantly more than other areas of the planet (IPCC, 2007). As well, the eco-system in this part of the world is particularly sensitive to changes in the climate given the harsh conditions. This highlights the importance of baseline hydrometerological datasets in these areas that can be used to increase the understanding of climate variability and change. Unfortunately, these areas of highest potential climate change impact also correspond to the areas within Canada with the greatest challenges in collecting measured data, and have thus lead to a scarcity of measurement stations in these areas. To make matters worse, there has also been a sharp decline in the number of measurement stations, in particular streamflow gauges, across the pan-Arctic region since the 1980s (Lammers *et al.,* 2001),.

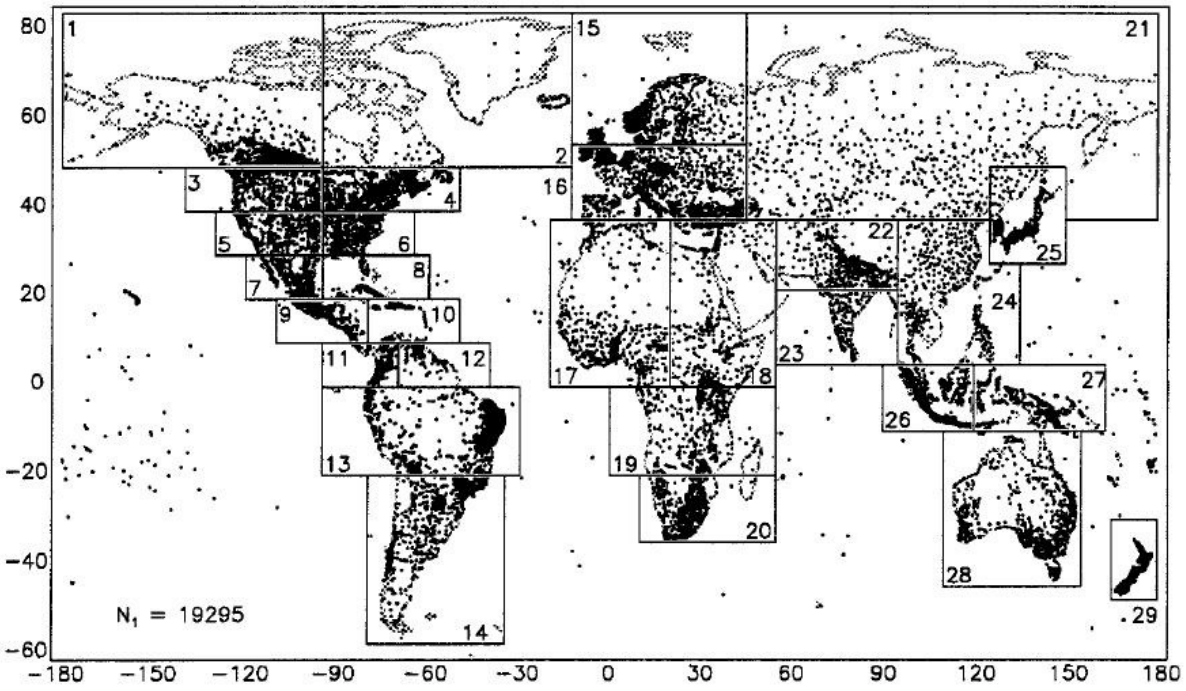

Figure 1.1: Location of stations with precipitation normals used by New *et al.* (1999).

Having a proper assessment of the past streamflow conditions is important for the design of engineering structures. As an example, consider the situation when a river crossing for a pipeline is

being designed in the Canadian Arctic. In order to properly design this crossing it is necessary to know the flow history of the river based on long-term measurements of the flow. However, there are few rivers in the Arctic where long-term streamflow stations exist; thus, most rivers are ungauged. A simple technique to create a simulated streamflow record would be to scale the readings from the nearest long-term gauged basin. But, depending on the location of the river, the nearest long-term gauged basin may be hundreds of kilometres away. The greater the distance from the nearest measured basin, the larger the uncertainty using this simple technique. As well, even if a measured basin was located near the basin of interest, because of differences in topography or land use, there may not necessarily be a linear relationship between the runoff in the two basins. Another possibility is that a streamflow station does exist, but it does not have sufficient record length (that is, 30 years) to be used in the design of the river crossing. Without this type of data, the engineering design will have to make assumptions that will most likely lead to added costs to the structure in the form of over-engineering in order to maintain public safety. The structure could perhaps be made just as safe if reliable data on the flow history of the river could be calculated.

Maps of runoff for Canada do exist, such as this one from the Canadian Atlas (Figure 1.2). Examining this map, there is a distinct lack of detail with large areas of the country divided by only a few contour lines. As well, there is not even an attempt to map the runoff on the Arctic islands; however, there are values given for the Arctic coast just to the south of the islands. This casts doubt on the validity of the readings on the Arctic coast.

In their paper, Andreassian et al. (2007) state that one of the factors contributing most to undermining present-day hydrologic science is that too much time is spent on the modelling of individual basins on short time scales. This leads to models that are very specific to each basin and do not perform well when either taken out of their original basins or used during time periods when extreme hydrological conditions may occur that were not encountered during the short time period when the model was developed. They suggest that there are many good reasons for working on larger sets of basins over longer time periods, including better assessment of the robustness and generality of the model and a better understanding of the variability between basins.

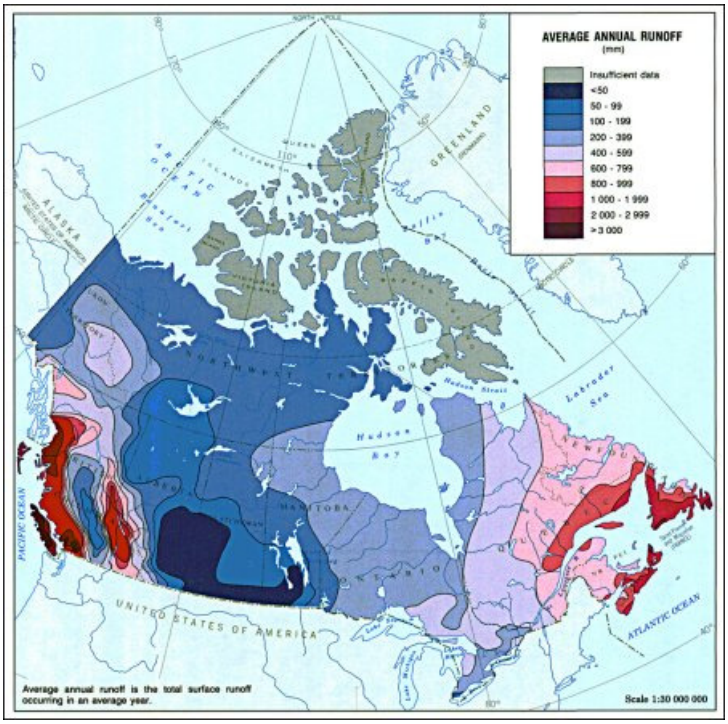

Figure 1.2: Map of average annual runoff from the Water Survey of Canada (source: The Atlas of Canada)

When considering these example, some questions arise about the current state of the measurement and modelling of hydrological variables including:

- How can the current network of meteorological stations in Canada be best utilized within a hydrological model in order to create national hydrometeorological datasets?
- What is the uncertainty in these datasets?
- What are the challenges involved in creating a drainage database and implementing a hydrological model across the entire country?
- What is the usefulness of the datasets given the spatial and temporal scales that have been used to create them?
- Do these datasets have enough reliability in order to make decisions on flow frequency estimation for ungauged basins that can be used for such applications as engineering design?
- How can this type of analysis be used in the prediction of changes to the components of the hydrological cycle under the influence of climate change, particularly in the Canadian Arctic?

This thesis presents methods designed to gain understanding of these questions and in doing so hopefully advances the science of hydrological modelling. The methods developed are particularly well designed to use the relatively low density of measurement stations that are a reality within all of Canada, but particularly the remote areas of the country.

1.2 Objectives

The overall objective of this thesis was to establish the best possible estimates of the hydrological variables, in particular runoff, for Canada over the period 1961-2000 based on measured data on a monthly time scale. Having a database of these variables will serve as a valuable reference for researchers in many different fields. The time period is especially important to those researchers involved in the study of climate variability. As well, there are other gridded products currently in development based on satellite imagery, output from numerical prediction models, field measurements, or a combination of all of these that will need to be verified. The type of gridded product created here, based on measured data, will provide a good basis upon which to compare these other products.

In order to achieve the overall goal of creating this gridded time series, a hydrological model was implemented across the entire country at a spatial scale that was small enough for the model assumptions to be respected and the data to reflect regional differences. While at the same time, the spatial scale had to be large enough so that the time to run the model would not be so large as to prevent proper calibration of the model. This leads not only to the objective of implementing the model across the country but also to evaluate the usefulness of the data at this scale.

Another objective was to evaluate the uncertainty in the hydrological variable estimates. Too many times in hydrological studies, simulated output from models is given as a single number without an indication of what the reasonable uncertainty bounds are on the number. Although some researchers question whether or not users of the data will see the uncertainty as an admission of the failure of the simulation, the inclusion of uncertainty adds to the utility of the data. As well, it has been suggested that operational personnel in charge of flow structures are more interested in knowing the probability of a certain flow rather than being given a single number (Dr. Sean Carey, personal communication, 2007).

Finally, another objective was to devise a method that could be used to create long-term streamflow records for any location in Canada that are based on the best available data and the best available techniques. Again this is particularly needed in areas of sparse data density where measured streamflow may either not exist or not have been measured over a sufficient period of time to make design decisions.

The objectives of this thesis fit in well with the goals of the International Association of Hydrological Sciences' (IAHS) initiative Predictions in Ungauged Basins (PUB). This is an international effort to increase skill in understanding key hydrological processes within ungauged basins and thus allow for better predictions of hydrological processes within these basins (Sivapalan, et al., 2003).

More specifically, the science program of PUB contains the following objectives:

1. Advance our ability to predict with confidence the fluxes of water and associated constituents from ungauged basins, evaluated with data from selected basins in different biomes or hydroclimatic regions, including quantification of the uncertainty in these predictions in a routine manner.

2. Advance the technological capability around the world to make predictions in ungauged basins, firmly based on local knowledge of the climatic and landscape controls on hydrological processes, along with access to the latest data sources, and through these means to constrain the uncertainty in hydrologic predictions.

3. Increase the awareness of the value of data, especially the gauging of hydrologic variables, for the management of water resources and water quality around the world, and demonstrate the need for targeted gauging of currently inadequate or nonexistent data sources by quantifying the links between data and predictive uncertainty.

All of these objectives of PUB were advanced by the research done in this thesis, and in particular, it focused in on some of the unique challenges of working with ungauged basins in the Canadian environment.

Another interesting aspect of PUB is that its overall organizing principle is to "Design the process, not the product." This thesis was organized along the same principle; although a set of final products was presented at the end, the most important part of the thesis was the set of techniques that were developed to achieve these products. The thesis laid out a series of techniques and procedures that could be used in many different studies for predictions in ungauged basins. For example, the model grid used for this study was a polar stereographic projection and a 51-km grid spacing. However, the exact same technique could be used for a smaller study area with a UTM projection and a 1-km grid spacing, if that were the requirement of the study.

In the hydrological modelling field, there is a push towards "community" modelling, where different researchers can contribute to the overall modelling efforts by providing their own ideas to certain parts of the process. The work in this thesis was designed to be "modular" in nature, with different parts being applicable to other research projects. Although the techniques have been used here to produce certain types of products with certain specifications, the very same techniques could be used with other specifications to products that could have uses in other scientific fields.

Thus it is not assumed that every technique designed in this thesis will be applicable to every other researcher, but it is hoped that most researchers in the field will be able to use at least some parts of the techniques developed here to help improve their own research goals.

1.3 Thesis organization

Chapter 2 provides a summary of the literature on interpolation methods used for meteorological data, hydrological models, the creation of drainage databases need to run hydrological models, and a history of past calculations of distributed runoff.

Chapter 3 describes the development of a technique to create drainage characteristics over large areas that can be used in the Waterloo Flood Forecasting Model (WATFLOOD) (Kouwen and Mousave, 2003). The technique is then used to create a drainage database for Canada that is evaluated at various locations throughout the country.

Chapter 4 develops a technique to interpolate measured station data based on the physiographic characteristics of the land surface surrounding each station. The technique is compared to the inverse weighted distance method for both precipitation and temperature. The technique is then modified to interpolate daily data and a simple disaggregation is performed to create an hourly dataset ready to be used by WATFLOOD.

Chapter 5 describes the implementation and calibration of the WATFLOOD hydrological model. WATFLOOD is calibrated using the Dynamically Dimensioned Search (DDS) algorithm (Tolson and Shoemaker, 2007), with the difference between the measured and simulated streamflow used as the objective function.

Chapter 6 presents the results of WATFLOOD runs as gridded time series of the hydrological variables: actual evapotranspiration, runoff, snow water equivalent, and soil moisture. An assessment is then made of the parameter uncertainty as well as an examination of the effects of climate change on the hydrological variables.

Chapter 7 summarizes the major conclusions of the thesis and presents recommendations for future research that would progress the science of hydrological research.

Chapter 2
Literature Review

2.1 Interpolation methods

Long-term gridded monthly precipitation and temperature values are fundamental data required for many climatological studies (Nadler and Wein, 1998; Venier *et al.*, 1999; McKenney *et al.*, 2001; Shen *et al.*, 2001). These are typically derived using measurements from irregularly spaced climate stations that are then interpolated onto a grid by various geostatistical methods.

The interpolation of meteorological variables onto a regular grid has been attempted for many years (Baumgartner and Reichel, 1975; Arnell, 1995; Willmot and Robeson, 1995; Thornton *et al.*, 1997). The first methods used to interpolate station data were numerical methods; these methods are generally simple to implement and generally perform well in areas of dense data availability. Numerical methods involve the calculation of a value at any point based on the values of surrounding measured point data.

In these methods, a numerical function is developed that is then used to estimate a regularly spaced grid from irregularly spaced point data (Daly *et al.*, 1994). Examples of numerical interpretation are: inverse weighted distance, kriging, nearest neighbour, radial basis function, modified Shepard's method. However only first two methods listed are commonly used for gridding climate data and as such, they will now be explained in more detail.

One of the simplest examples of a numerical method is the inverse weighted distance (IWD) method first introduced by Shepard (1968). In this method, data are given a weighting such that the influence of one point relative to another declines with distance from the grid node of interest. Weighting is assigned to the data through the use of a weighting factor that controls how the factors decline with increasing distance from a grid node. As the weighting factor increases, points further from the grid node have less of an effect, and the grid node value approaches the value of the nearest point. Meanwhile, for a smaller power, the weights are more evenly distributed among the neighboring data points (Issaks and Srivastava, 1989). By definition, the fitted surface will pass through the known points and thus the method is classified as an exact interpolator.

Numerically the calculated value at any point is given by the equation:

$$F(x,y) = \sum_{i=1}^{n} w_i f_i$$

where n is the number of measurement points, w_i is the weighting factor, and f_i is the value at each measurement point.

The weighting function is defined by:

$$w_i = \frac{h_i^{-p}}{\sum_{j=1}^{n} h_j^{-p}}$$

where h is the distance between the measurement point and the grid node and p is the weighting factor. The distance between the measurement point and the grid node is simply:

$$h_i = \sqrt{(x - x_i)^2 + (y - y_i)^2}$$

where (x,y) are the coordinates of the grid node and (x_i,y_i) are the coordinates of the measurement point.

This method is very simple and quick to implement, but its performance is greatly affected when the measured values are not closely spaced. Having sparse measurement points results in a single point having an influence for many hundreds or even thousands of kilometres in a situation like the Canadian north where there are very few measurement stations.

The other popular numerical method for the interpolation of meteorological data is kriging. This method assumes that the difference of the value of interest of two points is correlated with the distance between the two points. This is referred to as the semi variance and is calculated using the following formula:

$$y^*(h) = \frac{1}{2n}\sum_{i=1}^{n}(z(x_i) - z(x_i + h))^2$$

Where $y^*(h)$ is the calculated value of the semi variance at distance h, z is the attribute value, x_i is the location of the one of the pair of points, $x_i + h$ is the location of the other point, and n is the number of pairs of sample points separated by h. The plot of semi variance for all the distance values of h is referred to as a semivariogram.

In practice, the semivariogram is created by examining successive pairs of points; for each pair, the distance between the points is recorded, as well as the difference in the attribute value at the points. Intervals of the distance between the pairs (sometimes referred to as bins) are set up, and for each distance interval the average value of the difference in the values of the pair of points is used in the semivariogram. It is assumed that points that are closer together will have less of a difference in their data than points that are further apart; this leads to the typical shape of the semivariogram (Figure 2-1).

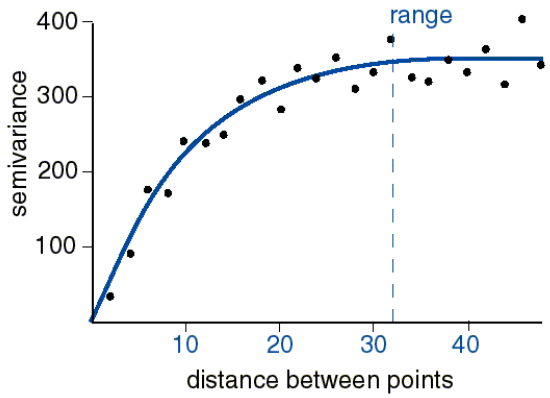

Figure 2-1: Typical semivariogram

The measured semivariogram is then modeled using a mathematical function that best describes the shape of the measured semivariogram. Typical functions that are commonly used to fit the semivariogram are: exponential, spherical, and Gaussian (Figure 2-2).

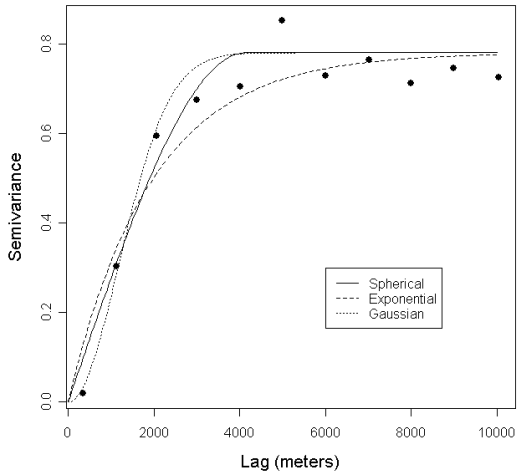

Figure 2-2: Semivariogram models

Once the semivariogram has been defined, it is then used to calculate the values for the grid nodes based on the relationship of the modeled semivariogram.

There are many different types of kriging, but the most common type that is used for the interpolation of meteorological data is called ordinary kriging. This type of kriging assumes two different characteristics about the data: that there is wide-sense stationarity in the data and that a semivariogram can be created from the data (Isaaks and Srivastava, 1989).

The first assumption of wide-sense stationarity implies that both the mean and variance of the error function (or probability distribution) of the data is constant throughout the area. The second assumption, being able to create the semivariogram, requires that there must be enough known points to determine the characteristics of the semivariogram in a reliable fashion. It has been suggested that at least 30 points are needed at each distance interval in order to create a reliable semivariogram (Journel and Huijbregts, 1978).

There are various parameters that can be adjusted during the kriging process that strike a balance between fitting the known points exactly and smoothing the final field. Thus kriging may or may not be an exact interpolator depending on the parameters chosen.

In their paper, Mueller *et al.* (2004) examined numerous studies that have compared the IWD and kriging techniques for the interpolation of meteorological data. Interestingly, they found that there were numerous studies that indicate that the IWD technique results in a better interpolation, others that side with the kriging technique, and still many others that conclude that neither technique was superior for their test cases. From this it was concluded that there is no evidence that either technique will be superior in all situations.

As these purely numerical techniques rely solely on measured data, they have been found not to work well in areas of sparse measurements (Creutin and Obled, 1982; Lebel *et al.*, 1987; Hevesi *et al.*, 1992). It is likely that the sparse nature of meteorological data and its dependence on topography make it difficult to use pure numerical methods to interpret it. This may cause large errors in the interpolation of data in difficult situations, such as sparse data or mountainous terrain (Daly *et al.*, 1994).

As well, kriging has specifically been criticized for requiring questionable assumptions and subjectivity in creating and interpreting the necessary semivariograms before the best fit surface can be created (Price *et al.*, 2000).

In Canada, most of the long-term climatic measurement stations are located in developed areas in the southern part of the country, leaving very few stations in the remote northern parts of the country. As well, the stations that are located in mountainous areas are usually located in lower elevations, for example along rivers and valleys (Flemming *et al.*, 2000). Thus any method that ignores topographic characteristics will have difficulty in properly predicting the values in areas of higher elevation between the measured station points.

The deficiencies of the numerical techniques were recognized and led to the development of techniques that combined topographic information with station measurements.

An example of one of these methods is the Precipitation-elevation Regressions on Independent Slopes Model (PRISM) (Daly *et al.*, 1994). This method assumes that precipitation increases in a linear manner in relation to elevation; this relationship is further assumed to be similar for topographically similar slopes, called facets. These facets are regionalized by using the slope and aspect of the grid elements of a Digital Elevation Model (DEM), defined as a contiguous area with similar slope orientation. However, in order to ensure that a reasonable number of stations are available in each facet, the original facets are filtered and combined with other neighbouring facets.

The PRISM model then develops a precipitation/elevation relationship for each facet using a regression analysis on the measured data points within that facet. This relationship is then used to calculate the values for the grid nodes in the rest of the facet.

A strength of the method is that as it doesn't use the same precipitation/elevation relationship for the entire study area; thus, it adapts to the local effects of topography in each region of a study area. It has been shown to give better results than kriging, detrended kriging, and cokriging in a study over the western United States (Daly *et al.*, 1994).

One limitation of the method is that it may not work well in areas where the precipitation amount is not solely correlated to the elevation. Such areas include, for example, areas where the precipitation is more influenced by the distance to the nearest water body or areas where there is not a large amount of topographic difference where it may be difficult to assign DEM squares to similar slope and aspect.

The PRISM method has also been criticized for its difficulty to implement, the amount of parameterization that is necessary, and the length of time it takes to run the model making it difficult to make detailed runs over large areas (Dodson and Marks, 1997).

ANUSPLIN is another popular method that uses topographic information to supplement numerical interpolation that was developed by the Australian National University (Hutchinson, 1995). The method uses thin-plate surface-fitting techniques to fit a surface to the station data points. Other supplemental data such as elevation, latitude, and longitude are also incorporated into the interpolation. The amount of smoothing is determined objectively by minimizing the error of the fitted surface.

As with other non-numerical methods, ANUSPLIN is also difficult to implement and is computationally taxing (Dodson and Marks, 1997). Even though non-numerical methods come with more of a computational cost, this complexity is a necessity in order to make better interpolations. However, with the ever-increasing availability of faster computer resources, the added computational cost may no longer be a significant obstacle.

A limitation of any of these interpolation methods is that as they rely on using their closest neighbour to evaluate interpolated values they will always be influenced by areas that have a greater station density. These effects can be minimized by parameter selection in the kriging method and the thin-plate fitting technique, but there will always be a strong influence of individual points on the final pattern of the data.

This can be seen in interpolated maps by the presence of "bulls-eye" patterns around the measurement stations (Figure 2-3). In this example, the only reason that the circles appear at those locations is because of the presence of measurement stations; it would be desirable to use an interpolation technique that it not directly affected by the station locations.

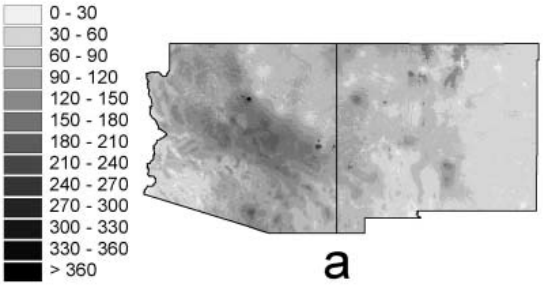

Figure 2-3: Kriging results showing the influence of the locations of the measurement points (from Brown and Comrie, 2002).

This has led to the development of methods that use regression methods with both the measured station data and topographic information. Although these techniques use measured station data to create the regression equations, as the interpolation is based on these equations, the resulting interpolated fields show no biases towards the specific locations of the measurement stations.

Interpolation methods using regression techniques exist that use solely elevation data (Fleming *et al.*, 2000), elevation along with latitude and longitude (Ninyerola *et al.*, 2000; Price *et al.*, 2000), but most common are those that use elevation along with a host of other topographically derived parameters (Prudhomme *et al.*, 1999; Agnew and Palutikof, 2000; Fassnacht *et al.*, 2003; Perry *et al.*, 2005).

In their study, Price *et al.* (2000) developed a method called GIDS based on a regression technique that uses elevation, latitude, and longitude. However, in their conclusions, they state that their results could be further refined by adding such parameters as distance from ocean or slope as independent

variables to their regressions. Mitas and Mitasova (1999) also note that the next generation of interpolation methods will have to incorporate topographic information.

The technique used for this study is an interpolation method known as the Waterloo Multiple Physiographic Parameter Regression (WATMPPR), based on the technique originally developed by Solomon *et al.*, (1968). WATMPPR is a technique that uses elevation, latitude, longitude, and a number of derived physiographic characteristics as independent variables in a regression analysis. The technique was developed in Canada for hydrometric network planning purposes and has been used subsequently in a number of studies including the Mackenzie Basin in Canada (Soulis *et al.*, 1994) and in the Colorado River basin (Fassnacht *et al.*, 2003). The WATMAPPR technique will be explained in detail in Chapter 4.

2.2 Hydrological models

Hydrologic models are simulations of the flow of water as it travels through a watershed starting at the point when the water enters the watershed from the atmosphere as precipitation until it leaves the watershed through the river network. Of course, there are many processes that occur between these two points that are simulated by hydrologic models.

These models can be used for such problems as water resources assessment, development, and management. Examples include analysis of quantity and quality of watershed runoff and streamflow, operation of reservoir systems, development and protection of groundwater, and operation of water distribution systems (Wurbs, 1998).

The first broad classification of hydrological models divides them into stochastic and deterministic models (Abbott and Refsgaard, 1996). Stochastic models examine the past sequence of a hydrological variable and use the statistical properties of that sequence to predict future patterns. In deterministic models, the output is based on the response of a basin to a set of inputs.

Most deterministic hydrologic models are based on the simple water balance equation:

$$P - ET = R + \Delta S$$

where P is the precipitation, ET is actual evapotranspiration, R is runoff, and ΔS is the change in storage. The differences between these hydrological models are the techniques and the assumptions they use to calculate the different components of the water balance.

Just as there are many different kinds of deterministic hydrological models, there are also many different ways to classify them (Singh, 1995; Wurbs, 1998; Todini, 1988). All deterministic models can be broadly classified into two types: physically based models and empirical models. Physically based models are founded on the mathematical solution of equations governing overland flow, flow through porous media and channel flow. Empirical models do not take into account the detailed geometry of the ground surface and sub-surface, but consider the watershed as an ensemble of

interconnected conceptual storages (Jothityangkoon *et al.*, 2001). These are two ends of a continuous spectrum, as there are physically based models that model certain processes of hydrological cycle in an empirical way.

Scaling and domain are other ways to distinguish models. These terms can describe both the spatial and temporal characteristics of the model. Spatially, the scale refers to the smallest unit that is distinguishable in the model, while the domain is the total size of the basin or length of the simulation. As a result, a model may have both a large scale and large domain or a small scale and a large domain.

The spatial scale of the model also dictates how the various physical processes are modeled within a basin. As stated by Singh and Frevert (2002), the interactions between land surface and pedologic, lithospheric, hydrospheric, and atmospheric processes have a direct relation with the spatial scale. The non-uniformity of hydrologic processes is a direct result of the spatial scale to be employed.

Temporally, the scale is the time step of the physical processes being modeled, which can be on the order of seconds all the way up to years. While the temporal domain is the total length of time being modeled, this can range from hours (event basin models) to centuries (climate models). Once again, models can have different levels of temporal scale and temporal domain.

As a general rule, as the scale of a model gets smaller, both spatially and temporally, the complexity of the model will increase.

The terms “lumped” and “distributed” are used interchangeably to describe spatial and temporal scaling, leading to much confusion. In general, a model is considered lumped if the forcing data (that is, temperature and precipitation) is averaged over the entire basin, while distributed models allow for different forcing data in different areas of the watershed. Once again this is a continuous scale as every distributed model can be considered a lumped model at some scale.

These are the general classifications of hydrologic models, but these classifications can be augmented by examining how each model simulates the different physical process that dictate the amount and timing of runoff in a watershed. These processes include evaporation, infiltration, rainfall-excess, runoff production, snowmelt, surface runoff routing, channel flow, interflow, groundwater flow, and storage terms. Depending on the hydrological model, it may or may not include the above processes or may add other ones depending on the processes that exist in the watershed being studied. For example, in a mountainous region, it may be necessary to include the process of glacier melt, but this would not be necessary in a desert region.

Jothityangkoon *et al.* (2001) discuss the development of catchment scale models using the downward or top-down approach of Klemes (1983). This approach started with a simple model at a large spatial and temporal scale. The model was forced with precipitation and temperature and the resulting simulated streamflow was compared to measured streamflow. The spatial and temporal

scales were then reduced and the streamflows were once again compared. If there was not adequate agreement between the measured and simulated hydrographs, the reasons for the poor fit were determined and more and more processes were added to the model until an adequate fit was achieved. These steps were then repeated to get the level of complexity needed for the spatial and temporal scale of interest.

Jothityangkoon *et al.* (2001) varied the spatial scale from about 2500 km^2 to 13 km^2 and the temporal scale went from yearly down to daily. The study found that for a yearly time scale, a very simple model that partitioned annual rainfall into evaporation and excess runoff was sufficient. This model required only three parameters: soil depth, average porosity, and percentage interception loss.

Once a monthly time step was used, the model needed to incorporate additional processes, most importantly the generation of subsurface runoff with a linear storage-discharge relationship and a partitioning of evaporation into bare soil evaporation and transpiration. It also required the addition of six more parameters dealing with soil, topography, and vegetation.

As expected, more processes had to be added in order to simulate the streamflow correctly with a daily time step. These processes included a non-linear storage-discharge relationship for subsurface runoff, multiple soil stores in series as various depths, and deep groundwater storage. This model required a total of 10 parameters: 7 for soil and topography, 2 for vegetation and 1 routing parameter.

The major limitation of this study was that the study area was located in southwestern Australia without the presence of snow. In order to simulate flow in most areas of Canada at a monthly time scale, it would be necessary to simulate snow storage, as it has a major effect on both the winter and early spring flows. This would have led to a model with even more complexity and more parameters.

Since the wide spread accessibility of computing power beginning in the late 1960s, many different hydrological models have been developed all around the world by many different organizations. Many of these have been developed for specific regions or to capture specific processes; however there have also been models that have been shown to work in many different basin around the world. Generally these models have to account for all of the major processes that can reasonably be expected to be encountered around the planet.

Examples of the most well-known hydrological models include: The UBC model (Quick and Pipes, 1976), the SRM model (Rango and Martinec, 1979), the NWSRFS model (Anderson, 1973), The TOPMODEL (Beven and Kirkby, 1979), the MIKE-SHE model (Refsgaard and Storm, 1995), the HBV model (Bergstrom and Forsman, 1973), and the VIC model (Liang and Lettenmaier, 1994). All of these models have different strengths and weaknesses and the choice of model to use for a particular study depends on the availability of the data needed to run the model and a determination of whether or not the model adequately considers the important hydrological processes occurring in the study basins.

The hydrological model used in this study was the Waterloo Flood Forecasting Model (WATFLOOD) developed at the University of Waterloo; WATFLOOD is a physically based semi-empirical distributed hydrologic model (Kouwen and Mousavi, 2002). A full description of the model is given in Appendix A.

2.3 Creation of the drainage database

An integral component of gridded hydrological models is the creation of the drainage database. This database consists of information on the topography of the watershed so that sub-grid physiographic features such as drainage direction, channel elevations, or ground slope, can be parameterized for each grid. These physiographic parameters are key to describing both the vertical transfer of water within each grid, as well as the horizontal transfer of water between grids. The segmentation process in these models condenses the data to a format that preserves as much as possible of the input information, while greatly reducing the memory requirements of the models (Kouwen and Mousavi, 2002).

When hydrological models were first developed, manual methods were used to partition watersheds into grid squares and create the drainage database. Principally this involved the determination of the flow network between the different grid squares as well as other physiographic parameters using topographic maps.

One of the limitations of these manual methods was that only small basins could be modeled because of the time needed to create the drainage database for larger basins. Also, these manual methods were very subjective and prone to error, thus making the resulting drainage database dependent on the particular person performing the analysis.

With the growing availability of Digital Elevations Models (DEMs) in the 1990s, automatic methods were developed to create the drainage database. This not only allowed for drainage databases to be created for much larger watersheds, but by using automatic methods, there was more consistency in the derived drainage database.

The resolution of global DEMs continues to improve with spatial resolutions of 1 km or less becoming common (USGS, 1997; Rabus *et al.*, 2003). However, most of the current distributed mesoscale hydrological models are not capable of resolving the earth's surface down to such a resolution, either because of computing limitations (Fekete *et al.*, 2001) or because some of the assumptions made about the hydrological processes are no longer valid when considering grid squares less than around 1 km (for example in WATFLOOD it is assumed that there is a river channel in each grid square, something that may not be true for small grid squares).

Thus techniques are needed that will take information from the smaller DEM pixel scale (typically on the order of kilometres) to create the drainage database for the mesoscale hydrological model grid scale (typically on the order of 10s of kilometres) (Figure 2-4).

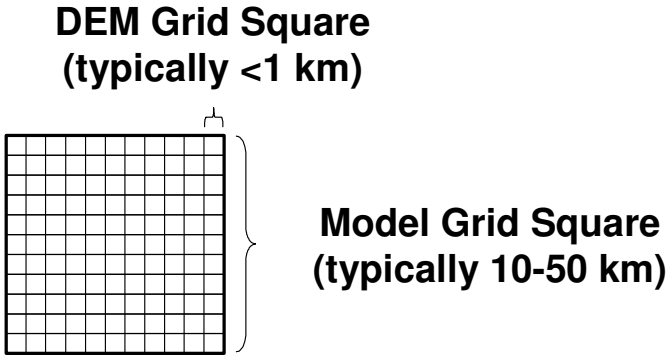

Figure 2-4: The relationship between model grid scale and DEM grid scale.

Thus there are two steps to create the drainage database on the model grid scale: first, the flow network must be determined at the DEM grid scale; second, this information must be scaled up to the model grid scale.

Although it would be possible to simply use elevation information at the scale of the model grid square to determine the flow network, this scale is typically not fine enough to accurately capture the physiographic features that influence the flow of water. This is especially true in mountainous regions where the presence of a valley may be masked by the elevation of the valley walls.

It has been shown that using the average elevation at the model scale leads to an inaccurate calculation of the drainage network (Shaw *et al.,* 2005). It is assumed that the resolution of the DEM pixel will be fine enough to allow the flow network to be accurately simulated.

Thus, as a first step, the flow network at the DEM scale must first be determined. It must be remembered that the flow network derived using a DEM is only the "potential" river network or where water would flow if there was enough water to fill the channels. However, the "active" river network (where water does actually flow) is determined by the climate and water uses of the region; thus, not all of the river channels in the potential river network will necessarily have flow (Vorosmarty *et al.*, 2000). For example, the "potential" river network in the southwestern United States shows the Colorado River draining a large area before emptying into the Pacific Ocean. However in reality, the Colorado River no longer flows into the Pacific Ocean as a result of the water demands before the water reaches the ocean.

One obstacle to creating the flow network at the DEM scale is that many DEMs created using automatic methods inevitably contain errors. Usually these errors show up as sinks; these are areas that are lower than their surroundings and, as a consequence, any flow into these areas cannot be connected to the outside of the DEM. In order to determine the flow network at the DEM scale, it is necessary to create what is called a depression-less DEM.

In the simplest method to correct the elevation within these sinks, the elevation of the pixels inside a sink are adjusted until all pixels within the sink are at the same elevation as the edge of the sink. Other more complicated pit-filling procedures also exist that use the shape of the sink area and location of the final outflow from the sink to create a more realistic flow pattern, both inside and outside the sink (Tribe, 1992; Garbrecht and Martz, 1997; Soille, 2003).

Once all the sinks have been filled and all pixels flow to the edge of the DEM, then a depression-less DEM has been created. It is now possible to calculate the flow direction for each pixel.

The most basic method of determining the flow direction at the DEM scale is called the D8 method (O'Callaghan and Mark, 1984) and has subsequently been used in many studies (Band, 1986; Jenson and Domingue, 1988; Morris and Heerdegen, 1988).

In the D8 method, it is assumed that flow will follow the direction of the greatest elevation difference between the current cell and the eight surrounding cells. In the case of two (or more) of the surrounding cells both having the greatest elevation difference, either a random method or one based on some prescribed algorithm can be used to determine the flow direction. This situation can often result as a consequence of the corrections made to create the depression-less DEM (that is, the filling of the sinks).

As an alternative to using the D8 technique, Tartoban (1997) used a method that calculated the angle of flow from a cell based on the elevation differences of the neighbouring pixels. The flow from the cell is then proportioned between the two neighbouring cells that border this angle of flow. Although the technique was shown to perform better than the D8 technique, the added complexity is probably not necessary for most studies.

Unfortunately, even with all of these adjustments, there sometimes still exist situations where the flow network derived using automatic methods must be corrected. This can either be done by "burning in" the flow network based on known flow paths or manually updating portions of the DEM to ensure the derivation of the proper flow network.

Once the flow network at the DEM scale results in the correct flow network to be simulated, this information can now be transferred to the model grid scale.

One of the techniques available to scale up information from the DEM scale is the one proposed by O'Donnel (1999). In this technique, the outside rows of the DEM pixels of each grid square are

first examined and the pixel with the greatest outflow from the grid square is used to determine the overall flow from the grid square.

In the O'Donnel study, the automatic technique was compared to a flow network derived from manual methods and there was general agreement between the two techniques. However, the authors caution that even after using their technique, there may still be a need to manually adjust the derived flow network to ensure it complies with the actual flow network.

Another technique to create drainage database from a DEM is SLURPAZ (Lacroix *et al.*, 2002). The SLURPAZ interface takes flow data from the TOPAZ model (Garbrecht and Martz, 1997) to create files needed to run the SLURP semi-distributed hydrological model (Kite, 1997). The input needed for the TOPAZ model is a DEM and land-cover database, while the output from SLURPAZ are the characteristics of the Aggregated Simulation Areas (ASAs) used in SLURP. But as these ASAs are based on sub-watersheds and not grids, the flow path is strictly from a single ASA to another ASA. This avoids the necessity to "scale-up" the flow data at the DEM scale in the same manner as would be necessary for a gridded hydrological model.

In their paper, Fekete *et al.* (2001) describe their river network scaling algorithm (NSA) designed to rescale finer-resolution networks to a coarser resolution. In this algorithm, the drainage area is calculated for each cell of the fine-resolution grid, and then, for each grid in the coarser-resolution grid, the largest value of the drainage area for the finer-resolution grid is found and is used for the coarse grid. Then the drainage direction is calculated in a manner analogous to the D8 method using drainage area instead of elevation. Other drainage characteristics of the river network can then be calculated.

Although the authors had success in applying the method to various European rivers, a few limitations to the method were found. To address some of these, a modification to the algorithm was developed that ensures that the calculated flow direction only occurs between squares that are in the same sub-basin. This was now called the network-scaling algorithm with basin enhancement (NSABE) and improved the results on the European basins. However, even with the NSABE modification, the authors state that there are inherent errors in the method that cannot be completely eliminated.

Doll and Lehner (2002) described a method similar to Fekete *et al.* (2001) where the drainage directions of coarser-resolution grids were based on the flow accumulation values from finer-resolution grids. The difference in the Doll and Lehner algorithm was that instead of choosing the highest flow accumulation in the neighbouring coarse-resolution grid, the highest flow accumulation had to be found within a prescribed distance of the finer-resolution grid. This prescribed distance was assigned to be the size of the coarse-resolution grid.

The method was shown to have less symmetric error than the Fekete *et al.* (2001) method when comparing basin areas provided by the Global Runoff Data Centre (GRDC, 1999). However, the method still required manual corrections based on published vector maps of river networks. The drainage directions of 35% of the coarse-resolution cells needed to be adjusted in order to conform to the published maps.

Reed (2003) presented the cell outlet tracing with an area threshold (COTAT) method that examines the accumulated flow at the outlet pixel of the model grid square. The accumulated flow from the next model grid square downstream is then compared to the previous one and if it is greater than a threshold value the flow is assumed to occur between the two model grid squares. The initial flow direction field will contain flow directions that cross paths between neighbouring model grid squares. There is then a need to post-process the flow direction field to remove these cross paths. The COTAT method resulted in higher mean absolute errors in drainage areas when compared to simple grid resampling method.

Another very interesting dataset was the Hydrological data and maps based on Shuttle Elevation Derivatives at multiple Scales (HydroSHEDS) product (USGS, 2006) that was created from the Shuttle Radar Topography Mission (SRTM) DEM (Rabus *et al.*, 2003). A very large portion of the data set development was focused on the sink filling routines and subsequent "burning-in" of river channels from another data source. With the detail of the STRM data even obstacles such as bridges provide barriers to the assumed flow of water and had to be removed. The results of HydroSHEDS were a hydrologically conditioned elevation model and a drainage direction map at a resolution of 3 arc-seconds. Unfortunately, the documentation fails to discuss how the areas north of 60 degrees latitude were dealt with as they were not part of the SRTM.

The other product from HydroSHEDS were upscaled drainage directions at resolutions of 15 arc-seconds and 30 arc-seconds. The technique used to upscale the drainage directions from the original 3 arc-seconds involved first upscaling the DEM data. Any sinks that had been created in the upscaled DEM were then filled and the river network that had been derived from the 3 arc-second DEM was burned in to the upscaled DEM. This upscaled DEM was then used to calculate the drainage directions the lower resolution.

One of the most important aspects of aggregating flow to the model grid scale is the treatment of diagonal flow. There are very few references that discuss how to handle this diagonal flow. One of these comes from O'Donnell (1999), which described a technique that decides on whether or not to assign diagonal flow based on first determining where the maximum flow from a grid cell occurs. If this flow occurs within a prescribed distance from the edge of the corner of the square, the flow is further followed as it flows into the neighbouring squares. Depending on how the flow behaves in the neighbouring squares, the flow direction of the initial grid cell will be defined as either diagonal or straight.

Chapter 3 of this study will show why the correct determination of diagonal flow is important in creating an accurate drainage database.

2.4 History of distributed runoff calculations

Attempts at quantifying the different elements of the water balance for the entire globe have been recorded as early as L. Buffon in 1749. The first reported attempt to quantify the water balance of England occurred in 1802, by John Dalton, who is also notably credited for the first calculation of evaporation from water surfaces. It was not until 1905 that E.A. Bruckner proposed a general scheme for a closed water cycle of the earth that included precipitation and evaporation from the ocean surfaces (Unesco, 1978).

A big step forward in the estimation of world runoff came during the first International Hydrological Decade (IHD) from 1965 to 1974. This effort led to the publication of "The World Water Balance" in 1975 by Baumgartner and Reichel. It was designed as a compilation of all available global water balance data that was available at the time. The balance was determined using the best available estimates of precipitation, evaporation, and runoff that were then interpolated in areas of missing data. The authors admit that the available data for the northern part of Canada and Arctic islands were very sparse, and as a result, their reported numbers were estimates.

In 1978, UNESCO published the World Water Balance and Water Resources of the Earth. It was based on precipitation and temperatures from 1891 to 1960. Again they performed a water balance using the best currently available estimates of precipitation, evaporation, and runoff.

For precipitation, all available station data were used, while for evaporation, a potential evaporation function was developed by Budyko that the authors claim is more accurate than the other popular potential evaporation functions of Penman or Thornthwaite (Unesco, 1978).

The calculation of runoff was based on measured discharge at streamflow stations; the overall average was one streamflow station for every 2650 km^2 of land area. Where there were large ungauged basins, they used indirect methods based on precipitation and evaporation.

Bishop and Church (1992) used a variety of interpolation and regression methods to create runoff contours for the northeastern United States for the water year 1984. All of these methods relied on a base map of runoff created using 1951-1980 streamflow data from 441 stations. The base map was created by calculating the runoff at each streamflow station using the stations drainage area, putting that runoff at the centroid of the watershed, and then drawing contours around the centroid values.

The comparison points for the methods were located at 405 precipitation stations in the study area. For each of the methods, runoff was calculated at the precipitation stations using values from the interpolated runoff base map used as the actual values. An uncertainty analysis was also performed,

in which 50 of the original streamflow stations were left out of the analysis and runoff values at these stations were compared to the values derived by the various methods. They concluded that the most satisfactory method was one that calculated the runoff to precipitation (R/P) ratio for each station, combined these into regional mean values, and then used these regional mean values of R/P to calculate the runoff at each precipitation station. Finally a contour map was created using both the calculated runoff at the precipitation stations as well as the runoff calculated at the streamflow stations.

All of these methods have presented some good results; however, they rely on a dense network of both streamflow and precipitation measurement stations, as well as having long-term data at these stations.

As pointed out by Arnell (1995), most of the runoff maps that had been produced up to that point were isoline maps. He states that these maps are more appropriate for showing the variability of continuously variable quantities such as elevation or point precipitation, while runoff does not lend itself well to such a presentation. Instead, he proposed gridded choropleth maps for runoff; because the units of runoff are a value-per-unit area, they are easier to compare to gridded climatic data sets.

Fekete *et al.* (2001) created a gridded runoff field that was derived from the output of a hydrological model. They used a climatologically averaged monthly temperature and precipitation data set as input into the Water Balance Model (WBM) (Vorosmarty *et al.*, 2000) at a global scale.

The WBM is a relatively simple model that assumes runoff when the water surplus (precipitation minus evaporation) exceeds the soil-moisture deficit; calculates type of precipitation, snowmelt, and evaporation based on temperature; and has a single runoff-detention pool in order to delay the runoff reaching the streams to account for water travelling through the ground.

The NSA method was used to connect the grid squares at the resolution of WBN. The drainage network had a resolution of 30 minutes that was approximately 120 km at 60 degrees latitude.

The runoff simulated from WBM was compared to measured annual streamflows at 861 streamflow stations around the world. Unfortunately, the simulated streamflow was found to be much higher than the measured values, which the authours attributed to unrealistic input precipitation. For example, in some instances, the measured runoff was greater than the input precipitation. The precipitation was adjusted so that the simulated streamflow better fit the measured values.

The authors argue the case for using a hydrological model to calculate distributed runoff by showing the result of calculating distributed runoff based on measured streamflow and assuming that the runoff is constant throughout the basin (Figure 2-5). From that figure, it can be seen that the resulting distributed runoff is very “patchy”, since a single value for runoff is used over very large areas. The runoff map created using the output from the WBM (Figure 2-6) is much more realistic showing the differences in runoff no matter where the streamflow gauges were located.

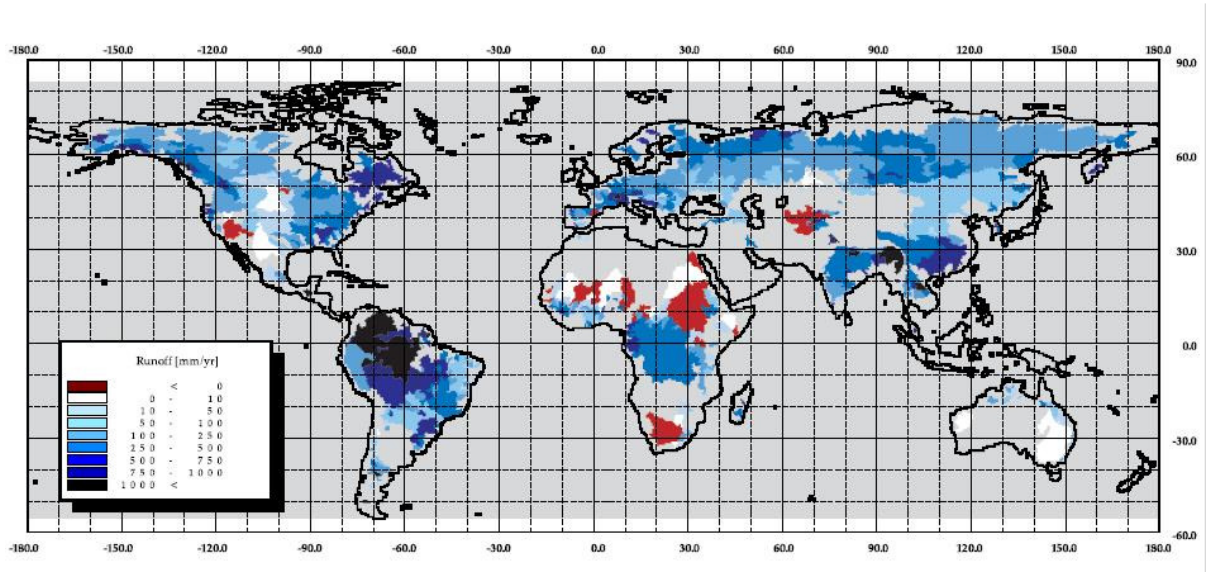

Figure 2-5: Distributed annual runoff based on measured streamflow (from Fekete *et al.*, 2002).

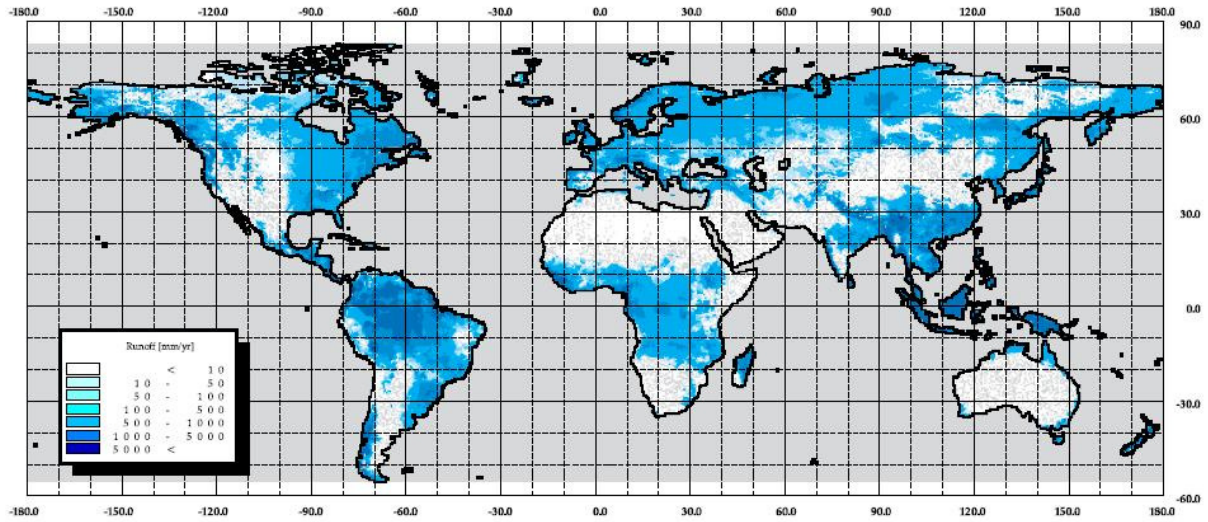

Figure 2-6: Distributed annual runoff based on output from WBM (from Fekete *et al.*, 2002).

One limitation of the Fekete *et al.* (2001) study was that the WBM model used may not adequately simulate some of the hydrological processes that are important in Canada. There were also questions

as to the reliability of the input precipitation as it had to be adjusted in order to correctly simulate the measured streamflow hydrographs. There was also no presentation of any hydrological variable apart from runoff and for this variable there was no attempt to gauge the uncertainty in its prediction.

Maurer *et al.* (2002) present a selection of different hydrological variables such as precipitation, ET, runoff, baseflow, soil moisture, snow water equivalent, and temperature based on either measured data or output from the VIC model. The dataset spanned the time period of 1950 to 2000 at a resolution of an eighth of a degree and the range of the study covers Canada up to a latitude of 53°N. Simulated streamflows were calculated for a selection of rivers around the country and the soil parameters were calibrated to the measured streamflows. As only temperature and precipitation were measured with enough spatial density to be interpolated, other input variables such as dewpoint temperature and incoming solar radiation were calculated from the temperature and precipitation data. Gridded precipitation was scaled to better match the long-term averages from the PRISM precipitation climatology. The authours do a good job of comparing the simulated soil moisture, surface fluxes, and snow extent to measured station data or satellite data.

Using the same approach as Mauer *et al.* (2002), the University of Washington calculates a near real-time gridded product of runoff, soil moisture, and snow water equivalent for the United States, this system is called the Surface Water Monitor (Wood, 2008). These datasets are created using the VIC model implemented at a spatial resolution of an eighth of a degree and using input precipitation and temperature from a real-time meteorological station dataset and long term average wind speed. As well as near real-time presentation of the data, they also provide an archive of the datasets going back to 1915. The current products are used as input into various drought products produced by the American government.

Chapter 3
Creation of the Drainage Database

3.1 Chapter introduction

In this chapter, the development of the WATMAP technique was described and then the technique was used to create the drainage database for all of Canada. The goal of the chapter was to create a drainage database that was, as best as possible, true to the drainage characteristics of the actual landscape.

In the early days of hydrological modelling, the process of creating the drainage database was a manual task using paper maps. However, this manual method became impractical with the desire to model larger basins at finer spatial scales. The introduction of spatial datasets of elevation called Digital Elevation Models (DEMs) since the early 1990s led to the development of automated techniques to create the drainage database, usually for specific hydrologic models (Martz and Garbrecht, 1993; Tarboton, 1997; O'Donnel et al., 1999; Vorosmarty et al., 2000; Fekete et al., 2001).

The Waterloo Mapping technique (WATMAP) was designed to create the drainage database necessary to model a watershed using the WATFLOOD hydrological model. However, it is important to note that the products created by the WATMAP technique can be adapted to be used by other hydrological models that need distributed drainage information.

The WATMAP technique also provided a consistent method for determining the components of the drainage database. Creating the drainage database using the manual method was heavily reliant on the experience of the person performing the derivation and thus the resulting drainage database could have been different if it was created by another operator even using identical input data. Using a technique such as WATMAP allows for the drainage database to be consistent no matter the skill of the operator.

3.1.1 Manual technique for determining the drainage database

When WATFLOOD was first developed in the early 1970s, computing power limited its use to relatively small basins that were usually contained within a small number of 1:50 000 scale topographic maps. To create the drainage database for these relatively small watersheds (less than 200 grid squares), all that needed to be done was to draw grids on a map, determine which grids were within the watershed, and then for each grid determine its flow characteristics to create the drainage database. These characteristics were then manually input into text files that could be used by WATFLOOD.

As part of the Mackenzie GEWEX study (Soulis and Seglenieks, 2007) the entire Mackenzie River watershed needed to be modelled using WATFLOOD. The size of the basin (1.8 million square kilometres) posed problems in using the manual technique to create the drainage database.

The geographical projection needed for the drainage database was the first problem. In smaller basins, the Universal Transverse Mercator (UTM) coordinate system is used as the geographical projection. In this system, the surface of the earth is split into 60 zones that each cover 6 degrees of longitude, and in each of these zones, the spherical surface of the earth is projected onto a flat surface using a unique set of characteristics. Consequently maps from both sides of an intersection between two UTM zones do not line up. The Mackenzie Basin covers seven UTM zones and thus even if all the over 200 maps would have been acquired; the differences between the zones would have caused inconsistencies in the drainage database.

To overcome the problem of using the UTM projection, it was decided to use a polar stereographic projection as it had less distortion in the polar regions. Unfortunately, paper maps are not routinely produced in this projection especially at the scale needed for hydrological modelling.

But even if paper maps had been available, another problem arising from the manual technique would have been the time needed to create the drainage database. With over 4000 grid squares making up the drainage database, it was estimated that it would have taken approximately 6 months to create it manually.

The third problem of using the manual method is the possibility of errors when calculating the drainage database for such a large basin. With the number of grid squares required in the drainage database it is quite likely that some of the characteristics of the basin would be derived incorrectly.

It was this need to create drainage databases for larger basins at finer resolutions with non-standard projections that made it necessary to automate the creation of the drainage database.

3.1.2 DEM scale and model scale

The resolution of global DEMs continues to improve with spatial resolutions of 1 km or less becoming common (USGS, 1997; Rabus *et al.*, 2003). However, most of the standard distributed mesoscale hydrological models are not capable of resolving the earth's surface down to such a resolution, as many of the assumptions made about the hydrological processes are no longer valid when considering grid squares less than 1 km. For instance, in the WATFLOOD model, it is assumed that there is always a stream channel in each grid, something that is not always true when using smaller grid sizes. As well, the computer resources needed to model the earth's surface at a small resolution (1 km) over a large domain (continental scale) are currently prohibitive and will continue to be in the near future, even with the inevitable increase in computer speed and storage.

The WATMAP technique uses characteristics derived at the DEM pixel scale (typically on the order of kilometres) to create the drainage database for the mesoscale hydrological model grid scale (typically on the order of 10s of kilometres) (Figure 3.1).

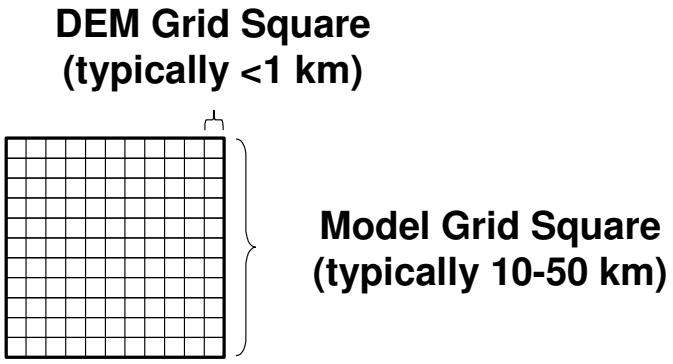

Figure 3.1: The relationship between model grid scale and DEM grid scale.

It would be possible to simply use the average elevations of a model grid square to derive the drainage database assuming that flow always occurs in the direction of the lowest neighbouring grid square. However, in most situations, this resolution would not capture the physiographic features that influence the flow of water. For example, in a mountainous region, this average elevation would reflect the characteristics of the valley slopes and mountain tops rather than the valleys where the rivers actually flow. Shaw *et al.* (2005) noted that, by incorporating sub-grid elevation information and respecting the true hydraulic pathways, drainage directions and other physiographic features can be preserved.

Of course, even at smaller DEM resolutions, the elevation value of a particular grid is an average of the elevation within that grid. It is generally assumed that at these smaller resolutions the drainage network will be adequately represented by the DEM, resulting in the derivation of the proper drainage database. However, there are situations where this is not true and even at these smaller DEM resolutions the derived drainage network has to be corrected.

3.1.3 Components of the drainage database needed for WATFLOOD

The WATMAP technique described in this study was originally designed specifically to create the drainage database needed for the WATFLOOD hydrological model. For this model, there are seven components in the drainage database that need to be calculated for each grid: elevation, drainage direction, drainage area, river type, channel density, land slope, and land class.

The elevation of each model grid is designated as the midpoint of the main channel within that grid. Elevations are used to estimate channel slope between grid elements for hydraulic routing. In the manual method, the elevation is interpolated from elevation contours at the midpoint of the main channel. Typically, the elevation of the grid has the units of metres.

Drainage direction is the direction of flow of the main channel from the grid. The main channel is not necessarily the channel that drains the most amount of area from that particular grid, but rather the channel that carries the greatest amount of cumulative flow out of the grid. The values for each of the eight drainage directions are shown in Figure 3.2.

The drainage area for each grid is the area of that grid that drains in the drainage direction of the main channel. For example, in Figure 3.3, only 60% of the grid drains in the direction of the outflow of the main channel. However, the other 40% of the grid is not lost as the drainage area of the grid to the left would be increased by 25% and the drainage area of the grid below would be increased by 15%. Thus it is possible for a single grid to have a value for drainage area of over 100%. Grids on the outer edge of the basin will have values of less than 100%, while values of 0% indicate the grid is outside of the basin. The only situation where the value would by 100% would be if the entire grid drains in the same direction and there is no contribution to the flow from neighbouring grids. This usually only occurs in flat areas. Keeping track of the flow area is very important to ensure that the calculated drainage areas are correct. Typically, the value ranges between 50% and 150%.

A river type is assigned to each grid in order that river roughness and other river channel specific variables can be assigned for different parts of the basin. It is common that the generally steeper river channels in the headwaters of basin will have different flow characteristics than the flatter river channels near the outlet of a basin. The value can range between 1 and 99, but even large basins rarely have more than five river classifications.

Channel density is needed as part of the river-routing algorithm used in WATFLOOD. This information is used in the model by assuming that in general large channels are more efficient at conveying water than smaller channels for the same runoff production. The value represents the number of approximately equal-sized flows that exit the grid square and has a value between 1 and 5.

The final element of the drainage database is the land slope. This parameter represents the land slope of the grid rather than the channel slope. Although it would be a simple matter to compute the average slope between squares in the grid cell, past experience indicates that using the maximum internal slope rather than the average internal slope is a better indicator of the rate of surface flow (Nick Kouwen, personal communication). In the manual technique, this value was determined by counting the maximum number of elevation contours that crossed a line the length of one side of the grid square. As a result, the value of land slope is expressed as an integer number between 0 and 99, with a higher number representing a greater slope.

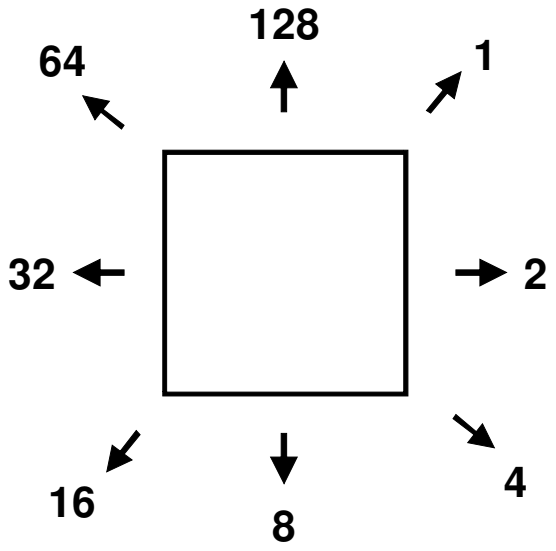

Figure 3.2: Drainage direction values.

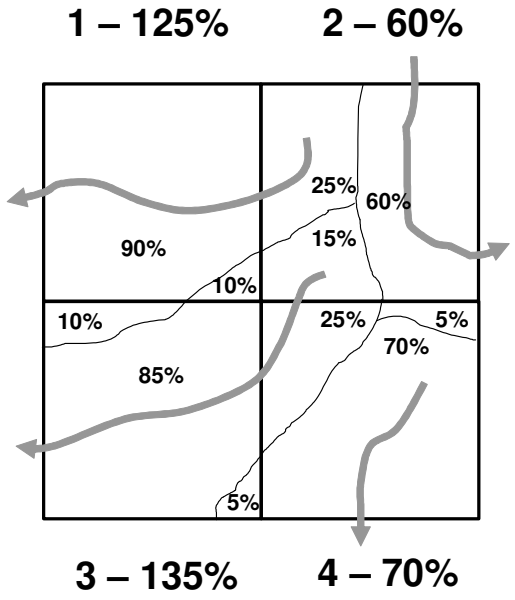

Figure 3.3: Fractional area totals for four model grid squares calculated using flow from neighbouring model grid squares. Thick grey lines represent river channels and the thin black lines show the watershed divides.

The one component of the drainage database that is not dependent on the topography of the basin is the land class. Although it is possible to run most hydrological models with just a single land class, better results are usually obtained in the simulations if the basin is split into different types of land. This allows different parameters to be assigned to each of these different land classes.

Typically, the division of these land classes is based on the land cover types derived from the classification of some type of remotely sensed imagery. This is common as it is a relatively simple procedure to classify a satellite image into different land cover types. However, it is also possible to define these land classes based on slope, soil type, distance to the outlet, or a combination of these factors. As this may require information collected on the ground, it may not be feasible to classify the land surface in this way over a large domain.

3.2 The WATMAP technique

The WATMAP technique created the components of the drainage database based on information from a DEM and a land-cover map. To do this, it upscaled the information from the finer-resolution DEM grid to the coarser-resolution model grid. Depending on its size, there were generally many river channels within a single model grid square. Most of the components of the drainage database depended on the characteristics of the main river channel that flowed through each model grid square. The main channel within a model grid square was defined as the channel that would have carried the most amount of flow.

The land slope was the only component of the drainage database that could be derived directly from information at the DEM grid scale. To calculate the others, the value of the DEM grid surrounding each model grid was examined to determine the locations of the inflows and outflows from the model grid. But in order to calculate these inflows and outflows, characteristics of each DEM grid had to be determined. Using these DEM grid characteristics, the rest of the components of the drainage database were calculated.

3.2.1 Calculation of land slope

The first component of the drainage database that was calculated was the land slope, as it was based solely on the individual DEM pixels. However, as previously discussed, the land slope calculated by the original manual technique for deriving the drainage database was not simply the average slope between pixels but rather a measure of the maximum land slope within the grid square.

Hence, the land slope was determined using a technique which mimicked the contour counting of the manual method for determining internal slope. WATMAP calculated the cumulative absolute difference in elevation between cells for each row and column of the grid square individually and

identified the highest cumulative difference. This value represented the maximum land slope; however, the protocol for this variable in the manual technique was an integer number ranging between 0 and 99. Thus as part of the WATMAP technique, this value was multiplied by a contour factor, which was determined by comparing land slopes using the manual method and WATMAP on various sample watersheds, to give a final value between 0 and 99.

3.2.2 DEM grid characteristics

To determine the rest of the drainage database components, the WATMAP technique analyzed the basin at the DEM grid resolution. For each DEM grid, a set of characteristics were calculated, these were: flow direction, flow accumulation, incremental watersheds, and pour points. All of these characteristics can be calculated using standard routines available in most GIS processing software.

The following is a description of these DEM grid characteristics:

- The most basic information about each DEM grid was the flow direction of that grid. This was usually determined using the D8 technique which assigned the direction of flow towards the lowest neighbouring grid.
- The flow accumulation was the number of DEM grids that were upstream from the pixel of interest. Thus grids at the divide between two basins had flow accumulations of 0, while the value of flow accumulation at the outlet of the basin was total number of grids in that basin.
- It was necessary to divide the basin into smaller incremental watersheds in order to use the WATMAP technique. The locations of these incremental watersheds were based on the flow accumulation values.
- Pour points were defined as the DEM grids where flow was connected between different incremental watersheds. They were used by WATMAP to determine which incremental watersheds were connected to each other.

3.2.3 Obtaining the grid scale inflows and outflows

Using the DEM grid characteristics, the WATMAP technique examined the outer layer of DEM grids that surrounded each model grid square. For each of the DEM grids, the DEM grid flow direction was used to determine if the flow at each of the DEM grids was into or out of the model grid square. This information was combined with the flow accumulation for each of the DEM grids to rank the magnitude of the inflows into the model grid square and the outflows out of the model grid square.

It was generally assumed that the greatest inflow and outflow represented the entry and exit points of the main channel of the model grid square. However, because of the erratic nature of river channels, there were situations that made the determination of flow direction difficult, such as when a river channel left and re-entered the same grid. This resulted in the greatest inflow not necessarily representing the entry point of the main channel of the grid square.

As an illustration, consider a model grid square where the main channel came into the top of the model grid and exited to the right with a smaller tributary joining the main channel from the bottom (Figure 3.4a). In this situation, Outflow 2 had the highest outflow and would have represented the outflow of the main channel, while the inflow with the greatest flow accumulation value was Inflow 2. However, as the same channel left and re-entered the same model grid square, the true inflow of the main channel into the model grid square was actually Inflow 1.

Another situation that caused confusion and could lead to the incorrect choice of the main channel inflow and outflow was illustrated in Figure 3.4b. Here two tributaries joined inside of the model grid square and, since Outflow 1 was greater than Outflow 2, Outflow 1 represented the outflow of the main channel from the model grid square. In the simple case, Inflow 2 would have been the largest inflow and thus would have been matched up with Outflow 1 to represent the main channel of the model grid square.

However, there could have also been the situation where the other channel that flowed through the model grid had a higher inflow (that is, Inflow 3 was the highest inflow) even though Outflow 2 was less than Outflow 1. This could have happened if the combined flow of Inflows 1 and 2 was greater than the flow of Inflow 3. Here, simply taking the highest inflow (Inflow 3) and the highest outflow (Outflow 1) would have resulted in an incorrect pairing of the flows, and calculations made using this as the main channel would have been incorrect.

Consequently, a method was needed to determine the connection of the flow accumulation channels. This was done by using the incremental watershed information contained in the DEM grid characteristics. Thus, if multiple inflows were determined to be part of the same incremental watershed, then the intermediate inflows (for example, Inflow 2 in Figure 3.4a) were ignored. Similarly, flows from different incremental watersheds (for example, Inflow 3 in Figure 3.4b) would not have been paired with their incorrect partners.

After this process, the result was that the number and magnitude of the unique inflows and outflows of each model grid square was known.

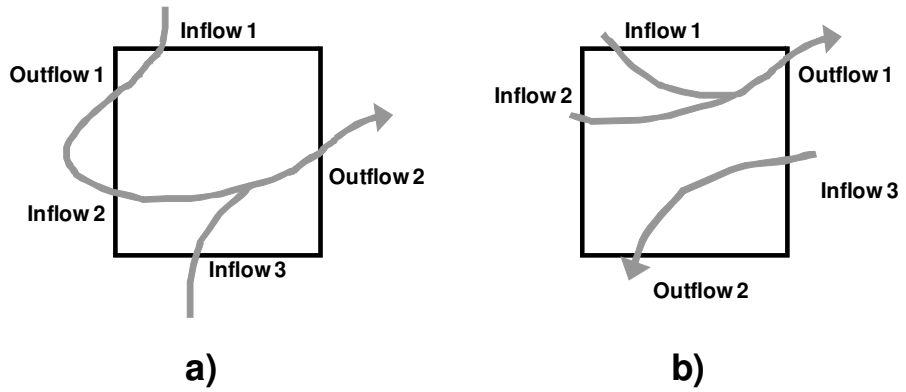

Figure 3.4: Model grid squares showing multiple inflows and outflows.

3.2.4 Calculation of river type, elevation, drainage area, and channel density

Once the unique inflows and outflows were known, most of the remaining components of the drainage database could be calculated. To calculate river classification, the watershed would be split into different river types based on the amount of flow accumulation of the main channel. To do this, only a threshold value was needed to distinguish headwater basins from downstream basins. This threshold value would be determined by examining the nature of each specific basin. As well, the drainage database could be manually modified if a specific type of river channel was needed.

The channel elevation was calculated by taking the average of the elevations of the DEM grids at the locations of the inflow and outflows of the main channel.

The drainage area of the model grid square represented the amount of that model grid square that was drained out of the main channel. To calculate the drainage area of each of the model grid squares, the inflow and outflow information was combined with the incremental watershed information, allowing for the determination of the amount of the model grid square that was drained through each of the outflows. The flow area was the amount of area that was drained by the outflow corresponding to the main channel, along with the extra flow area coming from the surrounding grid squares. The extra flow area was the percentage of each of the surrounding squares that did not flow out of the main channel.

The WATFLOOD-specific parameter known as channel density was the number of similar-sized rivers within a grid square. As the flow accumulation was known for all river channels exiting the grid square, a simple determination was made to determine how many of the outflows had a flow accumulation within 20% of that of the main channel.

3.2.5 Calculation of drainage direction

The final component of the drainage database that needed to be calculated was the drainage direction. The drainage direction from a grid square could have simply been assumed to be the same as the direction of the outflow of the main channel at the DEM scale. However, using this method would have only allowed for diagonal flow in the very rare situation where the main channel exited the square at a corner directly into the corner of its neighbouring square. Thus a majority of the grid squares would only have had drainage directions in the four major directions. The consequence of this would have been that the river channels would have had lengths that are longer than actual and may have led to situations where the incorrect drainage area was calculated. Thus it was necessary in WATMAP to allow for the possibility of diagonal flow.

To illustrate the proper calculation of diagonal flow, consider a situation where flow left a grid square and then entered the corner of another grid before moving on to the next grid, as shown in Figure 3.5a. Using the assumption that the flow direction of the model grid square was the same as the maximum DEM grid outflow, the flow of cell 1 would have been down and the flow from cell 3 would have been to the right (Figure 3.5b). This would that have been the incorrect flow direction for both cell 1 and cell 3. However, if performing this manually, an operator would have classified the flow as going diagonally from square 1 to 4 and the flow of cell 3 to be towards the bottom, as shown in Figure 3.5c.

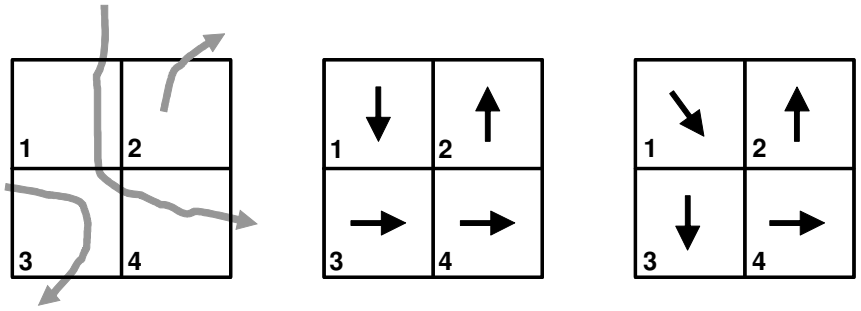

Figure 3.5: Flow network showing diagonal flow from cell 1 to cell 4, with model grid square drainage directions determined using b) a simple technique and c) WATMAP.

Thus WATMAP had to be able to recognize that in this situation, the small amount of cell 3 that was drained by the main channel was not significant. WATMAP did this by examining the amount of

area of the grid square that was drained by the main channel. In this example, the main channel only drained about 5% of cell 3 with 95% of the cell drained by another channel that left the cell towards the bottom. The technique would determine that the main channel did not drain a significant amount of cell 3 and it then would examine the path of the main channel after it left cell 3. Seeing that the main channel then went to cell 4, it would adjust the drainage direction of cell 1 to be diagonally connected to cell 4 and allow the flow of cell 3 to be towards the bottom.

A threshold called the diagonal factor was created that represented the maximum percentage of a model grid square that would have to be drained by the main channel that would lead to the triggering of diagonal flow calculations. Thus if the diagonal factor was set at 10% and the main channel drained 15% of a model grid square then diagonal flow would not be assumed, however if the main channel only drained 5% then diagonal flow would be assumed. The optimal value of the diagonal factor has been found to be between 5% and 20%.

Other methods to determine flow directions when scaling up from the DEM scale to the grid scale consider diagonal flow to occur if the flow out of the grid square occurs near the corner of the grid square (O'Donnell *et al.*, 1999). However, this does not allow for the possibility of the river channel changing direction once it leaves the grid square and could have led to the incorrect determination of flow direction.

Another situation that commonly occurred and affected the calculation of drainage direction was the situation where the main channel entered a neighbouring channel along one of the sides of the model grid (Figure 3.6a) and then returned to the same grid (referred to here as "side-swiping"). In this case, using simple assumptions in the calculation of flow direction would have resulted in the flow direction of cell 2 going toward cell 1, resulting in the actual flow from cell 2 channel not being seen (Figure 3.6b). However, a manual operator would have determined that the flow did not significantly enter cell 2 and thus the flow direction of cell 2 would not have been adjusted.

Although this situation does not directly involve diagonal flow, the diagonal factor was again used to determine if the amount of the neighbouring cell drained by the main channel was significant. Assuming that the amount of area drained by the main channel from cell 2 was less than the diagonal factor, WATMAP would have triggered the diagonal flow calculations. WATMAP would have then recognized that when the main channel briefly went into cell 2, it didn't drain enough of the area of cell 2 to adjust the drainage direction of cell 2. Rather, the flow direction of cell 2 would have been determined from the second-highest outflow from the grid square. This would have resulted in a more realistic overall flow pattern (Figure 3.6c).

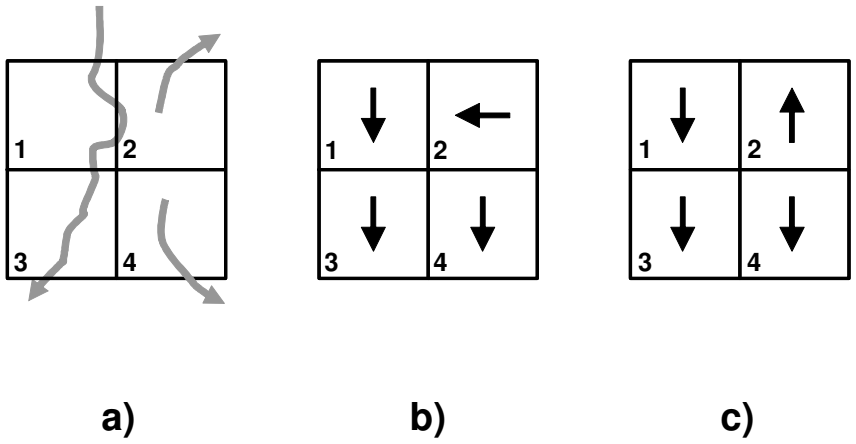

Figure 3.6: Flow situation demonstrating side-swiping a), with drainage directions determined using a simple technique b) and WATMAP c).

3.2.6 Calculation of land class

The calculation of land class at the model grid scale was simply the percentage of each type of land class within the model grid square. As the WATFLOOD model was based on the GRU concept, the location of the land classes within the grid did not need to be considered. This made the calculation of this component of the drainage database a simple matter of examining the land-class map, summing the area of each land class, and dividing by the total amount of area of the model grid square.

3.2.7 Creation of the final drainage database

With all the components of the drainage database calculated, files could now be created with information for each model grid square. These files could then be used by hydrological models to simulate the flow of water in the river basins.

3.3 Use of WATMAP to create drainage database for Canada

The WATMAP technique was then used to create the drainage database for all of Canada. As the technique depended on characteristics derived from a DEM, it was imperative to ensure that the DEM properly represented the actual flow network. Unfortunately, most DEMs contain defects that make it necessary to perform pre-processing before they can be used to create the drainage database. After this pre-processing was done on the DEM for Canada, a projection and resolution were selected for the model grid and WATMAP could then be used to create the drainage database.

3.3.1 Source of the elevation data

The elevation data used to create the drainage database was a combination of the GTOPO30 database produced by the United Stated Geological Survey (USGS, 1997) and the Shuttle Radar Topography Mission 30 second product (SRTM30) created jointly by the National Geospatial-Intelligence Agency (NGA) and the National Aeronautics and Space Administration (NASA) (Rabus *et al.*, 2003).

The SRTM30 dataset was considered to be more accurate than GTOPO30 as it was created using a single data source over a short time period as opposed to GTOPO30 which combined different data sources collected over many years. However, the orbits of the shuttle missions resulted in the SRTM30 dataset only covering up to 60 degrees North latitude, making it necessary to include the GTOPO30 information for that part of Canada (Figure 3.7).

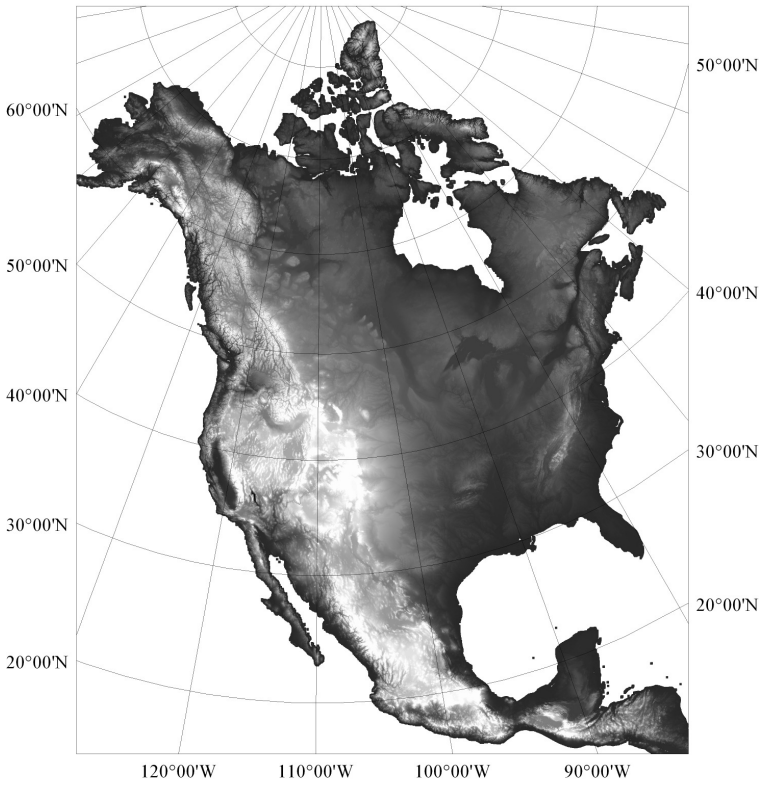

Figure 3.7: Elevation data from SRTM30 and GTOTO30 for North America, lighter colours represent higher elevations and darker colours represent lower elevations.

Unfortunately the use of two different datasets resulted in a discontinuity at 60 degrees latitude at the border between the two datasets (Figure 3.8). In general, the SRTM30 data had more topographic detail while the GTOPO30 was smoother, although the absolute elevation values were similar.

It was found that the calculated flow network at the discontinuity only presented a problem over a very small area and the overall drainage patterns were not affected. Thus it was decided to use the combined dataset to calculate the drainage database even with the discontinuity.

Both of these DEMs had a resolution of 30 arc seconds, which translated to a resolution that ranged from about 0.9 km over the southern United States to about 0.5 km in northern Canada.

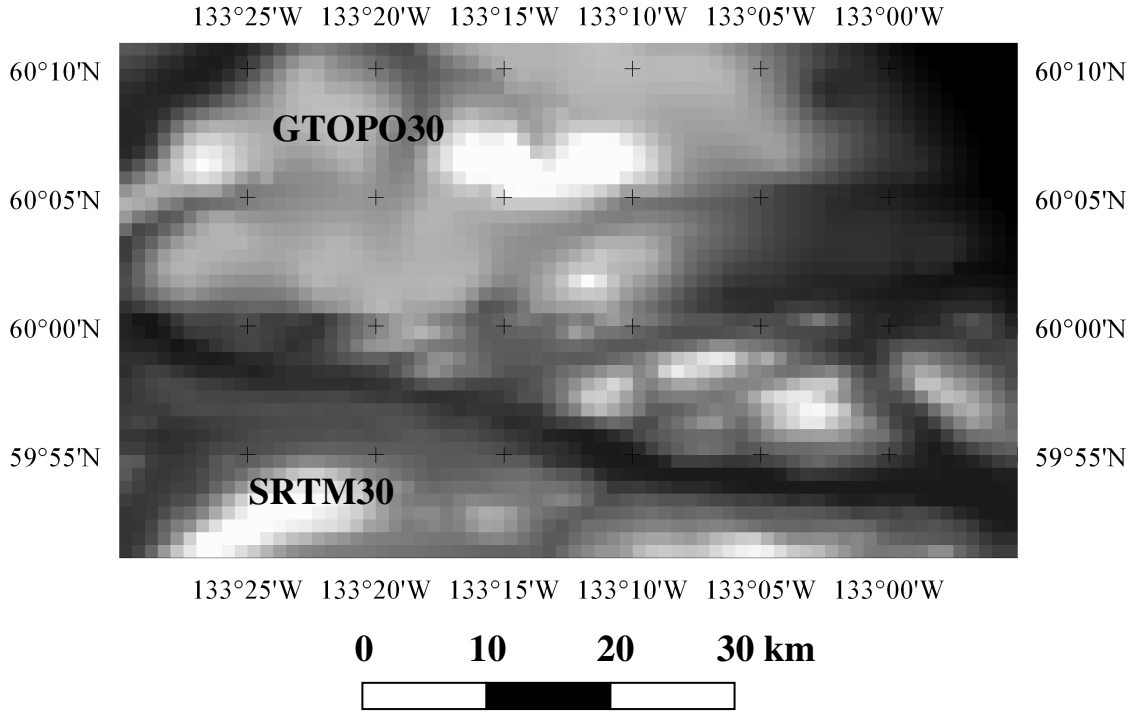

Figure 3.8: Close up of the discontinuity between the SRTM30 DEM and the GTOPO30 DEM. The SRTM30 DEM occupies the bottom of the figure and the GTOPO30 DEM occupies the top.

3.3.2 Creation of the depression-less DEM

The first step in ensuring that the DEM resulted in the proper flow network was to ensure that the DEM was depression-less, that is, that it did not contain sinks. These sinks were areas of lower

elevation that did not allow flow to the outside of the DEM. Both GTOPO30 and to a lesser extent SRTM30 contained sinks that had to be removed in order to create the depression-less DEM.

A basic sink-filling routine was used that simply raised the elevation of DEM pixels sufficiently to allow for flow out of the pit. The flow network was then derived using this modified DEM performing a simple D8 technique. The resulting flow network generally did a poor job a when compared to a flow network derived from topographic maps (Figure 3.9). In particular, some major Canadian river basins such as the Mackenzie, Saskatchewan, and the St. Lawrence were not even connected to the oceans. Thus although the DEM was now depression-less, further modification was needed in order for it to properly represent the correct drainage network.

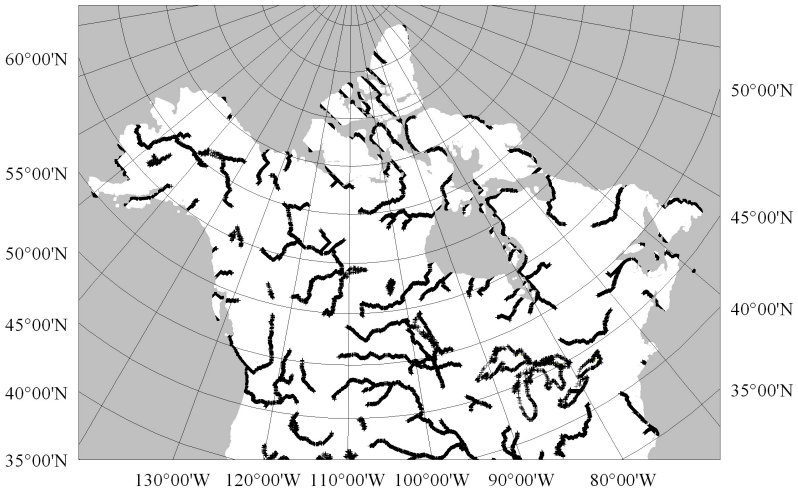

Figure 3.9: Flow network derived using the uncorrected depression-less DEM.

3.3.3 Creation of the modified DEM

As a result of the poor representation of the actual drainage network using the depression-less DEM, it was necessary to manually update the DEM. Generally, the problems in the derived drainage network were a result of flat areas or valleys where the incorrect path was chosen by the D8 method. This demonstrated that although the scale of the DEM was small, it was still not detailed enough to properly capture every part of the flow network.

In order to quantitatively compare the derived flow network to the actual drainage network, points were chosen where the drainage areas were known. This made it possible to compare the drainage area from the derived drainage network to the known drainage areas at these points. The measured

drainage area at each of these points was obtained from the HYDAT CD-ROM produced by Water Survey of Canada (Environment Canada, 2002).

Through an interactive process, the DEM was modified, the flow network was derived, and the drainage areas of the simulated and measured flow network were compared. This process was repeated until the error between the simulated and measured drainage areas was less than 5% at the comparison points (Table 3-1).

Table 3-1: Comparison of measured and simulated drainage areas from the flow network derived at the DEM grid scale after modification of the DEM.

Station Name	Measured Drainage Area (km^2)	Simulated Drainage Area (km^2)	Difference
Nipigon River at Pine Portage	24,600	24,010	-2.4%
Saugeen River near Port Elgin	3,960	3,707	-6.4%
Grand River at Brantford	5,210	5,043	-3.2%
Thames River at Thamesville	4,300	4,251	-1.1%
Ottawa River at Britannia	90,900	93,595	3.0%
Saint-Laurent (Fleuve) a Lasalle	1,200,000	1,162,430	-3.1%
Moose River at Moose River	60,100	60,439	0.6%
Red River near Lockport	287,000	278,452	-3.0%
Churchill River at Sandy Bay	212,000	203,345	-4.1%
Churchill River above Red Head Rapids	289,000	277,088	-4.1%
Thelon River above Baker Lake	154,000	159,130	3.3%
Thelon River below outlet of Schultz Lake	152,000	154,156	1.4%
Athabasca River below Mcmurray	133,000	129,943	-2.3%
Peace River at Peace River	186,000	190,147	2.2%
Fraser River at Mission	228,000	228,115	0.1%
Yukon River at Dawson	264,000	264,849	0.3%
Yukon River at Eagle	294,000	288,342	-1.9%
Liard River at Fort Liard	222,000	224,262	1.0%
Mackenzie River at Arctic Red River	1,700,000	1,690,283	-0.6%
Peel River above Canyon Creek	25,700	24,825	-3.4%
Anderson River below Carnwath River	57,800	59,577	3.1%
Burnside River near the mouth	16,800	16,814	0.1%
Allice River near the mouth	16,900	17,180	1.7%
Baillie River near the mouth	14,500	13,910	-4.1%
Back River above Hermann River	93,900	96,065	2.3%
Hayes River above Chantrey inlet	18,100	18,322	1.2%
Big River above Egg River	3,640	3,617	-0.6%
Sylvia Grinnell River near Iqaluit	2,980	2,822	-5.3%
Spanish River at Espanola	11,400	11,249	-1.3%
Saguenay at Caron	73,800	75,780	2.7%
Average of absolute differences			2.3%

After this process, the result was a corrected, depression-less DEM where the resulting flow network properly represented the flow network (Figure 3.10). Comparing this to the flow network

using the raw DEM (Figure 3.9), the improvement was obvious with all of the major Canadian rivers in their correct geographic positions and all of them flowing to the ocean.

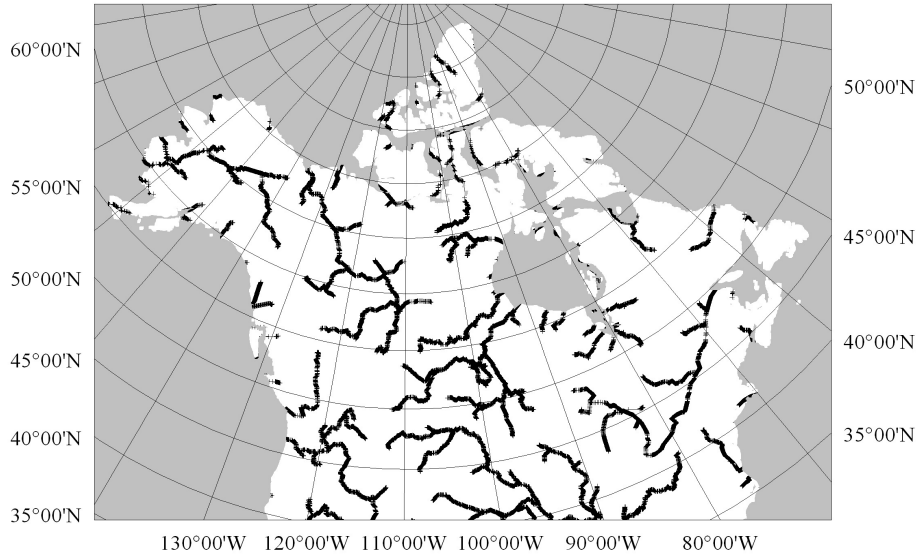

Figure 3.10: Flow network derived using the corrected depression-less DEM.

3.3.4 Derivation of the DEM grid characteristics

From the corrected depression-less DEM, the DEM grid characteristics discussed in Section 3.2.2 were calculated using the Geomatica software product from PCI industries (PCI, 2004). Figure 3.11 displays a close up of these characteristics (elevation, drainage direction, flow accumulation, pour points, and incremental watersheds) for an area over western Canada. This information at the DEM grid scale could then be upscaled by WATMAP to create the drainage database at the model grid scale.

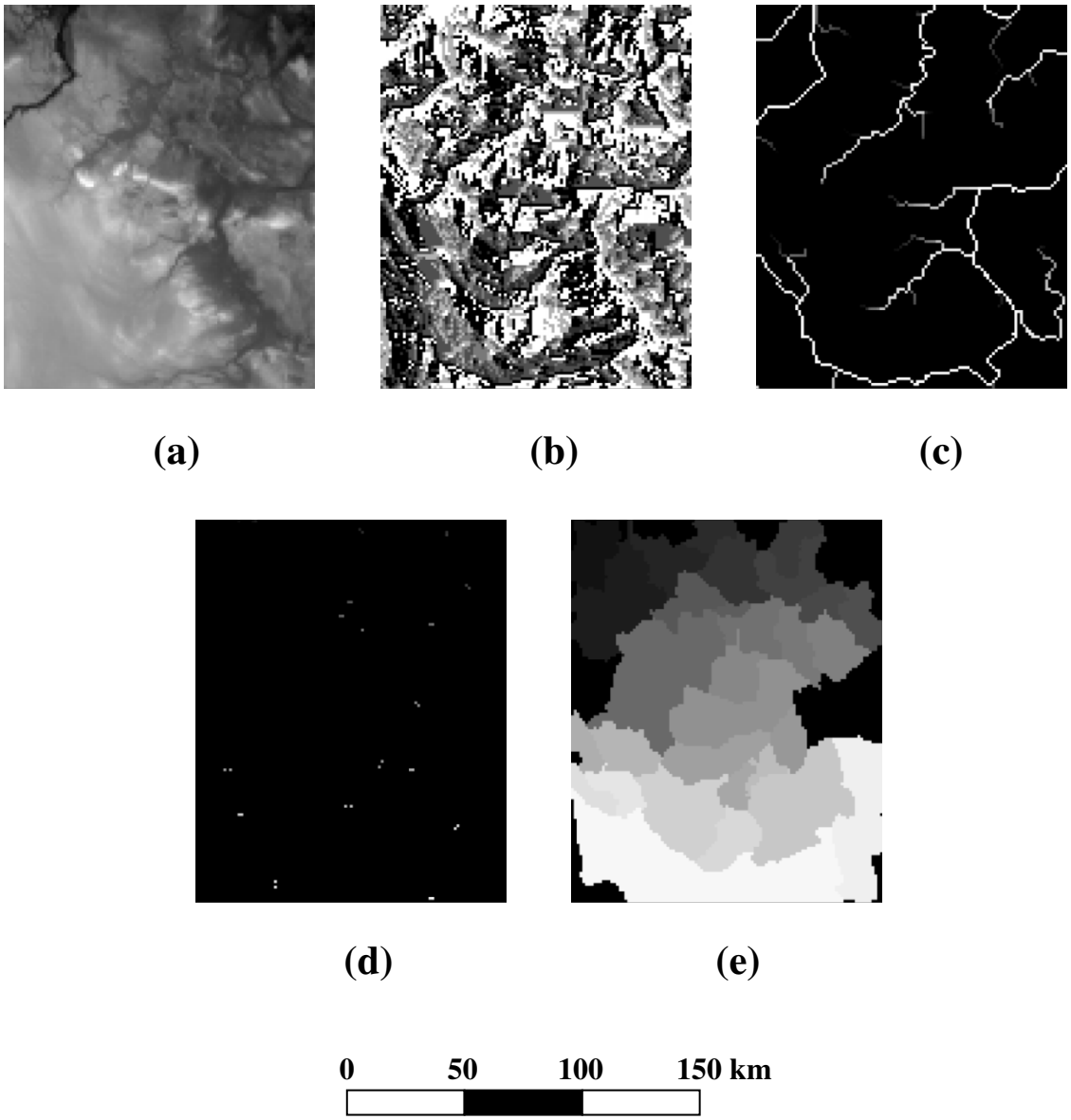

Figure 3.11: DEM grid characteristics for an area over western Canada (a) elevation, (b) drainage direction, (c) flow accumulation, (d) pour points, and (e) incremental watersheds

3.3.5 Projection and model grid size of the drainage database

There were many criteria that had to be considered when deciding on the projection and model grid size of the drainage database. If the study area was contained within a single UTM zone, it would have been preferable to use the UTM coordinate system. However, as Canada stretches over 15 UTM zones it would be impossible to use this projection.

There were various projections that were available for areas this large, each with its own advantages and disadvantages. In collaboration with Environment Canada, a projection was chosen for this study that coincided with one used by the Canadian Regional Climate Model (CRCM) (Caya and Laprise, 1999). This projection was polar stereographic with a true origin of 109° 36" W and 60° N using a normal sphere ellipsoid with a radius of 6 370 997 m. A grid size was chosen that coincided with the CRCM grid, this resulted in grids that were 51 km on each side.

Although this grid size was chosen based on the requirements of the CRCM, the typical range of grid sizes that is thought to be reasonable for the application of the WATFLOOD model is between 1 km and 50 km. When considering the upper limit to the range, one assumption is that all the areas within the grid are subjected to the same meteorological forcings. This assumption may not have been correct in the mountainous areas of Canada where large differences in meteorological readings can be seen over 50 km. However, as the forcings were calculated on a 1 km grid and then averaged to the 51 km model grid, the values used at the model grid scale should have been adequate to be used in the hydrological model.

Hydraulic routing considerations must also be taken into account when using large grid sizes. As only one routing element per grid square is used to represent streamflow in WATLOOD, the sub-grid element travel times are assumed to be small in comparison to the main channel of the grid square. With larger grid squares these sub-grid travel times may start to impact on this assumption.

As there are watersheds that cross the border between Canada and United States, the drainage database was also created for part of the United States. The extents of the modelled area had an upper left corner of approximately 150° E and 60° N and lower right corner of approximately 80° E and 35° N (Figure 3.12).

Using this projection and grid size, the WATMAP technique was performed on the corrected depression-less DEM to create the drainage database.

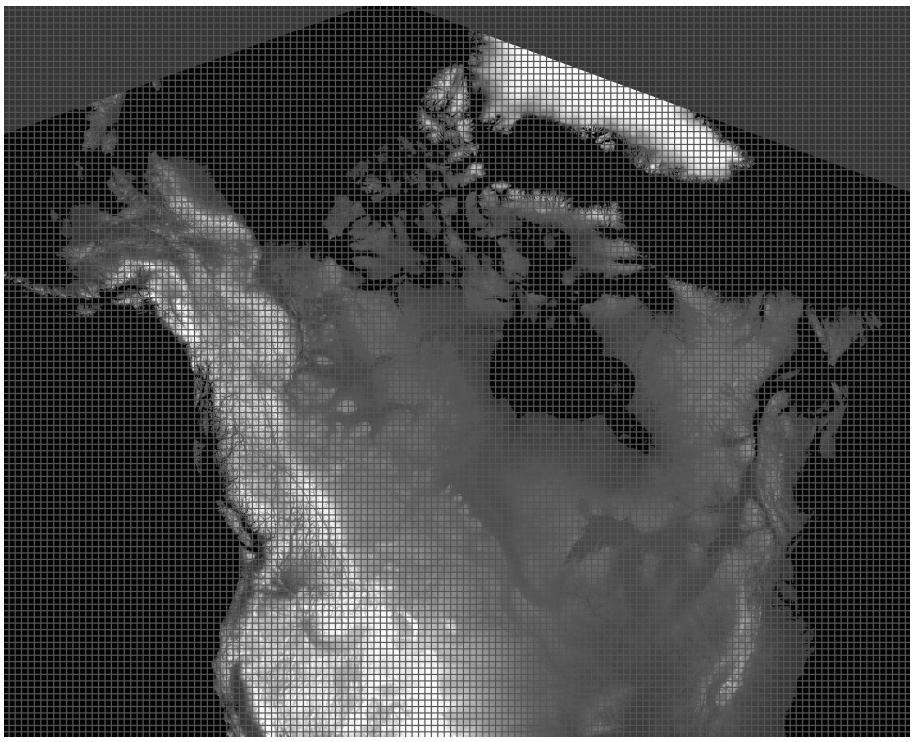

Figure 3.12: Projection of the model grid square domain used for the drainage database.

3.3.6 Land cover information

The land-cover information (the component of the drainage database that was not derived from the DEM) used was the global land-cover characteristics database created by the USGS (Loveland *et al.*, 2000). This data set had 24 land classes for North America and a resolution of 1 km. This number of land classes was too computationally expensive to be practical for running the WATFLOOD hydrological model. Thus the 24 original land classes were aggregated into 9 principal land classes (Table 3-2). This was done by examining the distribution of the original land classes and looking for natural groupings. For example, the four different types of tundra in the original classification (herbaceous, wooded, mixed, and bare ground) were consolidated into a single tundra land class. The distribution of the aggregated land classes can be seen in Figure 3.13.

For each of the model grid squares, the landcover information was analyzed and the percentage of each land class within each model grid square was calculated. This information was then added to the drainage database.

Table 3-2: Original and aggregated land classes from the USGS land cover data set

Original land Class	Aggregated land class
Urban and Built-Up Land	Urban
Dryland Cropland and Pasture	Agricultural
Irrigated Cropland and Pasture	Agricultural
Mixed Dryland/Irrigated Cropland and Pasture	Agricultural
Cropland/Grassland Mosaic	Agricultural
Cropland/Woodland Mosaic	Agricultural
Grassland	Low Vegetation
Shrubland	Low Vegetation
Mixed Shrubland/Grassland	Low Vegetation
Savanna	Low Vegetation
Deciduous Broadleaf Forest	Deciduous Forest
Deciduous Needleleaf Forest	Deciduous Forest
Evergreen Broadleaf Forest	Coniferous Forest
Evergreen Needleleaf Forest	Coniferous Forest
Mixed Forest	Coniferous Forest
Water Bodies	Water
Herbaceous Wetland	Wetland
Wooded Wetland	Wetland
Barren or Sparsely Vegetated	Low Vegetation
Herbaceous Tundra	Tundra
Wooded Tundra	Tundra
Mixed Tundra	Tundra
Bare Ground Tundra	Tundra
Snow or Ice	Glacier

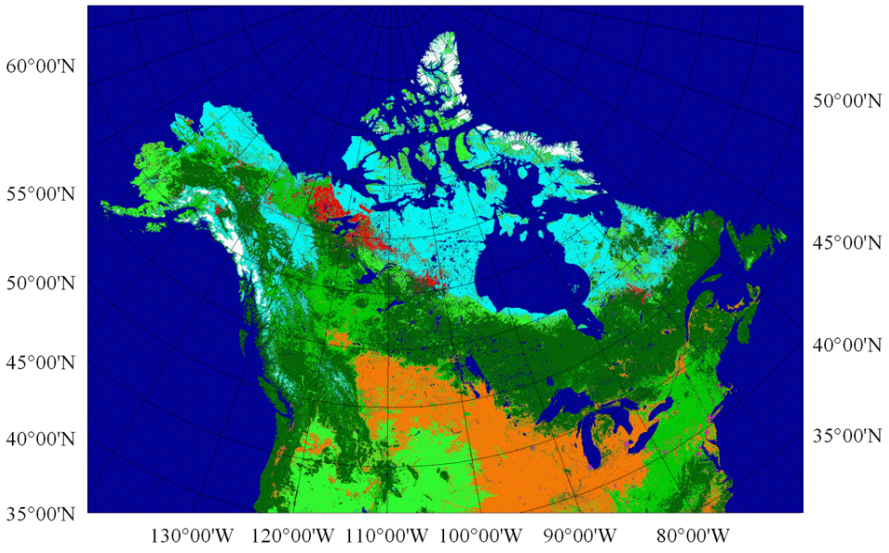

Figure 3.13: Distribution of the aggregated land classes derived from the USGS Global Land Cover Characteristics database (dark blue – water, dark green – coniferous forest, medium green – deciduous forest, light green – low vegetation, orange – agricultural, light blue – tundra, red – wetland, white - glacier)

3.3.7 Determination of the diagonal factor

Different values of the diagonal factor were examined to determine the most appropriate value to be used to calculate the drainage database. To quantify the differences between the simulated and measured flow networks for the different values of diagonal factor, the measured and simulated drainage areas were compared at the same set of points as used in Section 3.3.3 (Table 3-3 and Table 3-4). In general the larger basins had less percentage error than the smaller basins.

Note that it was not possible to match the measured versus simulated drainage areas to within 5% for all basins as was the case the simulated flow network at the DEM grid scale. As the area of each model grid in the simulation was 2600 km^2, it was difficult to match up the drainage areas in some of the smaller basins.

Looking at the average of the absolute differences for all of the basins, the drainage factor of 0.15 gave the lowest value at 5.0%. Thus this value was used by the WATMAP technique to create the drainage database.

Table 3-3: Comparison of measured and simulated drainage areas using diagonal factors of 0.00, 0.05, and 0.10.

Station Name	Measured	Diagonal factor 0.00		Diagonal factor 0.05		Diagonal factor 0.10	
	Drainage Area (km^2)	Simulated Drainage Area (km^2)	Difference	Simulated Drainage Area (km^2)	Difference	Simulated Drainage Area (km^2)	Difference
Nipigon River at Pine Portage	24,600	24,111	2.0%	23,487	4.5%	23,487	4.5%
Saugeen River near Port Elgin	3,960	3,329	15.9%	3,329	15.9%	3,329	15.9%
Grand River at Brantford	5,210	4,604	11.6%	4,604	11.6%	4,604	11.6%
Thames River at Thamesville	4,300	3,355	22.0%	3,355	22.0%	3,355	22.0%
Ottawa River at Britannia	90,900	94,104	-3.5%	94,859	-4.4%	94,859	-4.4%
Saint-Laurent (Fleuve) a Lasalle	1,200,000	1,215,343	-1.3%	1,213,263	-1.1%	1,213,263	-1.1%
Moose River at Moose River	60,100	59,771	0.5%	59,771	0.5%	59,771	0.5%
Moose River above Moose River	60,100	59,771	0.5%	59,771	0.5%	59,771	0.5%
Red River near Lockport	287,000	326,842	-13.9%	319,091	-11.2%	319,091	-11.2%
Churchill River at Sandy Bay	212,000	215,727	-1.8%	215,311	-1.6%	215,311	-1.6%
Churchill River above Red Head Rapids	289,000	294,303	-1.8%	293,887	-1.7%	293,887	-1.7%
Thelon River above Baker Lake	154,000	152,835	0.8%	152,835	0.8%	152,835	0.8%
Thelon River below outlet of Schultz Lake	152,000	152,835	-0.5%	152,835	-0.5%	152,835	-0.5%
Athabasca River below Mcmurray	133,000	138,737	-4.3%	138,737	-4.3%	138,737	-4.3%
Peace River at Peace River	186,000	191,382	-2.9%	191,382	-2.9%	191,382	-2.9%
Fraser River at Mission	228,000	233,414	-2.4%	230,969	-1.3%	230,969	-1.3%
Yukon River at Dawson	264,000	257,655	2.4%	257,655	2.4%	257,655	2.4%
Yukon River at Eagle	294,000	292,196	0.6%	292,196	0.6%	292,196	0.6%
Liard River at Fort Liard	222,000	225,221	-1.5%	225,221	-1.5%	225,221	-1.5%
Mackenzie River at Arctic Red River	1,700,000	1,664,926	2.1%	1,664,926	2.1%	1,664,926	2.1%
Peel River above Canyon Creek	25,700	24,475	4.8%	24,475	4.8%	24,475	4.8%
Anderson River below Carnwath River	57,800	57,586	0.4%	57,586	0.4%	57,586	0.4%
Burnside River near the mouth	16,800	21,042	-25.3%	21,042	-25.3%	21,042	-25.3%
Allice River near the mouth	16,900	16,464	2.6%	16,464	2.6%	16,464	2.6%
Baillie River near the mouth	14,500	13,759	5.1%	13,759	5.1%	13,759	5.1%
Back River above Hermann River	93,900	93,948	-0.1%	93,948	-0.1%	93,948	-0.1%
Hayes River above Chantrey inlet	18,100	17,115	5.4%	17,115	5.4%	17,115	5.4%
Big River above Egg River	3,640	3,199	12.1%	3,199	12.1%	3,199	12.1%
Sylvia Grinnell River near Iqaluit	2,980	2,705	9.2%	2,705	9.2%	2,705	9.2%
Spanish River at Espanola	11,400	12,901	-13.2%	12,901	-13.2%	12,901	-13.2%
Saguenay at Caron	73,800	73,244	0.8%	68,614	7.0%	68,614	7.0%
Average of absolute differences			5.5%		5.7%		5.7%

Table 3-4: Comparison of measured and simulated drainage areas using diagonal factors of 0.15, 0.20, and 0.25.

Station Name	Measured	Diagonal factor 0.15		Diagonal factor 0.20		Diagonal factor 0.25	
	Drainage Area (km^2)	Simulated Drainage Area (km^2)	Difference	Simulated Drainage Area (km^2)	Difference	Simulated Drainage Area (km^2)	Difference
Nipigon River at Pine Portage	24,600	23,487	4.5%	23,487	4.5%	14,019	43.0%
Saugeen River near Port Elgin	3,960	3,329	15.9%	3,329	15.9%	3,329	15.9%
Grand River at Brantford	5,210	4,604	11.6%	4,604	11.6%	4,604	11.6%
Thames River at Thamesville	4,300	3,381	21.4%	3,225	25.0%	3,355	22.0%
Ottawa River at Britannia	90,900	94,859	-4.4%	94,859	-4.4%	95,093	-4.6%
Saint-Laurent (Fleuve) a Lasalle	1,200,000	1,203,821	-0.3%	1,203,821	-0.3%	1,204,809	-0.4%
Moose River at Moose River	60,100	59,849	0.4%	59,849	0.4%	59,849	0.4%
Moose River above Moose River	60,100	59,849	0.4%	59,849	0.4%	59,849	0.4%
Red River near Lockport	287,000	320,313	-11.6%	320,313	-11.6%	315,033	-9.8%
Churchill River at Sandy Bay	212,000	213,906	-0.9%	213,906	-0.9%	213,906	-0.9%
Churchill River above Red Head Rapids	289,000	290,766	-0.6%	290,766	-0.6%	289,075	0.0%
Thelon River above Baker Lake	154,000	152,861	0.7%	152,861	0.7%	153,147	0.6%
Thelon River below outlet of Schultz Lake	152,000	152,861	-0.6%	152,861	-0.6%	153,147	-0.8%
Athabasca River below Mcmurray	133,000	136,995	-3.0%	136,995	-3.0%	133,900	-0.7%
Peace River at Peace River	186,000	191,382	-2.9%	191,382	-2.9%	196,324	-5.6%
Fraser River at Mission	228,000	230,995	-1.3%	230,995	-1.3%	230,111	-0.9%
Yukon River at Dawson	264,000	257,733	2.4%	257,733	2.4%	259,112	1.9%
Yukon River at Eagle	294,000	292,196	0.6%	292,196	0.6%	293,575	0.1%
Liard River at Fort Liard	222,000	225,221	-1.5%	225,221	-1.5%	225,377	-1.5%
Mackenzie River at Arctic Red River	1,700,000	1,682,041	1.1%	1,682,041	1.1%	1,667,397	1.9%
Peel River above Canyon Creek	25,700	24,475	4.8%	24,475	4.8%	24,475	4.8%
Anderson River below Carnwath River	57,800	57,586	0.4%	57,586	0.4%	57,586	0.4%
Burnside River near the mouth	16,800	17,271	-2.8%	17,271	-2.8%	17,271	-2.8%
Allice River near the mouth	16,900	16,464	2.6%	16,464	2.6%	16,464	2.6%
Baillie River near the mouth	14,500	13,759	5.1%	13,837	4.6%	13,759	5.1%
Back River above Hermann River	93,900	95,691	-1.9%	95,691	-1.9%	95,691	-1.9%
Hayes River above Chantrey inlet	18,100	19,820	-9.5%	19,820	-9.5%	21,016	-16.1%
Big River above Egg River	3,640	3,199	12.1%	3,199	12.1%	3,199	12.1%
Sylvia Grinnell River near Iqaluit	2,980	2,705	9.2%	2,705	9.2%	2,705	9.2%
Spanish River at Espanola	11,400	12,901	-13.2%	12,901	-13.2%	12,017	-5.4%
Saguenay at Caron	73,800	68,614	7.0%	68,614	7.0%	67,106	9.1%
Average of absolute differences			5.0%		5.1%		6.2%

Presented are the derived flow networks for the entire study area using a diagonal factor of 0.0 (Figure 3.14) and a diagonal factor of 0.15 (Figure 3.15). From these it was seen that as the drainage factor was increased a higher percentage of the flow between grid cells became diagonal. This resulted in a much less-jagged flow pattern that more closely followed the true drainage pattern of the rivers.

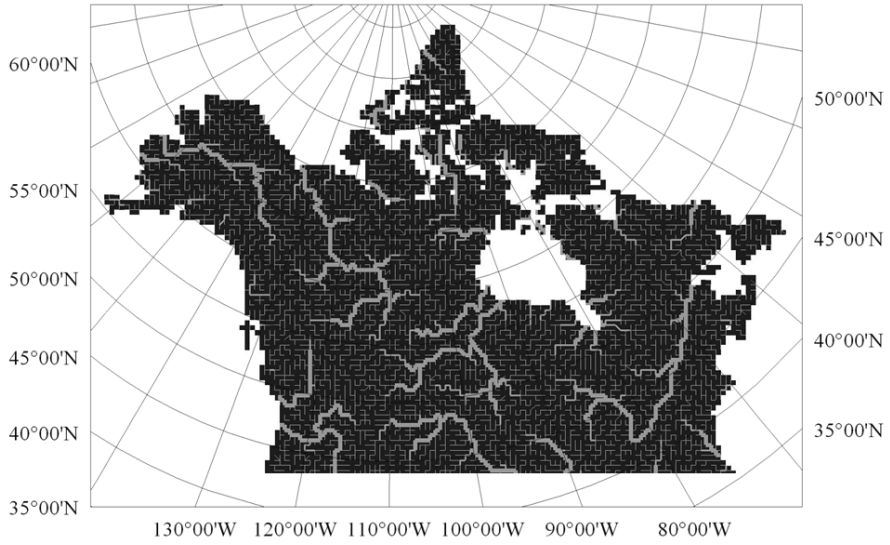

Figure 3.14: Flow network derived using diagonal factor of 0.00.

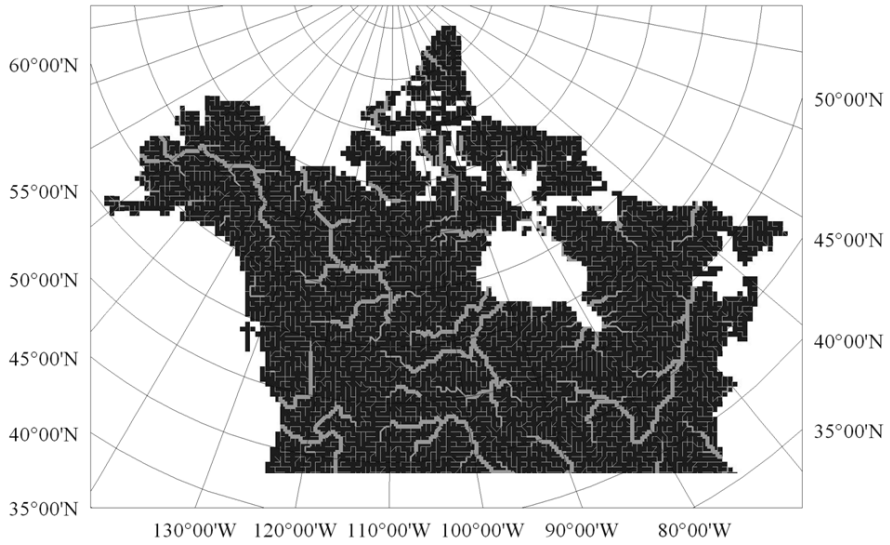

Figure 3.15: Flow network derived using diagonal factor of 0.15.

Examining a branch of the Athabasca River, when the flow network was derived using a drainage factor of 0.00, the results was a series of very blocky flow with no diagonal connectors (Figure 3.16a). Using a drainage factor of 0.15, the flow network had a much for realistic pattern with fewer blocky connections (Figure 3.16b). Comparing the simulated flow network to the actual flow network (Figure 3.16c) it was seen that the flow network derived using the drainage factor of 0.15 was a much better representation of the true pattern.

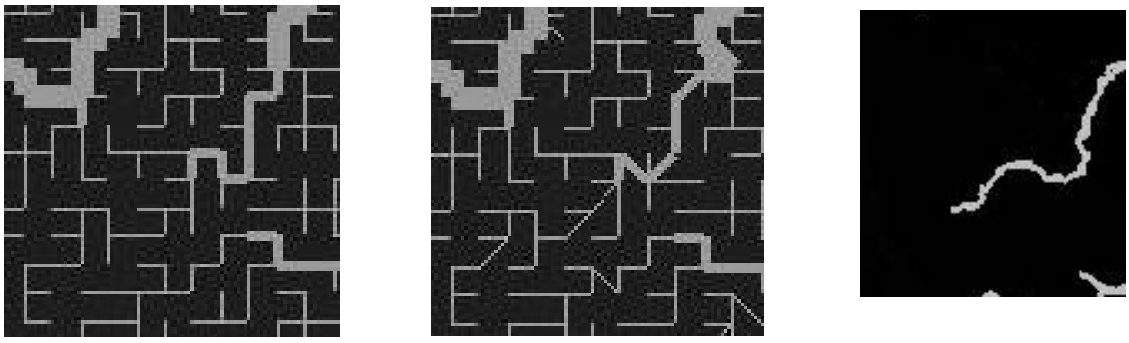

Figure 3.16: The derived flow network of part of the Athabasca river using a diagonal factor of a) 0.00, b) 0.15, and c) the approximate actual location of the main river channel.

3.3.8 Presentation of the drainage database for Canada

Using a diagonal factor of 0.15, the WATMAP technique was used on the modified depressionless DEM to compute the components of the drainage database. Presented here are the components of the drainage database: elevation (Figure 3.17), fractional area (Figure 3.18), drainage direction (Figure 3.19), channel classification (Figure 3.20), contour number (Figure 3.21), and number of similar channels (Figure 3.22). Note that no scale is given in these figures as they were meant to show the relative value of the different components of the drainage database.

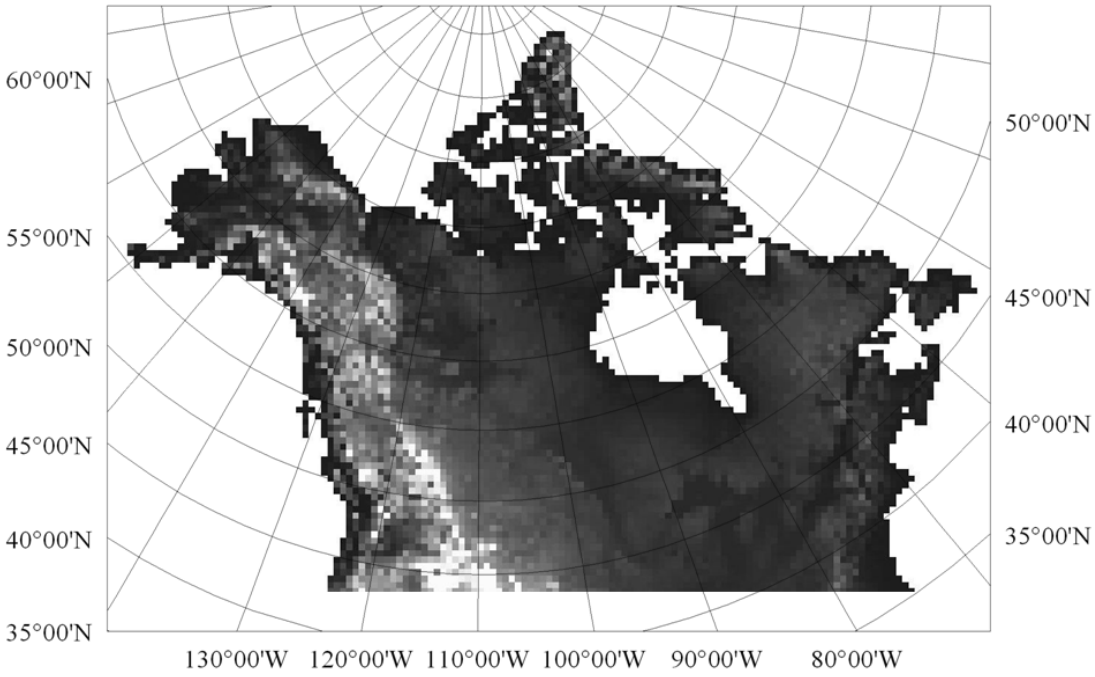

Figure 3.17: Elevation component of the drainage database.

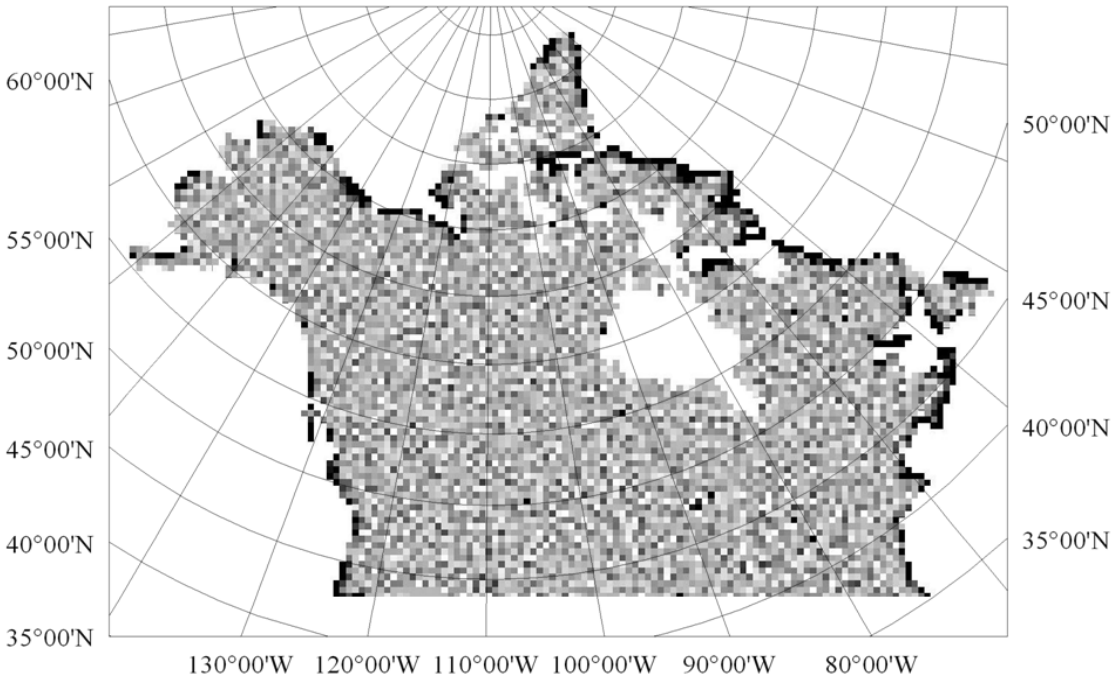

Figure 3.18: Fractional area component of the drainage database.

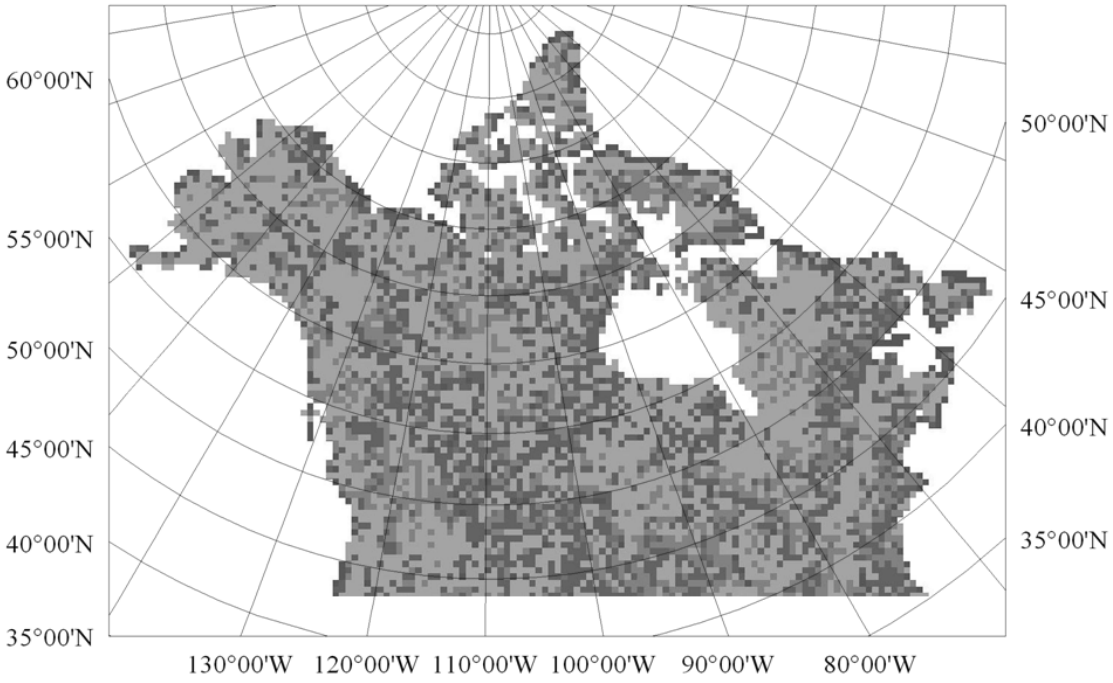

Figure 3.19: Drainage direction component of the drainage database.

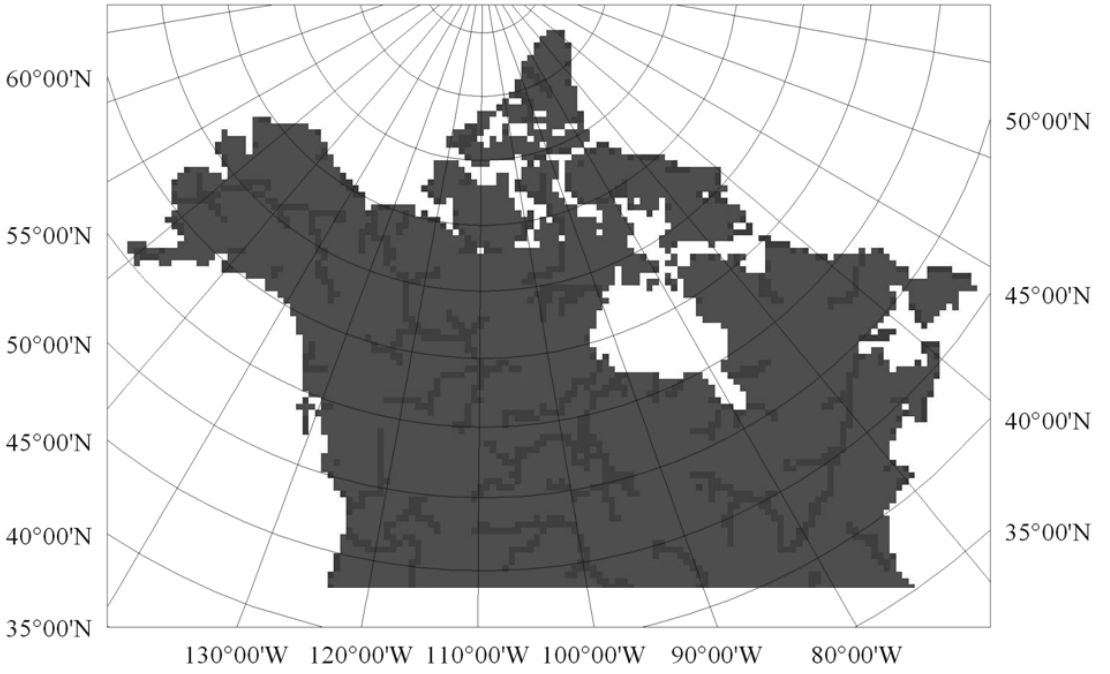

Figure 3.20: Basin number component of the drainage database.

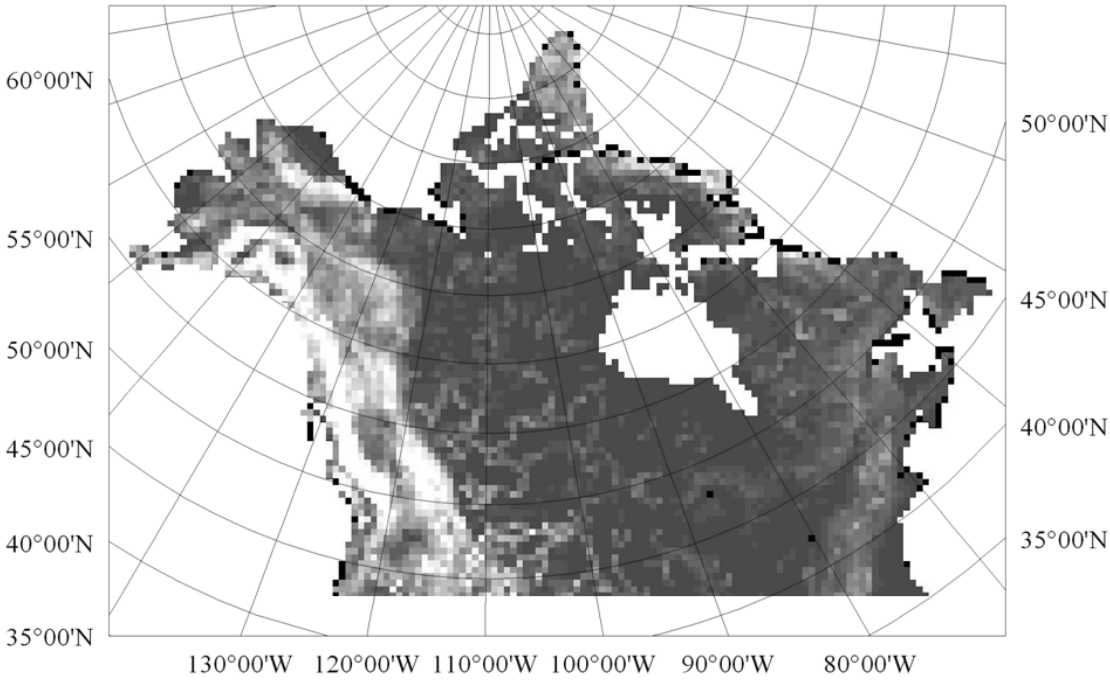

Figure 3.21: Contour number component of the drainage database.

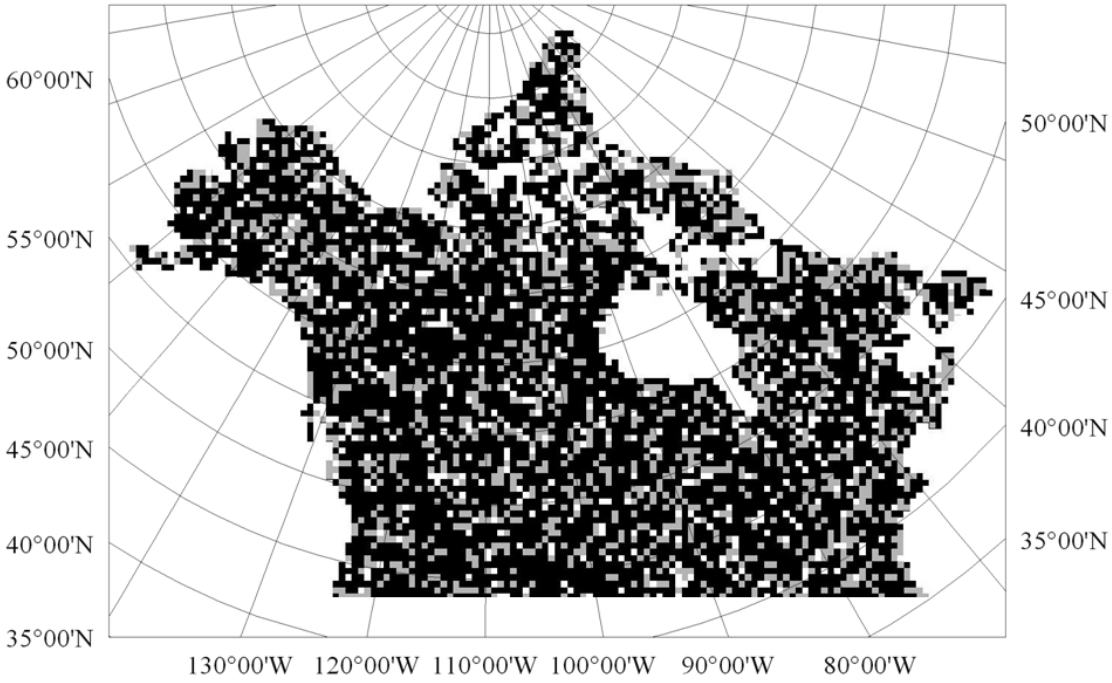

Figure 3.22: Number of similar channels component of the drainage database.

3.3.9 Flow network comparison – using the D8 technique at the model grid scale

In order to demonstrate the effectiveness of the WATMAP technique, the flow network that was simulated with WATMAP was compared to other techniques. As a first comparison, the flow network was calculated using a simple D8 drainage technique using the average elevation of each model grid square. In essence, this was how the flow network would have been determined without using the WATMAP technique.

The resulting flow network (Figure 3.23) gave a very poor representation of the drainage network with all major rivers in western Canada merged into one, the Mackenzie River emptied into the Arctic Ocean early and the St. Lawrence was not defined.

This technique resulted in a poor representation of the flow network because the average elevation of the 51-km model grid square was unable to properly represent the part of the model grid square where the drainage channel was likely to occur. Thus when the D8 technique decided on the direction of flow between model grids, it did not make the decision based on characteristics that affected the actual flow of water out of the model grid.

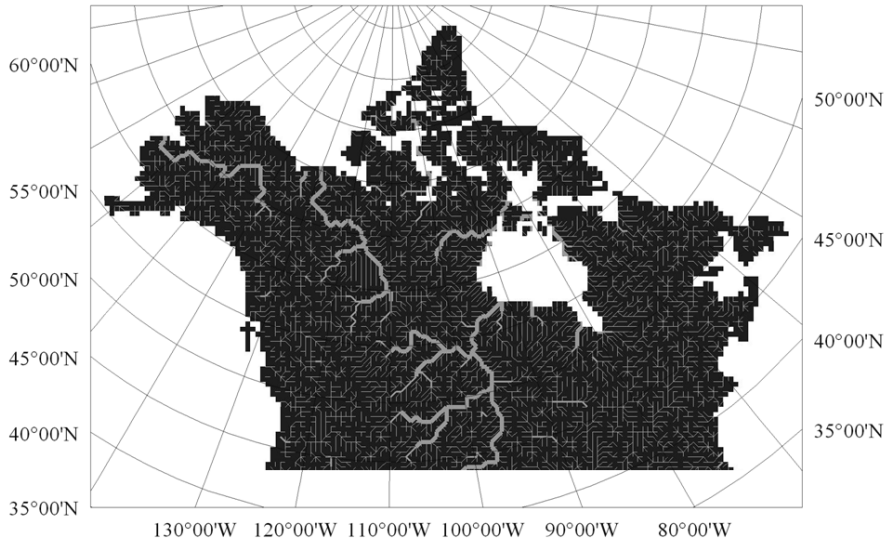

Figure 3.23: Derived flow network using the D8 technique on the average elevation of the 51-km grid squares

3.3.10 Flow network comparison – the effect of 100 percent fractional area

A comparison was also made between the derived drainage area using the value for fractional area of 100% for all model squares and the fractional area that was calculated by WATMAP. By using a value of 100%, it would have been assumed that all flow from a grid square would have flowed in the main drainage direction (see section 3.1.3). The drainage areas at the comparison points were calculated using a drainage factor of 0.15 for both techniques (Table 3-5).

This comparison showed that using a 100% value for fractional area causing a marked increase in the absolute error between the measured and the simulated values. The effect was seen more on the smaller basins, since, on these basins, improperly partitioning the flow of five or six model grid squares with an area of 2600 km^2 could have a large impact on the calculation of the total drainage area. For example, the measured drainage area at the Burnside River was 16 800 km^2; using WATMAP, the drainage area for this basin was 17 271 km^2. However, assuming fractional areas of 100%, the drainage area was calculated to be 18 207 km^2.

In larger basins, this improperly partitioned flow would eventually cancel each out and as a result the derived drainage areas are similar (when considering percentage difference).

As the overall average of the absolute difference between the measured and simulated drainage areas greatly increased when the fractional area was assumed to be 100% for each grid, it showed that

such an assumption was not valid, and thus the technique used by WATMAP should be used when calculating the drainage database.

Table 3-5: Comparison of measured and simulated drainage areas using different area fractions.

Station Name	Measured	Using calculated area fractions		Using area fractions of 100%	
	Drainage Area (km^2)	Simulated Drainage Area (km^2)	Difference	Simulated Drainage Area (km^2)	Difference
Nipigon River at Pine Portage	24,600	23,487	4.5%	28,611	-16.3%
Saugeen River near Port Elgin	3,960	3,329	15.9%	2,601	34.3%
Grand River at Brantford	5,210	4,604	11.6%	7,803	-49.8%
Thames River at Thamesville	4,300	3,381	21.4%	5,202	-21.0%
Ottawa River at Britannia	90,900	94,859	-4.4%	96,237	-5.9%
Saint-Laurent (Fleuve) a Lasalle	1,200,000	1,203,821	-0.3%	1,201,662	-0.1%
Moose River at Moose River	60,100	59,849	0.4%	59,823	0.5%
Moose River above Moose River	60,100	59,849	0.4%	59,823	0.5%
Red River near Lockport	287,000	320,313	-11.6%	332,928	-16.0%
Churchill River at Sandy Bay	212,000	213,906	-0.9%	210,681	0.6%
Churchill River above Red Head Rapids	289,000	290,766	-0.6%	286,110	1.0%
Thelon River above Baker Lake	154,000	152,861	0.7%	150,858	2.0%
Thelon River below outlet of Schultz Lake	152,000	152,861	-0.6%	150,858	0.8%
Athabasca River below Mcmurray	133,000	136,995	-3.0%	148,257	-11.5%
Peace River at Peace River	186,000	191,382	-2.9%	189,873	-2.1%
Fraser River at Mission	228,000	230,995	-1.3%	236,691	-3.8%
Yukon River at Dawson	264,000	257,733	2.4%	265,302	-0.5%
Yukon River at Eagle	294,000	292,196	0.6%	296,514	-0.9%
Liard River at Fort Liard	222,000	225,221	-1.5%	228,888	-3.1%
Mackenzie River at Arctic Red River	1,700,000	1,682,041	1.1%	1,714,059	-0.8%
Peel River above Canyon Creek	25,700	24,475	4.8%	26,010	-1.2%
Anderson River below Carnwath River	57,800	57,586	0.4%	57,222	1.0%
Burnside River near the mouth	16,800	17,271	-2.8%	18,207	-8.4%
Allice River near the mouth	16,900	16,464	2.6%	18,207	-7.7%
Baillie River near the mouth	14,500	13,759	5.1%	13,005	10.3%
Back River above Hermann River	93,900	95,691	-1.9%	101,439	-8.0%
Hayes River above Chantrey inlet	18,100	19,820	-9.5%	20,808	-15.0%
Big River above Egg River	3,640	3,199	12.1%	5,202	-42.9%
Sylvia Grinnell River near Iqaluit	2,980	2,705	9.2%	2,601	12.7%
Spanish River at Espanola	11,400	12,901	-13.2%	15,606	-36.9%
Saguenay at Caron	73,800	68,614	7.0%	72,828	1.3%
Average of absolute differences			6.1%		10.6%

3.4 Chapter discussion

The WATFLOOD model could now be used with the drainage database created in this chapter in order to help create the gridded time series of hydrological variables. Although the drainage database created was specifically designed to be used with the WATFLOOD model, the information contained in the drainage database is useable by other hydrological models. For example the VIC model created at the University of Washington (Liang *et al.*, 1994) also has requirements for a flow direction file and a fraction file that are analogous to the drainage direction and fractional area discussed in this chapter.

The drainage database created in this chapter is also compatible with the Modélisation Environnementale Communautaire (MEC) Surface and Hydrology (MESH) modelling system (Pietroniro *et al.*, 2007) being developed at Environment Canada's Hydrometeorology and Arctic Laboratory. This model is a combination of the WATFLOOD routing system with the Canadian land surface scheme (CLASS) (Verseghy, 1991).

Also, the technique presented here is not limited to the 1-km DEM grid and 51-km polar stereographic model grid. Any resolution and projection of grids could be used, but the technique would not be as effective if the size of the model grid scale was similar to the DEM grid scale. Experience using WATMAP indicates that at a minimum there should be at least 10 DEM grids along each side of the model grid, in order for the WATMAP technique to properly function.

As well, other input DEMs can easily be used by WATMAP to upscale to different resolutions. For instance, the HydroSHEDS hydrologically conditioned elevation model could be used as the depression-less DEM to derive the drainage database. The HydroSHEDS model went through a considerable amount of processing to ensure the derived river channels were correct. However, the upscaled products only consist of drainage direction (generally more information is needed to run complex hydrological models) and are only available at scales of 15 and 30 arc-seconds. Inevitably models will be needed to be used at different resolutions requiring a technique such as WATMAP.

In the future it will be possible to use finer resolutions of the model grid with the inevitable increase in available computer resources. This will make the correct calculation of diagonal flow and the partitioning of the flow from each model grid even more important. If these are not considered, it is impossible to properly simulate the actual drainage area of a watershed, problems that will be more evident when smaller model grid sizes are used.

Chapter 4
Creation of the Meteorological Dataset

4.1 Chapter introduction

It was the goal of this chapter to produce the most accurate gridded dataset of precipitation and temperature for all of Canada based on measured data from 1961-2000 on a daily basis. A technique was developed to produce gridded values of both temperature and precipitation that was not biased against areas that have a scarcity of data.

As measurement stations are located at randomly distributed points, in order to create gridded meteorological datasets from this station data, it is necessary to be able to interpolate. Consequently, there are many different techniques available to interpolate different kinds of meteorological data. However, temperature and precipitation are the only meteorological variables that are measured with enough spatial and temporal density across the country to perform meaningful interpolations.

But this is not the only method available to create gridded estimates of historical meteorological variables, as techniques have been developed that use a combination of measured data and numerical weather model output to create gridded estimates. These are called Land Data Assimilation Systems and have resulted in products such as the North American LDAS (Mitchell *et al.*, 2004) and the Global LDAS (Rodell *et al.*, 2004). These systems begin each of their forecast time steps by prescribing the current state of the atmosphere and ground surface. This is done using output from numerical weather prediction (NWP) models, station observations, ground radar observations and satellite observations. The future time steps are then forecasted using NWP models that allow for the creation of gridded data where modeled output is used for areas where no station data exist.

Development of these LDAS systems has resulted in the creation of re-analysis products; agencies such as the National Centres for Environmental Prediction (NCEP) and the European Centre for Medium-Range Weather Forecasts (ECMWF) have produced global datasets of many meteorological variables for time series going back to the 1940s (Uppala *et al.*, 2005; Kalnay *et al.*, 1996). While the LDAS systems are constantly evolving by incorporating more and more data, these re-analysis products have tried to create a consistent dataset by using the same LDAS system throughout the analysis time period.

These techniques also have their weaknesses when used to create longer time series. Mitchell and Jones (2005) concluded that station data are preferred to satellite data in creating long-term climate series they have longer record lengths (satellite data is only available after 1970) and satellite measurements have to measure surface conditions through the atmosphere instead of on the earth's surface. They also state that the latter reason is also applicable to blended data that uses data from satellites to expand the coverage of station data. As well, as stated by Maurer *et al.* (2002) the use of

measured data to run a land surface model that has been calibrated to measured streamflow is likely to produce better estimates for land surface water budget simulations than re-analysis products.

Overall, these re-analysis techniques are very intriguing and certainly represent the future of hydrological and climate sciences and in fact they may result in more reliable and consistent gridded products than can be derived from measured station data alone. However, as these new datasets need to be verified, it emphasizes the need for the comparison of these or any other future re-analysis products to gridded data based on measured station data. A measured gridded database of meteorological data will always represent the most reliable basis of comparison, as there is a danger of solely assessing the output from one model with the output from another model. As these re-analysis products are partly based on a "modeled" component, they should always be verified against the best available "measurement-based" data source, such as the one derived in this chapter.

4.2 Previous gridded temperature and precipitation datasets

There have been various previous studies that have produced gridded temperature and precipitation time series based on measured station data, some going back to the beginning of the 20th century.

The work of Wilmott and Matsuura (1995) produced a global gridded time series of temperature and precipitation at a resolution of 0.5 degrees called the Global Historical Climatology Network. They used measured station data taken between 1950 and 1999 that was interpolated using the inverse weighted distance method. For temperatures they used a lapse rate of 6.0° C per km to normalize the data to sea level.

For both temperature and precipitation, they employed a method called Climatologically Aided Interpolation where the difference between the monthly climate variable at each station and the monthly climatological average was the factor that was used in the interpolation. The interpolated difference was then added back to the average fields to calculate the final value of the factor at each location.

Another global gridded dataset was created by the Climate Research Unit, which is part of the University of East Anglia in Norwich, UK. Various versions of their global gridded dataset exist, but the one with the highest spatial resolution was referred to as CRU TS 2.1, which contained worldwide monthly temperature, precipitation, diurnal temperature range, vapour pressure, cloud cover, sunshine duration, and wet days at a resolution of 0.5 degrees for the time period of 1901-2002 based on measured station data (Mitchell and Jones, 2005).

As the dataset required data from many different agencies from around the world, a lot of work was done to ensure the data quality of all the readings. This involved creating reference series from

neighbouring stations to fill in missing data and to detect problems with data series. It was the anomalies of the different variables relative to the 1961-90 normal that were used for the time series rather than the absolute values. For stations that did not contain any data, an anomaly of zero was assumed and then the anomalies were interpolated to the grid. The interpolation method is not described, but it is assumed that it would have been the inverse weighted distance method that was used in previous version of the CRU gridded data series.

The global precipitation climatology project (GPCP) was created by the World Climate Research Program (WCRP) to combine precipitation information available from different sources into a final merged product (Adler *et al.*, 2003). Sources of precipitation used to create the final product include various satellite data (infrared and longwave sensors) and measured station data. As the dataset relies on satellite data, data are only available starting in 1979 while the spatial resolution is only 2.5 degrees.

Sheffield *et al.* (2006) produced a global dataset of forcing data sets including temperature, precipitation, incoming shortwave, and incoming longwave radiation. The dataset goes from 1948 to 2000 as a spatial resolution of one degree and a time step of 3 hours. The basis for the dataset is the NCEP-NCAR reanalysis product that was corrected using various global-observation based datasets including the ones from CRU and the GPCP. This correction was necessary as the NCEP-NCAR reanalysis has been shown to have problems with some of their products most notably in relation to precipitation. The NCEP-NCAR dataset was also spatially downscaled from its native resolution of approximately 1.9° latitude by 1.875° longitude to the 1° final product from the study.

Apart from the work by Maurer *et al*. (2002) presented in Chapter 2, none of the previously generated gridded temperature and precipitation datasets based on measured station data that have been published were found to interpolate to areas of sparse data with anything more than a modifed inverse weighted distance interpolation method. It is hoped that the interpolation method developed in this chapter that incorporates information on the physiography of the surface will result in a more reliable interpolation.

4.3 Observed data

Data were used from stations in the Environment Canada database that were in operation between 1961 and 2000. The daily temperature and precipitation were obtained from each station as well its location and elevation. The period from 1961 to 2000 was chosen as a time when the maximum number of meteorological stations was present in Canada, although they have seen a sharp decline in numbers since the early 1990s (Figure 4-1).

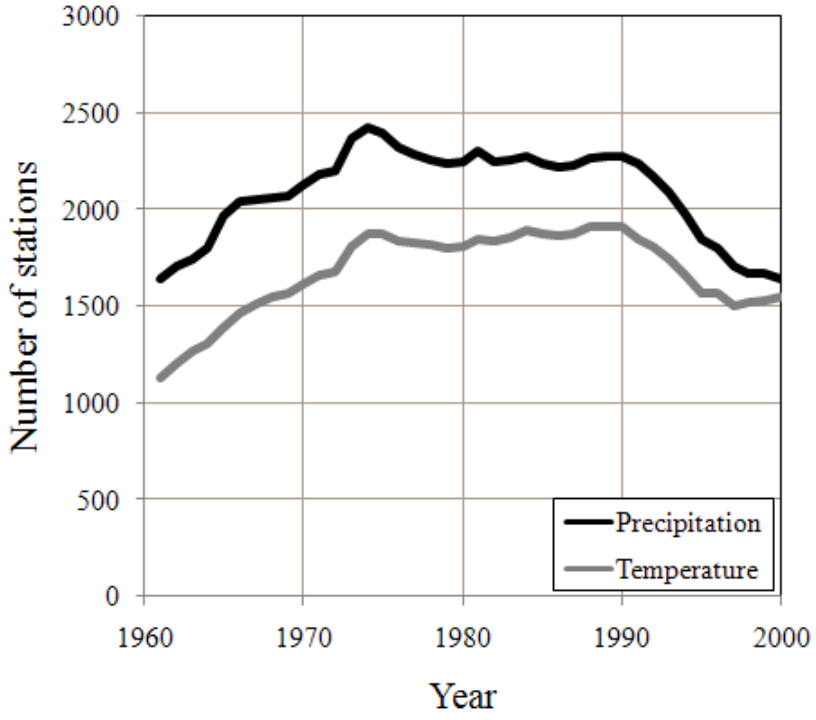

Figure 4-1: Number of climate stations in Canada between 1960-2000.

In total, 11 202 stations had some data recorded (although not necessarily precipitation and/or temperature) during 1961-2000, but not all the stations were available for the entire period, thus standards were needed in order to decide when to reject a station from the analysis. This was necessary as a station that was only reporting data for a small number of years may skew the overall analysis. It was decided that at least 20 years of data would be necessary in order for a station to be considered in the analysis.

Using this criterion, the total number of precipitation stations available was 1986 (Figure 4-2) while the number of maximum and minimum temperature stations was 1762 (Figure 4-3 and Figure 4-4). It can be seen that most stations were located in southern Canada with relatively few in the northern part of the country. A notable exception was the line of stations just south of the Arctic islands that were set up by the American and Canadian military as part of their Distant Early Warning (DEW) line after the Second World War.

All the interpolations done in this chapter were performed using the identical projection as the one that was used to create the drainage database files. However, instead of the 51-km grid used for the drainage database file, the grid size used for the interpolation of the meteorological dataset was 1 km.

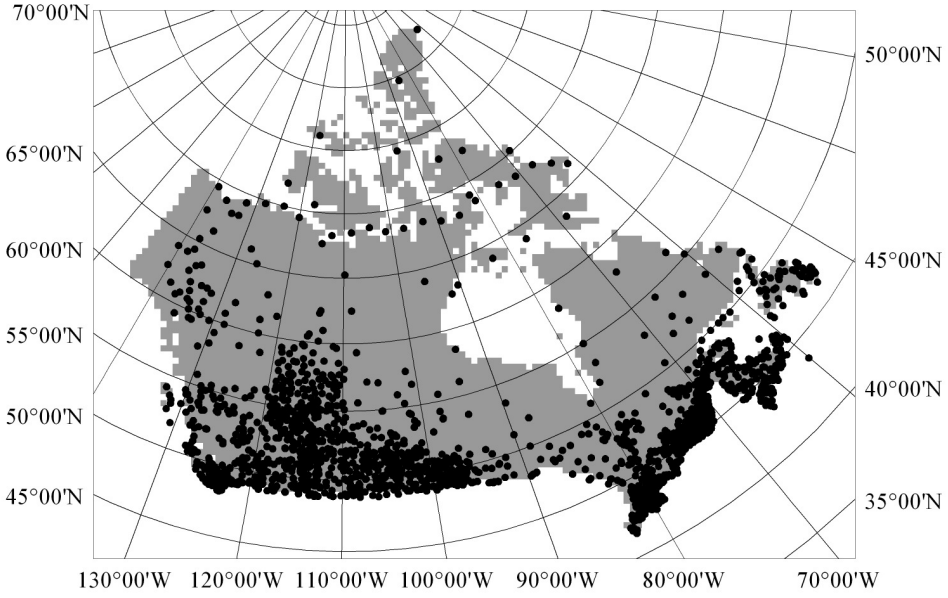

Figure 4-2: Precipitation stations with at least 20 years of data.

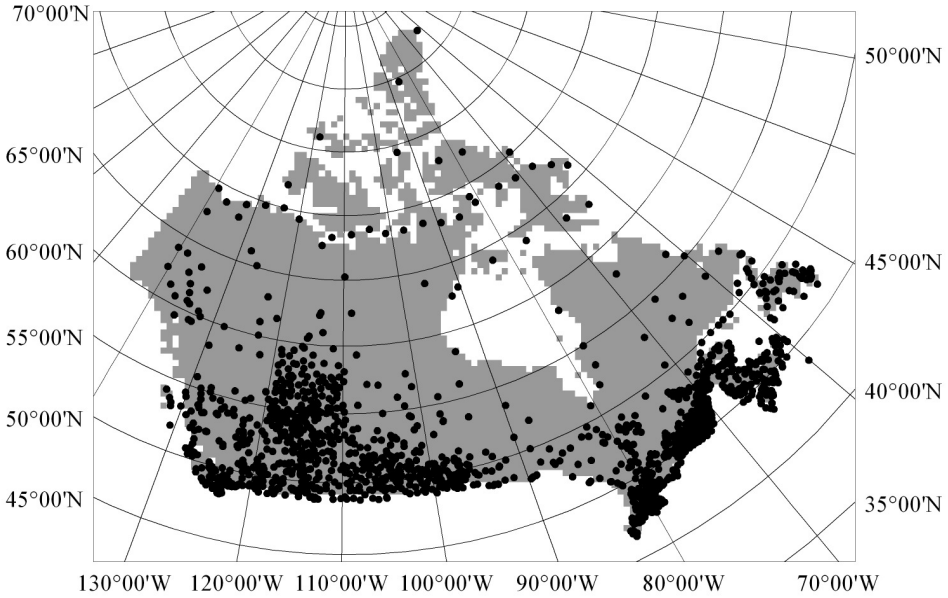

Figure 4-3: Stations with at least 20 years of maximum temperature data.

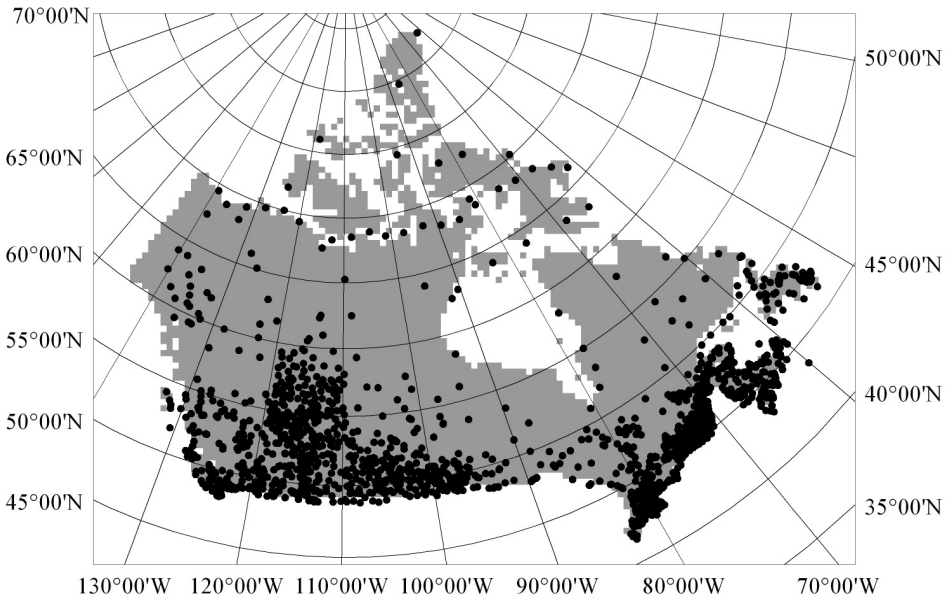

Figure 4-4: Stations with at least 20 years of minimum temperature data.

4.4 Interpolating the data - Monthly

As a first step in the interpolation of the meteorological data, the monthly averages or totals of the data were interpolated. The average monthly precipitation was simply the sum of all the precipitation for that month. The average monthly maximum temperature was the average of all the daily maximum temperatures for that month. The same method was used to calculate the average monthly minimum temperature.

It was important not to let missing data skew the overall average for a particular month. For example, in southern Canada, the temperature during the month of April typically increases sharply between the beginning and the end of the month. Thus even if only 5 days of data were missing from the temperature record from the end of the month, it would greatly affect the average for the month. Thus only months that contained daily readings for each day of that month were used in the calculation of the monthly averages.

4.4.1 IWD technique – monthly precipitation

In the paper by Mueller *et al.* (2004), the authors examined many different studies using both the inverse weighted distance (IWD) and the kriging technique and found that there was no conclusive evidence that either technique produced significantly better results. As the kriging technique is more

difficult and time-consuming to implement (Hartman and Hossjer, 2008), the IWD technique was used to interpolate the monthly temperature and precipitation data as a comparison to the technique developed later in this chapter.

The only tuning factor available for the IWD technique was the weighting factor that determines the balance between how much the interpolated value for the current point was influenced by the nearest point and how much by the overall average (the weighting factor was further defined in Section 2.1).

The limitations of the IWD technique were seen when a weighting factor of 2.0 was used to interpolate the June total precipitation (Figure 4-5). The interpolation showed the tent-pole effect inherent in the IWD technique where the influence of the measured points was consistently at a local high point as shown in Figure 4-6 (Vieux, 2004).

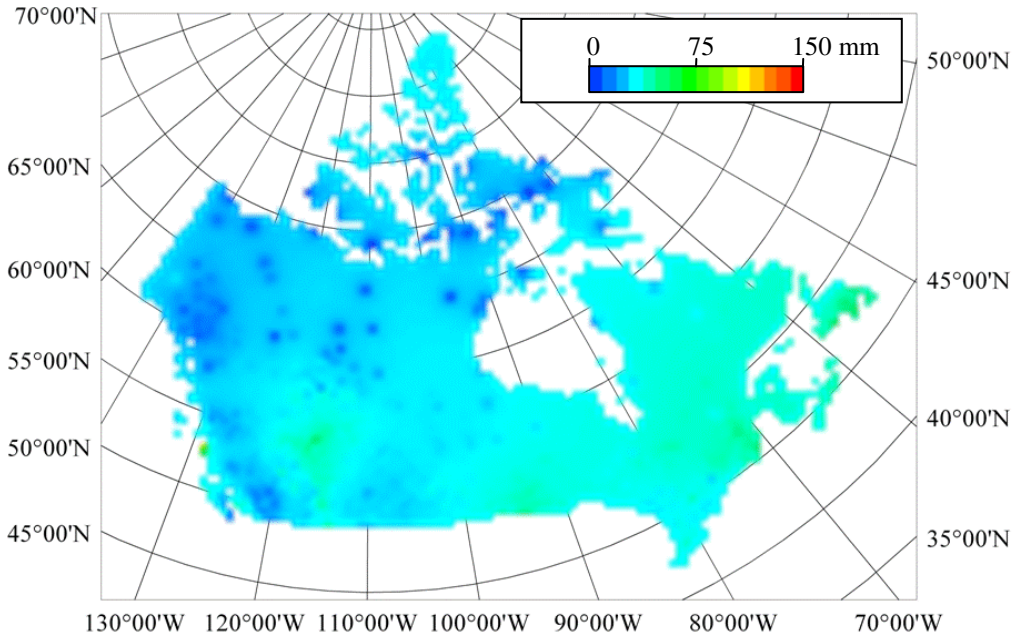

Figure 4-5: IWD interpolation of June total precipitation using a factor of 2.0.

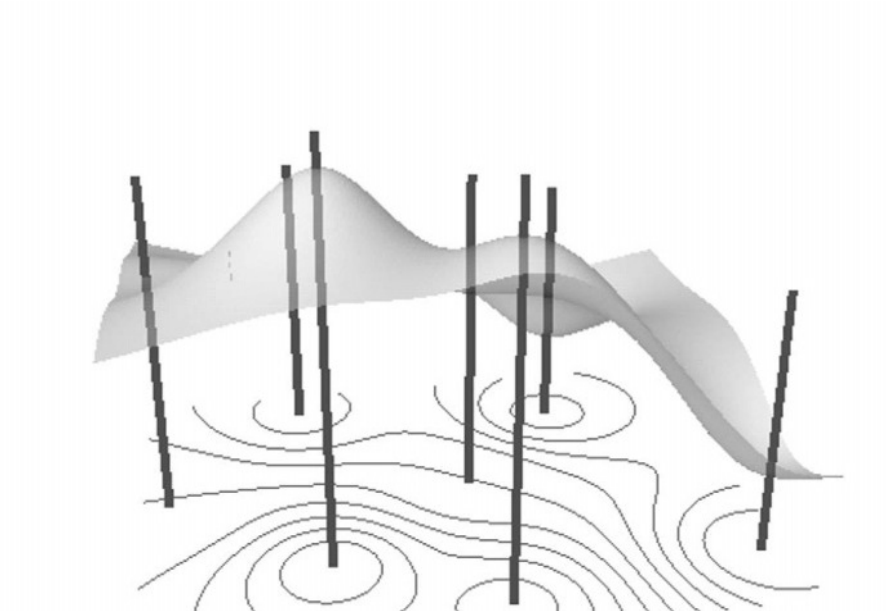

Figure 4-6: Tent-pole effect of IWD interpolation (from Vieux, 2004).

When using larger values of the weighting factor, the influence of each measured station was seen over a much larger area and less of the interpolation reverted back to the average value. Thus with a value of 1.0 (Figure 4-7a) the interpolation showed a series of small areas where the individual stations had a great influence surrounded by areas where the interpolated value was just the average all the stations. The other end of the scale was when the weighting factor was raised to 20.0 (Figure 4-7f) and the final interpolation was a mosaic where the value of each station was used until halfway to the next station in each direction giving an appearance similar to Thiessen polygons.

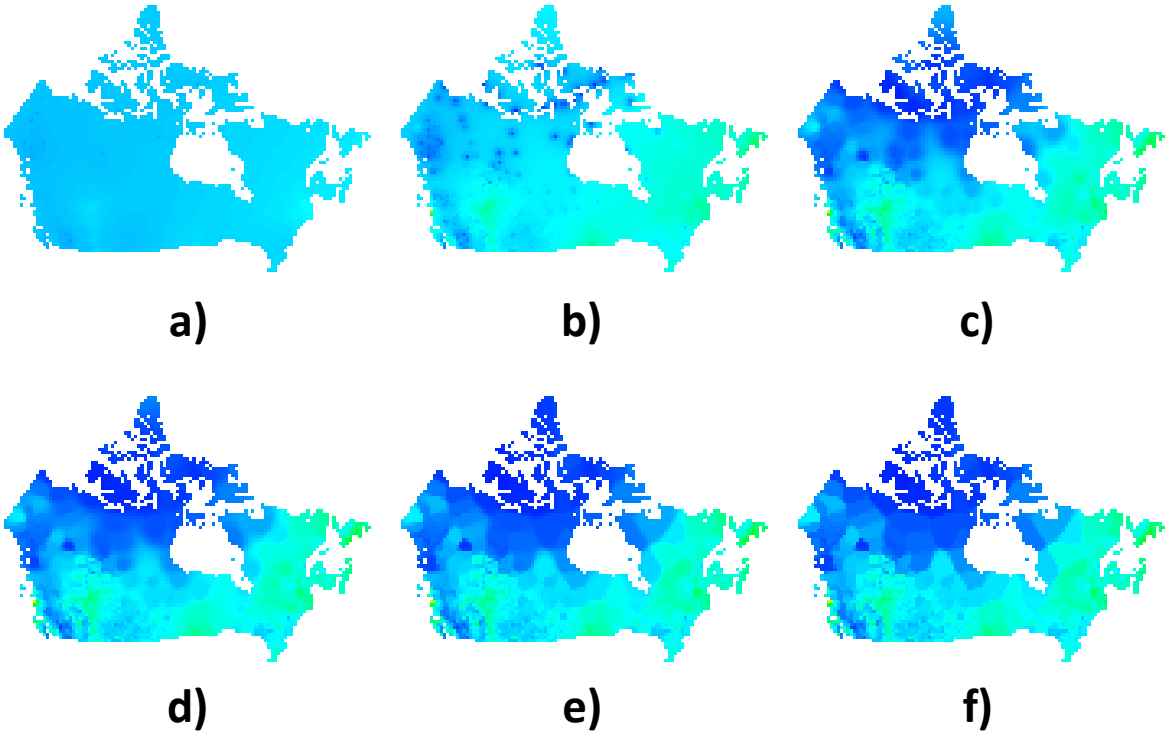

Figure 4-7: IWD interpolation on June total precipitation using different weighting factors a) 1.0 b) 2.0 c) 4.0 d) 5.0 e) 10.0 f) 20.0.

In order to make an accuracy comparison between the different weighting factor, a leave one out cross-validation technique was employed where each point was sequentially left out of the analysis and then the interpolated value at the point was compared to the measured value at that point. This was then repeated for each measured point in the analysis.

Two measures of fit were evaluated; the root mean squared error (RMSE) which is the square root of the sum of the squares of the differences between the measured and interpolated values and the mean error (ME) which is the average of the differences between the measured and interpolated values. The RMSE gave an indication of the accuracy of the interpolation while the ME gave an indication of the bias of the interpolation. Both the RMSE and ME values were normalized by the average measured values which gave the results as a percentage.

When considering monthly precipitation, the minimum value of the RMSE error using different values of the IWD factor occurred at an IWD factor of 4.0 (Figure 4-8). However, the IWD factor that resulted in the lowest RMSE error was dependent on the parameter under consideration and thus was recalculated for different situations.

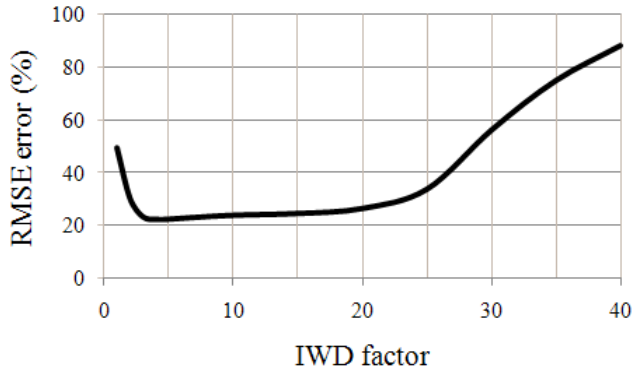

Figure 4-8: RMSE error values using different values of weighting factors on the average monthly precipitation.

Maps were created using the IWD technique and this weighting factor for precipitation, presented here are the final interpolated fields for January (Figure 4-9) and July (Figure 4-10). The maps for the rest of the months are presented in Appendix B.

Even at this scale, the general pattern of the interpolation was not very realistic, as individual stations had an influence for many hundreds of kilometres while the interpreted values themselves had no consideration of the underlying topography. As well, any detail in the interpreted values was merely a result of closely spaced measurement stations and conversely homogeneous interpreted values were found in areas of sparse measurement stations.

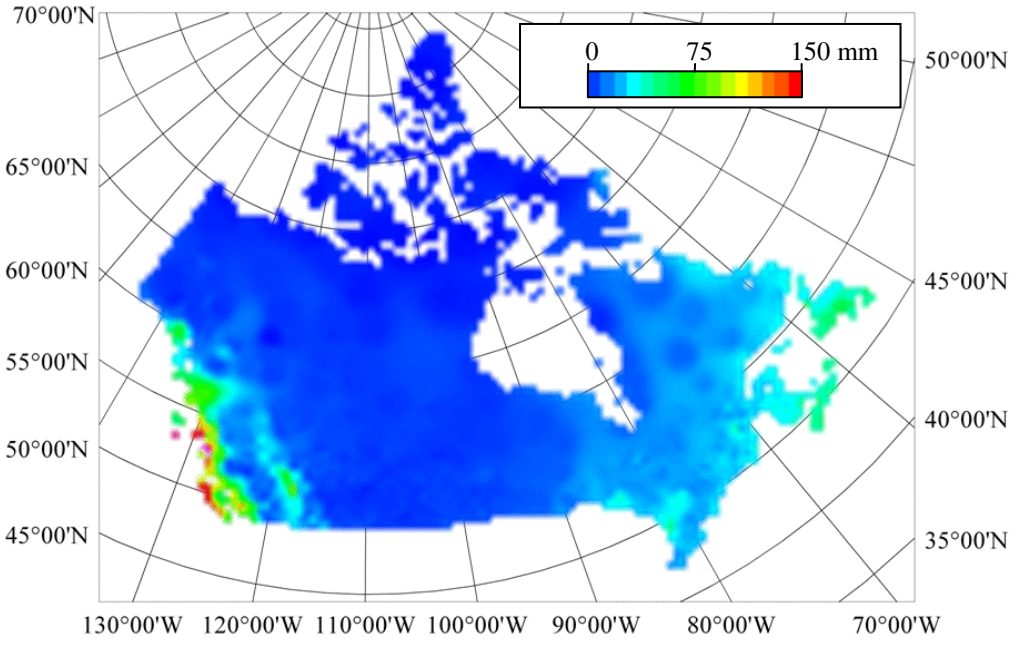

Figure 4-9: IWD interpolation of January total precipitation.

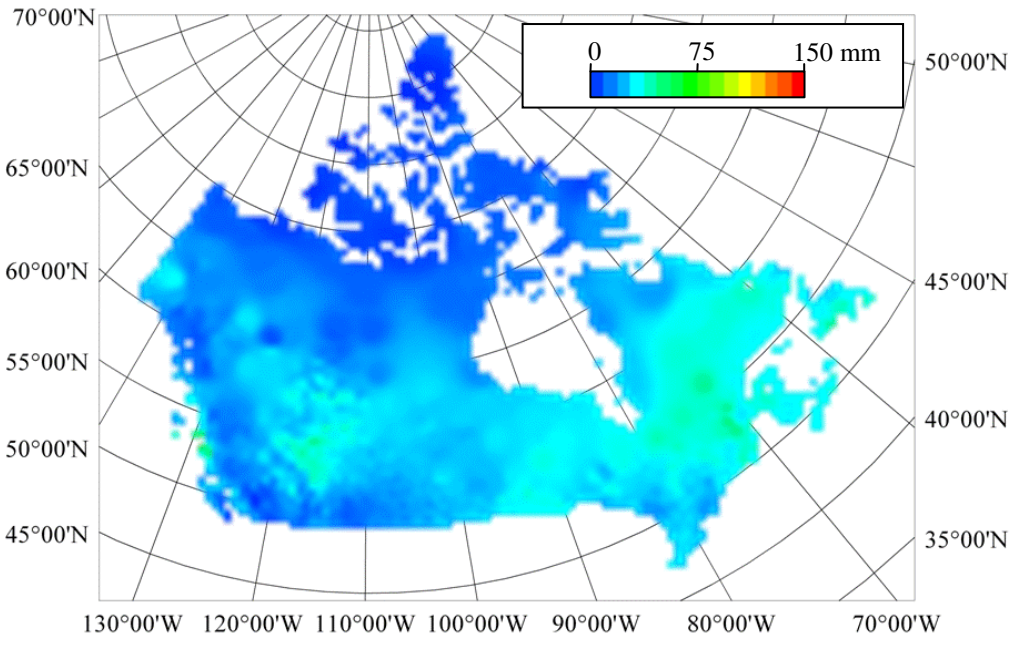

Figure 4-10: IWD interpolation of July total precipitation.

Table 4-1 shows the RMSE and ME values derived for each month as well as an overall annual value for the IWD interpolated precipitation. The interpolation performed much better in the summer than in the winter with an RMSE value of 12.7% in July compared to 32.6% in January. While the interpolation showed a negative bias (ie. the values from the interpolation were lower than the measured values) in all of the months with generally higher absolute values of ME in the winter.

Table 4-1: RMSE and ME values for IWD interpolation of average monthly precipitation for all of Canada.

	IWD	
Month	RMSE	ME
Jan	32.6%	-0.64%
Feb	36.3%	-0.62%
Mar	30.4%	-0.44%
Apr	25.6%	-0.28%
May	16.2%	-0.09%
Jun	13.5%	-0.12%
Jul	12.7%	-0.24%
Aug	12.7%	-0.58%
Sep	19.6%	-0.86%
Oct	32.5%	-1.08%
Nov	30.9%	-0.84%
Dec	32.8%	-0.59%
Ann	24.6%	-0.53%

It was also possible to create an error map for the interpolation by using the results of the leave one out analysis used to create the RMSE table. This was done by plotting the difference between the calculated and measured values on a map at the station locations. Error values for the areas between the station locations were then interpolated using IWD (Figure 4-11). In the figure, areas of red and orange indicated areas where the interpolation technique overestimated the value of the parameter at that point, areas of blue were areas that are underestimated by the interpolation, and areas of green indicate regions where there was little difference between the measured and interpolated value.

Obviously the goal was to have an error map that showed as few differences as possible (ie. mostly green) while also showing no regional bias to the errors (ie. having the non-green areas evenly distributed across the country). It should be noted that errors in the northern regions of Canada had a greater visual impact in the error maps as their values had an influence over a larger area as a result of the sparseness of the data.

Figure 4-11 shows the error map produced from the IWD interpolation of precipitation for January. The map contained generally green areas across the country with some overestimation in the northern part of Quebec and small pockets of both over and underestimation on the west coast and Rocky Mountains.

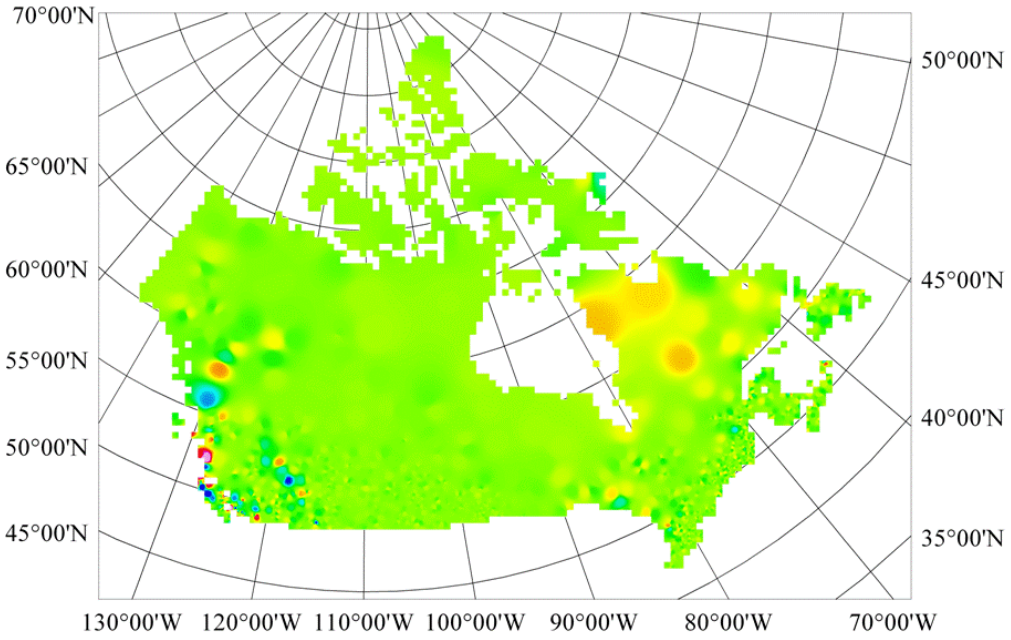

Figure 4-11: Error map for precipitation using the IWD interpolation technique.

4.4.2 IWD technique – monthly temperature

The average monthly temperature values were then interpolated using the IWD technique, again with an influence factor of 4.0. Maps are presented for average daily maximum temperature for January (Figure 4-12) and July (Figure 4-13) as well as the daily minimum temperature for January (Figure 4-14) and July (Figure 4-15). As with the precipitation, maps of all of the months of interpolated temperature are presented in Appendix B.

The interpolated temperatures were much smoother than their precipitation counterparts with the temperature mostly influenced by the elevations of the stations (colder as you go higher up), latitudes of the stations (colder as you go further north) and the distance from the coast (colder in the interior of the continent).

The influence of individual stations (ie. the tent pole effect) was seen in the temperature interpolations more than in the precipitation interpolation.

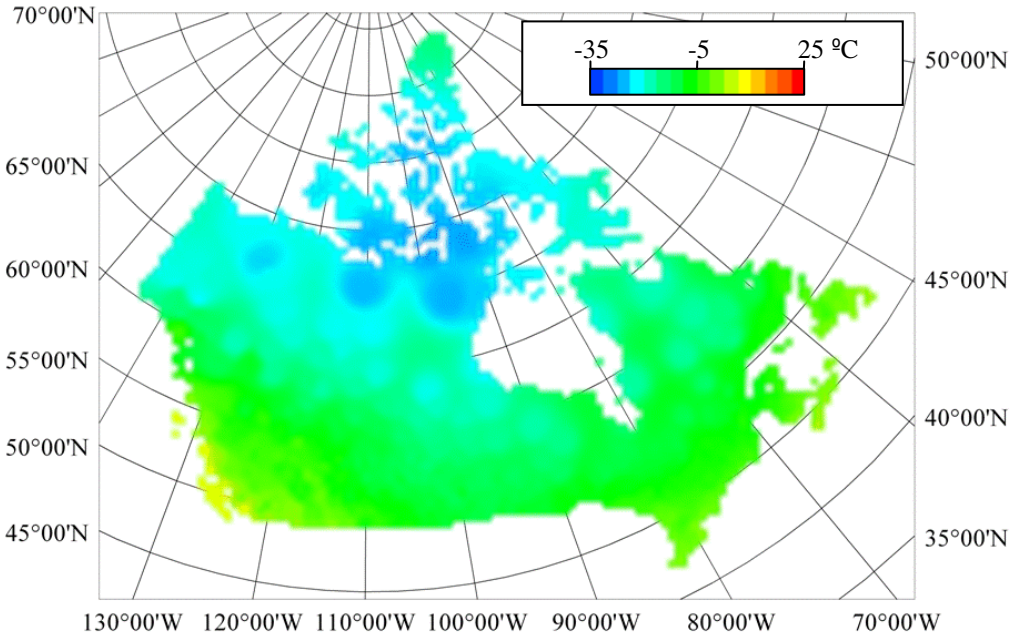

Figure 4-12: IWD interpolation of January maximum temperature.

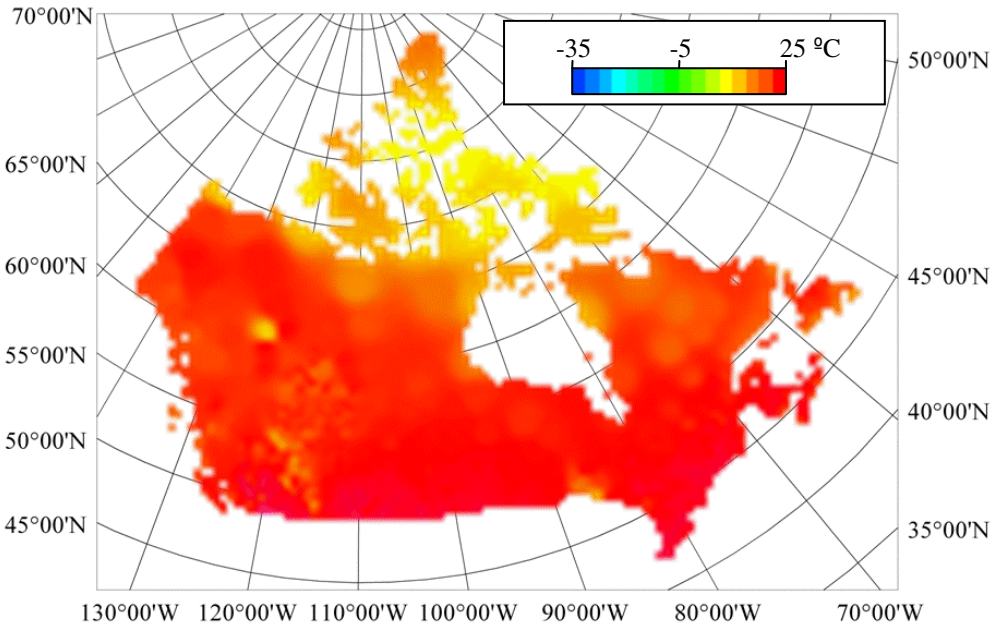

Figure 4-13: IWD interpolation of July maximum temperature.

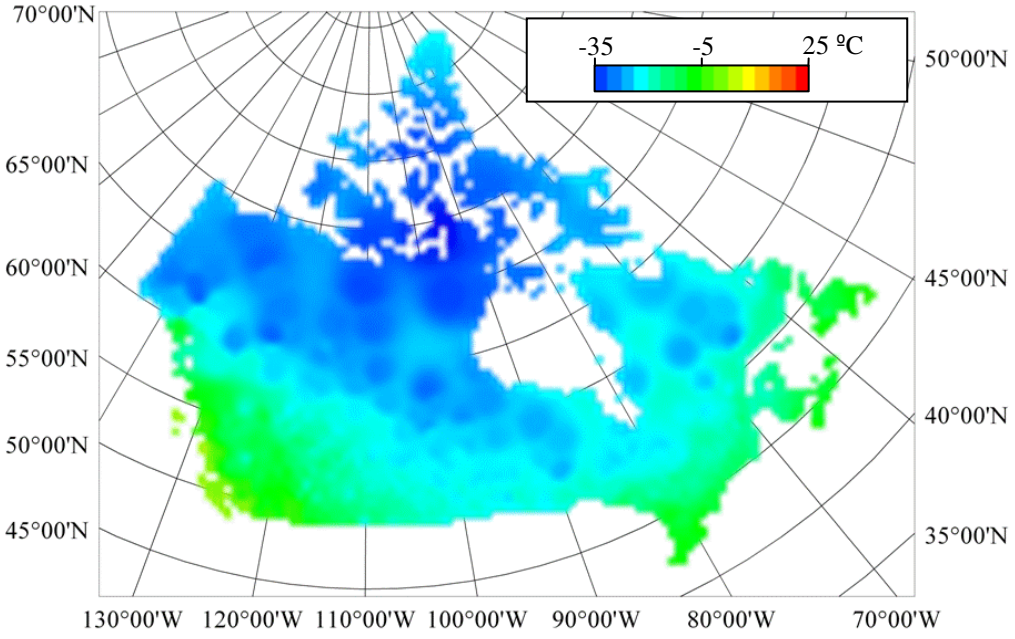

Figure 4-14: IWD interpolation of January minimum temperature.

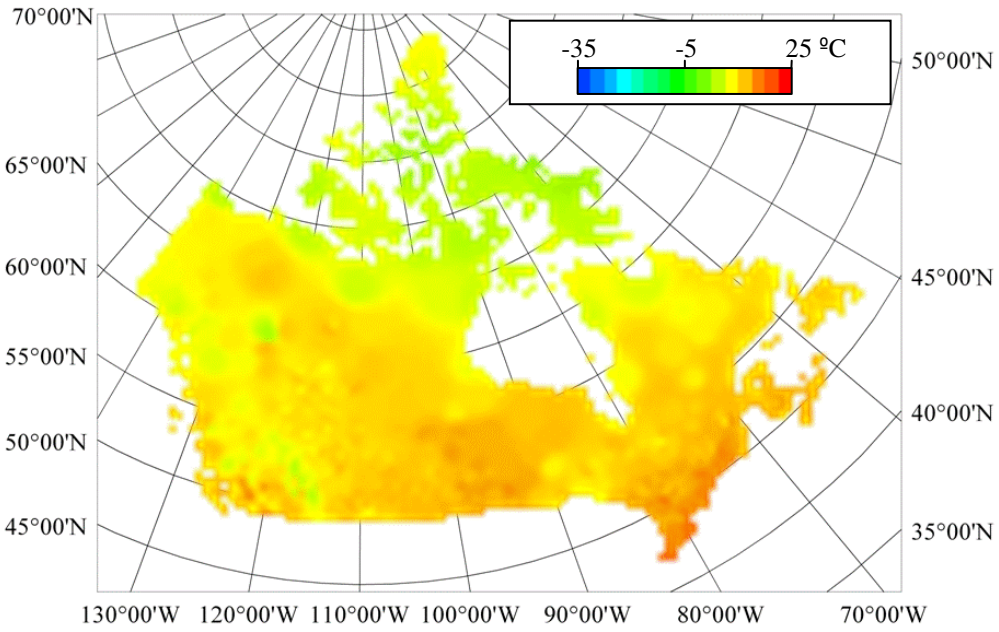

Figure 4-15: IWD interpolation of July minimum temperature.

Again the RMSE and ME were calculated, however the results were not normalized as temperature values are instantaneous values and not accumulations. The IDW factor that resulted in the lowest RMSE for average monthly temperature was 5.0 for both maximum and minimum temperatures.

Although the overall average of the RMSE for the average monthly maximum temperature (Table 4-2) was the same as the average monthly minimum temperature (Table 4-3), the monthly patterns were quite different. For the maximum temperatures, the higher values for RMSE were seen in the spring and summer months, while for the minimum temperatures, the highest values occurred during the winter.

When looking at the ME, not only were the overall averages similar, but the patterns were also generally the same with the highest values during the winter months. All of the ME values were positive, indicating that the interpolated values were generally higher than the measured values at the station values.

Error maps for the IWD interpolation of both maximum temperature (Figure 4-16) and minimum temperature (Figure 4-17) showed the same general patterns with large areas of overestimation of temperature around Hudson Bay and another large area on the northern Arctic islands.

Table 4-2: RMSE and ME values for IWD interpolation of average monthly maximum temperature for all of Canada (all values in degrees).

IWD		
Month	RMSE	ME
Jan	1.21	0.198
Feb	1.09	0.180
Mar	1.22	0.204
Apr	1.75	0.189
May	1.75	0.192
Jun	1.84	0.143
Jul	1.73	0.132
Aug	1.69	0.134
Sep	1.25	0.142
Oct	1.02	0.164
Nov	1.02	0.158
Dec	1.15	0.165
Ann	1.39	0.167

Table 4-3: RMSE and ME values for IWD interpolation of average monthly minimum temperature for all of Canada (all values in degrees).

	IWD	
Month	RMSE	ME
Jan	1.65	0.234
Feb	1.65	0.243
Mar	1.62	0.258
Apr	1.55	0.215
May	1.29	0.165
Jun	1.20	0.125
Jul	1.22	0.122
Aug	1.25	0.115
Sep	1.24	0.127
Oct	1.24	0.137
Nov	1.36	0.179
Dec	1.57	0.203
Ann	1.40	0.177

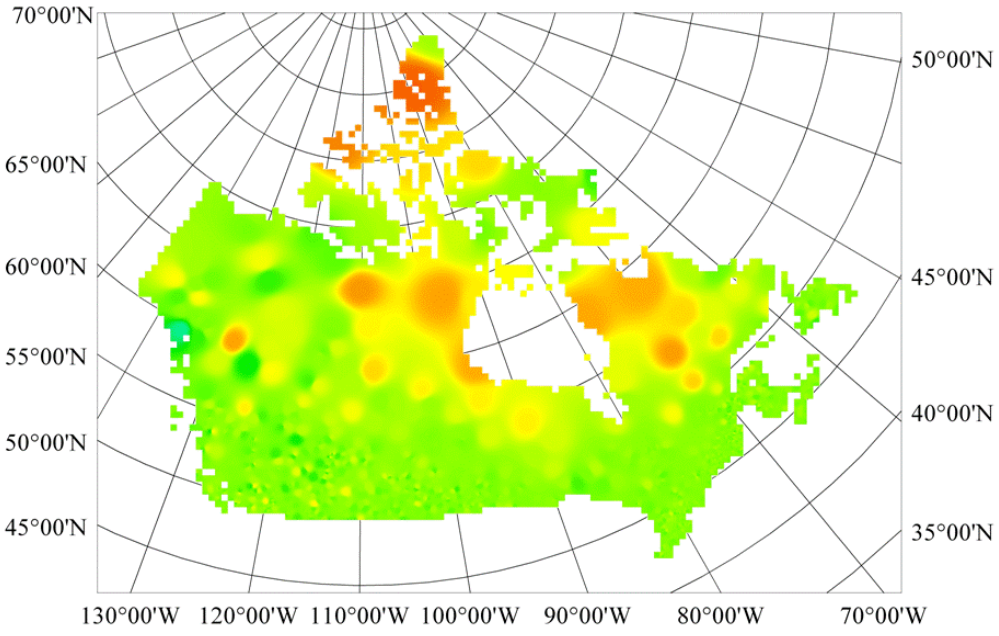

Figure 4-16: Error map for maximum temperature using the IWD interpolation technique.

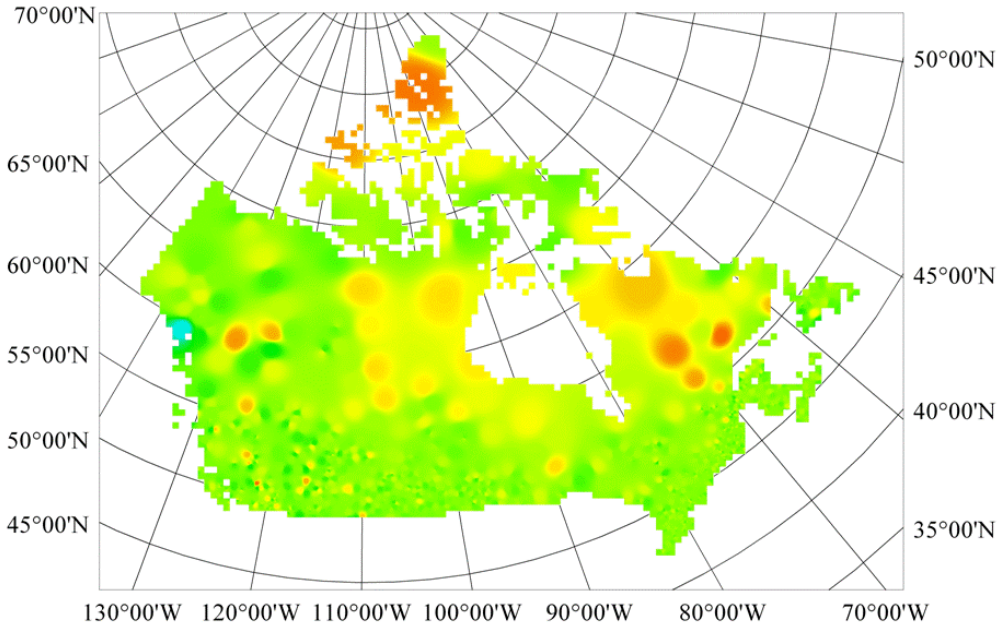

Figure 4-17: Error map for minimum temperature using the IWD interpolation technique.

4.4.3 WATMAPPR technique

In the late 1960s, Solomon *et al.* (1968) developed an interpolation technique called the "square grid" method. The name was derived from the fact that the method divided the study area into distinct square grids each with its own physiographic characteristics. The method used in this study was a modification of the original "square grid" method that was renamed the Waterloo Multiple Physiographic Parameter Regression (WATMAPPR) technique to better reflect the nature of the interpolation. Using this technique, regression equations were derived for an area based on the values of physiographic parameters using the locations of measurement stations.

Some of these parameters, called station parameters, were based solely on the properties of the individual grid or neighbouring grids, while others, called derived parameters, were calculated using terrain features between the station location and the ocean in each of eight directions (that is, N, NE, E, SE, S, SW, W, and NW) and reset to zero when the elevation of a grid was found to be sea level.

The following is a description of the station parameters used in the WATMAPPR technique:

- Elevation – The average elevation of the grid.
- Latitude – The latitude of the grid.
- Longitude – The longitude of the grid.

- Slope – The difference in elevation between the grids on either side of the station grid divided by the horizontal distance between the grids.

The following is a description of the derived parameters used in the WATMAPPR technique:

- Distance to ocean - The horizontal distance from the grid to the ocean in a certain direction.
- Shield effect - The sum of the elevation difference of all ascending stretches of terrain in a certain direction.
- Barrier height - The difference between the elevation of the grid and the highest elevation encountered in a certain direction.

All of these physiographic parameters were calculated for the entire study area. Then the grids that contained measurement stations were identified and the values of the physiographic parameters were put into a database along with the climate data from those stations.

Once all of the values for the physiographic parameters and climate data were available, a stepwise forward selection linear regression was performed. The climate data – for example, long-term average precipitation for January – were the dependent variable in the regression while the physiographic parameters were the independent variables. The objective function used to evaluate each regression was the results of the leave-one-out analysis, making the goal to minimize the objective function.

In the stepwise regression, each independent variable was put into the regression individually and the resulting value of the objective function was determined. The independent variable that resulted in the lowest value of the objective function was the first variable to enter the regression. The process was then repeated with the first variable and each of the remaining variables entered individually into the regression. The variable that gave the lowest value of the objective function was then the second variable to enter the regression. Other variables were added to the regression until resulting objective function no longer decreased by a certain threshold amount.

The result of this process were equations that related the value of the climate data to the physiographic parameters. These equations were then used to calculate the expected value of the climate data at all points in the study area based on the values of the physiographic parameters at those points. The WATMAPPR technique is a non-exact interpolation, since the interpolated value at a measurement station may not necessarily be the measured value at that station.

4.4.4 Modifications to the square-grid technique

It was necessary to make modifications to the original square-grid technique, as the original technique was developed for small areas where the same meteorological and climatic effects would

influence the entire study area. The modifications generally involved adjustments to the derived physiographic parameters.

The first change to the original technique was in the definition of the ocean; since the derived parameters reset at the sea level, the location of the ocean was critically important. The original technique reset the derived parameters whenever a sizeable water body was encountered or the elevation was found to be sea level. This did not have many consequences when examining a smaller area, but when calculating the derived parameters across Canada, a small inlet could cause a reset of a parameter that would then have effects lasting hundreds or thousands of kilometres.

Thus, for the WATMAPPR technique used in this study, the parameters were only reset outside of the continent (Figure 4-18). Figure 4-19 shows the effect that this had on the derived parameter distance to the ocean to the northeast. When using the modified ocean definition, the parameter was much smoother than using the original ocean definition.

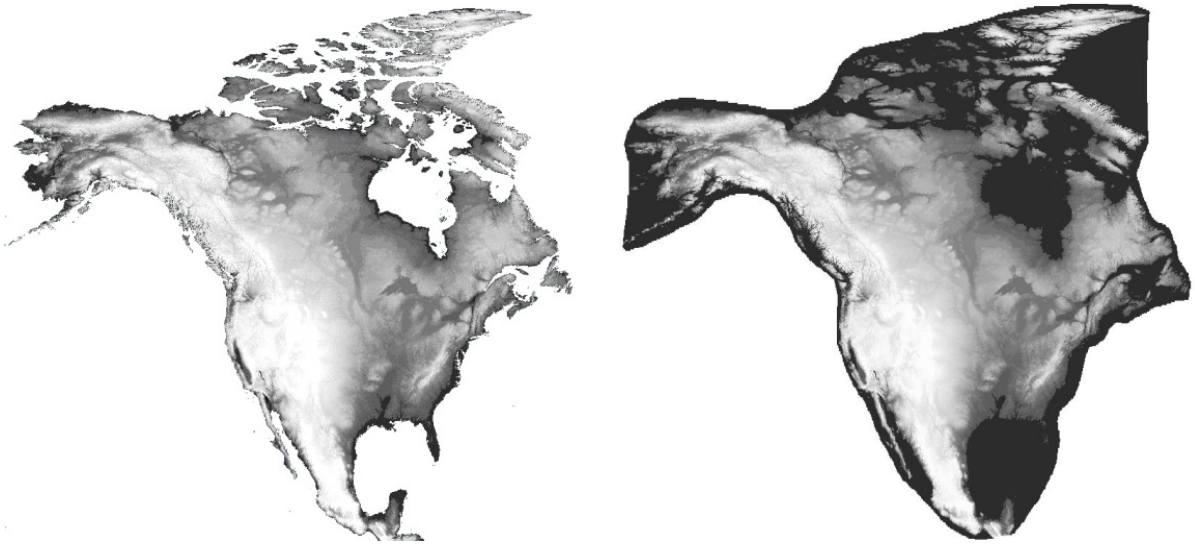

Figure 4-18: Location of ocean for resetting the derived parameters shown in white: a) original ocean definition; b) modified ocean definition.

a) b)

Figure 4-19: Effect of ocean definition on distance to ocean to the northeast: a) original ocean definition; b) modified ocean definition.

Also, in the original square-grid technique, the influence of a physiographic feature had a constant influence no matter how far away it was from the station of interest. For example, when calculating barrier height, the value was dependent on the single greatest elevation between a station location and the ocean in a certain direction. But it was thought that is was not realistic that this elevation should have the same influence on a point that is 100 km away as one that is 1500 km away.

To account for this dwindling influence, a decay factor was put into the derived parameters so that their influence would lessen further away from the physiographic feature. In the original formulation of barrier height from the west (Figure 4-20a), the values calculated after crossing the Rocky Mountains were constant over the rest of the continent. However, the modified barrier height (Figure 4-20b) shows the influence of the Rocky Mountains starting to diminish over the Prairies and other points of high elevation affecting the value of the barrier height on the eastern part of the continent.

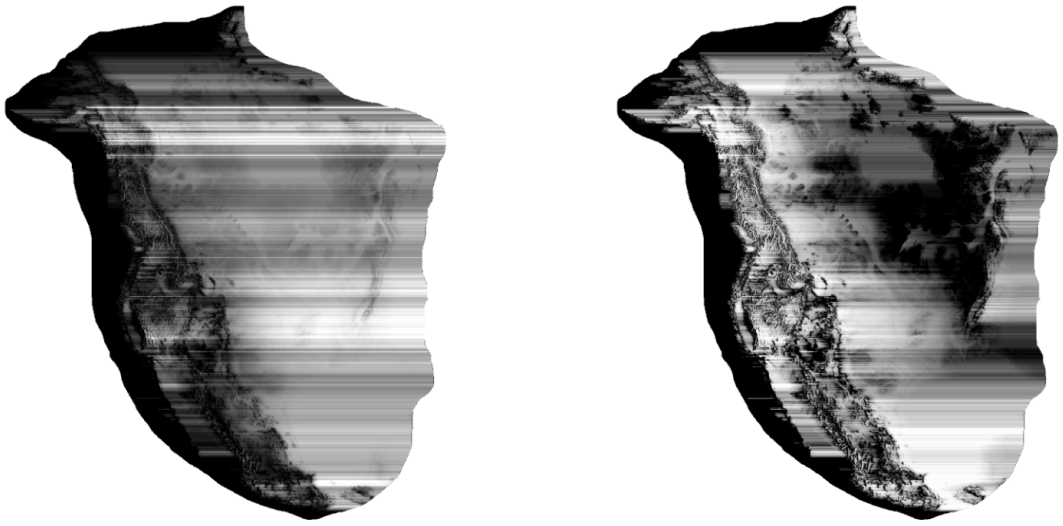

a) **b)**

Figure 4-20: Barrier height from the west: a) without decay; b) with decay.

4.4.5 WATMAPPR technique – monthly precipitation

As a first step, the WATMAPPR technique was used assuming the same regression equations for all of Canada, that is, treating the entire country as one region. The interpolation of total precipitation for July (Figure 4-21) resulted in an interpolation that was very homogeneous and did not show known areas of high precipitation such as along the west coast.

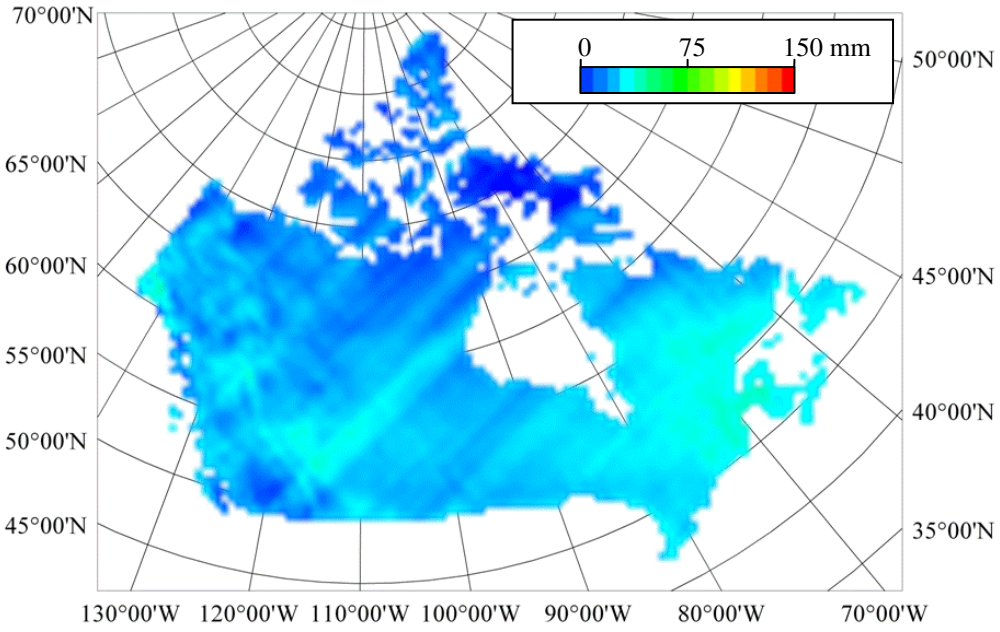

Figure 4-21: WATMAPPR interpolation of July total precipitation using a single region.

When comparing the RMSE results using both interpolation techniques (Table 4-4), the error was much lower using the IWD interpolation, although the same general monthly patterns existed with generally better results in the summer.

Examining the ME results from the WATMAPPR interpolation it was seen that the nature of the regression interpolation caused very little bias in the interpolated values. The ME values were in general one to two orders of magnitude less than in the IWD interpolation while the fact that some months are positive and some are negative resulted in the overall average to be very close to zero (0.003 %).

Table 4-4: RMSE and ME values for both IWD and WATMAPPR interpolation of average monthly precipitation using a single region.

IWD		
Month	RMSE	ME
Jan	32.6%	-0.64%
Feb	36.3%	-0.62%
Mar	30.4%	-0.44%
Apr	25.6%	-0.28%
May	16.2%	-0.09%
Jun	13.5%	-0.12%
Jul	12.7%	-0.24%
Aug	12.7%	-0.58%
Sep	19.6%	-0.86%
Oct	32.5%	-1.08%
Nov	30.9%	-0.84%
Dec	32.8%	-0.59%
Ann	24.6%	-0.53%

WATMAPPR		
Month	RMSE	ME
Jan	43.9%	0.00%
Feb	50.0%	0.25%
Mar	40.8%	-0.01%
Apr	36.5%	0.05%
May	23.7%	0.01%
Jun	20.8%	0.00%
Jul	20.3%	0.02%
Aug	20.2%	0.01%
Sep	27.5%	0.01%
Oct	44.6%	0.02%
Nov	42.7%	0.01%
Dec	42.6%	0.01%
Ann	34.5%	0.03%

The WATMAPPR interpolation of precipitation for January (Figure 4-22) resulted in many regions with high error values, especially on the west coast and Arctic regions of Canada. Although no area of the country showed very good results.

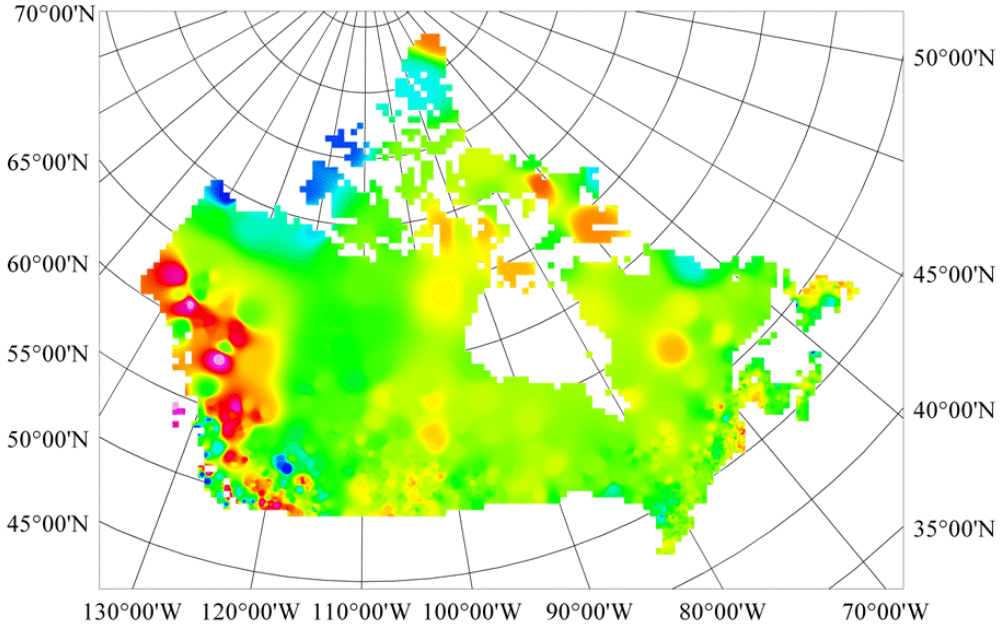

Figure 4-22: Error map for precipitation using the WATMAPPR interpolation technique with one region.

An assumption of the WATMAPPR technique was that the differences in the dependent variables for all the points in the study area were related to the same factors. For the station parameters (such

as elevation, slope, and so on) it generally does not depend on the location of the station. However, when considering the derived parameters (such as shield effect from the west), the influence of a parameter such as distance to the ocean to the west would be much greater for a point on the west coast as compared to a point on the east coast.

Thus it was unrealistic to assume that the same influence factors that were important on the west coast of Canada would also be relevant on the east coast. This demonstrated the need to separate the country into different regions when using the WATMAPPR technique on an area of this size. It was hoped that a minimum number of regions would be necessary as there was often a discontinuity in the interpolation at the boundaries between the regions.

As a first attempt at regionalization, the country was divided into three regions representing the Western, Central, and Eastern regions of the country (Figure 4-23). This was done both on the basis of the error maps produced from the interpolation and using knowledge of the general weather patterns across the country.

The boundary between the West and Central regions was the easiest to designate at it was assigned to be at the eastern edge of the Rocky Mountains. However, the demarcation between the Central and Eastern regions was more arbitrary. It was eventually decided to split the regions in Northern Ontario where areas to the west of the boundary would show a more continental climate with weather systems approaching from the north and west while areas to the east of the boundary would be more typically influenced by weather systems approaching from the American mid-west.

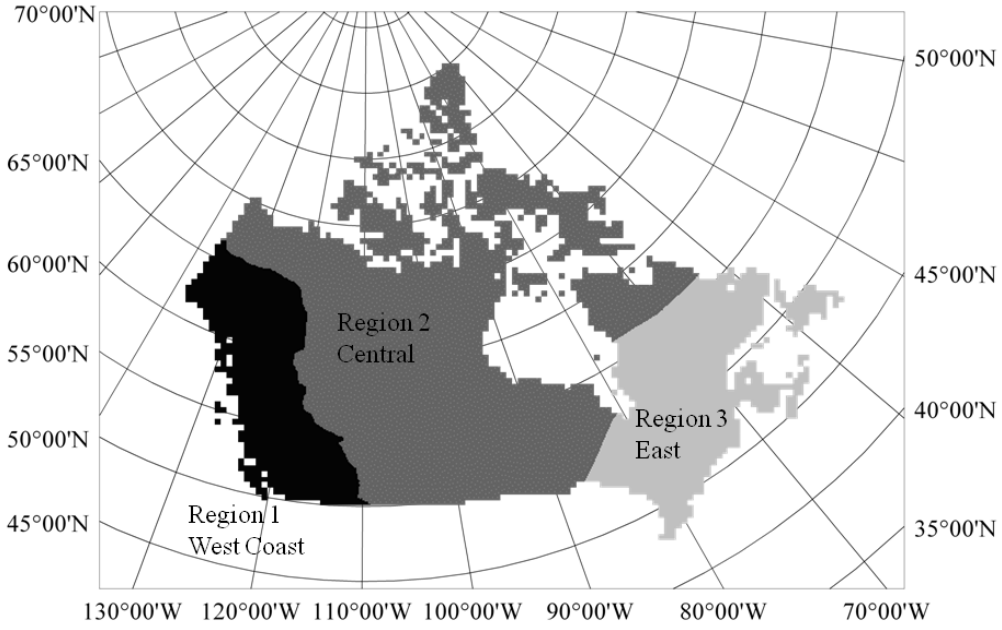

Figure 4-23: Map showing the locations of the three regions used in the WATMAPPR technique.

The WATMAPPR technique was then implemented separately on each region. However, when creating the regression equations, not only were stations within that region used, but also stations that were less than 200 km from the border with the neighbouring regions. It was thought that this would allow for a smoother transition in the interpolated values between the regions. The results from the RMSE and ME analysis using the WATMAPPR technique were now closer to the values obtained using the IWD interpolation (Table 4-5). The IWD factors that resulted in the lowest RMSE for the IWD interpolation were also recalculated and for Region 1 the best IWD factor was now 3.0 and for both Regions 2 and 3 a factor of 5.0 resulted in the lowest RMSE.

In Region 1 (West Coast), the average RMSE for the IWD was less than that for the WATMAPPR while the absolute value of ME was less using WATMAPPR in all months. The ME was negative using IWD and positive using WATMAPPR. Both techniques saw generally worse results in the winter months.

For Region 2 (Central), the overall average of RMSE was close to 20% using both techniques, with some months having lower values using IWD and some using WATMAPPR. Both techniques resulted in better values in the winter months with the summer months not performing as well. Once again the ME values were better for the WATMAPPR technique.

The IWD interpolation resulted in a smaller value of RMSE in Region 3 (East Coast) then WATMAPPR in both the overall average and for each of the individual months. For the IWD technique the summer and fall months showed a negative ME value, while the winter and spring months had positive values. These ME values were up to an order of magnitude larger than the corresponding values using WATMAPPR.

The error map for the WATMAPPR interpolation of precipitation using three regions (Figure 4-24) showed a marked improvement over using just a single region (Figure 4-22). In general, more of the error map was green in colour and there was an overall reduction in the number of underestimated and overestimated regions (that is, less red and blue areas). In particular, the Arctic islands showed much less error and the areas of overestimation were much smaller in the Rocky Mountains.

Each of the three regions was then subdivided again, taking into consideration the location of the errors and the prevalent weather conditions. The West Coast was divided so that the very highest precipitation values on the extreme western areas of the region had their own region. The Central region was split so that the Prairie region and the Arctic regions could have separate equations. The dividing line coincided with the northern limit of tree line. The East Coast region was the most difficult to split but in the end, the Great Lakes region up to the Ottawa River was split from the Maritimes and Newfoundland and Labrador (Figure 4-25).

The values of RMSE and RSE were then calculated on the basis of the six regions for both the WATMAPPR and IWD technique (Table 4-6 and Table 4-7). The optimal value of the IWD factor was 3.0 for Regions 3,4, and 5, while both Regions 1 and 2 had a value of 4.0, and an IWD factor of 5 in Region 6 gave the lowest values for RMSE.

Table 4-5: RMSE and ME values for both IWD and WATMAPPR interpolation of average monthly precipitation using 3 regions.

IWD		
Region 1		
Month	RMSE	ME
Jan	22.2%	-2.22%
Feb	27.3%	-1.91%
Mar	24.9%	-1.50%
Apr	29.1%	-1.31%
May	20.3%	-1.36%
Jun	20.0%	-0.96%
Jul	19.6%	-1.87%
Aug	20.1%	-1.93%
Sep	26.8%	-2.30%
Oct	31.5%	-2.97%
Nov	20.5%	-1.36%
Dec	19.9%	-1.39%
Ann	23.5%	-1.76%

WATMAPPR		
Region 1		
Month	RMSE	ME
Jan	39.4%	0.48%
Feb	46.9%	0.44%
Mar	45.4%	0.55%
Apr	45.0%	0.40%
May	34.5%	0.50%
Jun	27.4%	0.46%
Jul	27.3%	0.41%
Aug	30.2%	0.44%
Sep	40.7%	0.54%
Oct	47.1%	0.69%
Nov	40.5%	0.45%
Dec	41.4%	0.42%
Ann	38.8%	0.48%

IWD		
Region 2		
Month	RMSE	ME
Jan	27.8%	3.96%
Feb	27.9%	4.02%
Mar	24.4%	3.34%
Apr	19.7%	1.80%
May	14.7%	1.22%
Jun	12.9%	1.00%
Jul	13.1%	0.85%
Aug	12.4%	0.33%
Sep	13.4%	0.31%
Oct	19.1%	1.31%
Nov	24.8%	2.48%
Dec	27.5%	3.75%
Ann	19.8%	2.03%

WATMAPPR		
Region 2		
Month	RMSE	ME
Jan	24.1%	0.41%
Feb	23.7%	0.27%
Mar	23.8%	0.35%
Apr	15.6%	0.10%
May	13.3%	0.16%
Jun	13.7%	0.53%
Jul	15.5%	0.30%
Aug	14.1%	0.38%
Sep	16.7%	0.90%
Oct	20.7%	0.85%
Nov	24.1%	0.66%
Dec	23.6%	0.46%
Ann	19.1%	0.45%

IWD		
Region 3		
Month	RMSE	ME
Jan	16.5%	0.08%
Feb	15.5%	0.38%
Mar	13.4%	0.31%
Apr	11.3%	0.33%
May	9.1%	0.29%
Jun	9.3%	-0.08%
Jul	9.1%	-0.33%
Aug	8.5%	-0.45%
Sep	10.3%	-0.34%
Oct	10.2%	-0.13%
Nov	11.5%	-0.12%
Dec	14.4%	0.36%
Ann	11.6%	0.03%

WATMAPPR		
Region 3		
Month	RMSE	ME
Jan	18.5%	-0.07%
Feb	15.9%	0.00%
Mar	14.2%	-0.01%
Apr	12.4%	-0.02%
May	9.8%	-0.01%
Jun	10.6%	-0.08%
Jul	11.2%	-0.08%
Aug	9.2%	-0.03%
Sep	10.9%	-0.08%
Oct	11.8%	-0.10%
Nov	13.3%	-0.04%
Dec	15.6%	-0.06%
Ann	12.8%	-0.05%

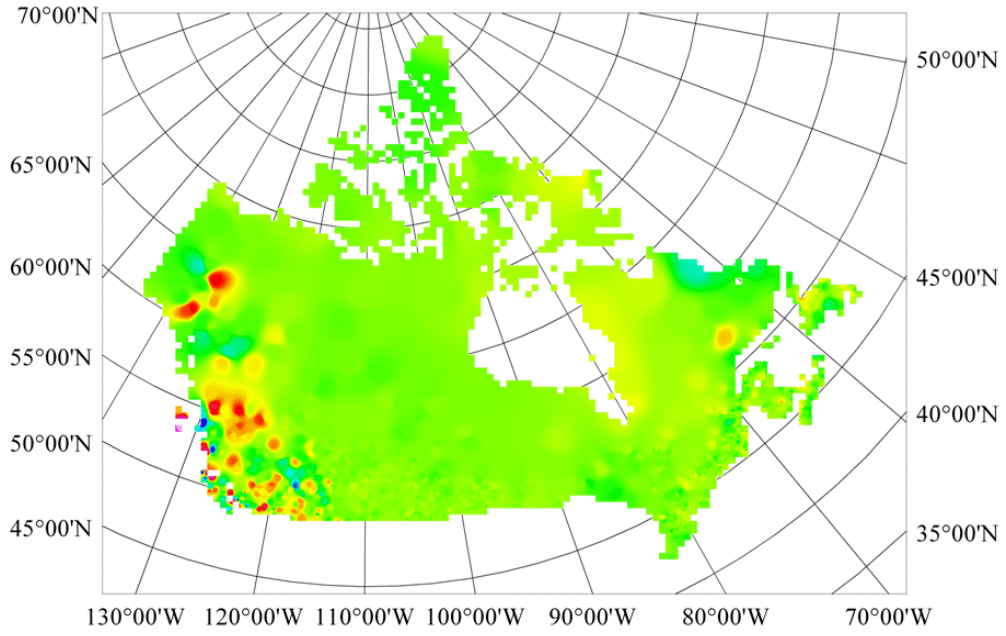

Figure 4-24: Error map for precipitation using the WATMAPPR interpolation technique with three regions.

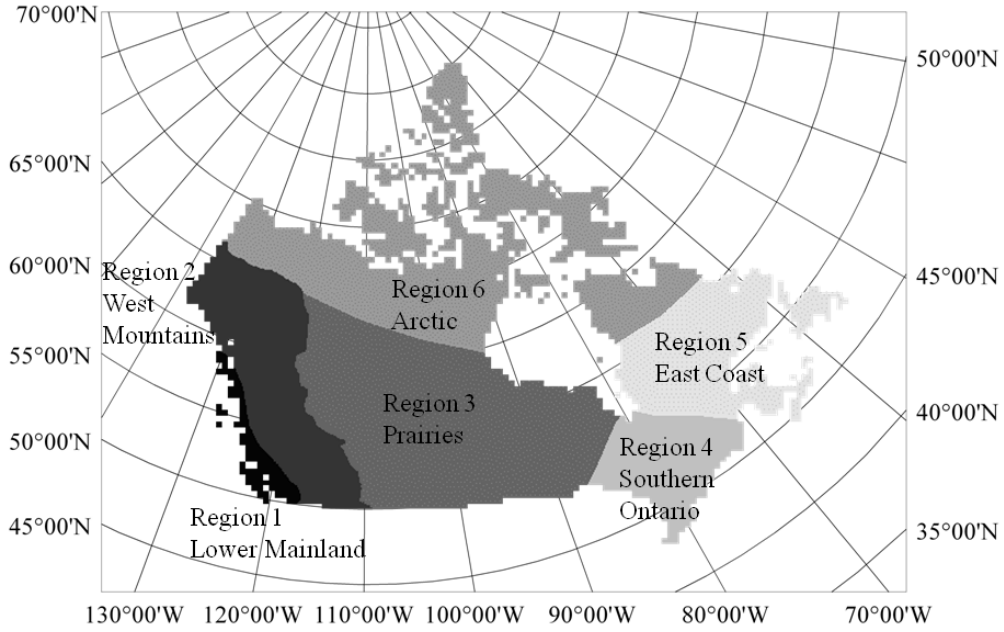

Figure 4-25: Map showing the locations of the six regions used in the WATMAPPR technique.

For Region 1 (lower mainland), the WATMAPPR technique resulted in lower RMSE values during almost all months (the 27.9% value of using WATMAPPR in June was slightly higher than the 26.9% value from IWD) and a much lower overall value (28.4% compared to 32.0%). Both techniques showed a negative bias, but at -0.3%, the WATMAPPR technique results were much smaller than the 3.0% seen using IWD.

Region 2 (west mountains) was one of the regions in which neither technique consistently resulted in lower RMSE values, although the pattern of better results in summer was seen using both. Overall the RMSE was lower using IWD (30.4%) compared to using WATMAPPR (34.6%). The absolute ME values were consistently smaller using WATMAPPR for all months. One reason this is a difficult region in which to interpolate precipitation data may be a result of undercatch of the precipitation caused by wind. This problem would be greatest in the mountainous areas as they generally have higher wind speeds than other areas of the country and have higher wind speeds in the winter (Glazer *et al.*, 2005)

For eight of the months of the year, the RMSE values were lower using WATMAPPR in Region 3 (prairies) and the values were very close in the other four months. The overall average of 14.1% using WATMAPPR was lower than the 15.0% using IWD. Once again the ME value was an order of magnitude lower using the WATMAPPR technique.

Region 4 (southern Ontario) resulted in a eight months of the year having a lower RMSE using the IWD technique and the same the overall average of 9.7%. This was also the region that had the lowest overall value of RMSE of any region, perhaps as a result of the density of measurement stations and relatively flat terrain.

The results from Region 5 (east coast) again showed lower RMSE in most months using the WATMAPPR technique and a slightly lower overall average RMSE (12.5% compared to 12.8% using IWD) along with generally lower absolute ME values. However the overall average ME is lower as a result of there being some large values that were both positive and negative that cancelled each other out when calculating the average.

The results in Region 6 (Arctic) were much better using WATMAPPR with lower values in all the months and a much lower value of ME. However, in general the Arctic region had the highest overall RMSE values, this could be a result of the low density of measurement stations. It was also encouraging to see the WATMAPPR technique do well in this region as it should perform better than the IWD technique in areas of sparse data.

Table 4-6: RMSE and ME values for both IWD and WATMAPPR interpolation of average monthly precipitation using six regions; Regions 1, 2, and 3 shown here.

IWD		
Region 1		
Month	RMSE	ME
Jan	29.6%	-2.56%
Feb	34.0%	-3.07%
Mar	33.1%	-2.98%
Apr	35.6%	-3.29%
May	31.6%	-3.19%
Jun	26.9%	-2.13%
Jul	28.8%	-2.09%
Aug	28.6%	-2.88%
Sep	38.0%	-4.28%
Oct	37.4%	-3.98%
Nov	30.0%	-2.87%
Dec	30.9%	-3.00%
Ann	32.0%	-3.03%

WATMAPPR		
Region 1		
Month	RMSE	ME
Jan	24.3%	-0.07%
Feb	30.2%	0.04%
Mar	28.8%	-0.39%
Apr	32.5%	-0.26%
May	28.8%	-0.61%
Jun	27.9%	-0.27%
Jul	27.1%	-0.38%
Aug	26.3%	-0.26%
Sep	32.8%	-0.13%
Oct	30.2%	-0.31%
Nov	25.8%	-0.10%
Dec	26.6%	-0.22%
Ann	28.4%	-0.25%

IWD		
Region 2		
Month	RMSE	ME
Jan	37.2%	-2.10%
Feb	43.9%	-1.67%
Mar	43.7%	-1.16%
Apr	30.9%	-0.26%
May	18.0%	-0.89%
Jun	18.5%	-0.94%
Jul	16.1%	-1.49%
Aug	17.3%	-1.62%
Sep	24.8%	-1.61%
Oct	38.4%	-1.89%
Nov	38.4%	-1.44%
Dec	37.9%	-1.43%
Ann	30.4%	-1.37%

WATMAPPR		
Region 2		
Month	RMSE	ME
Jan	50.7%	0.78%
Feb	19.0%	1.32%
Mar	70.6%	0.38%
Apr	60.0%	0.12%
May	34.3%	-0.24%
Jun	21.6%	-0.23%
Jul	18.1%	0.55%
Aug	25.4%	0.57%
Sep	22.8%	0.19%
Oct	21.3%	0.50%
Nov	30.1%	0.89%
Dec	40.9%	1.23%
Ann	34.6%	0.50%

IWD		
Region 3		
Month	RMSE	ME
Jan	19.0%	2.18%
Feb	18.7%	1.90%
Mar	17.9%	1.64%
Apr	14.7%	0.43%
May	11.7%	0.36%
Jun	11.1%	0.32%
Jul	11.5%	0.21%
Aug	11.0%	-0.51%
Sep	11.7%	-0.65%
Oct	15.6%	-0.63%
Nov	18.9%	0.31%
Dec	18.6%	2.14%
Ann	15.0%	0.64%

WATMAPPR		
Region 3		
Month	RMSE	ME
Jan	17.1%	0.00%
Feb	17.9%	-0.18%
Mar	16.2%	0.00%
Apr	13.0%	0.15%
May	11.8%	0.15%
Jun	11.6%	-0.05%
Jul	11.5%	-0.24%
Aug	10.6%	-0.13%
Sep	11.8%	-0.06%
Oct	13.6%	0.05%
Nov	17.4%	-0.01%
Dec	16.9%	0.16%
Ann	14.1%	-0.01%

Table 4-7: RMSE and ME values for both IWD and WATMAPPR interpolation of average monthly precipitation using six regions; Regions 4, 5, and 6 shown here.

IWD		
Region 4		
Month	RMSE	ME
Jan	15.3%	-0.63%
Feb	14.1%	-0.13%
Mar	10.8%	-0.29%
Apr	7.9%	0.35%
May	7.0%	0.34%
Jun	7.3%	0.03%
Jul	7.8%	-0.03%
Aug	7.1%	-0.20%
Sep	7.8%	-0.03%
Oct	8.7%	-0.02%
Nov	9.5%	0.00%
Dec	13.5%	-0.19%
Ann	9.7%	-0.07%

WATMAPPR		
Region 4		
Month	RMSE	ME
Jan	17.7%	0.05%
Feb	14.4%	-0.03%
Mar	10.8%	0.04%
Apr	8.1%	0.05%
May	7.0%	-0.02%
Jun	6.6%	-0.07%
Jul	6.5%	-0.05%
Aug	7.5%	-0.03%
Sep	9.2%	0.00%
Oct	9.0%	-0.04%
Nov	9.8%	0.03%
Dec	9.3%	0.06%
Ann	9.7%	0.00%

IWD		
Region 5		
Month	RMSE	ME
Jan	16.6%	0.75%
Feb	15.3%	0.83%
Mar	14.4%	0.79%
Apr	14.1%	0.41%
May	11.4%	0.10%
Jun	11.4%	-0.51%
Jul	10.7%	-0.71%
Aug	9.9%	-0.56%
Sep	12.4%	-0.73%
Oct	11.0%	0.01%
Nov	12.7%	-0.19%
Dec	14.2%	0.77%
Ann	12.8%	0.08%

WATMAPPR		
Region 5		
Month	RMSE	ME
Jan	16.6%	0.06%
Feb	15.3%	0.18%
Mar	14.4%	0.18%
Apr	14.2%	0.25%
May	10.7%	0.26%
Jun	11.8%	0.39%
Jul	10.4%	0.38%
Aug	9.4%	0.37%
Sep	12.0%	0.30%
Oct	9.9%	0.15%
Nov	11.7%	0.15%
Dec	14.1%	0.04%
Ann	12.5%	0.23%

IWD		
Region 6		
Month	RMSE	ME
Jan	71.8%	35.59%
Feb	69.5%	33.43%
Mar	55.8%	25.19%
Apr	53.4%	21.93%
May	45.6%	24.51%
Jun	33.3%	20.69%
Jul	28.7%	13.72%
Aug	27.6%	9.44%
Sep	31.8%	10.77%
Oct	32.9%	14.74%
Nov	45.5%	23.70%
Dec	66.1%	27.71%
Ann	46.8%	21.79%

WATMAPPR		
Region 6		
Month	RMSE	ME
Jan	69.6%	3.74%
Feb	57.6%	1.41%
Mar	36.5%	6.18%
Apr	34.8%	-1.97%
May	28.3%	0.93%
Jun	27.8%	1.68%
Jul	21.7%	1.29%
Aug	15.0%	-0.05%
Sep	18.4%	-0.37%
Oct	28.9%	-0.50%
Nov	31.6%	1.48%
Dec	62.6%	4.05%
Ann	36.1%	1.49%

The error map for the WATMAPPR interpolation using six regions had very few areas of red or blue with most of the map green in colour, indicating that most of the country had small errors in the interpolation (Figure 4-26). As well, the errors that did occur were generally well distributed across the country.

There were still some errors seen in the west coast and Rocky Mountains, but these had been reduced to a small number of stations. The error map also compared well with the error map derived from the IWD interpolation technique (Figure 4-11) with generally the same distribution of error; however, the WATMAPPR technique did show less error in northern Quebec.

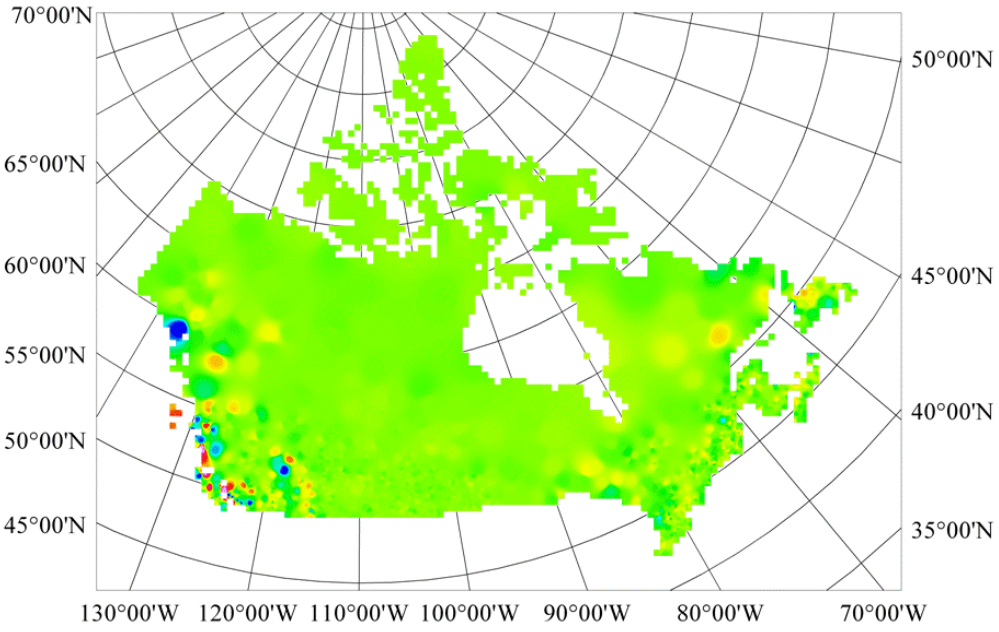

Figure 4-26: Error map for precipitation using the WATMAPPR interpolation technique with six regions.

Again the interpolated maps are presented for January (Figure 4-27) and July (Figure 4-28), while the other months are presented in Appendix B.

When compared to the IWD interpolation, the WATMAPPR interpolation had a much more realistic pattern that did a better job of conforming to the actual physiography of the land surface as well as showing more detailed variations in the precipitation. For example there are variations in the July precipitation over the northern Prairie region that correspond to areas of higher elevation and

thus increased slope. It is not unreasonable that this type of landform would affect the amount of precipitation.

However, there were also some deficiencies in the WATMAPPR interpolation. For instance there were discontinuities at the boundaries between the different regions. This was the most noticeable at the southern boundary of the Arctic region where the average monthly precipitation value appeared to take a sharp jump. In reality there was probably a more gradual transition between the values in the different regions.

Another negative consequence of the WATMAPPR technique was that for some months, particular physiographic parameters that entered into the regression early caused an undulating pattern in the interpolated precipitation fields. This was seen most prominently in the Arctic region, for example in the January map (Figure 4-27). This effect was probably a result of these parameters being significant at the locations of the measured stations and then this relationship was transferred to the rest of the region.

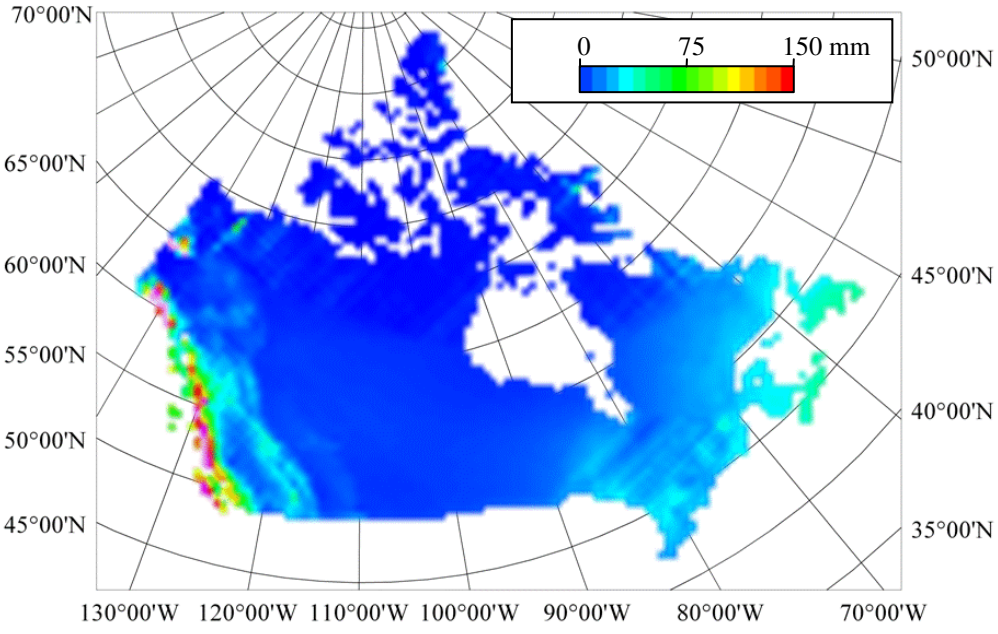

Figure 4-27: WATMAPPR interpolation of January total precipitation using six regions.

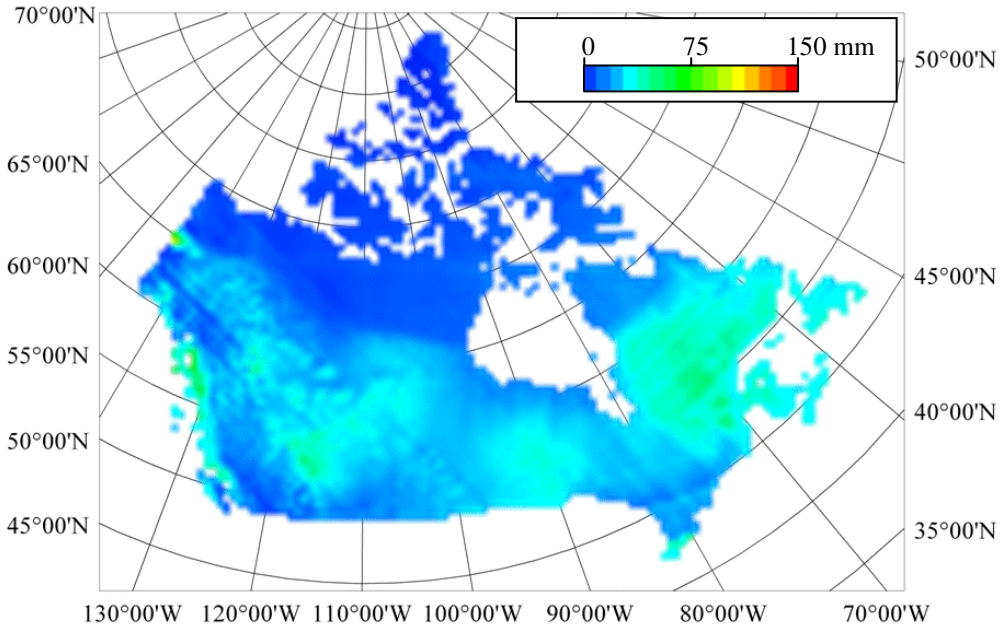

Figure 4-28: WATMAPPR interpolation of July total precipitation using six regions.

4.4.6 WATMAPPR technique – monthly temperature

The WATMAPPR technique was then used to interpolate the monthly maximum and minimum temperatures. As with precipitation, as a first step, the same regression equations were used over the entire country. Once again, the RSME and ME values were not as good as the results from the IWD technique (Table 4-8 and Table 4-9).

Comparing the maximum temperature results, although the WATMAPPR technique performed better in some of the months, the overall average of RMSE was higher than the IWD interpolation. The pattern of higher values in the summer months and lower in the winter months was the same using both techniques. As with the precipitation comparison, the ME for the WATMAPPR technique was a few orders of magnitude less than using IWD.

The minimum temperature results were overall better using IWD, with the WATMAPPR technique only performing better in a couple of months. The same reversal of the higher and lower RMSE values for different months was seen using the WATMAPPR technique and again the ME was much less using WATMAPPR.

Table 4-8: RMSE and ME values for both IWD and WATMAPPR interpolation of average monthly maximum temperature using a single region (all values in degrees).

IWD				WATMAPPR		
Month	RMSE	ME		Month	RMSE	ME
Jan	1.21	0.198		Jan	1.73	0.012
Feb	1.09	0.180		Feb	1.38	0.001
Mar	1.22	0.204		Mar	1.38	0.000
Apr	1.75	0.189		Apr	1.73	0.000
May	1.75	0.192		May	1.83	-0.001
Jun	1.84	0.143		Jun	2.00	-0.004
Jul	1.73	0.132		Jul	1.91	-0.001
Aug	1.69	0.134		Aug	1.75	-0.004
Sep	1.25	0.142		Sep	1.15	-0.001
Oct	1.02	0.164		Oct	1.00	0.001
Nov	1.02	0.158		Nov	1.22	0.001
Dec	1.15	0.165		Dec	1.61	0.002
Ann	1.39	0.167		Ann	1.56	0.001

Table 4-9: RMSE and ME values for both IWD and WATMAPPR interpolation of average monthly minimum temperature using a single region (all values in degrees).

IWD				WATMAPPR		
Month	RMSE	ME		Month	RMSE	ME
Jan	1.65	0.234		Jan	2.30	0.004
Feb	1.65	0.243		Feb	1.96	0.001
Mar	1.62	0.258		Mar	1.59	0.003
Apr	1.55	0.215		Apr	1.47	-0.001
May	1.29	0.165		May	1.32	-0.002
Jun	1.20	0.125		Jun	1.29	-0.001
Jul	1.22	0.122		Jul	1.28	-0.001
Aug	1.25	0.115		Aug	1.26	0.000
Sep	1.24	0.127		Sep	1.23	0.000
Oct	1.24	0.137		Oct	1.38	0.002
Nov	1.36	0.179		Nov	1.60	0.001
Dec	1.57	0.203		Dec	2.14	0.002
Ann	1.40	0.177		Ann	1.57	0.001

The error maps of the temperature interpolations (Figure 4-29 and Figure 4-30) generally showed that even using the WATMAPPR technique with a single region resulted in only a few areas of extreme error values. The only areas that resulted in large amounts of error were on the Arctic islands and in the northern Rocky Mountains.

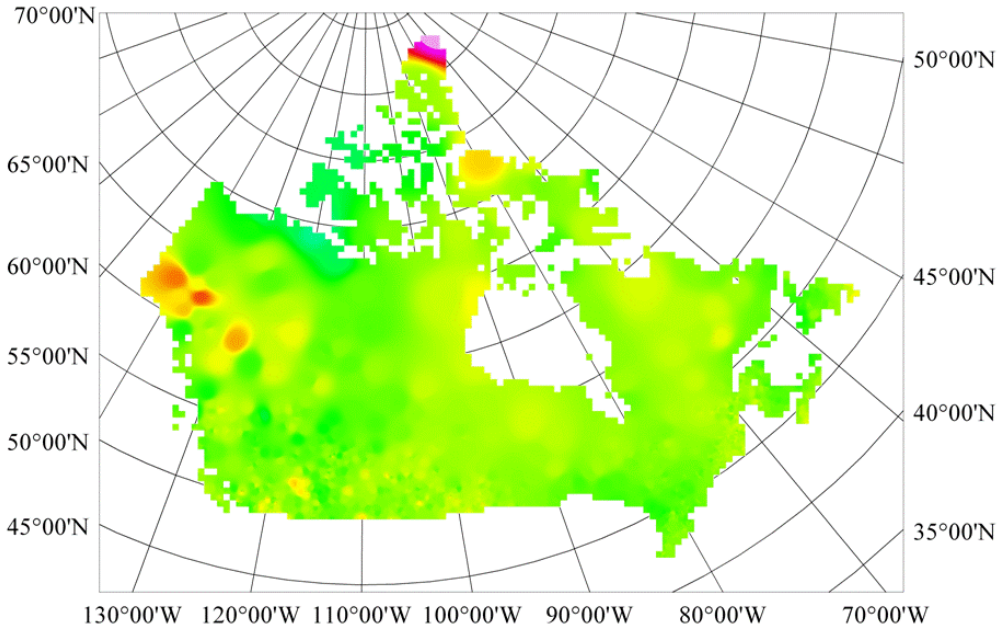

Figure 4-29: Error map for maximum temperature using the WATMAPPR interpolation technique with one region.

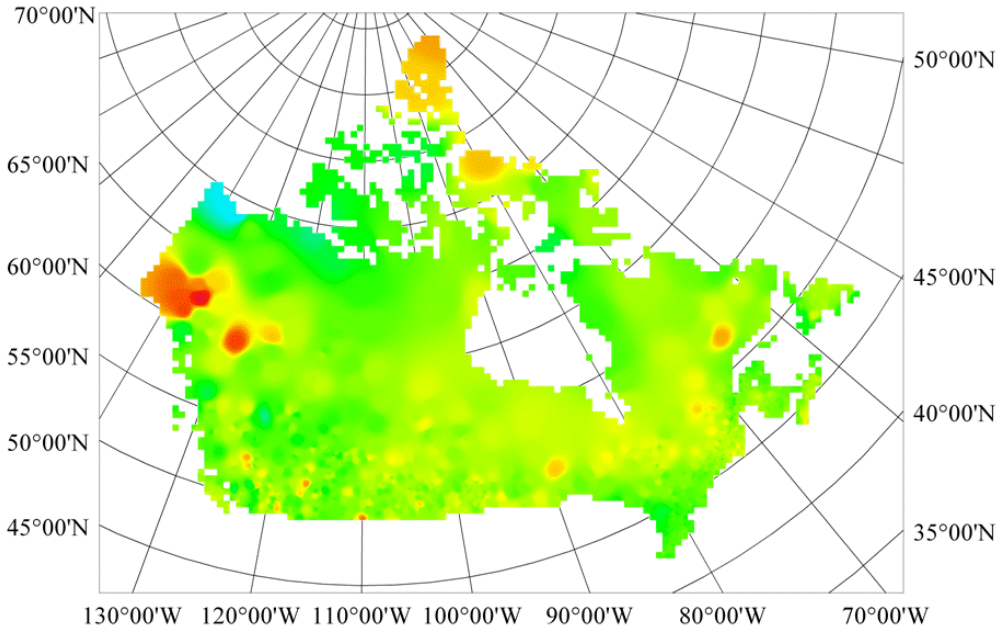

Figure 4-30: Error map for minimum temperature using the WATMAPPR interpolation technique with one region.

The WATMAPPR technique was then used to interpolate the temperature data based on the same three regions that were initially chosen for the precipitation interpolation. The results of the RMSE and ME analysis for maximum temperature on the three regions (Table 4-10) showed that the WATMAPPR technique produced a smaller RMSE in all but a few cases. The overall average RMSE was lower using WATMAPPR for all regions.

The same pattern of the highest RMSE values in the summer months was seen in all the regions. Similar values were found for RMSE in both Regions 1 and 2, while values for Region 3 were significantly lower. Again the ME values for the WATMAPPR technique were a few orders of magnitude less than the IWD technique.

For minimum temperature (Table 4-11), the WATMAPPR technique again resulted in lower values of RMSE for almost all months in all regions. As with the single-region analysis, the highest values of RMSE were seen in the winter or spring months; however, unlike the maximum temperature results, the results from Region 3 were not significantly better than for Regions 1 and 2.

For both the maximum and minimum temperature in Region 1 the best value for the IWD factor was 3.0 while it was 5.0 for Regions 2 and 3, also for both maximum and minimum temperature.

Table 4-10: RMSE and ME values for both IWD and WATMAPPR interpolation of average monthly maximum temperature using three regions (all values in degrees).

IWD			WATMAPPR		
Region 1			Region 1		
Month	RMSE	ME	Month	RMSE	ME
Jan	1.59	-0.052	Jan	1.43	0.004
Feb	1.34	0.010	Feb	1.30	0.005
Mar	1.62	0.108	Mar	1.60	0.002
Apr	1.77	0.112	Apr	1.77	-0.002
May	1.89	0.122	May	1.85	-0.001
Jun	2.47	0.045	Jun	2.31	-0.001
Jul	2.42	0.085	Jul	2.30	-0.004
Aug	2.45	0.063	Aug	2.31	-0.005
Sep	1.60	0.068	Sep	1.53	-0.002
Oct	1.24	0.112	Oct	1.19	0.000
Nov	1.43	0.096	Nov	1.31	0.006
Dec	1.62	0.002	Dec	1.53	0.003
Ann	1.79	0.064	Ann	1.70	0.000

IWD			WATMAPPR		
Region 2			Region 2		
Month	RMSE	ME	Month	RMSE	ME
Jan	1.37	0.500	Jan	1.33	-0.002
Feb	1.26	0.462	Feb	1.20	-0.002
Mar	1.34	0.433	Mar	1.35	0.002
Apr	2.42	0.269	Apr	1.79	0.006
May	2.14	0.186	May	1.76	0.003
Jun	1.83	0.097	Jun	1.56	0.000
Jul	1.61	0.061	Jul	1.34	-0.001
Aug	1.57	0.095	Aug	1.22	0.000
Sep	1.41	0.163	Sep	0.98	-0.001
Oct	1.19	0.282	Oct	0.89	0.000
Nov	1.04	0.298	Nov	1.18	-0.003
Dec	1.18	0.372	Dec	1.33	-0.005
Ann	1.53	0.268	Ann	1.33	0.000

IWD			WATMAPPR		
Region 3			Region 3		
Month	RMSE	ME	Month	RMSE	ME
Jan	0.80	0.128	Jan	0.75	0.000
Feb	0.76	0.095	Feb	0.69	0.001
Mar	0.74	0.105	Mar	0.69	0.000
Apr	0.83	0.130	Apr	0.81	0.001
May	1.10	0.176	May	1.13	0.002
Jun	1.19	0.163	Jun	1.25	0.001
Jul	1.17	0.162	Jul	1.21	0.001
Aug	0.98	0.149	Aug	0.96	0.001
Sep	0.74	0.130	Sep	0.71	0.001
Oct	0.69	0.115	Oct	0.60	0.000
Nov	0.70	0.110	Nov	0.62	0.001
Dec	0.77	0.106	Dec	0.75	0.001
Ann	0.87	0.131	Ann	0.85	0.001

Table 4-11: RMSE and ME values for both IWD and WATMAPPR interpolation of average monthly minimum temperature using three regions (all values in degrees).

IWD			WATMAPPR		
Region 1			Region 1		
Month	RMSE	ME	Month	RMSE	ME
Jan	2.18	-0.012	Jan	1.99	0.000
Feb	1.96	0.046	Feb	1.79	-0.002
Mar	1.87	0.076	Mar	1.75	0.001
Apr	1.56	0.109	Apr	1.48	0.000
May	1.50	0.088	May	1.47	-0.003
Jun	1.50	0.031	Jun	1.53	-0.005
Jul	1.50	0.050	Jul	1.51	-0.003
Aug	1.63	0.067	Aug	1.58	0.000
Sep	1.64	0.121	Sep	1.56	0.002
Oct	1.61	0.108	Oct	1.44	0.003
Nov	1.94	0.089	Nov	1.75	0.000
Dec	2.26	0.012	Dec	2.13	-0.001
Ann	1.76	0.065	Ann	1.66	-0.001

IWD			WATMAPPR		
Region 2			Region 2		
Month	RMSE	ME	Month	RMSE	ME
Jan	1.70	0.461	Jan	1.60	-0.002
Feb	1.84	0.448	Feb	1.56	-0.001
Mar	2.02	0.463	Mar	1.57	0.003
Apr	2.15	0.321	Apr	1.51	0.007
May	1.53	0.177	May	1.28	0.004
Jun	1.19	0.092	Jun	1.06	0.002
Jul	1.17	0.086	Jul	0.97	-0.001
Aug	1.10	0.089	Aug	0.98	-0.001
Sep	1.14	0.157	Sep	0.90	0.001
Oct	1.32	0.219	Oct	1.13	0.002
Nov	1.38	0.321	Nov	1.33	0.001
Dec	1.46	0.377	Dec	1.52	-0.014
Ann	1.50	0.268	Ann	1.28	0.000

IWD			WATMAPPR		
Region 3			Region 3		
Month	RMSE	ME	Month	RMSE	ME
Jan	1.27	0.193	Jan	1.28	0.000
Feb	1.32	0.183	Feb	1.16	0.001
Mar	1.06	0.191	Mar	0.81	0.000
Apr	0.83	0.159	Apr	0.63	0.001
May	0.84	0.148	May	0.70	0.001
Jun	0.90	0.143	Jun	0.82	0.001
Jul	0.97	0.135	Jul	0.94	0.000
Aug	1.02	0.114	Aug	1.46	0.000
Sep	1.05	0.083	Sep	0.92	0.000
Oct	0.98	0.092	Oct	0.87	0.000
Nov	0.95	0.117	Nov	0.88	0.000
Dec	1.19	0.168	Dec	1.22	0.000
Ann	1.03	0.144	Ann	0.97	0.000

Once again, the error maps showed that the three-region interpolation did a very good job of reducing the overall amount of error across the entire country, with bias only apparent in a few scattered stations (Figure 4-31 and Figure 4-32). The error maps using the WATMAPPR technique showed quite an improvement over those using the IWD technique (Figure 4-16 and Figure 4-17) with a significant reduction in the error in both the Arctic islands and the northern mainland of Canada.

Since using three regions produced reasonable RMSE results and the error maps did not show any large areas of incorrect temperatures, no further splitting of the regions was done for the temperature analysis.

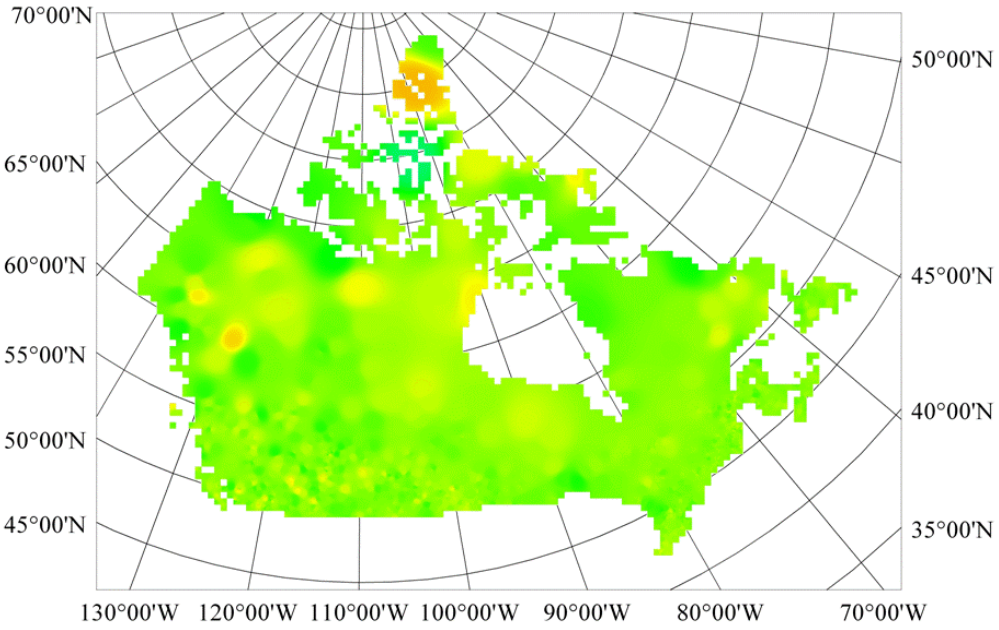

Figure 4-31: Error map for maximum temperature using the WATMAPPR interpolation technique with three regions.

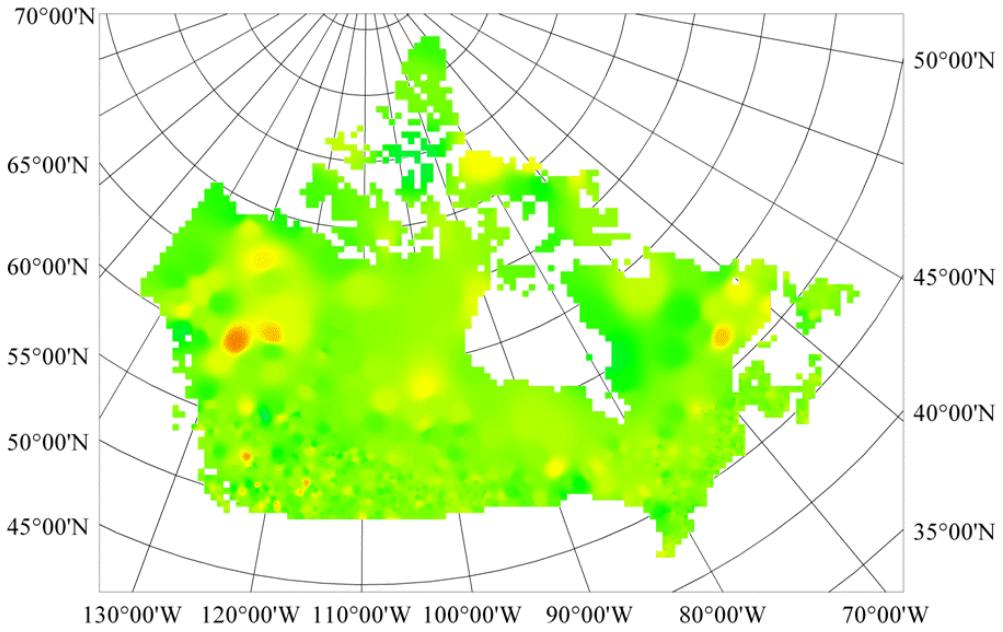

Figure 4-32: Error map for minimum temperature using the WATMAPPR interpolation technique with three regions.

Interpolated maps are presented of maximum temperature for January (Figure 4-33) and July (Figure 4-34) and of minimum temperature for January (Figure 4-35) and July (Figure 4-36), while the WATMAPPR interpolation for the other months are presented in Appendix B.

The general patterns of the WATMAPPR interpolated temperature data were not that surprising, with the overall pattern showing lower temperatures in areas of higher elevation and higher latitude.

As with the precipitation results, there were still some discontinuities at the borders between the regions, however with only three regions they were not as prevalent. As well, as variations were generally a result of changes in elevation and latitude, there was not as much variation in the results between the different regions. However, the undulating pattern seen in the precipitation results unfortunately were also visible in some of the temperature results.

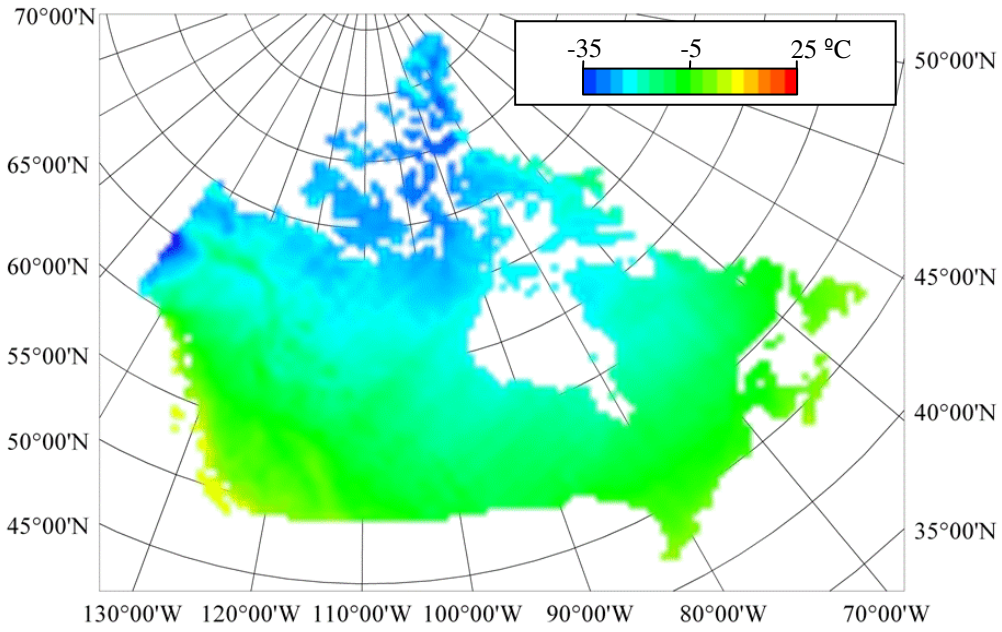

Figure 4-33: WATMAPPR interpolation of January maximum temperature using three regions.

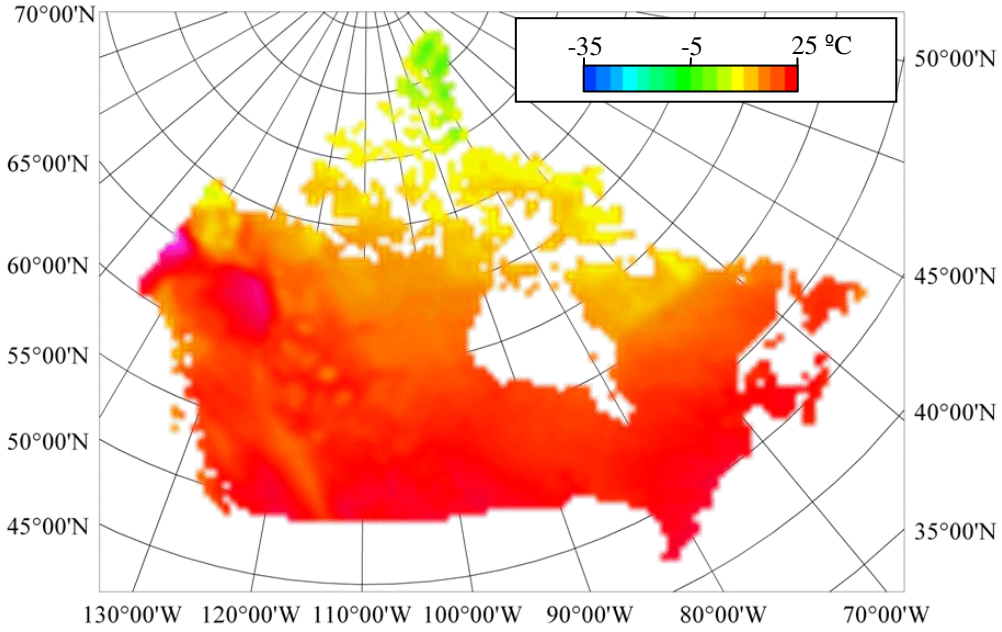

Figure 4-34: WATMAPPR interpolation of July maximum temperature using three regions.

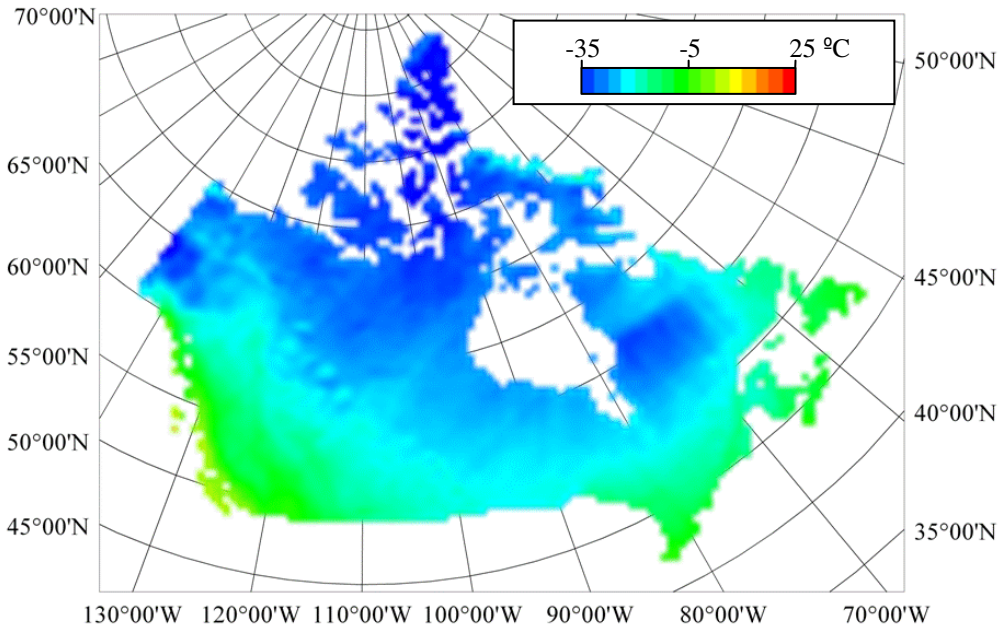

Figure 4-35: WATMAPPR interpolation of January minimum temperature using three regions.

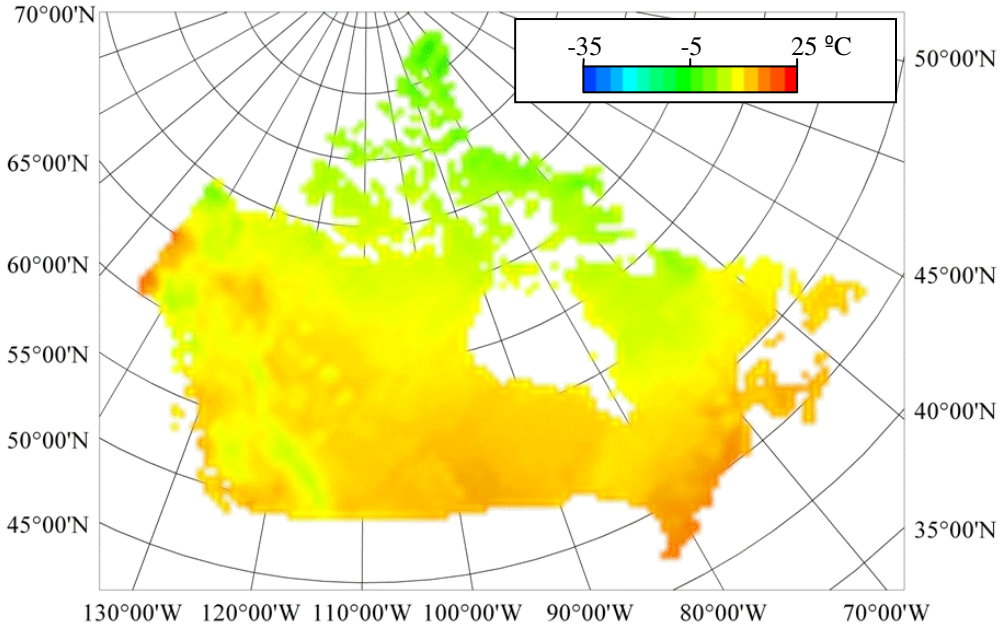

Figure 4-36: WATMAPPR interpolation of July minimum temperature using three regions.

4.5 Interpolating the data - Daily

When interpolating the daily station data, it was possible to use all available data for a particular day as there was no longer a requirement for 20 years worth of readings to be available for a station in order to be included in the analysis. This allowed for more data to be used in the daily interpolation than there was in the monthly interpolation; however the extra number of stations for the daily interpolation was rarely more than 50 for either precipitation or temperature.

4.5.1 IWD technique

The IWD interpolation of daily data was exactly the same technique that was used to interpolate the monthly data. However, when looking at the precipitation data on a daily basis, a majority of the readings for any given day had values of zero. Thus, the inherent weakness of this technique is that the interpolated values for these stations that should have zero values were influenced by the "average" value of the neighbouring stations and thus the technique generally calculated a small amount of precipitation in many areas.

When examining the interpolated daily precipitation for July 1, 1980 (Figure 4-37), the tent-pole effect was clearly seen as well as the interpolated values having a similar distribution around each measurement point.

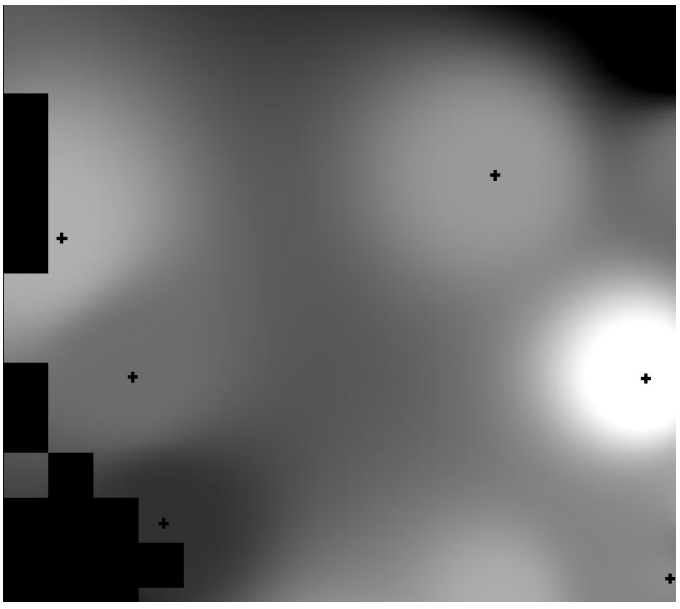

Figure 4-37: Interpolation of precipitation for July 1, 1980 using the IWD technique (image size is approximately 750 km by 750 km). The measurement stations are represented by black crosses.

As with the monthly interpolation, the RMSE was calculated at each point for each day using the leave-one-out technique. The results were summarized by grouping the average RMSE value by year (Figure 4-38) and by each day of the year (Figure 4-39).

The yearly summary showed no overall pattern, indicating that the interpolation is approximately the same for each year. It was thought that the RMSE might be influenced by the number of meteorological stations available for the interpolation (Figure 4-1), but this was not the case.

Interestingly, the pattern seen in the monthly RMSE results (Table 4-1) of precipitation using the IWD was not replicated in the daily RMSE results. Whereas the monthly results showed the highest RMSE values in the winter months and the lowest in the summer, the daily results showed the lowest RMSE values in the late winter and spring and the highest in the summer.

As the temperature was a different type of measurement with an instantaneous value rather than an accumulation, the IWD interpolation technique for the daily values was the same as the monthly values.

The yearly summaries of the daily RMSE numbers for maximum temperature (Figure 4-40) and minimum temperature (Figure 4-42) did not show any strong patterns except for a small downward trend during the study period.

The summary of the daily maximum temperature RMSE values for each day of the year (Figure 4-41) showed the lowest values in the fall and the highest during the winter. For minimum temperature the lower values persisted from the spring to the fall with winter having the highest values.

The RMSE values from the monthly IWD interpolation of the minimum temperatures (Table 4-2) tended to agree with the pattern seen in the daily RMSE values (Figure 4-43) while the maximum temperature monthly IWD interpolation of the minimum temperatures (Table 4-3) did not match well with their daily counterparts.

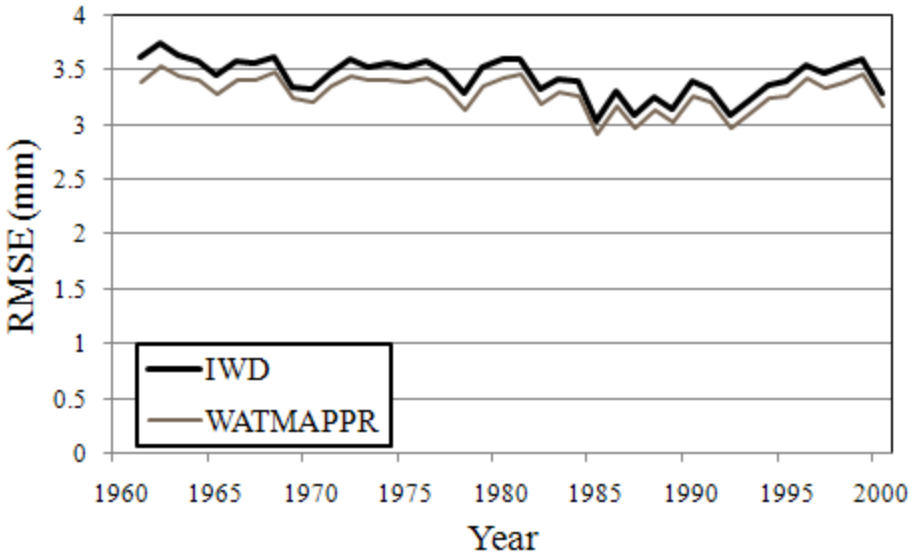

Figure 4-38: Yearly summary of RMSE value for daily IWD and WATMAPPR interpolation of precipitation.

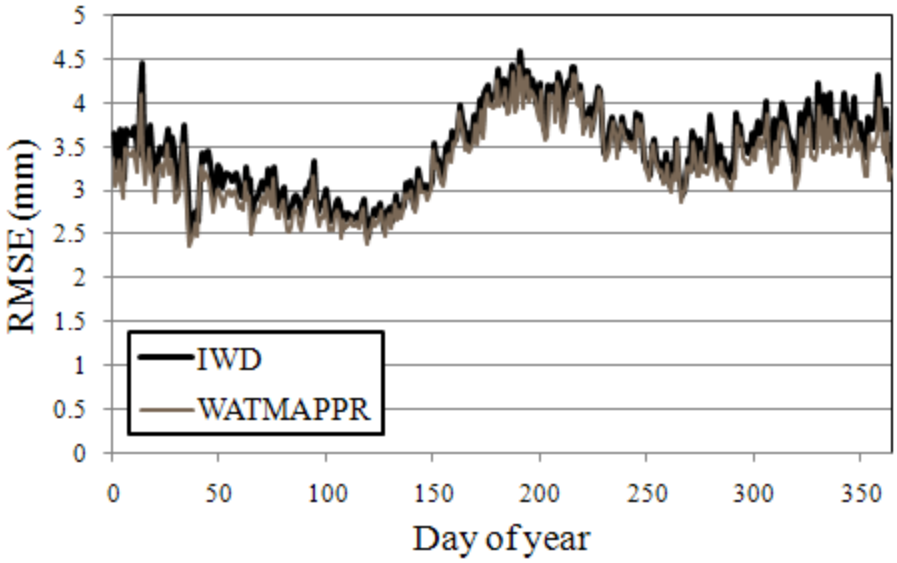

Figure 4-39: Daily summary of RMSE value for daily IWD and WATMAPPR interpolation of precipitation.

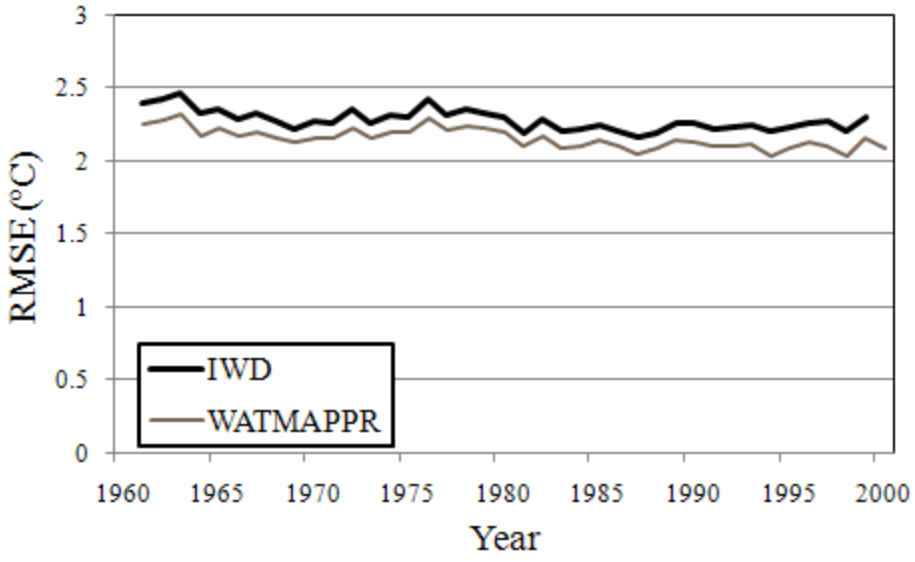

Figure 4-40: Yearly summary of RMSE value for daily IWD and WATMAPPR interpolation of average maximum temperature.

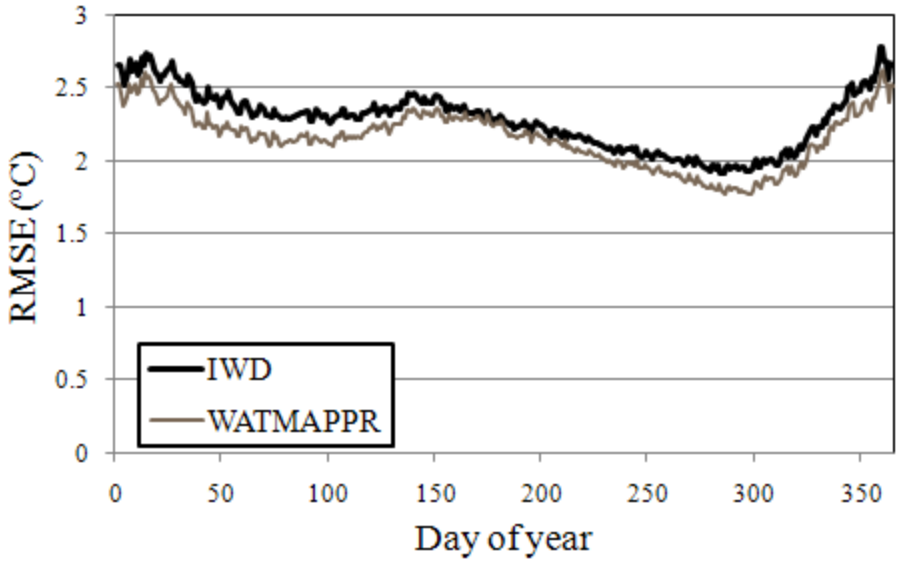

Figure 4-41: Daily summary of RMSE value for daily IWD and WATMAPPR interpolation of average maximum temperature.

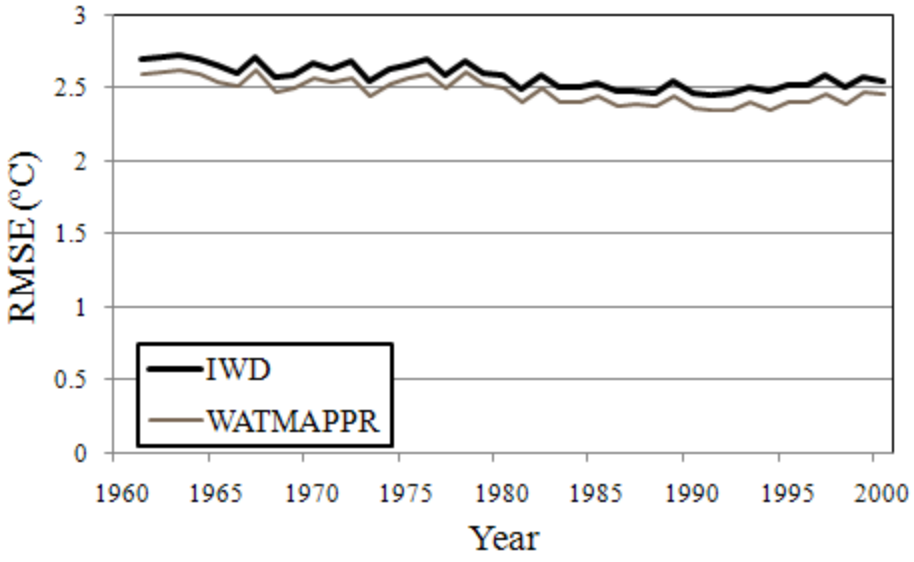

Figure 4-42: Yearly summary of RMSE value for daily IWD and WATMAPPR interpolation of average minimum temperature.

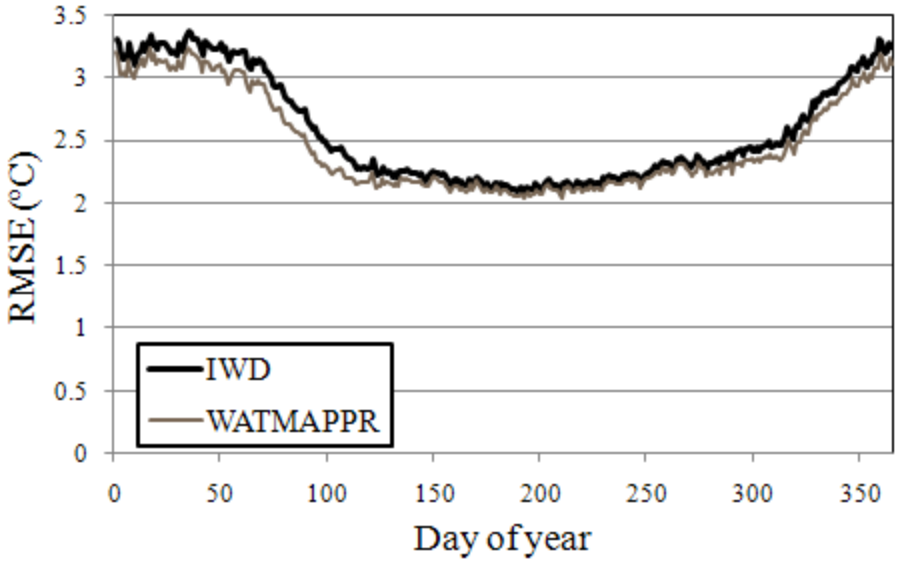

Figure 4-43: Daily summary of RMSE value for daily IWD and WATMAPPR interpolation of average minimum temperature.

4.5.2 WATMAPPR technique

There was a problem using the WATMAPPR technique (or any regression-based interpolation technique or the kriging technique) for the interpolation of daily precipitation data. This was a result of the large number of zero readings during a typical day.

As previously discussed, this was not seen in the temperature data, as there was always a meaningful reading for each station at each time step. This also did not occur using the monthly precipitation data, as there were no stations that reported a zero value of precipitation for any month in the 1961-2000 data. However, the daily precipitation data often had measured values of zero that are independent of topographical effects or distance between stations.

If these zero values had been used in the WATMAPPR technique they would have adversely affected the regression equations. Similarly for the kriging technique: the inclusion of the zero values would have skewed the semivariogram towards the y-axis and made fitting a model to the variogram very difficult. It would have been possible to just remove these zero precipitation values; however, these readings did contain important information that should not have just been discarded.

A modification to the WATMAPPR technique was devised that allowed the information from the stations that reported zero daily precipitation to be used without adversely affecting the regression. In order to do this, each station was considered in isolation. The daily precipitation total from that station was compared to the value from the WATMAPPR interpolation of the monthly total precipitation for the location of that station. The daily precipitation total was divided by the monthly precipitation readings to get a factor for that station for that day. This factor was zero for any station that reported zero precipitation for that day.

The entire field of the WATMAPPR interpolation of monthly precipitation was then multiplied by this factor to get an adjusted daily precipitation based on that station. At the location of the station, the adjusted daily precipitation would be the same as the measured daily precipitation; however around the station the adjusted daily precipitation would vary based on the WATMAPPR interpolation. This would result in the daily values of precipitation surrounding the station to vary based on the regression equations from WATMAPPR and thus would conform to the local physiographic conditions.

As an example, consider a measurement station located on the upslope of a mountain range where the precipitation increases up the side of the mountain and then drops off sharply on the downslope side of the mountain. An IWD interpolation would simply project the daily value to the surrounding areas equally in all directions depending on the next closest station. However, using the daily WATMAPPR technique a daily precipitation of 10 mm at the station could result in values of 15 mm further up the mountain and then sharply dropping to 2 mm on the other side depending on the WATMAPPR interpolation.

Of course this station does not have influence over the entire country and its influence will gradually drop off towards the next measured station. Thus a map also had to be created that showed the extent of the influence of that station based on the measurement stations that were available for that day. This influence map was created by using a simple IWD technique with each station having a value of 1, this caused each station to have greater influence on areas close to the station and then have the influence gradually fade out. This resulted in an influence map that had a value of 1 for the location of the measurement station and less than one everywhere else eventually fading to 0 closer to the next measurement station.

The adjusted daily precipitation was then multiplied by the influence map to get the final precipitation surrounding that station for that day. This process was repeated for each of the stations and the precipitation field based on each station was added together to get the final total daily precipitation for that day for the entire country.

When this process was used for the daily precipitation on July 1, 1980 (Figure 4-44), the overall effect was not very noticeable; however, when examined closely, it could be seen that the interpolated values showed more variation then using the IWD technique. It was assumed that these values were a more realistic representation of the actual precipitation patterns.

As with the IWD interpolation, RMSE was calculated for each day using the same leave-one-out analysis used for the monthly average data. The daily and yearly summaries for precipitation (Figure 4-38 and Figure 4-39) showed that in comparison to the IWD technique, the values of RMSE using the daily WATMAPPR technique were always lower. The same general patterns were seen in both the IWD and the WATMAPPR interpolation techniques.

Even though temperature is an instantaneous value and not an accumulation like precipitation, the same modified WATMAPPR technique used to interpolate daily precipitation was also used to interpolate daily maximum and minimum temperatures.

For the yearly summaries of both the maximum temperatures (Figure 4-40) and the minimum temperatures (Figure 4-42), the WATMAPPR technique produced consistently lower values than the IWD technique. The daily leave-one-out summaries of maximum temperature (Figure 4-41) and minimum temperature (Figure 4-43) showed better results using WATMAPPR for all times of the year except for the summer when the RMSE values were very close.

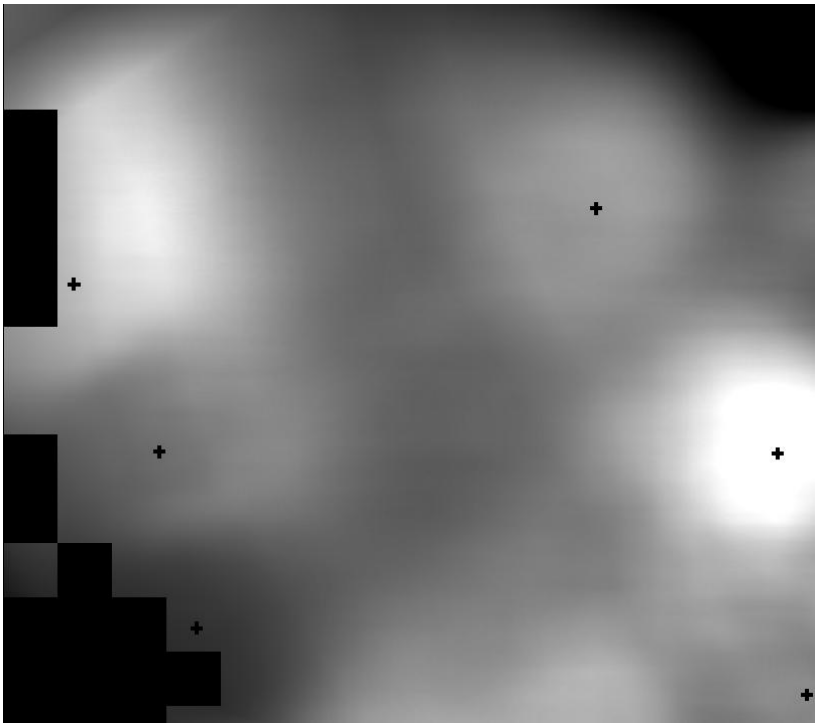

Figure 4-44: Interpolation of precipitation for July 1, 1980 using the WATMAPPR technique (image size is approximately 750 km by 750 km), the measurement stations are represented by black crosses.

4.6 Interpolating the data - Hourly

The hydrological model WATFLOOD that was used in the next part of this study was run on an hourly time step. Thus the gridded daily data had to be disaggregated into hourly readings in order to be used by the model.

Sheffield *et al.* (2006) highlight various temporal downscaling techniques such as the use of probability distributions of precipitation statistics, multi-fractal cascade methods, and stochastic rainfall generators. But in the end the authors use a relatively simple stochastic sampling approach.

The focus of this study was not to examine the effect of different temporal downscaling techniques, thus the one used here was merely done to address the issue in a simple fashion that was more realistic than merely assuming the entire days precipitation would occur in a single hour.

4.6.1 Disaggregating the precipitation data

There were different philosophies that were considered to disaggregate the daily precipitation data. For instance, all of the precipitation that had been recorded for a particular day could be assumed to

fall during the first hour of that day and then zero precipitation assumed for the rest of the day. However, this amount of precipitation appearing during one time step in most hydrological models would lead to unrealistic runoff. In this case, the ground surface would have become saturated during the hour of very intense precipitation, leading to an unrealistic situation where most of the rainfall would have flowed over the ground surface and very little would have infiltrated into the soil (this of course would depend not only on the hydrological model, but also on the soil parameters of the model, but in general most models would simulate a great deal of surface flow in response to a day's worth of precipitation occurring in a single hour). This may have also caused the soil layers to dry out, cutting off the supply of water for evapotranspiration, resulting in an underestimation of total evapotranspiration.

There is also a problem if the opposite situation was assumed to have occurred, that is, all of the precipitation recorded for each day occurring at a constant intensity over the full 24-hour period of the day. In this situation, the surface layer of the hydrological model might never have reached saturation and the water would have slowly infiltrated into the deep soil layers. This could have led to a situation where there was little fast response to a storm and most of the flow would have been baseflow. Having an almost permanently saturated top soil layer may also lead to a situation where there is always a supply of water for evapotranspiration, resulting in an overestimation of evapotranspiration.

Considering these situations, it was decided that the best way to disaggregate the daily precipitation was to assume a distribution of the daily precipitation over a certain time period of the day. A distribution supplied by Environment Canada was used in this study that was based on the measured distribution of precipitation at various stations in the Canadian Prairies (Figure 4-45) (Al Pietroniro, personal communication). Ideally, distributions could have been calculated for other areas of the country, but such data were not available.

It was assumed that this storm would have occurred in the time between the warmest and coldest temperature of the day. A bias could have been introduced if the precipitation was always assumed to occur during either the warmest or coldest part of the day. Thus it seemed reasonable to simulate the precipitation when the temperature was close to the average for that day.

Of course the limitation to using a single distribution for the entire period is that this distribution likely is different for different regions of the country as well as being different during different times of the year. However, it was beyond the scope of this study to obtain and examine the hourly precipitation data that would have been necessary to develop individual distributions for each region for each month.

However, to examine just how much of an impact spreading the daily precipitation had on the simulated streamflow, an experiment was performed where the daily precipitation was evenly spread

over a different fraction of the day. The rainfall was spread over the following number of hours: 1, 4, 8, 12, 16, 20, and 24 and the average annual flow was determined for the station located at the Mississagi River at Mississagi Chute in central Ontario (Figure 4-46). This watershed has a drainage area of 9300 km^2.

As a result of the non-linear processes that are involved when a hydrological model partitions the precipitation (Marani, *et al.*, 1997), the final result was that if the precipitation was assumed to be evenly spread over the entire day the resulting average flow was higher than if the precipitation was assumed to occur during a single hour of the day. These results were similar to the ones found by Maurer *et al.*, (2002).

The experiment also showed that there wasn't a large difference in the flow when the daily precipitation was spread between 1 hour or 12 hours. It really wasn't until the daily precipitation was spread over 16 or more hours that there was a significant difference in the flow. Consequently, although the daily precipitation was distributed based on data from only a single region, it was hoped that as long as the actual average distribution was not more than 16 hours, the simulated streamflow using a 6 hour distribution would not be significantly affected.

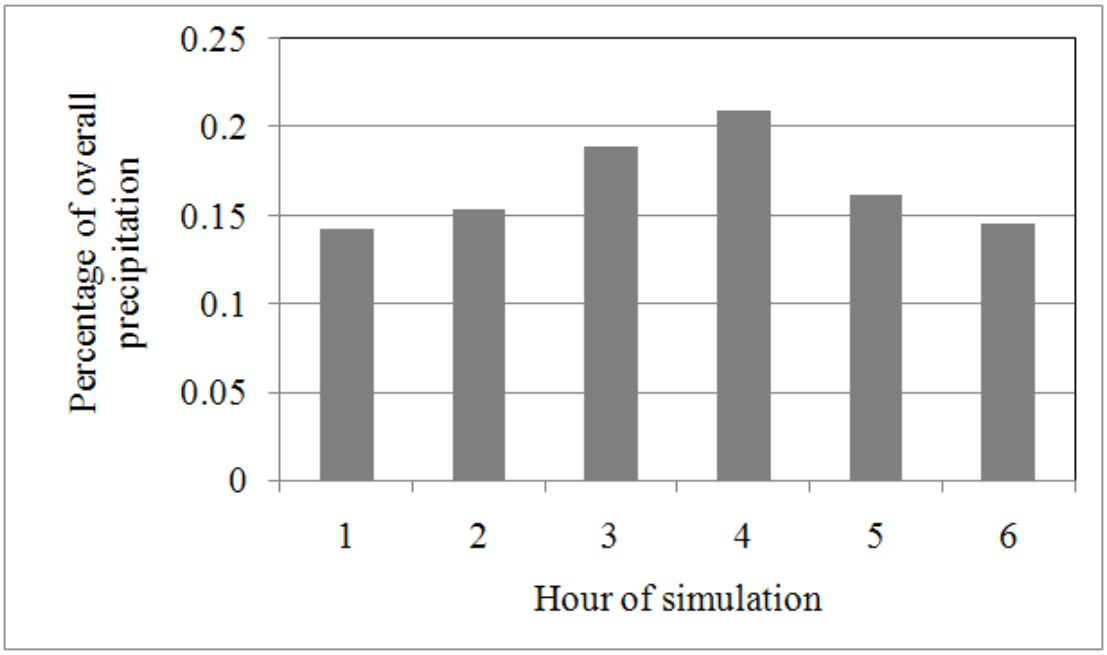

Figure 4-45: Assumed distribution of hourly precipitation data.

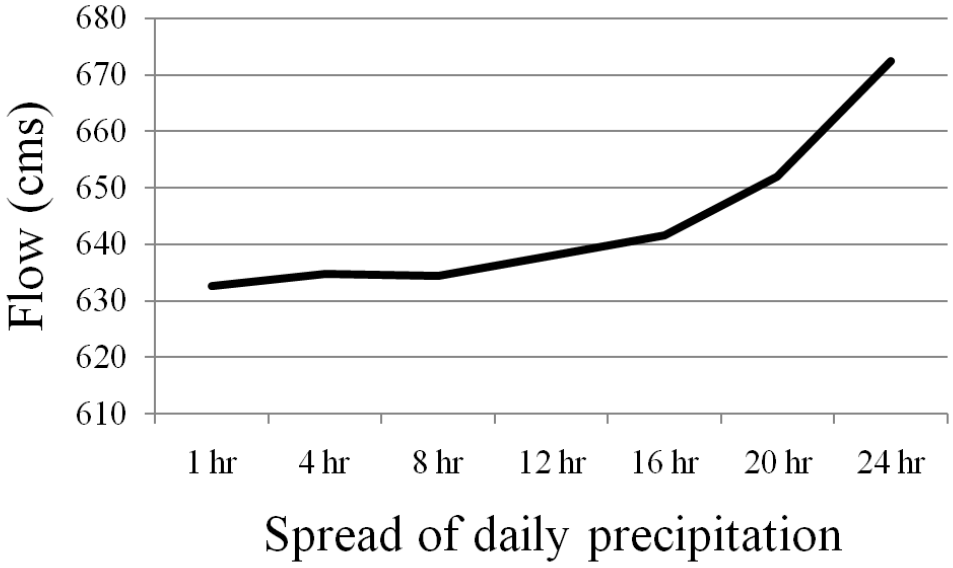

Figure 4-46: Effect of spreading the daily precipitation over a different number of hours during the day on the average flow of on the Mississagi River at Mississagi Chute.

4.6.2 Disaggregating the temperature data

In a similar argument to the disaggregation of the precipitation data, using only the average daily temperature would result in the loss of sensitivity of the hydrological model to the diurnal cycle. This would be most evident in the calculation of snowmelt, but may also be seen in the calculation of evapotranspiration if the equation used to calculate evapotranspiration was a function of temperature.

The influence of the disaggregation method on snowmelt would be particularly noticeable when the maximum temperature for a day was just above the base temperature (the base temperature is the temperature used by a hydrological model above which snowmelt begins to occur). Figure 4-45 demonstrates this concept with a hypothetical three-day period, showing the high and low temperatures for each day, the disaggregated three-hour temperatures, the base temperature, and the simulated snowmelt periods using both the daily and the three-hour data.

If we only use the daily data, then we have to assume that each temperature is persistent for 12 hours. Thus, snowmelt would not occur for the entire 12 hours that the temperature is less than the base temperature and snowmelt would occur for the 12 hours that the temperature is above the base temperature. However, if we interpolate the temperature between the daily maximum and minimum temperatures on a simple linear basis into three-hour segments, snowmelt would occur for only the

three-hour segments that the temperature is more than the base temperature. This example demonstrates how much of a difference this makes in the length of the snowmelt periods. Thus, splitting the daily data into three-hour segments will lead to a more realistic simulation of the snowmelt than just using the daily high and low temperature as actual time of snowmelt will be simulated better.

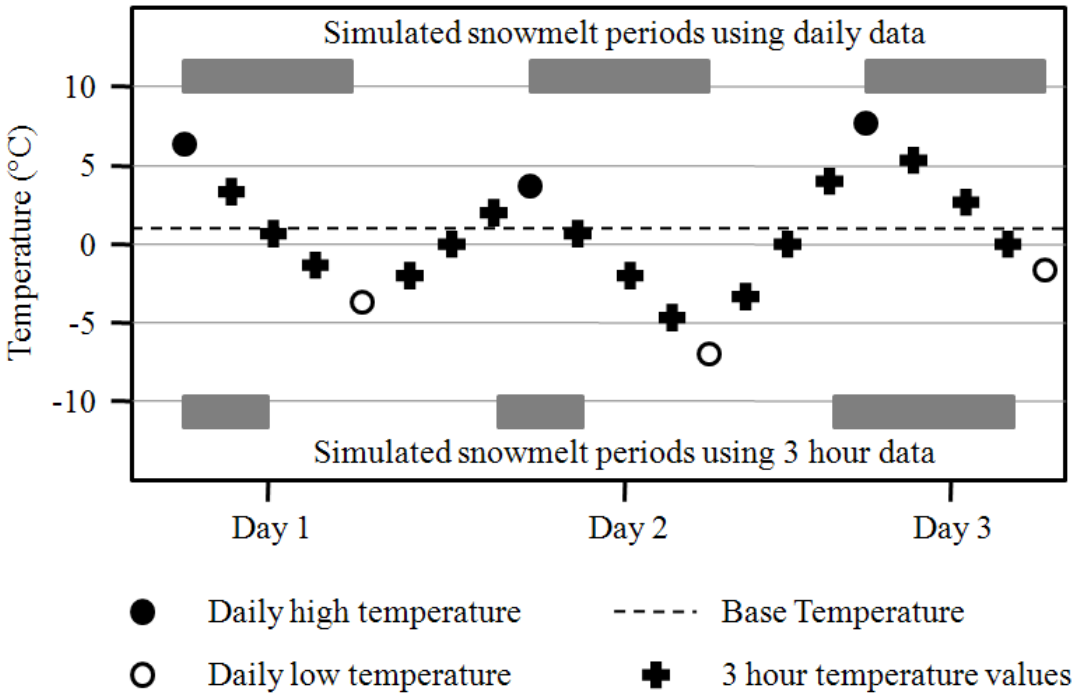

Figure 4-47: Comparison of simulated snowmelt periods using daily and three-hour data.

4.7 Chapter discussion

After the implementation of the WATMAPPR interpolation technique in this chapter, a gridded dataset of temperature and precipitation had been created for all of Canada based on measured values. This interpolation was not biased by the location of measurement stations, but still used all the available information from the measurement stations. These interpolated values will be most valuable in areas between measurement station where long-term estimates of temperature and precipitation are necessary to make planning, engineering, and watershed management decisions.

Although the WATMAPPR technique was not as simple to implement as the IWD technique, the added complexity was necessary to create a better interpolated product especially in areas of sparse

data. The findings of this chapter support the conclusions of Mitas and Mitasova (1999) that the next generation of interpolation methods will have to incorporate topographic information.

The technique developed in this chapter to create the daily precipitation files based on a regression-based interpolation is truly unique and will become even more important as the time scales in datasets are reduced. For instance, although the current results from future climate scenarios are generally only available as monthly averages, future climate scenarios are becoming available on a smaller time scale that will need to be spatially interpolated.

However, it should also be recognized that the choice of the hourly time step was made because of the requirements of the hydrological model and thus the techniques used to create the hourly data were not meant to be a rigorous into data disaggregation. The arbitrary nature of how the hourly data was created (6 hour spread at the same time each day) suggest that any conclusions made from the results of the hydrological model should only be made at a timestep greater than daily. For example, the diurnal differences in simulated flow should not be considered as significant as they would arise solely from the choice of how the daily data was disaggregated.

The selection of the regions that were necessary to properly implement the WATMAPPR technique may seem arbitrary, however it is interesting to note the similarities between the regions found in this study and the concepts commonly used in the field of climatology (UCAR, 2007). In climatology, effects are often separated into those that occur on the mesoscale, the synoptic scale, and the global scale. The mesoscale is generally considered to have the scale between 2 and 2000 km, while the synoptic scale effects are generally seen at scales at over 2000 km. The global scales refer to effects seen around the entire planet that are a result of the earth's rotation and orbit around the sun.

The mesoscale effects seen in climatology refer to such processes as downslope winds, sea breezes, or lake-effect precipitation. In this study, that scale is captured by the physiographic parameters that were derived from the elevation data.

The synoptic scale drivers are such things as air masses, air mass boundaries, jet streams, and mountain ranges. These synoptic scale drivers determine the overall climate of an area and result in the formation of climate zones. The regions that were developed for this study could be thought of as resulting from these synoptic scale drivers.

As the gridded datasets that were created in this chapter used the same projection as the drainage database created in Chapter 3, these datasets could then be used in Chapter 5 as inputs into the WATFLOOD hydrological model.

Chapter 5
Implementation and Calibration of the WATFLOOD Hydrological Model

5.1 Chapter introduction

This chapter describes the implementation and calibration of the WATFLOOD hydrological model. The model was run using the drainage database derived in Chapter 3 and the gridded hourly temperature and precipitation datasets created in Chapter 4. The goal of this chapter was to derive the best possible simulation of the streamflow for gauges located across Canada using calibration.

Ideally, all the parameters needed by a hydrological model could be directly measured leaving no question as to their values. This may be possible in purely physical hydrological models, but such a model could not have been implemented over the entire country. In any semi-empirical hydrological model, there will always exist parameters that cannot be directly measured. Thus there will always be a need to perform parameter calibration in any empirical hydrological model.

In order to do this, values of the parameters for each GRU were systematically adjusted with the goal of reducing an objective function based on the difference between measured and simulated streamflows. Other hydrological variables could have been used in the calculation of the objective function, however detailed measurements were not available for these variables and thus the only practical choice for the calculation of the objective function was to use streamflow.

Although multi-objective calibration techniques exist in hydrological modelling (Yapo *et al.*, 1998), for this study a calibration procedure was used that relies on a single objective function. This objective function was based on the average of the assessment of the measured streamflows for a number of different basins.

5.2 Hydrological models runs

WATFLOOD is a semi-empirical, distributed hydrological model that uses the inputs of precipitation and temperature to calculate the flow of water through a river basin. A full description of the WATFLOOD model is given in Appendix A.

The WATFLOOD hydrological model was implemented using the drainage database calculated for Canada in Chapter 3 and was run using with input data derived in Chapter 4. The model was run for the time period 1961-2000 using a one-hour time step on the 51-km polar stereographic grid described in Chapter 3.

Initial conditions for soil moisture and snow depth were estimated at the beginning of the model run; however, for the rest of the model run, these values were adjusted by WATFLOOD. Experience

with the model has shown that the value of these initial conditions has an effect on the simulation that only lasts on the order of a few weeks for soil moisture and up to a few months in the case of snow depth.

Although the model runs started in 1961, simulated results from the first year were not used in the model evaluation giving the model a one-year "spin-up" period to minimize any effect of the initial values that were chosen. Thus, as long as the initial conditions were reasonable (that is, not initializing the runs with 100 m of snow over all of Canada) it was assumed that their values would not affect the overall results of the model runs.

5.3 Model calibration

To run any hydrological model, each land unit type – whether it is based on land cover, soil composition, slope, and so on – must be given a set of parameters that govern how it will transport, store, and evaporate water. With semi-empirical models, some of these parameters are conceptual while others are physically based.

For conceptual parameters, the only method to derive their values is calibration. For the physically based parameters, there are scaling issues that sometimes make it difficult (or impossible) to take measurements that can be directly related to the parameter values.

These scaling issues were discussed by Bevin (1996) in the context of soil conductivity. This conductivity can be measured using a small grab sample on the scale of centimetres, using time domain reflectivity on the scale of 10s of centimetres, or using borehole techniques on the scale of metres. This leads to the question: which of these measurements best represents the soil conductivity parameter used in a hydrological model with grid squares on the order of kilometres? Thus it is often only possible to determine the most appropriate value of a physically based parameter through the use of calibration.

The next section describes how the objective functions were decided upon and the one following then describes the method for the choice of which parameters to use in the calibration. A description is then given of how the streamflow stations were selected that were used to create the objective functions.

There were two different objective functions that were used as a comparison of the measured and simulated streamflows: volume difference and timing difference. For each of these objective functions, a sensitivity analysis was first done to determine which parameters should be used in the calibration. Then an initial calibration was done where only the parameters for a particular land class were calibrated individually, as only basins were used that were dominated by one or two land classes. The results of this calibration were then used as the starting point for another calibration run

where the parameters for all the different land classes were calibrated at the same time using all the basins.

The final calibration used information gathered from the other calibration runs to initialize 100 separate calibrations runs using different search patterns. The information from these 100 calibration runs was then combined to create the final data set.

The steps of the calibration will now be described in detail.

5.3.1 Selection of the objective function

The objective function is the measure by which the model performance will be judged. In the end, the calibration technique used in this study will use a single value of the objective function to judge whether or not a particular set of variables produced better results than the previous one.

Unfortunately, it is impossible to define an objective function that will properly evaluate all aspects of the model that are important. Thus an objective function must be chosen that will be a good overall measure of validity of the model, even though it may not be perfect in all aspects. It is also possible that certain objective functions can be used for calibrating certain parameters and other objective functions will be used for other parameters.

The most commonly used objective functions in hydrology are based on the differences between the streamflow simulated by the models and those measured at points in the basin. Streamflow has been described as the hydrological variable that can be measured with the most accuracy after temperature (Krahe and Grabs, 1996). However, the objective function does not exclusively have to be derived from streamflow simulations. One of the strengths of using measured streamflow (that it is an aggregation of all the hydrological processes that are occurring in a river basin) is also one of its weaknesses (that deficiencies in the simulation of certain parts of the hydrological cycle can be masked by the deficiencies of the simulations of other parts of the hydrological cycle).

In essence, the streamflow could be right for the wrong reasons. For example, a model could have simulated the beginning of snowmelt earlier than it actually occurred in the basin. However, this could have been compensated for in the model if the simulated river roughness was too high, causing a delay of the excess water from the snowmelt in reaching the streamflow gauge. As a result, when the simulated and measured flows were compared, it would have appeared that the model did a good job of simulating the hydrological processes in the basin. In this case, it would have been beneficial to have used measures of other hydrological variables to create other objective functions. These could have included such measures as the amount of snow water equivalent or the amount of soil moisture.

This being said, however, in order to incorporate these other hydrological variables into the objective function, detailed field measurements of these variables would have been needed. Such measurements were generally only recorded at a few specific basins throughout the country, and these data would have been difficult to obtain.

Scale issues must also be considered when evaluating an objective function that is not based on streamflow. For instance, does taking a snow-depth measurement at one location in a grid properly represent the snow depth over the entire grid? If one is not enough, can it be determined how many are needed to properly represent the grid?

In the end, streamflow was the only measurement that was available with enough spatial and temporal density that it could be used for the objective function in a study of the entire country over multiple decades.

5.3.2 Selection of calibration parameters

Even after the decision had been made to use streamflow as the basis for the objective function, there were still different methods available to compute the objective function.

As previously discussed, the choice of objective functions will influence which parameters should be part of the calibration. For example, the amount of evapotranspiration from a basin will greatly affect the overall water balance of the basin, but will not be as important to the timing of the peak flows. In the same manner, the speed at which water flows once it is in the river channels will affect the timing of the peak flows, but will have little impact on the overall water balance.

The influence that a certain parameter has on an objective function is usually determined using a sensitivity analysis. In this analysis, the value of each parameter is changed individually in a prescribed manner and the effect on the value of the objective function is recorded. The parameters that had the greatest sensitivity to the objective function are the ones used in the calibration procedure.

Once the parameters that are to be used in the calibration have been decided upon, then reasonable limits must be established for the parameters. This is important to prevent the calibration from adjusting the parameters to unrealistic values. The limits for each parameter are generally decided upon using past experience running the models. It should not be assumed that these limits are always correct and any calibration that results in parameter values being chosen that are close to or at their limits should be examined.

5.3.3 Selection of streamflow stations

The simulated amount of water in the river network was calculated by WATFLOOD for each model grid square of the drainage database. However, measured streamflow gauges only existed in a limited number of model grid squares and, as with the meteorological stations, a majority of the streamflow gauging stations in Canada were located in the southern part of the country.

There were four factors considered when deciding upon which streamflow stations would be used for the calibration of the WATFLOOD model: location, record length, regulation of flow, and drainage area.

- Location: It was important to choose stations that were evenly distributed across the country, representing different climatic zones and land covers.
- Record length: As with the meteorological stations, only stations that had a minimum record length of 20 years were chosen for the calibration.
- Regulation of flow: Many of the larger rivers in Canada have some amount of regulation; if a significant portion of the flow is regulated, calibration of the hydrological model is difficult. This is because the outflow from the regulation is controlled by a set of rules that are typically based on the demand for power and/or flooding concerns. Even if these rules were fully known and they could be programmed into the hydrological model, the model could not be calibrated on these stations as the flow would not be affected by the choice of parameters. Thus, stations were chosen where a majority of the flow was not regulated.
- Drainage area: As each grid square in the drainage database had an area of 2600 km^2, it would have been difficult to simulate basins that had a drainage area of less than around 5000 km^2. This was because the GRU algorithm at the heart of WATFLOOD does not explicitly account for the location of the river channel within a grid square. Thus, although the actual river gauge could have been located anywhere within the grid square, WATFLOOD simulated the flow as if were at the outlet of the basin.

Although these were the general criterion, there were times when exceptions had to be made. For example, it was difficult to find large watersheds on the Arctic islands to satisfy the requirement of having basins that were distributed across the country. Thus, both the Big River on Banks Island and Sylvia Grinnell River near Iqaluit were used, even though they both have a drainage area less than 5000 km^2. The same reasoning was used for the selection of basins in Southern Ontario.

Overall, 17 streamflow stations were found that met the criteria and these were the ones that were used in the calibration. Details of these 17 streamflow stations are given in Table 5-1, while their locations are shown in Figure 5.1. Although many of the basins listed in the table indicate they had regulated flow, it must be remembered that if even if a small part of the basin was regulated, the

entire basin was considered to have regulated flow. However, for most of the basins in Table 5-1 that were classified as regulated, the regulated portions of the basins were small enough that they did not have a notable influence on the overall flow. The exception was the streamflow station located at Peace River at Peace River.

Table 5-1: Streamflow stations used in the calibration.

Reference number	Station number	Station name	Longitude	Latitude	Number of years of record	Regulation	Area (km^2)
1	02FC001	Saugeen River near Port Elgin	81 D 19' 35"	44 D 27' 23"	40	Yes	3 960
2	02GB001	Grand River at Brantford	80 D 16' 02"	43 D 07' 58"	40	Yes	5 210
3	02GE003	Thames River at Thamesville	81 D 58' 02"	42 D 32' 41"	40	Yes	4 300
4	02CE001	Spanish River at Espanola	81 D 46' 20"	46 D 16' 05"	34	Yes	11 400
5	04LG002	Moose River at Moose River	81 D 17' 40"	50 D 48' 50"	40	Yes	60 100
6	06MA003	Thelon River above Baker Lake	96 D 24' 37"	64 D 24' 25"	27	No	154 000
7	07DA001	Athabasca River below Mcmurray	111 D 24' 00"	56 D 46' 50"	40	No	133 000
8	07HA001	Peace River at Peace River	117 D 18' 46"	56 D 14' 41"	40	Yes	186 000
9	09EB001	Yukon River at Dawson	139 D 25' 30"	64 D 04' 12"	40	No	264 000
10	10ED001	Liard River at Fort Liard	123 D 28' 32"	60 D 14' 26"	40	No	222 000
11	10LC014	Mackenzie River at Arctic Red River	133 D 44' 13"	67 D 27' 22"	29	Yes	1 700 000
12	10MA001	Peel River above Canyon Creek	136 D 02' 10"	65 D 53' 40"	38	No	25 700
13	10NC001	Anderson River below Carnwath River	128 D 24' 48"	68 D 37' 56"	32	No	57 800
14	10QD001	Ellice River near the mouth	104 D 08' 27"	67 D 42' 42"	30	No	16 900
15	10RA002	Baillie River near the mouth	104 D 29' 26"	65 D 00' 38"	22	No	14 500
16	10TA001	Big River above Egg River	123 D 24' 02"	72 D 28' 54"	14	No	3 640
17	10UH001	Sylvia Grinnell River near Iqaluit	68 D 35' 02"	63 D 45' 38"	29	No	2 980

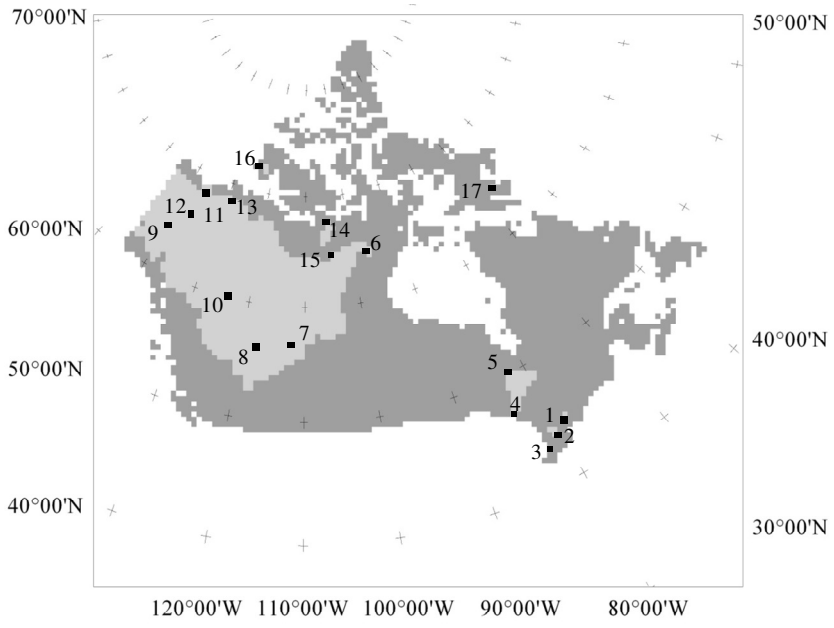

Figure 5.1: Locations of streamflow stations and their drainage areas used in the calibration (see Table 5-1 for reference numbers).

5.4 Calibration using streamflow volume as the objective function

The first objective function used to evaluate the calibration was based on minimizing the average difference between the measured and simulated total annual volume of flow at all the calibration streamflow gauges:

$$Volume\ difference = \frac{Total\ measured\ flow - Total\ simulated\ flow}{Total\ measured\ flow}$$

Note that even though only annual volumes were used for the objective function, the WATFLOOD model was still run on an hourly time step.

The difference value at each streamflow gauge was treated equally in the calculation of the total average; that is, the values at each gauge were not pro-rated based on the drainage area of that gauge. From Table 5-1, it can be seen that if the values had been pro-rated, then the gauge located at the Mackenzie River at Arctic Red River would have dominated the calibration because of its very large drainage area.

A sensitivity analysis was performed on all of the parameters available in WATFLOOD. This involved individually adjusting each of the parameters sequentially through its range of permitted values. This was done in 10 steps between the highest and lowest permitted values. The value of the objective function was recorded for each of these steps and the difference between the highest and lowest value of the objective function was used as the measure of sensitivity for each parameter.

Other methods exist to measure parameter sensitivity. For instance, it is common to individually adjust each parameter up and down by a certain percentage and use the change in the objective function as the measure of sensitivity. However, this method only examines the sensitivity of the parameter very close to the initial value. If this initial value is not well chosen, then the parameter may not show sensitivity in that range, but would have shown variation in the objective function using a different initial value. It was thought that examining the sensitivity of each parameter over the entire range of possible values would give a more accurate measure of its sensitivity.

The sensitivity analysis results indicated that when using the total annual volume simulated by the model as the objective function, the parameters that adjusted the amount of potential evapotranspiration were the most sensitive (Table 5-2). These parameters, referred to in WATFLOOD as FPET (the increase in interception evaporation for tall vegetation) and FTAL (the reduction in soil evaporation due to tall vegetation) were used to increase or decrease the amount of evaporation by simply multiplying the calculated value of potential evapotranspiration by these parameters. As these parameters were multiplied together, there was no benefit in calibrating their values individually and thus only the value of FPET was adjusted in the calibration.

Table 5-2: Sensitivity of WATFLOOD parameters using objective function based on annual volume (higher number indicates higher sensitivity, values higher than 0.1 shown in bold).

Lower zone drainage function parameter (LZF)	
	Volume
River type 1	0.005
River type 2	0.064

River channel Manning's n (R2)	
	Volume
River type 1	0.026
River type 2	0.029

Depression storage for bare ground (DS)	
Land class	Volume
Coniferous forest	0.000
Deciduous forest	0.000
Agricultural	0.000
Low vegetation	0.000
Tundra	0.000
Wetland	0.000

Depression storage for snow covered ground (DSFS)	
Land class	Volume
Coniferous forest	0.000
Deciduous forest	0.000
Agricultural	0.000
Low vegetation	0.000
Tundra	0.000
Wetland	0.000

Interflow depletion (RE)	
Land class	Volume
Coniferous forest	0.013
Deciduous forest	0.004
Agricultural	0.014
Low vegetation	0.004
Tundra	0.004
Wetland	0.002

Soil permeability for bare ground (AK)	
Land class	Volume
Coniferous forest	0.001
Deciduous forest	0.000
Agricultural	0.000
Low vegetation	0.000
Tundra	0.000
Wetland	0.000

Soil permeability under snow (AKFS)	
Land class	Volume
Coniferous forest	0.000
Deciduous forest	0.001
Agricultural	0.000
Low vegetation	0.001
Tundra	0.000
Wetland	0.001

Upper zone specific retention (RETN)	
Land class	Volume
Coniferous forest	0.046
Deciduous forest	0.023
Agricultural	0.097
Low vegetation	0.033
Tundra	0.037
Wetland	0.009

Upper zone drainage resistance factor for bare ground (AK2)	
Land class	Volume
Coniferous forest	0.008
Deciduous forest	0.002
Agricultural	0.012
Low vegetation	0.002
Tundra	0.001
Wetland	0.001

Upper zone drainage resistance factor under snow (AK2FS)	
Land class	Volume
Coniferous forest	0.013
Deciduous forest	0.012
Agricultural	0.009
Low vegetation	0.001
Tundra	0.005
Wetland	0.004

Overland flow roughness for bare pervious area (R3)	
Land class	Volume
Coniferous forest	0.000
Deciduous forest	0.000
Agricultural	0.000
Low vegetation	0.000
Tundra	0.000
Wetland	0.000

Overland flow roughness for snow covered pervious area (R3FS)	
Land class	Volume
Coniferous forest	0.000
Deciduous forest	0.000
Agricultural	0.000
Low vegetation	0.000
Tundra	0.000
Wetland	0.000

Impervious area roughness (R4)	
Land class	Volume
Coniferous forest	0.000
Deciduous forest	0.000
Agricultural	0.000
Low vegetation	0.000
Tundra	0.000
Wetland	0.000

Channel efficiency factor (CH)	
Land class	Volume
Coniferous forest	0.000
Deciduous forest	0.000
Agricultural	0.000
Low vegetation	0.000
Tundra	0.000
Wetland	0.000

Melt factor (MF)	
Land class	Volume
Coniferous forest	0.006
Deciduous forest	0.017
Agricultural	0.004
Low vegetation	0.003
Tundra	0.004
Wetland	0.002

Base Temperature for melt calculations (BASE)	
Land class	Volume
Coniferous forest	0.017
Deciduous forest	0.019
Agricultural	0.017
Low vegetation	0.003
Tundra	0.009
Wetland	0.002

All-wave albedo in each land class (ALLW)	
Land class	Volume
Coniferous forest	0.000
Deciduous forest	0.000
Agricultural	0.000
Low vegetation	0.000
Tundra	0.000
Wetland	0.000

Increase in interception evaporation for tall vegetation (FPET)	
Land class	Volume
Coniferous forest	**0.123**
Deciduous forest	0.025
Agricultural	**0.138**
Low vegetation	0.060
Tundra	0.035
Wetland	0.005

Reduction in soil evaporation due to tall vegetation (FTAL)	
Land class	Volume
Coniferous forest	0.073
Deciduous forest	0.023
Agricultural	0.099
Low vegetation	0.049
Tundra	0.024
Wetland	0.003

The finding that parameters governing evapotranspiration would affect the overall water balance was consistent with the governing equations used by the WATFLOOD model. In WATFLOOD, after water is put into the simulated watershed as precipitation, evapotranspiration is the only method to remove water from the simulated watershed.

Looking at the water balance equation:

$$P - ET = R + \Delta S$$

where P is the precipitation, ET is actual evapotranspiration, R is runoff, and ΔS is the change in storage. If the precipitation and total runoff are known, then the only unknown is the evapotranspiration (ET), assuming that over a simulation period of 40 years the change in storage of the basin will average out to be zero. In work done for the Mackenzie Basin GEWEX study, the assumption of having no overall change in storage was verified for a 40-year WATFLOOD simulation in the Mackenzie Basin (Soulis and Seglenieks, 2007).

Although there are other parameters that had an influence on the amount of evapotranspiration, such as those that effect the amount of water in the upper soil layer, their influence was order of magnitudes less than the parameters that determined the amount of potential ET.

Calibration was performed using the dynamic dimensioned search (DDS) algorithm (Tolson and Shoemaker, 2007). The DDS algorithm first does a global search for the best parameter sets, and then narrows down to a more local search in later runs. The algorithm was designed to be able to calibrate many parameters, does not need algorithm parameter tuning, and readjusts its search algorithm based on the number of runs that are available. The number of runs available is a function of the length of each simulation and the amount of available processor time.

It has been shown by Tolson and Shoemaker (2007) that DDS was able to find comparable solutions using only 15-20% of the runs needed using other algorithms. This was very important in this study, as each WATFLOOD model run took approximately 10 hours to complete and thus it would not have been possible to use an inefficient calibration algorithm because of processor time limitations.

Two different methods of using the DDS algorithm were tested: the first was to use all the streamflow gauges to calibrate all of the land classes at once; the second was to isolate the watersheds that were dominated by a particular land class and then to perform individual calibrations for each land class.

This first method simply involved performing a 200-trial DDS calibration. When the calibration was started, a value of 0.50 for the parameter FPET was used for all land classes while the bounds on the parameter were 0.01 and 10.0. Note that neither the glacier or water land classes were used in the calibration. The reason that the glacier land class was not calibrated was that it did not make up a

significant proportion of the calibration watersheds. The reason for not calibrating the water land class was that the calculation of evaporation in the water land class in WATFLOOD did not use the FPET parameter.

The results of this calibration (Table 5-3) showed that the FPET parameter value was very different for each of the land classes. Lower numbers for FPET (indicating less potential evapotranspiration) were seen in the tundra and wetland land class, while higher numbers were seen in the agricultural and low-vegetation land classes.

The volume difference at the beginning of the calibration run (that is, FPET having a value of 0.50 for all land classes) was 32.1%; after the calibration, the volume difference dropped to 26.5%.

Table 5-3: Values of FPET using volume as the objective function calibrating on all land classes at the same time.

Land class	FPET
Coniferous forest	0.48
Deciduous forest	0.66
Agricultural	1.09
Low vegetaion	0.56
Tundra	0.28
Wetland	0.29

In order to test the second calibration method, the dominant land classes were found for each watershed (Table 5-4). For some of the land classes, there were many watersheds where they were dominant (for example, coniferous forest or tundra) while for others there was only a single watershed (for example, wetland).

Table 5-4: Dominant land classes found in the calibration watersheds.

Station number	Station name	Coniferous forest	Deciduous forest	Agricultural	Low vegetation	Tundra	Wetland
10ED001	Liard River at Fort Liard	X	X				
10LC014	Mackenzie River at Arctic Red River	X	X				
07DA001	Athabasca River below Mcmurray	X				X	
09EB001	Yukon River at Dawson	X				X	
09ED001	Yukon River at Eagle	X				X	
04LG002	Moose River at Moose River	X					
04LG004	Moose River abvoe Moose River	X					
07HA001	Peace River at Peace River	X					
02GB001	Grand River at Brantford		X	X			
02FC001	Saugeen River near Port Elgin			X			
02GE003	Thames River at Thamesville			X			
10UH001	Sylvia Grinnell River near Iqaluit				X	X	
06MA003	Thelon River above Baker Lake					X	
06MA006	Thelon River below outlet of Schultz Lake					X	
10MA001	Peel River above Canyon Creek					X	
10QD001	Ellice River near the mouth					X	
10SB001	Hayes River above Chantrey Inlet					X	
10TA001	Big River above Egg River					X	
10NC001	Anderson River below Carnwath River						X

Six separate 200-trial DDS calibrations were then performed for each land class where the objective function was calculated only using the streamflow gauges that contained significant proportions of that land class. For all of the calibrations, the starting value of the FPET parameter was again set to 0.50.

The results of the calibrated FPET variable on the different land classes (Table 5-5) showed that the highest rate of potential evapotranspiration would occur in the agricultural land class, with the lowest rate seen in the low vegetation and tundra land classes.

Table 5-5: Values of FPET and volume different using volume as the objective function calibrating on all land classes individually.

Land class	FPET	Volume Difference	
		Before	After
Coniferous forest	0.49	26.6%	16.0%
Deciduous forest	0.10	32.9%	32.6%
Agricultural	1.04	23.3%	21.9%
Low vegetation	0.01	32.7%	31.6%
Tundra	0.01	34.1%	28.0%
Wetland	0.21	2.4%	0.2%

Using the results of the calibration instead of the starting parameters set improved the overall average absolute volume difference from 25.3% to 21.7%. The greatest improvement was seen in the

coniferous forest and tundra land classes. Note that these volume differences were not comparable to the values from the first method as these volume differences were not calculated on the same basins.

In order to directly compare the volume differences using the two methods, the model was run on all the watersheds using the FPET values for each land classes that resulted from the calibration on the individual land classes. The volume difference was then 28.6% compared to 26.5% when a single calibration was done on all the land classes at once. Thus the results of combining the calibrated parameters from the individual land classes were worse than the results when the calibration was done for all land classes at the same time.

It would have been impossible to find calibration basins that were exclusively composed of a single land class, since although a basin may be dominated by one or two land classes, they still contained some amount of other land classes. This was the reason that the results from the calibration done on the individual land classes did not give the best overall simulation results.

A third calibration method was then devised where all the land classes would be calibrated at the same time, but this time the starting values for FPET were the ones calculated using the DDS calibration on the individual land classes.

Once again a 200-trial DDS calibration was performed and it resulted in the lowest overall volume difference of any of the methods (23.6%), while the final calibration resulted in a smaller absolute volume difference in all but three of the basins (Table 5-1). Even though in two of the basins the increase in volume difference was large (0.5% to -7.3% in the Peace River and 2.4% to 14.8% in the Yukon River) the improvement in other basins resulted in the lower overall average.

Unfortunately, there were also some basins where the volume difference was over 40%, this amount of disagreement from the measured data indicates that there was something incorrect with either the drainage database or the input data. However this was not investigated further.

Table 5-6: Volume differences for individual basins using the original parameter set and the calibrated parameter set

Station name	Original parameter set	Calibrated parameter set	Lowest absolute volume difference
Saugeen River near Port Elgin	13.0%	-6.5%	Calibrated
Grand River at Brantford	71.2%	47.3%	Calibrated
Thames River at Thamesville	17.1%	-4.1%	Calibrated
Moose River at Moose River	51.1%	48.6%	Calibrated
Thelon River above Baker Lake	-30.9%	-6.4%	Calibrated
Athabasca River below Mcmurray	68.5%	52.8%	Calibrated
Peace River at Peace River	0.5%	-7.3%	Original
Yukon River at Dawson	2.4%	14.8%	Original
Liard River at Fort Liard	-18.1%	-19.7%	Original
Mackenzie River at Arctic Red River	2.9%	-0.2%	Calibrated
Peel River above Canyon Creek	-49.8%	-48.2%	Calibrated
Anderson River below Carnwath River	-13.7%	-2.3%	Calibrated
Ellice River near the mouth	-69.8%	-45.6%	Calibrated
Baillie River near the mouth	-25.3%	-21.0%	Calibrated
Big River above Egg River	-56.3%	-26.5%	Calibrated
Sylvia Grinnell River near Iqaluit	-29.7%	-27.2%	Calibrated
Spanish River at Espanola	24.3%	24.1%	Calibrated
Average of absolute volume differences	32.0%	23.7%	Calibrated

The final values for FPET using this method resulted in the highest potential evapotranspiration rates in the low-vegetation and agricultural land classes while the lowest rates were in the tundra and wetland land classes (Table 5-7).

Table 5-7: Values of the FPET using different calibration results.

Land class	All land classes at once, common starting value (100 DDS runs)	All land classes at once, common starting value (200 DDS runs)	Individual land classes, common starting value	All land classes at once, starting with results from individual land classes
Coniferous forest	0.48	0.49	0.49	0.49
Deciduous forest	0.66	0.70	0.10	0.86
Agricultural	1.09	1.01	1.04	0.96
Low vegetation	0.56	3.59	0.01	1.05
Tundra	0.28	0.10	0.01	0.01
Wetland	0.29	0.29	0.21	0.29

5.5 Calibration using streamflow timing as the objective function

After using the difference in total annual volume of flow as the objective function, the next step was to perform a calibration using the timing of the flow as the objective function. A very commonly used measure of fit between measured and simulated streamflow series is the Nash-Sutcliffe coefficient of efficiency or simply the Nash number (Nash and Sutcliffe, 1970).

Its formulation is as follows:

$$E_f = 1 - \frac{\sum \left(\hat{Y}_i - Y_i\right)^2}{\sum \left(Y_i - \bar{Y}\right)^2}$$

Where E_f is the Nash number, $\hat{Y}_i$ is the simulated value, Y_i is the measured value, and Y (bar) is the mean of the measured values. A monthly time step was used in the calculation of the Nash number.

The Nash number has a range of values that go from negative infinity to 1.0. Values of Nash number less than 0.0 indicate that the observed mean is a better predictor than the simulated results, while a value of 1.0 indicates a perfect fit for the simulated results (Legates and McCabe, 1999).

It has been noted that outliers, bias in magnitude, and bias in timing will have an adverse effect on the Nash number that may lead to rejection of good model that is simply biased (McCuen *et al.*, 2006). However, even with its shortcomings the Nash number is still a good measure of the goodness of fit of a simulated streamflow and was used as the objective function for this set of calibrations. The objective function was calculated as the average Nash number from each of the calibration basins with each basin treated equally regardless of the size of the basin.

A sensitivity analysis was performed to examine the sensitivity of each parameter to the value of the average Nash number (Table 5-8). The following were the parameters that were found to be the most sensitive:

- Lower zone drainage function (LZF) controls how much of the water in the lower zone storage will be passed onto the river channel each time step. A higher number will result in more water being transferred from the lower zone storage to the river channel.
- River channel roughness (R2) affects how fast water will travel in the river channels. A higher number will slow the flow of water in the river channels.
- Interflow depletion (RE) is the rate at which water from the upper-zone storage will be delivered to the river channel. A higher number will cause more water to be taken from the upper-zone storage to the river channel.
- Upper-zone specific retention (RETN) is the amount of water in the upper-zone storage that is not available to be drained to the lower-zone storage. A higher number results in more water being retained in the upper-zone storage where it is available for evaporation.
- Upper-zone drainage resistance factor for both bare (AK2) and snowcovered gound (AK2FS), controls how much of the water available from the upper-zone storage is allowed to flow to the lower zone storage each time step. A higher number results in more water being transferred from the upper-zone to lower-zone storage.
- The snowmelt factor (MF) controls the rate of snowmelt. A higher number will cause the snow to melt faster.
- The snowmelt base temperature (BASE) is the temperature at which snowmelt begins to occur. A higher temperature will delay the snowmelt.
- The evaporation parameters increase in interception evaporation for tall vegetation (FTAL) and reduction in soil evaporation due to tall vegetation (FPET) that were discussed in the previous section.

Table 5-8: Sensitivity of WATFLOOD parameters using objective function based on Nash value (higher number indicates higher sensitivity, values over 0.1 shown in bold)

Lower zone drainage function parameter (LZF)	
	Nash
River type 1	0.044
River type 2	**0.832**

River channel Manning's n (R2)	
	Nash
River type 1	0.082
River type 2	**0.177**

Depression storage for bare ground (DS)	
Land class	Nash
Coniferous forest	0.000
Deciduous forest	0.000
Agricultural	0.000
Low vegetation	0.000
Tundra	0.000
Wetland	0.000

Depression storage for snow covered ground (DSFS)	
Land class	Nash
Coniferous forest	0.000
Deciduous forest	0.000
Agricultural	0.000
Low vegetation	0.000
Tundra	0.000
Wetland	0.000

Interflow depletion (RE)	
Land class	Nash
Coniferous forest	0.082
Deciduous forest	0.029
Agricultural	0.034
Low vegetation	0.030
Tundra	0.008
Wetland	0.017

Soil permeability for bare ground (AK)	
Land class	Nash
Coniferous forest	0.004
Deciduous forest	0.000
Agricultural	0.000
Low vegetation	0.000
Tundra	0.000
Wetland	0.000

Soil permeability under snow (AKFS)	
Land class	Nash
Coniferous forest	0.001
Deciduous forest	0.003
Agricultural	0.006
Low vegetation	0.004
Tundra	0.000
Wetland	0.004

Upper zone specific retention (RETN)	
Land class	Nash
Coniferous forest	**0.141**
Deciduous forest	0.065
Agricultural	**0.144**
Low vegetation	0.077
Tundra	0.033
Wetland	0.015

Upper zone drainage resistance factor for bare ground (AK2)	
Land class	Nash
Coniferous forest	0.073
Deciduous forest	0.050
Agricultural	**0.106**
Low vegetation	0.042
Tundra	0.001
Wetland	0.006

Upper zone drainage resistance factor under snow (AK2FS)	
Land class	Nash
Coniferous forest	**0.199**
Deciduous forest	0.028
Agricultural	0.031
Low vegetation	0.030
Tundra	0.008
Wetland	0.041

Overland flow roughness for bare pervious area (R3)	
Land class	Nash
Coniferous forest	0.000
Deciduous forest	0.000
Agricultural	0.000
Low vegetation	0.000
Tundra	0.000
Wetland	0.000

Overland flow roughness for snow covered pervious area (R3FS)	
Land class	Nash
Coniferous forest	0.000
Deciduous forest	0.000
Agricultural	0.000
Low vegetation	0.000
Tundra	0.000
Wetland	0.000

Impervious area roughness (R4)	
Land class	Nash
Coniferous forest	0.000
Deciduous forest	0.000
Agricultural	0.000
Low vegetation	0.000
Tundra	0.000
Wetland	0.000

Channel efficiency factor (CH)	
Land class	Nash
Coniferous forest	0.000
Deciduous forest	0.000
Agricultural	0.000
Low vegetation	0.000
Tundra	0.000
Wetland	0.000

Melt factor (MF)	
Land class	Nash
Coniferous forest	**0.389**
Deciduous forest	0.089
Agricultural	**0.296**
Low vegetation	0.080
Tundra	0.013
Wetland	0.026

Base Temperature for melt calculations (BASE)	
Land class	Nash
Coniferous forest	**0.331**
Deciduous forest	**0.118**
Agricultural	**0.589**
Low vegetation	0.082
Tundra	0.017
Wetland	0.021

All-wave albedo in each land class (ALLW)	
Land class	Nash
Coniferous forest	0.000
Deciduous forest	0.000
Agricultural	0.000
Low vegetation	0.000
Tundra	0.000
Wetland	0.000

Increase in interception evaporation for tall vegetation (FPET)	
Land class	Nash
Coniferous forest	**0.794**
Deciduous forest	**0.328**
Agricultural	**0.459**
Low vegetation	**0.251**
Tundra	0.015
Wetland	0.031

Reduction in soil evaporation due to tall vegetation (FTAL)	
Land class	Nash
Coniferous forest	**0.452**
Deciduous forest	**0.265**
Agricultural	**0.387**
Low vegetation	**0.202**
Tundra	0.013
Wetland	0.031

Learning from the experience gained using volume as the objective function, a 200-trial DDS calibration was first done on the individual land classes using only the streamflow gauges that contain those land classes. For this phase of the calibration, the parameters based on the river class of the grid were not included. These two parameters were the river roughnesses and the lower zone storage function. If they had been included in the calibration for the individual land classes, it was likely that each calibration would have resulted in different values for these parameters. This would have made it difficult to combine the different values in the next step of the calibration.

The results of this calibration (Table 5-9) showed that the average Nash number increased in value for all land classes and, although the volume difference generally decreased, there was an increase seen in both the agricultural and wetland land class.

Table 5-9: Results for different land classes using Nash number as the objective function calibrating on all land classes at the same time.

Land class	Volume difference		Nash	
	Before	After	Before	After
Coniferous forest	16.0%	14.0%	0.313	0.397
Deciduous forest	32.6%	30.0%	0.204	0.327
Agricultural	21.9%	25.2%	0.115	0.377
Low vegetation	31.6%	21.2%	0.505	0.583
Tundra	28.0%	26.9%	0.261	0.354
Wetland	0.2%	5.9%	0.576	0.637

The calibrated parameter values (Table 5-10) showed that, based on the combination of melt factors and base temperatures, the coniferous forest land class would have seen the latest onset of melt with the tundra class having by far the slowest rate of melt. The fastest melt would have occurred in the agricultural and low-vegetation land classes.

The combination of the parameters affecting the flow of water through the upper- and lower-zone storages would have resulted in the greatest flow in the low vegetation and wetland land classes.

There was a notable difference in the evaporation parameter FPET. As the land class that had the highest value using volume difference as the objective function, low vegetation had the smallest value using the Nash number as the objective function.

Table 5-10: Parameter values for different land classes using Nash number as the objective function calibrating on all land classes at the same time.

Land class	RE	RETN	AK2	AK2FS	MF	BASE	FPET
Coniferous forest	0.553	45.300	0.121	0.542	0.481	3.820	1.200
Deciduous forest	0.174	3.520	0.198	0.311	0.382	-2.280	8.250
Agricultural	0.154	315.000	0.774	0.036	0.810	0.080	1.720
Low vegetation	0.989	178.000	0.015	0.054	0.812	-0.327	0.040
Tundra	0.725	8.330	0.333	0.426	0.062	-0.958	0.090
Wetland	0.989	196.000	0.182	0.238	0.100	-6.050	0.310

5.6 Final calibration

Next, a calibration was done on all the land classes at the same time, using the values from the previous calibration as a starting point. As this was the final calibration, a total of 100 separate 200-trial DDS runs were performed using different initial random search patterns. The parameters from the tundra and wetland land classes were not included in this calibration as the sensitivity analysis indicated that they did not significantly affect the average Nash values. Instead the parameter values for these land classes obtained from the previous calibration were used, but not adjusted, in the final calibration.

The capability to perform 100 separate 200-trial DDS runs, in a reasonable amount of time, was only possible through the use of the facilities of the Shared Hierarchical Academic Research Computer Network (SHARCNET). This is a high-performance computing consortium involving various universities and colleges across Ontario where clusters of thousands of processors are made available to researchers.

5.6.1 Final calibration results

In order to determine the best simulation from the results of the final calibration, a comparison was performed of different methods to calculate the average Nash number using the results of the 100 DDS runs. The first method simply used the simulated results from the DDS run that resulted in the highest average Nash number. As the average Nash number ranged from 0.329 to 0.387 in the 100 DDS runs, the highest average Nash using this method was 0.387.

The second method involved examining the parameter sets that results from each of the 100 DDS runs. Taking the average value of each parameter from the 100 runs resulted in a new parameter set. This average parameter set was used to run WATFLOOD and the resulting streamflow simulation

resulted in a average Nash number of 0.351. Thus using this average parameter set resulted in a lower average Nash number than just using the best individual result of the 100 DDS runs.

The third method looked solely at the simulation results from the 100 DDS runs. For each time step, the average simulated streamflow was averaged for the 100 DDS runs. Using this method the average Nash number was now 0.400. Thus the average of the simulated streamflows from all of the 100 DDS runs resulted in an average Nash number that was higher than any single DDS run. Similar results have been reported in the atmospheric sciences when performing ensemble forecasting (Richardson, 2000).

A comparison was then made between the average simulated streamflow results of the final calibration and the simulated streamflow using the initial parameter set from the beginning of the calibration process. As the objective function in the calibration was the average Nash number of all the calibration basins, it was informative to examine the Nash number for the individual calibration basins. Using the average simulated streamflows from all of the 100 DDS runs of the final calibration resulted in higher Nash numbers in most of the individual calibration basins (Table 5-11). Some basins showed a marked improvement in the Nash number, especially the Grand River at Brantford (up from -0.91 to 0.44) and the Yukon River at Dawson (up from -0.50 to 0.61).

However, there were also basins where even after all the calibration the Nash number decreased compared to the original parameter set. This indicates that there is a limitation to the amount of improvement to the simulation that can be done with calibration.

There were also other basins where although the Nash number increased during the calibration, the final value was so low that there was not much utility in using the model to simulate the flows. The results from these basins indicated that either the drainage database was not correct for that basin, the model was not correctly simulating certain processes that were occurring in the basin, or the input data for that basin were incorrect. As a result of some or all of these problems, no amount of calibration of the parameter set was able to result in a simulation that adequately represented the flow of water in the basin. In this situation, the individual basins would have to be examined to determine the reasons for the incorrect simulations and either the drainage database needed to be modified, additional processes would have to be added to the model or the input data would have to be modified.

Table 5-11: Nash numbers for the individual stations using the original parameter set and the average of the 100 DDS calibration runs.

Station name	Original parameter set	Calibrated parameter set	Lowest Nash number
Saugeen River near Port Elgin	0.34	0.55	Calibrated
Grand River at Brantford	-0.91	0.44	Calibrated
Thames River at Thamesville	0.14	0.51	Calibrated
Moose River at Moose River	0.37	0.64	Calibrated
Thelon River above Baker Lake	0.55	0.39	Original
Athabasca River below Mcmurray	-0.36	0.33	Calibrated
Peace River at Peace River	0.45	0.34	Original
Yukon River at Dawson	-0.50	0.61	Calibrated
Liard River at Fort Liard	0.56	0.46	Original
Mackenzie River at Arctic Red River	-0.08	0.73	Calibrated
Peel River above Canyon Creek	0.19	0.08	Original
Anderson River below Carnwath River	0.54	0.44	Original
Ellice River near the mouth	0.15	0.16	Calibrated
Baillie River near the mouth	-0.03	-0.04	Original
Big River above Egg River	0.23	0.35	Calibrated
Sylvia Grinnell River near Iqaluit	0.58	0.63	Calibrated
Spanish River at Espanola	-0.68	0.17	Calibrated
Total	0.09	0.40	Calibrated

5.6.2 Final calibration parameters

Although using the averages of the parameters of the 100 DDS calibration runs did not give a high value for the average Nash number, it was still informative to examine the averages of the parameter values for each land class (Table 5-12). For example, there was a striking difference in the calibrated river roughness values for the two different river classes. The calibrated roughness values in the river class that represented the lower reaches of the river systems were much less than the values for the headwaters. The effect of this would have been slower transportation of the water in the lower reaches.

The combination of higher base temperature values and lower melt factors for the coniferous forested land classes would have delayed the snowmelt in these land classes. The average values of the flow parameters that resulted from the calibration would have resulted in slower flow from the agricultural and low-vegetation land classes because the water would have spent more time in the upper- and lower-zone storages.

Table 5-12: Parameter values using Nash number as the objective function calibrating all the land classes at once.

River class	LZF	R2
Upper	1.67E-05	0.281
Lower	8.91E-06	1.196

Land class	RE	RETN	AK2	AK2FS	MF	BASE	FPET
Coniferous forest	0.484	69.3	0.250	0.641	0.592	2.208	3.147
Deciduous forest	0.266	54.1	0.187	0.584	0.438	-1.878	0.458
Agricultural	0.347	338.9	0.655	0.230	0.814	-0.126	2.097
Low vegetation	0.786	190.0	0.335	0.159	0.665	-0.179	3.883

The spread of the values of each of the WATFLOOD parameters were calculated from each of the individual calibrations (Figure 5.2). Although some of the parameters did show some clustering, there were many others that exhibited a spread throughout their ranges. This result gives support to the equifinality thesis proposed by Beven (2006), as the calibration demonstrated that there existed many different parameter sets that resulted in reasonable simulations. If only a few parameter sets existed that gave reasonable simulations then most of the parameters values would have showed distinct clustering instead of the observed spread of most of the parameters.

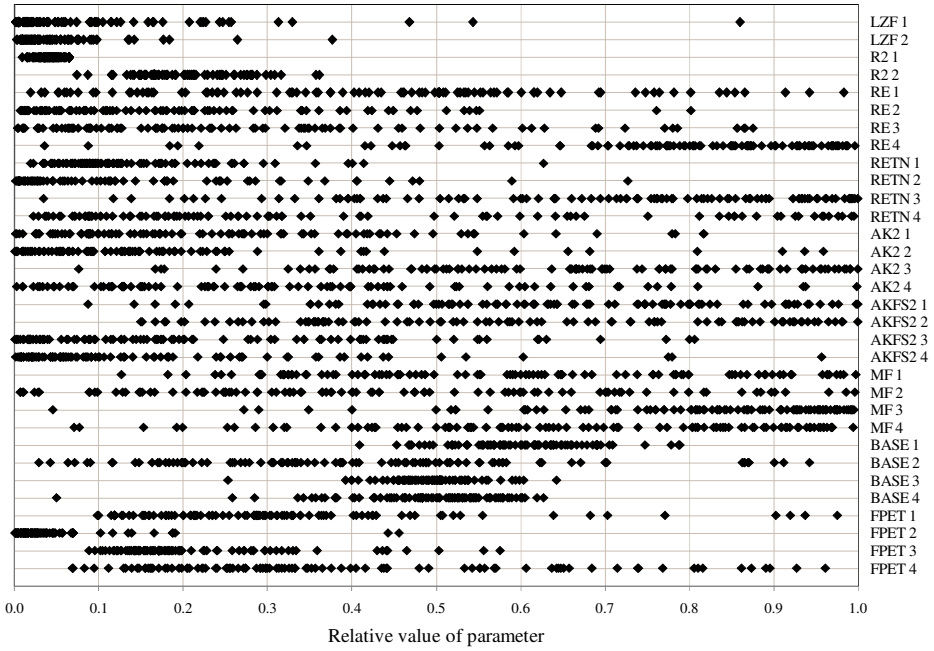

Figure 5.2: Spread of parameters from the 100 DDS calibrations.

5.6.3 Final calibration validation

To demonstrate the improvement of the simulation as a result of having performed the calibration, hydrographs were created from the streamflow station located at the Mackenzie River at Arctic Red River using the results of the different calibrations (Figure 5.3). Using the initial parameter set from the beginning of the first calibration in Section 5.4, the simulated streamflow did a poor job of matching the measured streamflow in regards to both the timing and the volume of the flow. There was a marked improvement using the parameter set from the objective function based on volume, with the simulated flow closer to the measured flow. The results shown for the final calibration were the average simulated streamflows of the 100 DDS runs that used the timing of the flow as the objective function. This calibration resulted in simulated streamflows that were the closest to the measured streamflows both in terms of timing and volume of flow.

The simulated hydrographs from all of the calibration stations using the results of the final calibration are presented in Appendix C.

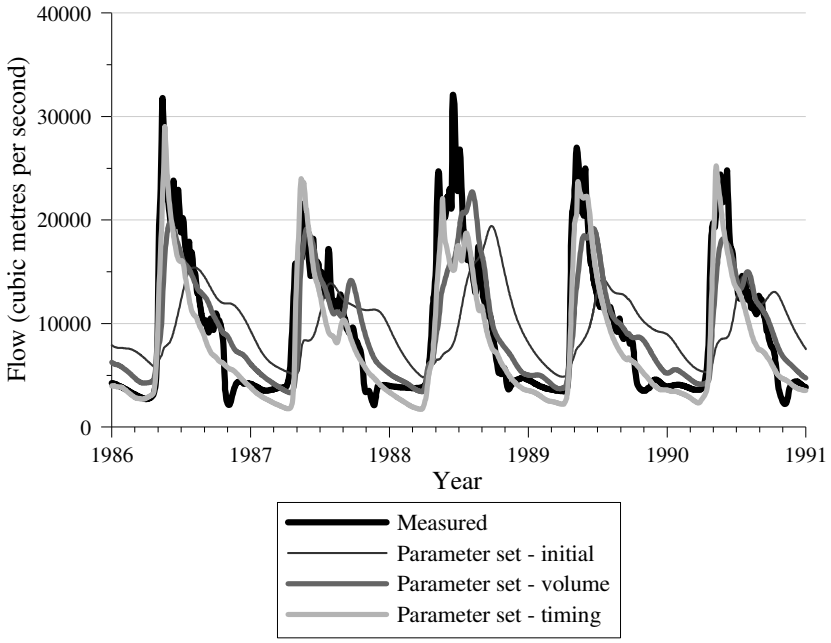

Figure 5.3: Hydrograph showing measured and simulated flows at the Mackenzie River at Arctic Red River using different parameter sets.

Another method to demonstrate the improvement of the simulation using calibration was to validate the simulated flows from the calibration on a set of data that was not used in the calibration.

Streamflow stations that were not used in the calibration were used for a validation of the final calibration results. These 13 stations were located throughout the country (Figure 5.4). These basins were not used in the calibration because they did not meet one or more of the criteria to become calibration basins. As these gauges were not used in the calibration, they gave an independent assessment of whether or not the calibration procedure improved the simulation in other basins.

A comparison was made looking at the simulated streamflow using the initial parameter set and the average of the simulated streamflows from the 200 DDS runs (Table 5-13). Using the average simulated streamflows of the 200 DDS runs increased the Nash number in all but two of the validation basins and had a higher overall average. There was also a substantial improvement in the simulation in many of the basins, for example the Nash number increased from 0.01 to 0.67 in the Grande River at Acazi streamflow gauge located in central Quebec.

However, as in the calibration basins, there were some basins where the final calibrated Nash values were less than zero indicating that the simulations from the model were not better than just using the average value of the measured flows. As with the calibration basins, the causes for these poor simulation results should be examined and corrected. For instance, the poor results on the three basins associated with the Saskatchewan River may very well have had too much regulation, making their simulation with a hydrological model impossible without specifically accounting for the rules of operation of the regulation structures.

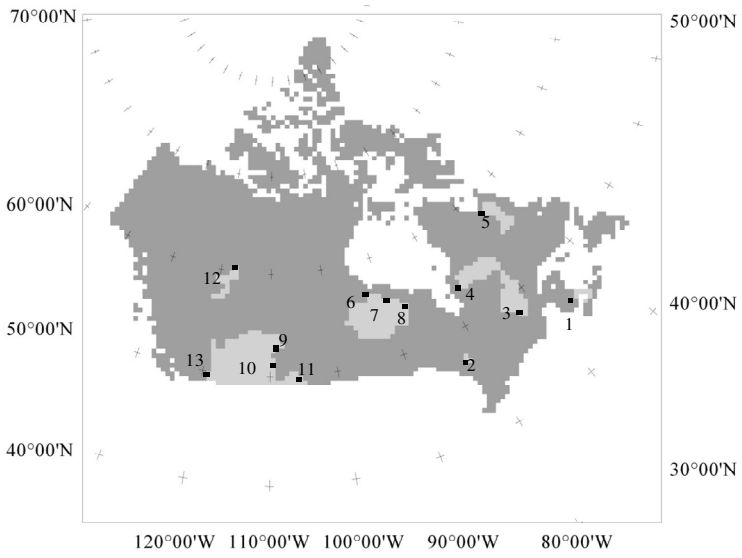

Figure 5.4: Location of validation streamflow gauges and their drainage areas (refer to Table 5-13 for reference numbers).

Table 5-13: Nash value comparison on validation streamflow gauges.

Station number	Station name	Area (km^2)	Number of years of record	Regulation	Original parameter set	Calibrated parameter set	Lowest absolute volume difference
1	Saint John River near east Florenceville	34 200	35	Yes	0.11	0.05	Original
2	Mississagi River at Mississagi Chute	9 300	40	Yes	-0.47	0.13	Calibrated
3	Ottawa River at Britannia	90 900	40	Yes	-3.14	-2.73	Calibrated
4	Grande Rivir at Acazi	96 600	19	No	0.01	0.67	Calibrated
5	Melezes River near the mouth	42 700	26	No	0.26	0.35	Calibrated
6	Hayes River below Gods River	103 000	28	No	0.04	0.39	Calibrated
7	Severn River at Limestone Rapids	94 300	24	No	0.19	0.47	Calibrated
8	Winisk River below Asheweig River tributary	50 000	35	No	-0.03	0.12	Calibrated
9	North Saskatchewan River at Prince Albert	131 000	40	Yes	-9.42	-1.66	Calibrated
10	South Saskatchewan River at St. Louis	148 000	36	Yes	-21.36	-4.96	Calibrated
11	Saskatchewan River below Tobin Lake	289 000	38	Yes	-15.78	-0.72	Calibrated
12	Hay River near Hay River	47 900	37	No	-0.31	0.22	Calibrated
13	Columbia River at international boundary	155 000	40	Yes	-0.45	-0.52	Original
	Average absolute value				-3.87	-0.63	Calibrated

5.7 Chapter discussion

The strength of using the technique described in this chapter was that the simulations were not only based on measured temperature and precipitation but were compared to measured streamflow. With this comparison to measured data, there was greater confidence in each of the elements of the water balance, in particular actual evapotranspiration which is the hardest one to measure.

Use of the DDS technique in the manner described in this chapter allowed for a consistent method of evaluating a model that was not dependent on the skill and/or the experience of the modeler. An example of where this might be useful would be in the evaluation of different implementations of a model. Here it would be advantageous to be able to have a consistent method of calibrating the model for each of the model implementations. If a modeler were to manually calibrate the model, the optimum solution may not be found for a specific model implementation, putting it at a disadvantage over the others.

Ideally, streamflow stations that met the criteria to become calibration stations would have been evenly distributed across the country. But this was not possible given the current locations of measurement stations. Firstly, this highlights the fact there is a need for more long-term measurement stations. Secondly, this kind of research can give an indication of where future streamflow gauges stations would have the most benefit to aid future researchers. Thirdly, if the resolution of the model grid were to be made smaller it could allow more streamflow stations to be chosen for calibration locations, as smaller basins could then be considered.

Although only streamflow was used in this study, there are many good reasons to the use other variables as the basis for the objective function of a calibration (Hamilton, 2007). One problem with using streamflow as the objective function is that the simulation of streamflow is a result of many

different hydrological processes, and thus many different parameters contribute to its calculation. As previously discussed, this may cause the model to be right for the wrong reasons.

As an example, consider a situation where the objective function is first based on the simulation of snow water equivalent. In the WATFLOOD model, there are only two parameters that control the amount of simulated snow water equivalent: base temperature and melt factor. If the model could be calibrated using an objective function based on measured snow water equivalent, then these two parameters could be set by the results of this calibration and need not be adjusted when running other calibrations using different objective functions. The problem with this approach is the availability of enough reliable field data to isolate the parameters for each process.

The initial set-up of the model would have been easier if there had existed a standard set of parameters for different land classes that could have been used as a starting point for the calibrations. A study that may aid in this goal is the Improved Process, Parameterisation, and Prediction in Cold Regions (IP3) study currently underway as a joint project between Environment Canada and various university researchers. In this study, detailed field observations are being collected in various research basins in northern Canada. Each of these research basins has different types of land cover and the combination of detailed field measurements and model calibration will hopefully allow for the creation of standard parameter values for different land classes.

The calibration results from this chapter were used in the next chapter to derive gridded time series of the other major hydrological variables apart from temperature and precipitation, namely: actual evapotranspiration, runoff, snow water equivalent, and soil moisture.

Chapter 6
Final Hydrological Variable Datasets

6.1 Chapter introduction

This chapter presents the gridded time series of the hydrological variables: actual evapotranspiration, runoff, snow water equivalent, and soil moisture, based on the output of the WATFLOOD hydrological model. The gridded datasets were created using the results of the final calibration in the previous chapter.

If the data had been available, it would have been possible to also interpolate these other hydrological variables from measured station data using the same technique as was done for temperature and precipitation. However, there were very few locations in Canada where these other hydrological variables were measured. For example, there were only 22 Environment Canada stations that measured evapotranspiration between 1961 and 2000, compared to the 1986 stations that measured precipitation. It would have been impossible to perform a meaningful interpolation based on such a small number of measured station locations over such a large area.

This is the situation not only in the remote areas of Canada but also in many areas of the world. Examining how these data-scarce regions could be better understood was one of the reasons for the creation of the PUB initiative. Hopefully, this chapter demonstrated how hydrological modeling was able to use knowledge gained from the analysis of measured basins to make informed decisions about the state of the hydrology in ungauged basins.

The second part of the chapter dealt with the predictive uncertainty inherent in the simulation results and demonstrated how the techniques developed in this thesis can be used to make predictions based on future climate scenarios.

6.2 Presentation of the hydrological variable datasets

It was demonstrated in Chapter 5, that the best simulation of streamflow (the highest average Nash number) was achieved by averaging the simulated streamflow from each of the 200 DDS runs of the final calibration. The same principle was used in this chapter to present the values of actual evapotranspiration, runoff, snow water equivalent, and soil moisture. Thus, for example, the gridded runoff results presented for a particular grid were the averages of runoff for that grid from each of the 200 DDS runs of the final calibration.

6.2.1 Actual evapotranspiration

The term evapotranspiration (ET) should always be used with the modifier "actual" or "potential", as there is a significant difference in each of the terms. The use of a hydrological model allows for the calculation of simulated actual ET (AET) as the model will track the amount of water available in the soil that is available for evapotranspiration. Potential ET (PET) is much easier to calculate as it only relies on the atmospheric conditions and not on the soil moisture conditions. However, when considering the water balance equation, it is not appropriate to use PET, since using it could result in situations where water is assumed to be evaporated when there is no water available in the soil.

To illustrate this point, consider a map showing precipitation minus PET and precipitation minus AET on an annual basis in the Mackenzie Basin (Figure 6-1). The precipitation minus PET map (Figure 6-1a) shows many areas of the basin where PET exceeds precipitation (that is, precipitation minus PET is negative). This is very unrealistic as this would make these areas appear to be arid implying a severe lack of available water, to the extent of hindering or even preventing the growth and development of plant and animal life.

A much more realistic situation is seen in the map showing precipitation minus AET (Figure 6-1b). Here the only areas where AET exceeds precipitation correspond to the large water bodies in the basin. As these water bodies contain mostly open water, they are indeed grids where the AET exceeds the precipitation, but of course they are not arid as they are supplied with water by upstream grids.

(a) (b)

Figure 6-1: (a) Precipitation minus potential evapotranspiration and (b) precipitation minus actual evapotranspiration. Areas with negative values are shown in black while areas with positive values are shown in grey.

The map of average annual actual evapotranspiration for the 1961-2000 period (Figure 6-2) showed that the highest AET occurs in the mountains of the west coast and in parts of Ontario and Quebec. As a result of both the low amount of precipitation and the low temperatures, there was little AET seen in the northern part of the county when compared with the southern part. The dividing line between these two areas generally coincided with the northern extent of the Boreal forest.

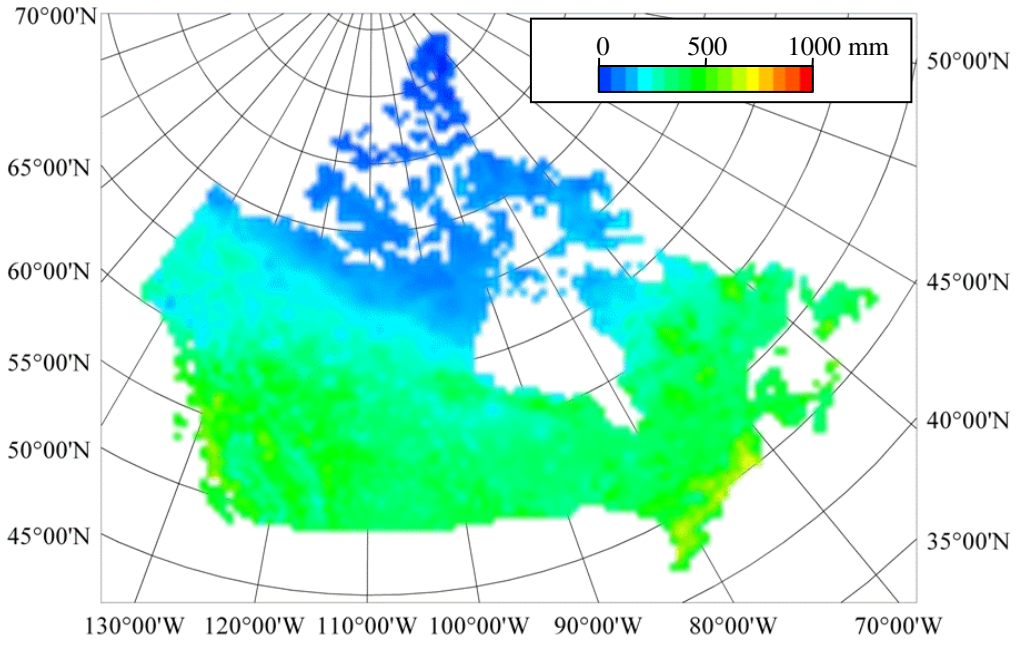

Figure 6-2: Average annual actual evapotranspiration for 1961-2000.

When examining the average monthly values of AET (Figure 6-3), very little AET occurred between the months of December and February in most of the country. The low temperatures are what prevented any meaningful AET from occurring during those months. There is also a vegetation effect that can be seen in both the months of June and July on the Prairies where there is high AET from the agricultural land class.

Conversely, the warmer temperatures between June and August caused them to be the most intense period of AET for most of the country with the highest values observed from the prairies to central Quebec. It is interesting to note that there was no real peak in the western mountains during the summer; rather they experienced a relatively constant amount of AET during the entire year.

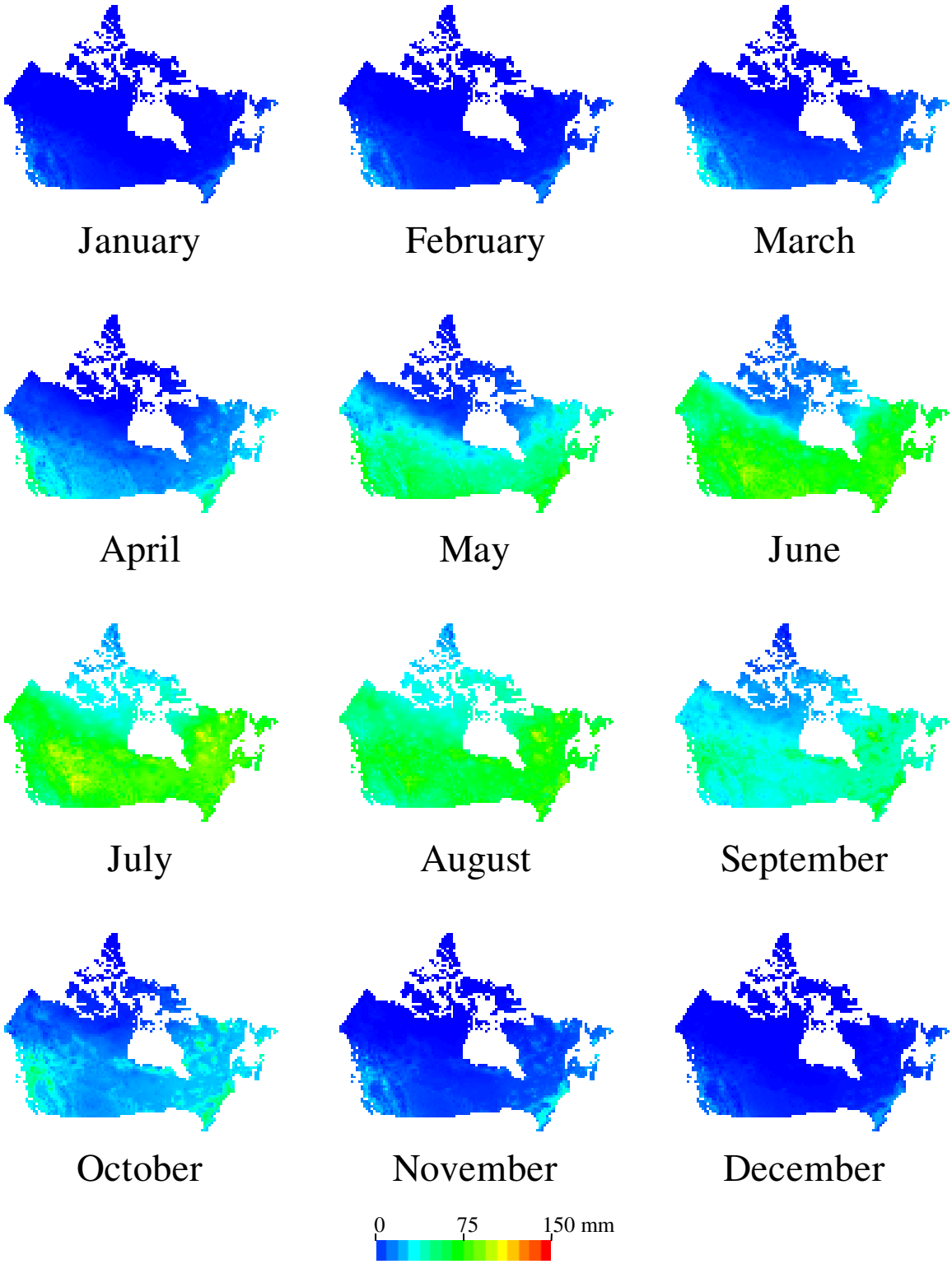

Figure 6-3: Average monthly actual evapotranspiration for 1961-2000.

In order to study the regional differences in more detail, six locations were chosen where the annual cycle of the parameters could be plotted and examined. These locations represented points in different climatic zones of Canada: west coast, mountains, Arctic, prairies, Ontario, and Newfoundland (Figure 6-4).

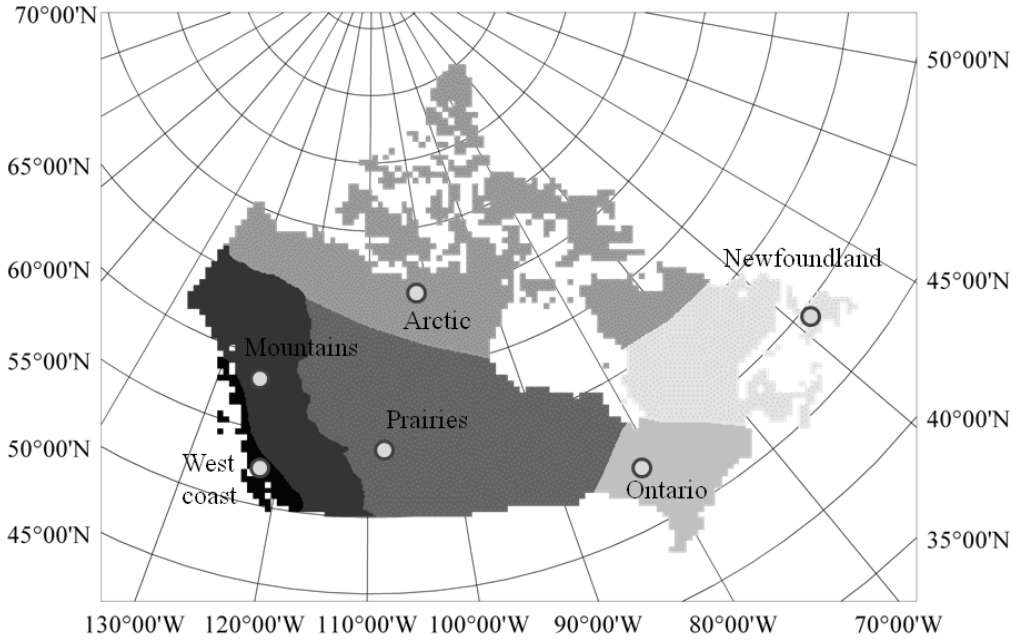

Figure 6-4: Locations of the points representing the different climatic zones.

The land cover mix for each of the points were summarized in Table 6-1, while their elevations, average annual precipitation, and average annual temperature were summarized in Table 6-2.

The west coast and central mountain point had a similar mix of land classes. Not surprisingly, the Arctic point was dominated by the tundra land class and the prairie point consisted mostly of the agricultural land class. Both the Ontario and Newfoundland points were dominated by the coniferous forest land class.

The west coast point had by far the highest average annual precipitation and temperature with the Arctic point having both the lowest precipitation and temperature. Apart from the mountain point which had an elevation of over 1000 m, the rest of the points had similar elevations.

Table 6-1: Land class percentages of the climatic zones points.

Land class	West coast	Mountains	Arctic	Prairies	Ontario	Newfoundland
Coniferous forest	55.0%	42.0%	2.0%	31.0%	84.0%	98.0%
Deciduous forest	8.0%	12.0%	0.0%	25.0%	12.0%	0.0%
Agricultural	1.0%	0.0%	0.0%	33.0%	0.0%	0.0%
Low vegetation	10.0%	6.0%	2.0%	9.0%	2.0%	0.0%
Tundra	16.0%	28.0%	87.0%	0.0%	0.0%	0.0%
Wetland	6.0%	7.0%	3.0%	0.0%	0.0%	0.0%
Glacier	0.0%	0.0%	0.0%	0.0%	0.0%	0.0%
Water	4.0%	5.0%	6.0%	1.0%	2.0%	2.0%
Urban	0.0%	0.0%	0.0%	1.0%	0.0%	0.0%

Table 6-2: Elevation, average annual precipitation, and average annual temperature of the climatic zones points.

Land class	Elevation (m)	Average annual preciptiation (mm)	Average annual temperature (°C)
West coast	279	1495.7	7.0
Mountains	1098	844.9	-1.1
Arctic	219	161.9	-13.5
Prairies	458	402.1	2.5
Ontario	266	817.1	0.8
Newfoundland	309	1170.8	2.9

Looking at the yearly pattern of AET in the different climatic zones (Figure 6-5), there was a comparable amount of AET in most of the regions. The exception was the Arctic which showed a much lower amount, likely due to the lower temperatures and lower amount of available water. There was a small amount of AET even during the winter months in the west coast, while in all other regions there was very little AET during this time. The highest peak value of AET was seen in the prairie region during the summer months.

6.2.2 Soil moisture

For soil moisture, it must be remembered that WATFLOOD only employs a very basic soil model and thus the amount of water in the storages are representative of the amount of moisture in the soil, but cannot be directly related to common soil properties such as volumetric or gravimetric water content.

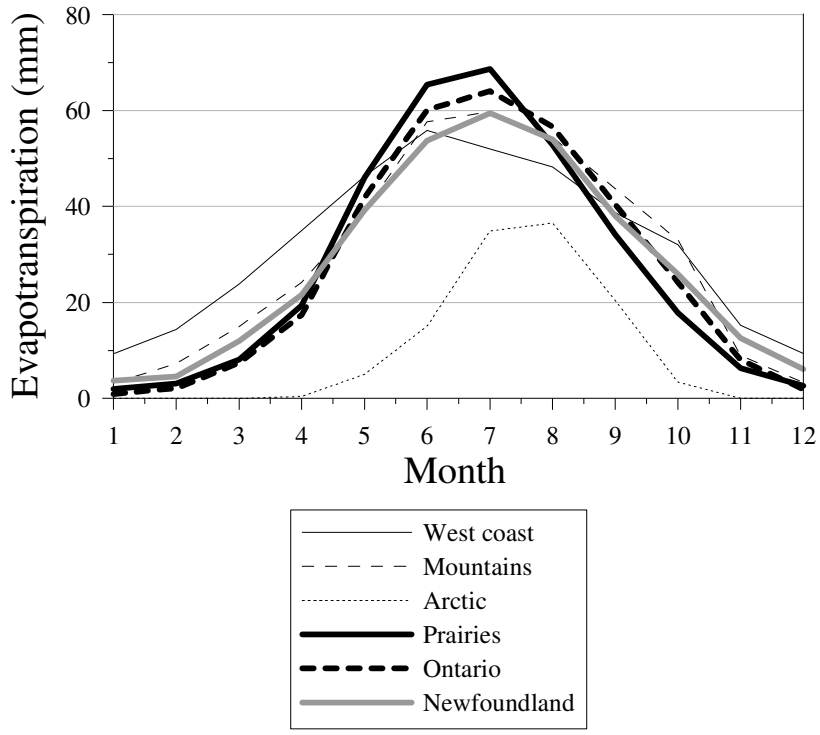

Figure 6-5: Monthly average actual evapotranspiration for different climatic zones.

In the WATFLOOD model, the soil moisture is represented by an upper- and a lower-zone storage. The upper-zone storage is conceptionalized as a fast-response storage such as interflow, while the lower-zone storage gives a slower response in the manner of baseflow.

Looking at the average monthly upper-zone storage (Figure 6-6) there was not much change in the upper-zone storage during the winter months. This represents a time when there is little activity in the soil layer. The melting of the snowcover during the spring then increased the upper-zone storage from the south to the north. During the summer, the entire country had about the same level of upper-zone storage except for an area of the prairies; this represents the filling of the upper-zone storage.

Examining the lower-zone storages (Figure 6-7), the values on the coasts peaked in the summer months and receded in the winter and once again there was little activity in the lower-zone storage in the central part of the country.

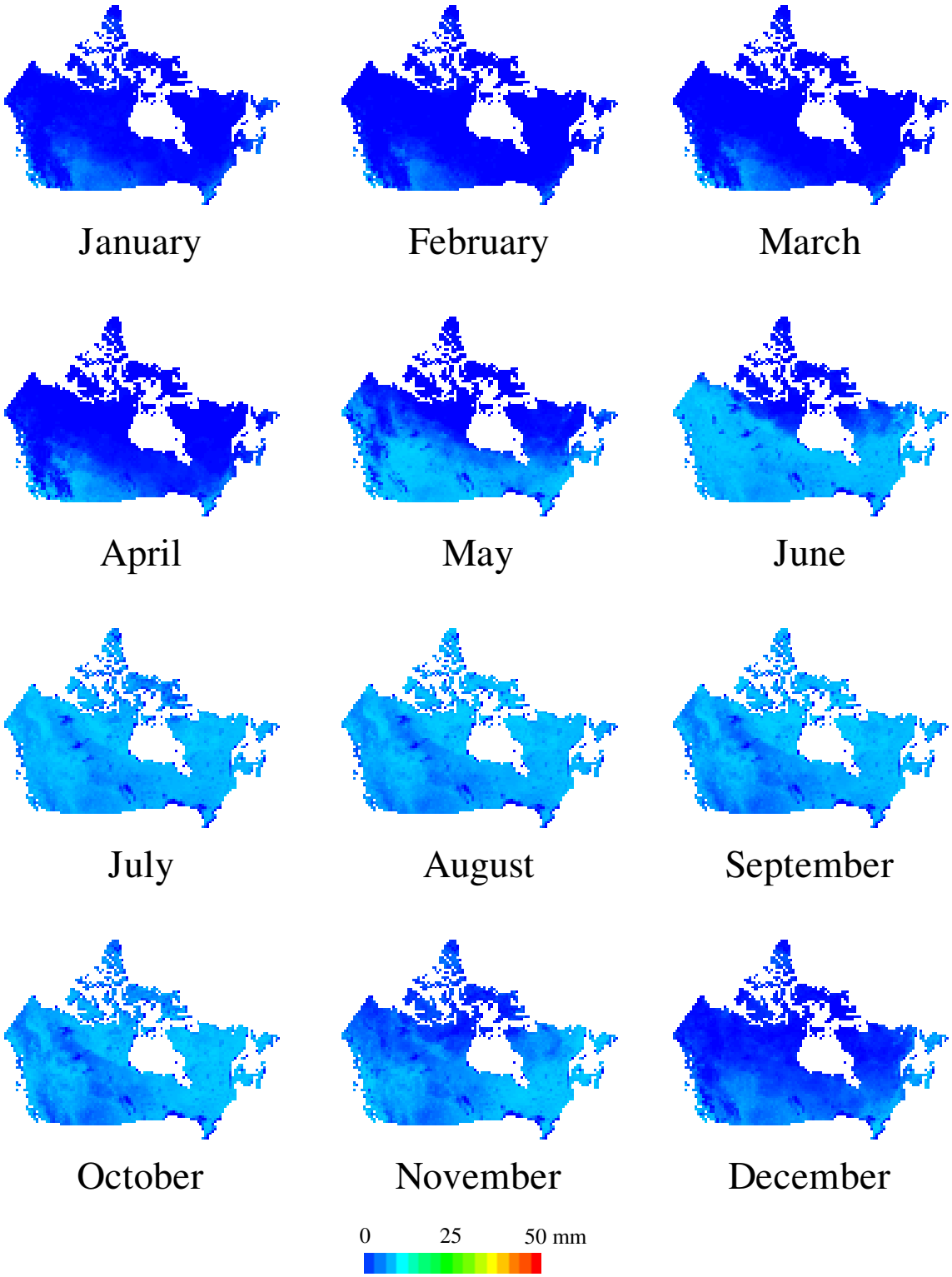

Figure 6-6: Average monthly upper zone storage for 1961-2000.

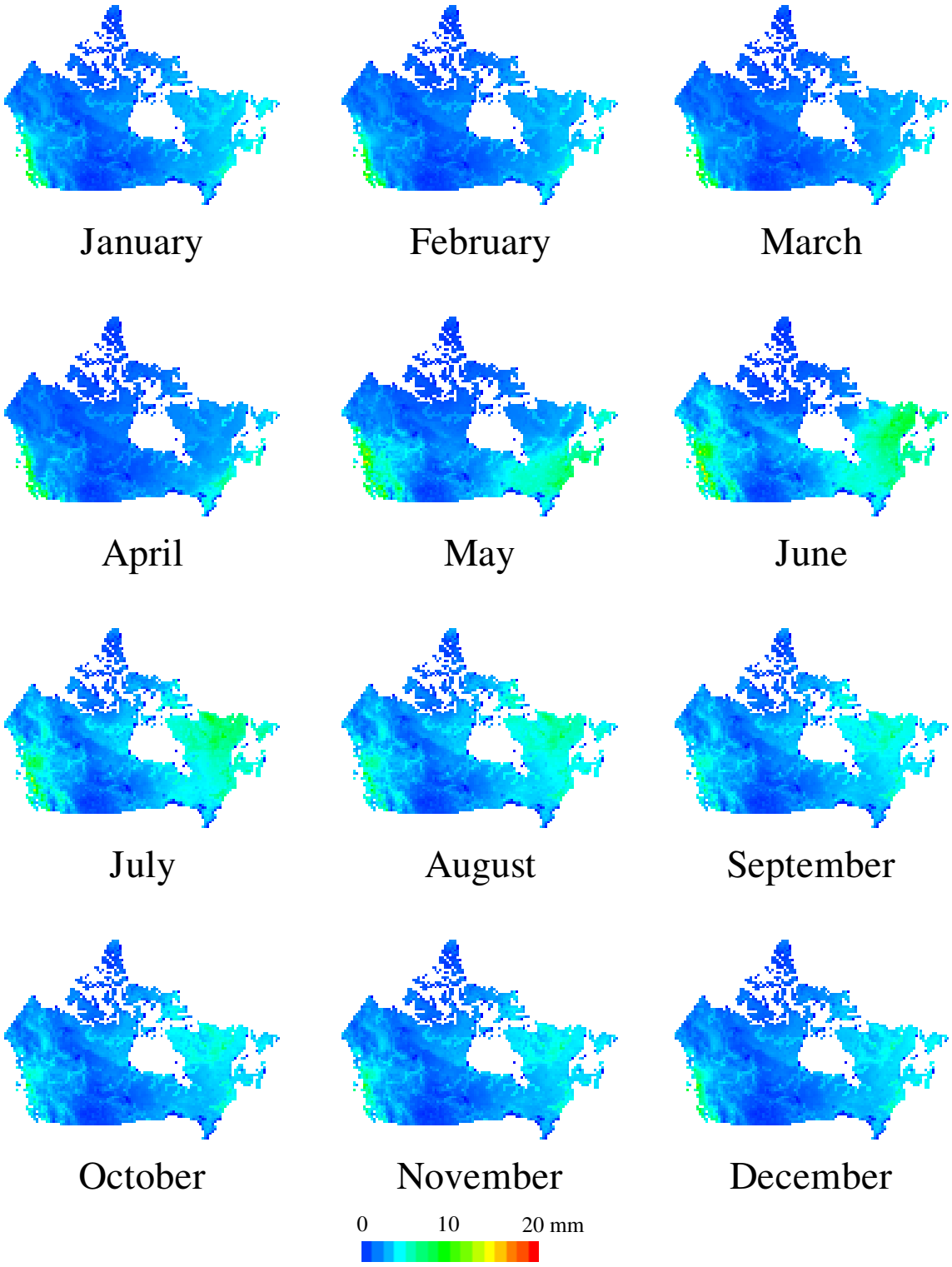

Figure 6-7: Average monthly lower zone storage for 1961-2000.

Looking at the annual cycle of upper-zone storage in the different climatic regions (Figure 6-8), all of the regions filled the upper-zone storage between the spring and the fall. The only exception was on the Prairies where there was always some moisture left in the upper-zone storage even in the winter months. The different maximum amounts seen were a result of the different capacities of the upper-zone storage reservoirs depending on the mix of land-cover types contained in that grid square.

On the lower-zone storage graph (Figure 6-9), once again the effects of the spring snowmelt were evident along with a drying out over the summer months. Most areas showed some replenishing of the lower-zone storage in the fall, an effect seen most dramatically on the west coast and in Newfoundland. The effect of the snowmelt was delayed until the summer months in the Arctic as well as the region containing less water in the lower-zone storage overall.

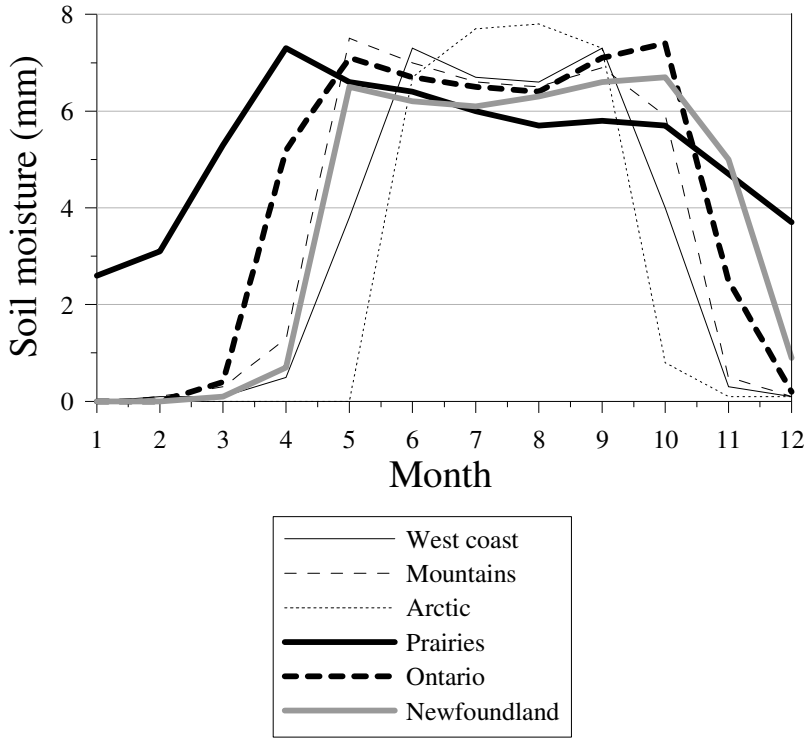

Figure 6-8: Monthly average upper-zone storage for different climatic zones.

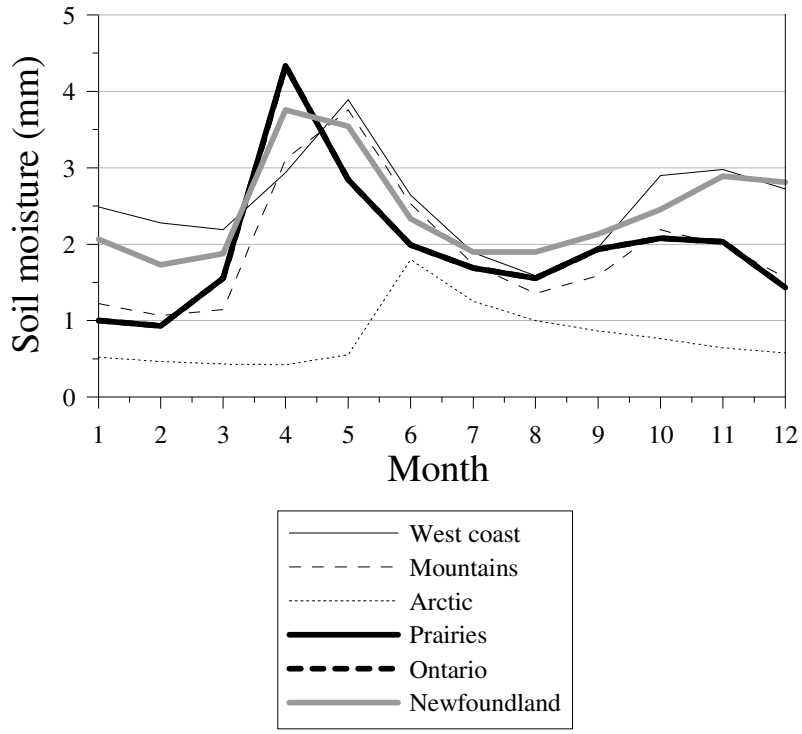

Figure 6-9: Monthly average lower-zone storage for different climatic zones.

6.2.3 Snow water equivalent

Not surprisingly, the monthly average snow water equivalent (SWE) values (Figure 6-10) showed a gradual rise in the fall months up to a peak in March and April, and then a rapid decline during the spring.

The highest values of SWE were seen in both the western and eastern parts of the country. Although the northern areas were cold, they did not have enough precipitation to produce large amounts of snow on the ground. During the summer months, the only areas with persistent snow cover were the higher elevations on the Arctic islands and in the mountains of the west coast that had significant amounts of glacial cover.

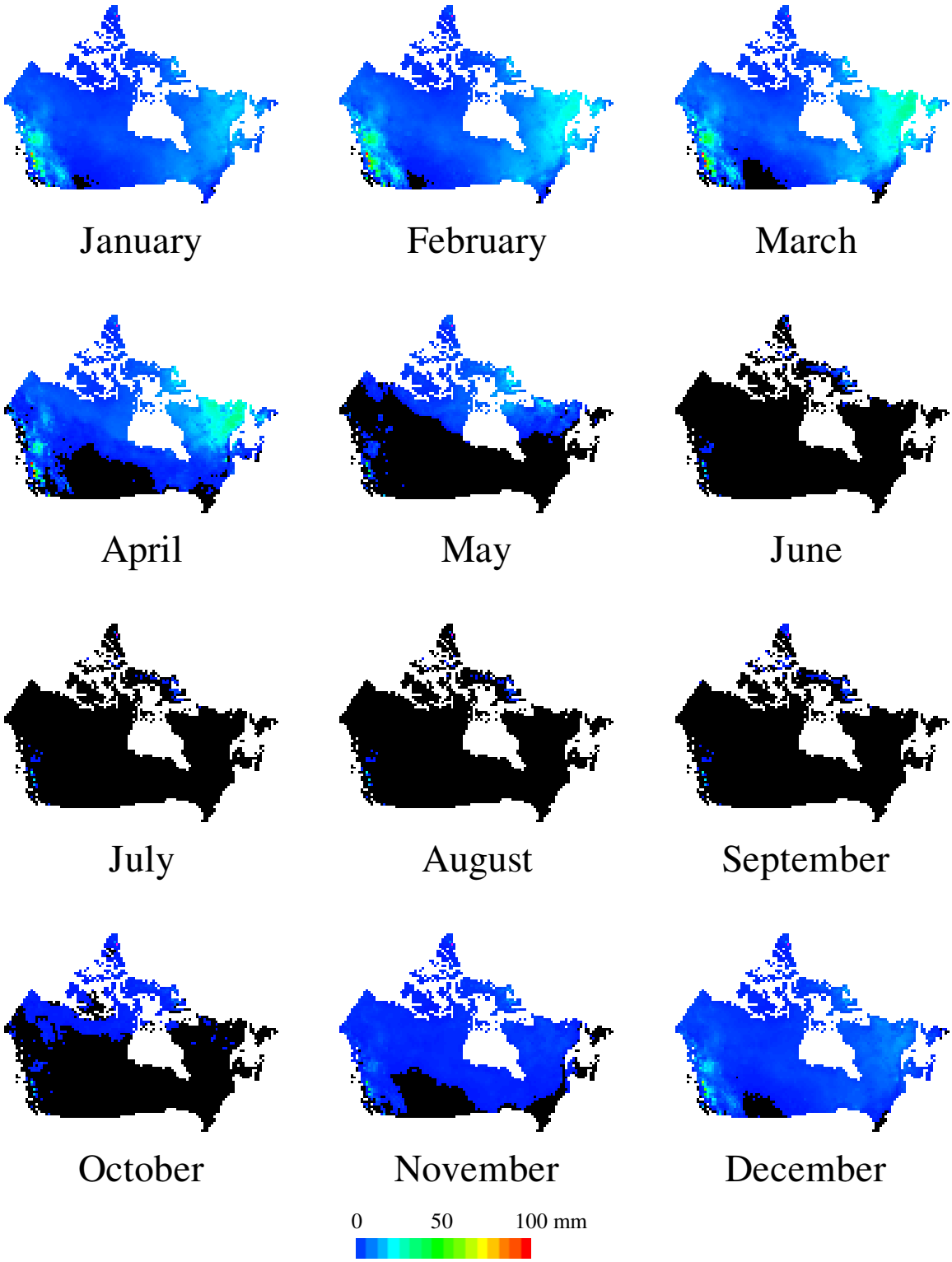

Figure 6-10: Average monthly snow water equivalent for 1961-2000.

The regional SWE graphs (Figure 6-11) showed that the west coast and mountains had by far the highest amount of SWE, while the lowest values were in the Arctic. The timing of the melt was relatively consistent with the peak in all areas occurring during March with the exception of the Arctic where the SWE peak only occurred in May.

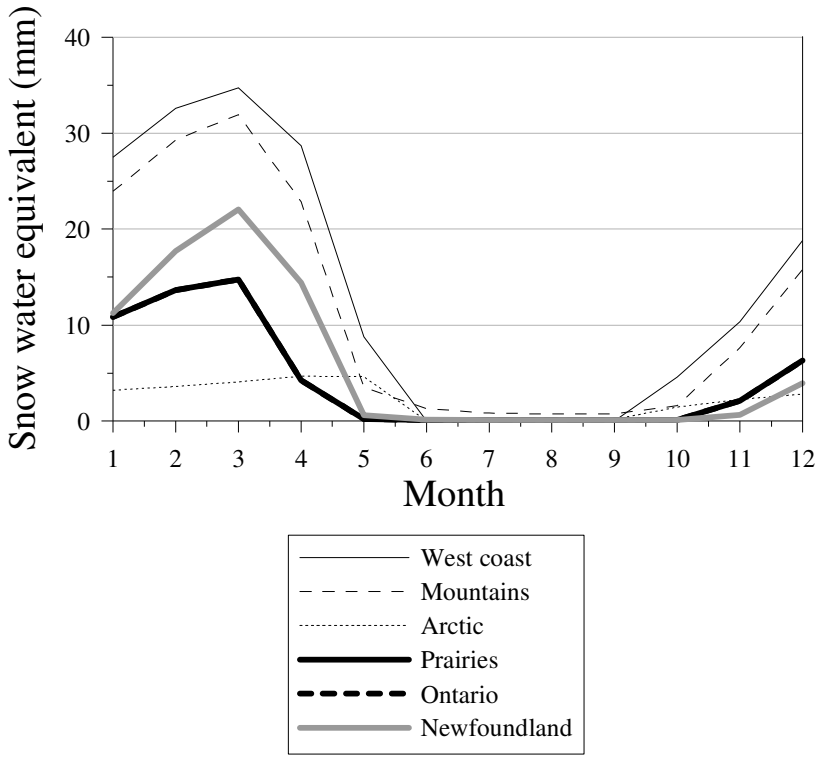

Figure 6-11: Monthly average snow water equivalent for different climatic zones.

6.2.4 Runoff

Because of its importance in design of structures or land-use development planning (especially in ungauged basins), runoff was the most important hydrological variable that was calculated during this study. In this study, runoff was defined as the total contribution of flow from the surface flow, interflow, and groundwater flow entering the river channel from all parts of the grid square.

The average annual runoff (Figure 6-12) showed that by far the highest values occurred along the west coast of the country, with the next highest values occurring along the east coast of Canada. The

values for Ontario and Quebec were also relatively high with the lowest values seen both across the prairies and in the Arctic.

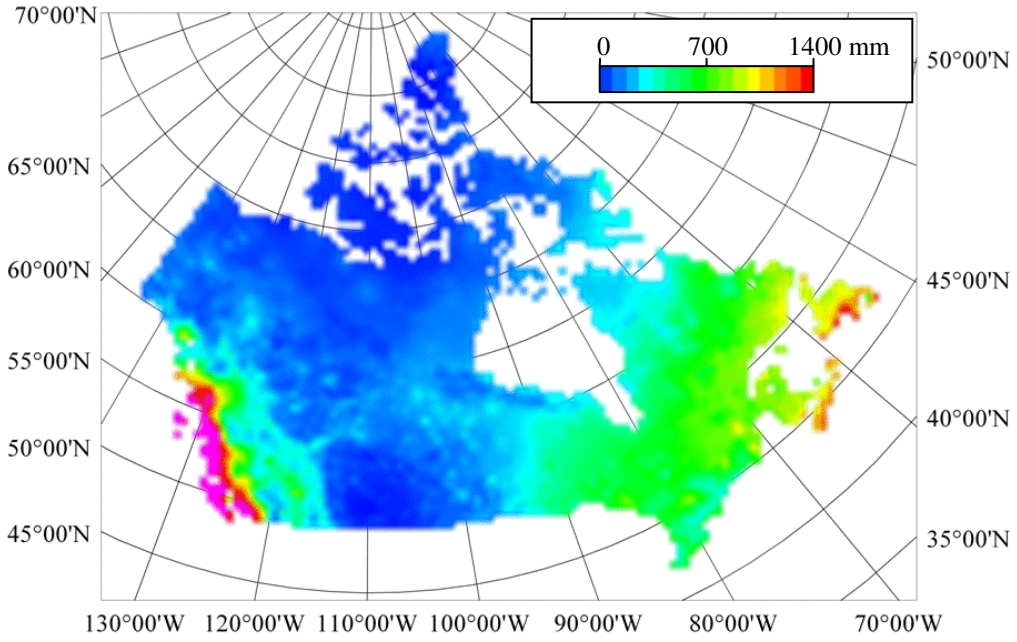

Figure 6-12: Average annual runoff for 1961-2000.

From the maps of average monthly runoff (Figure 6-13), a majority of the runoff occurred during the spring months as a result of melting snow for most of the country. This effect occurred in April in the southern part of the country, but did not occur until June in the north. Just like with some of the other hydrological variables, the runoff from the west coast was relatively consistent throughout the year, whereas in most other parts of the country the runoff shut down during the winter.

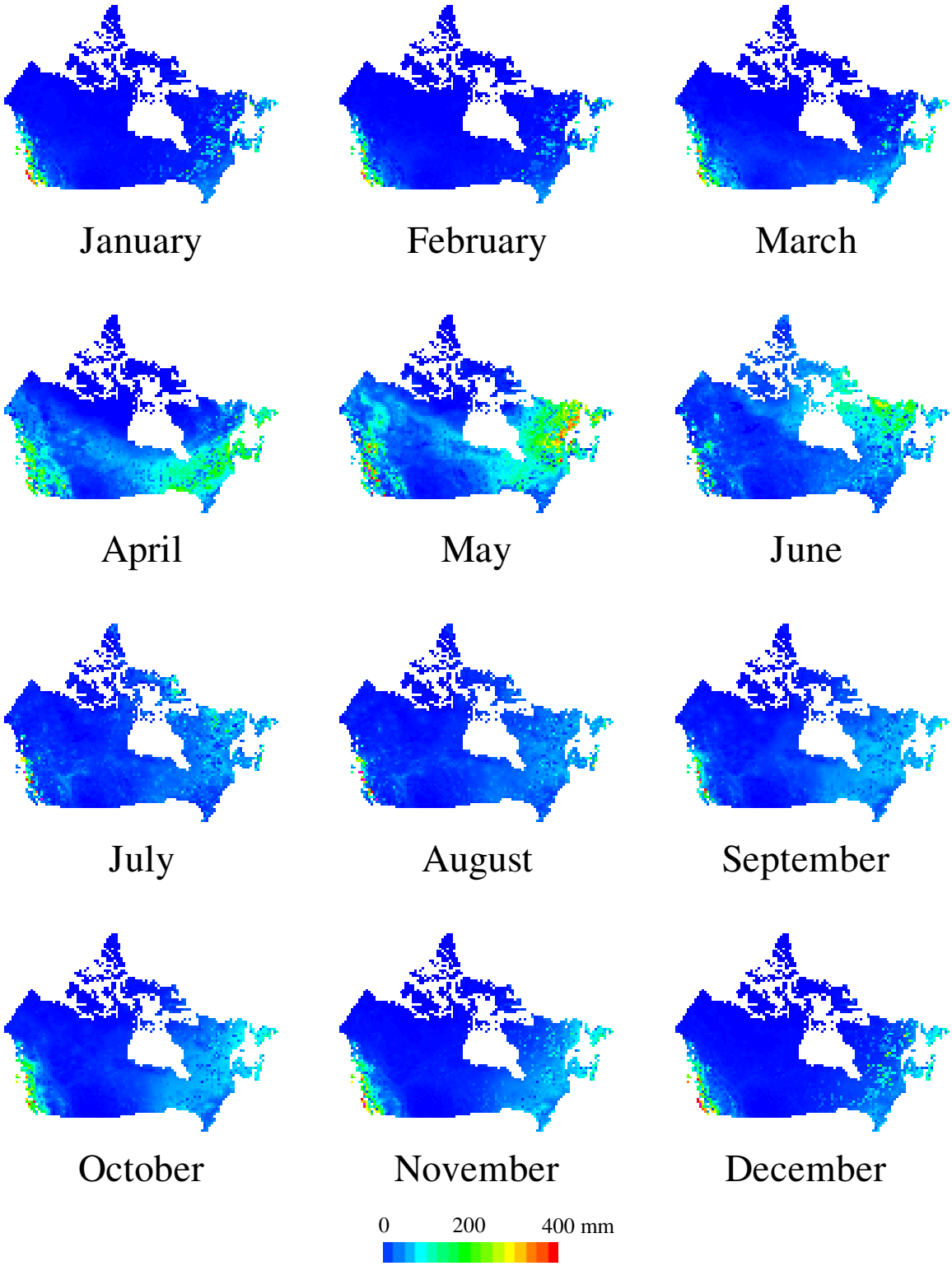

Figure 6-13: Average monthly runoff for 1961-2000.

The regional graph of runoff (Figure 6-14) confirmed that most of the regions have their largest runoff periods during the spring melt, although this effect was muted in the prairies and Arctic regions as a result of their relatively low amount of snow. Many of the regions also showed a smaller late fall peak.

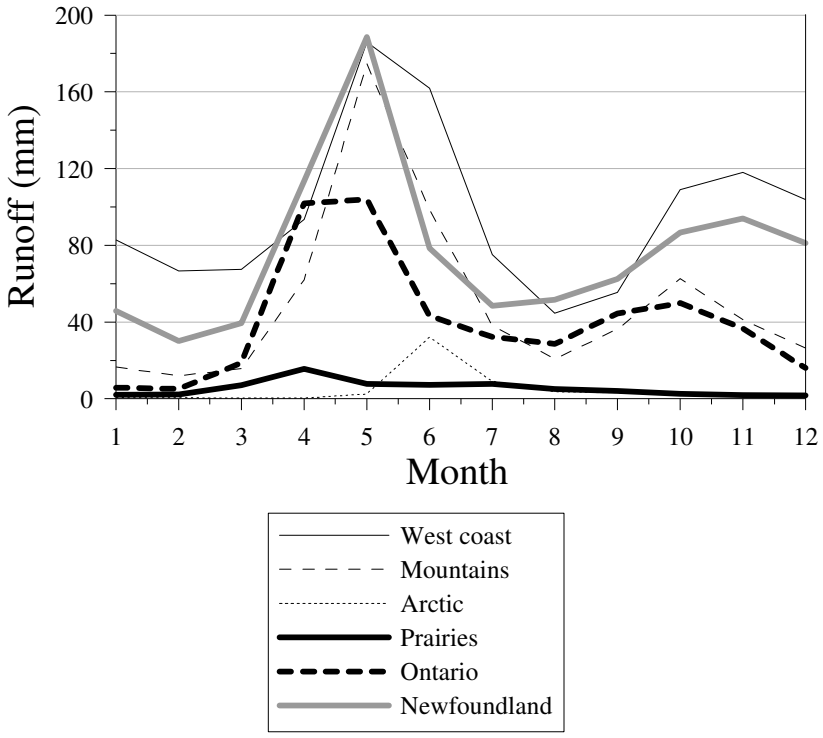

Figure 6-14: Monthly average runoff for different climatic zones.

6.2.5 Time series of hydrological variables

As well as the average monthly gridded products, there were also time series that were made from the hydrological model runs. These time series could be produced for any point in the basin for the entire length of the simulation (1961-2000). Examples are shown here for both SWE (Figure 6-15) and lower-zone storage (Figure 6-16) at the location in the prairie climate zone from the previous section.

The SWE time series appeared to show a trend, a lowering in the amount of SWE, that was consistent with a warming climate in recent decades. There were only a few winter seasons with high snow water equivalent values between 1983 and 2001 compared to the higher number of occurrences between 1961 and 1982.

There was no obvious overall trend in the lower-zone storage time series; however, it was interesting to contrast the years of 1986 that showed high values for a good portion of the spring and summer with 1987 when low values persisted throughout the year.

In order to properly investigate any trends in the data, a full analysis would have to be performed, such as pre-whitening of the data series and implementation of the Mann-Kendall technique (Burn and Hag Elnur, 2002). However, such an analysis was beyond the scope of this study.

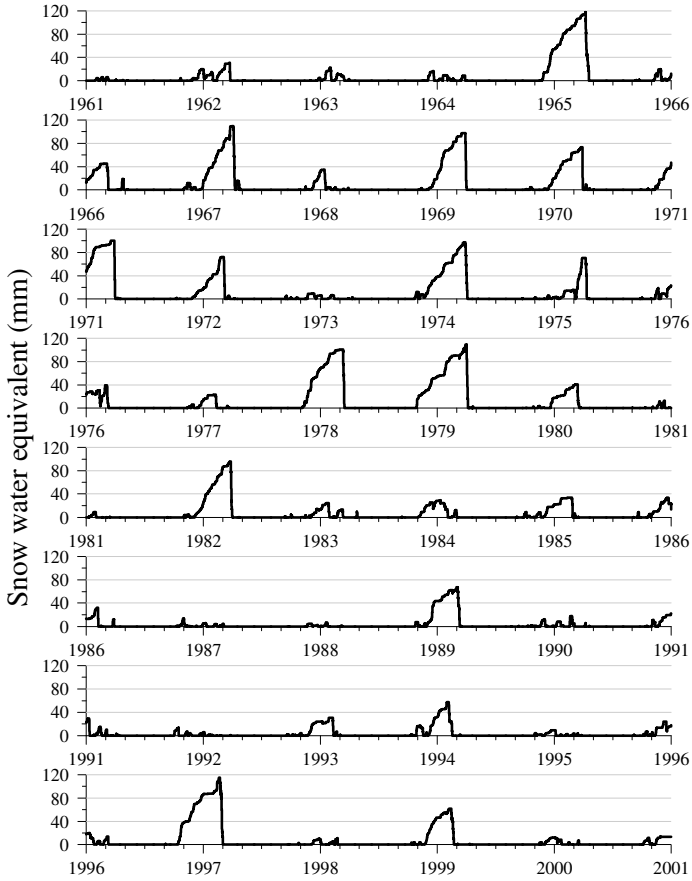

Figure 6-15: Time series of SWE for a point in the prairies.

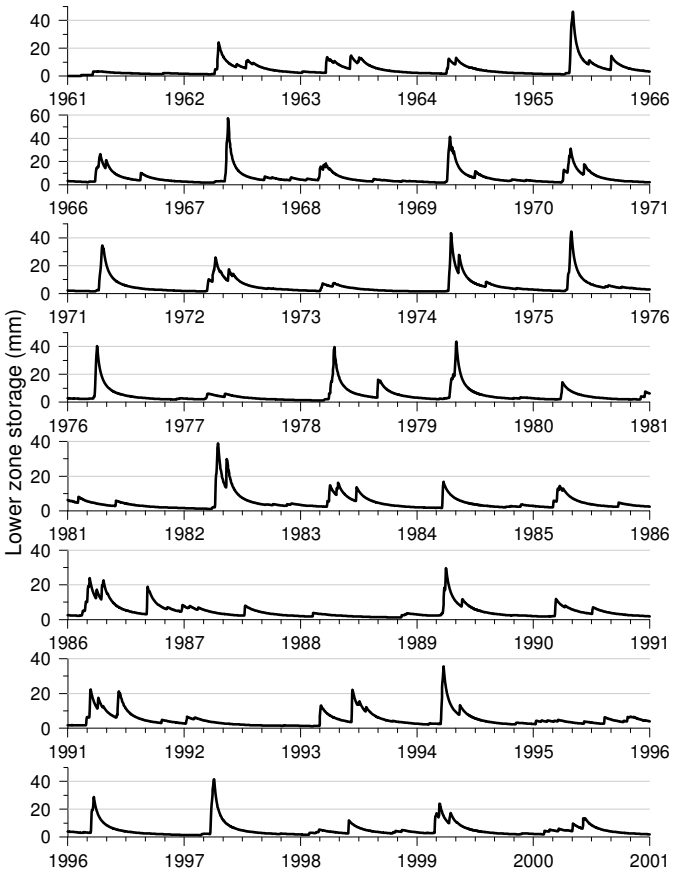

Figure 6-16: Time series of lower zone storage for a point in the prairies.

6.2.6 Runoff products

Runoff is unique in relation to the other the hydrological variables, as the runoff from each grid is transported (routed) through river systems to eventually empty into the oceans. As a result, the simulated routed runoff can be compared to measured streamflow. One of the important results of this study was that by using the simulated streamflow we could create time series of flow for any point in the country.

One of the uses for the simulation results is the creation of flow duration curves for any point along any of the rivers within Canada. An example of such a curve is given for the North Nahanni River at the mouth (Figure 6-17), a river that flows into the Mackenzie River north of Fort Simpson, NWT. This river has never been gauged and the use of simulations like this can be used in the design of an engineering structure, such as a pipeline or road, which has to cross the river. Without this kind of information, predictions of the flow in the river would have to be transferred from the closest measured basin. But depending on the distance to the nearest measured basin and the differences in

the characteristics of the two basins, simply pro-rating the flow from one to the other may lead to unpredictable and potentially dangerous results.

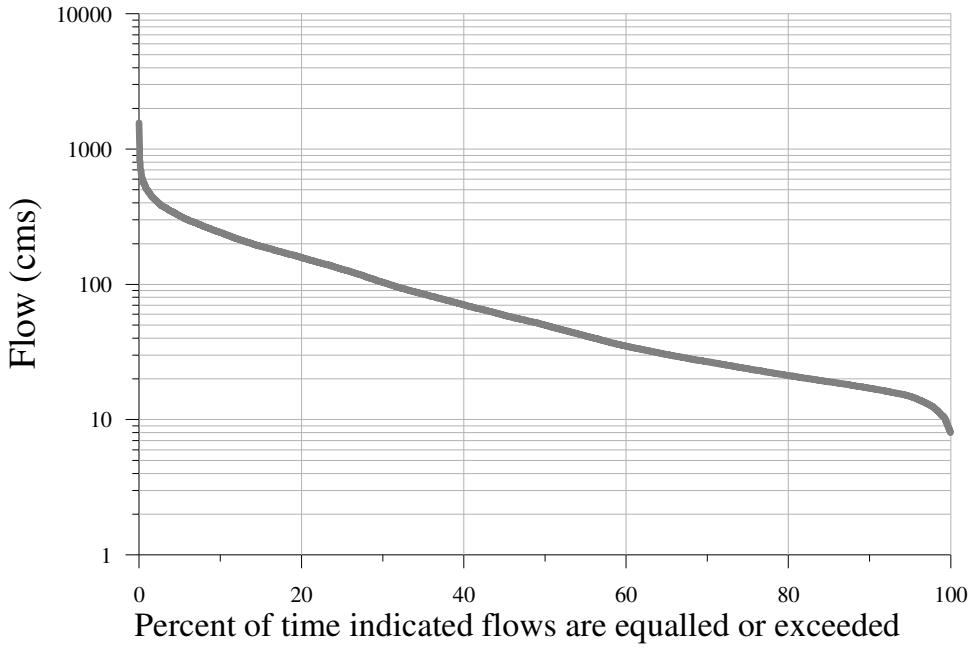

Figure 6-17: Example flow duration curve for the North Nahani River at the mouth.

In addition to their use in ungauged basins, the results can also be used in areas where the streamflow record may be incomplete. For example, the streamflow gauge along the Mackenzie River at Arctic Red River was only installed in the summer of 1972. As this is the largest single watershed in all of Canada, it would be beneficial to have an estimate of the flow from the watershed before 1972. Figure 6-18 shows the existing streamflow record along with the simulated values for streamflow for the entire period of 1961-2000.

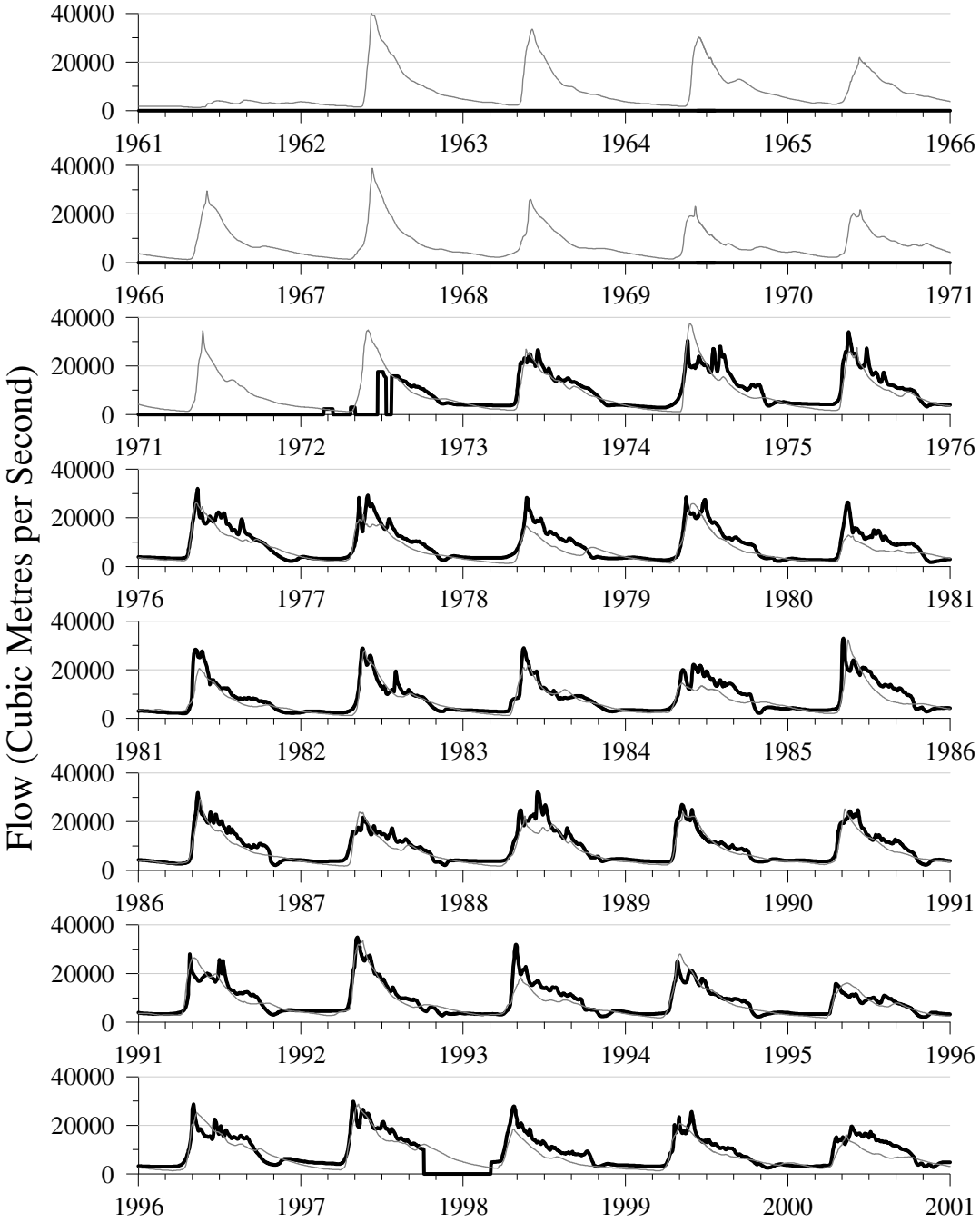

Figure 6-18: Measured (thick black line) and simulated (thin grey line) for the streamflow station Mackenzie River at Arctic Red River.

If a streamflow record covering only a short time period is used in the creation of a flow duration curve, it may be biased towards the meteorological conditions that occurred during that short time period. This may lead to incorrect assumptions being made about the long-term flow characteristics that could lead to improper and possible hazardous engineering designs. Figure 6-19 shows the difference in the flow duration curve between using only the 2 years of flows and the full 40 years of flows at the gauge located on the Athabasca River below Fort McMurray.

These examples demonstrate the utility of using the methods described in this thesis to determine the flow characteristics of ungauged basins that can then be used to make engineering and planning decisions.

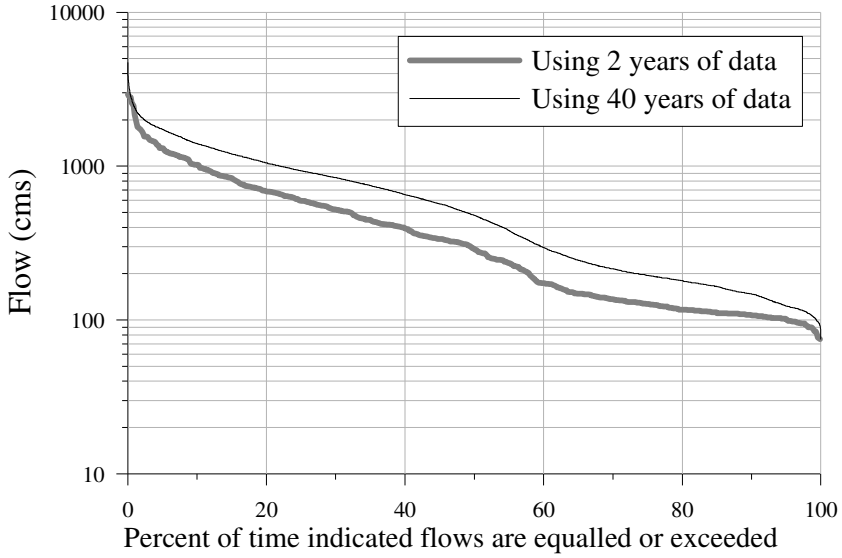

Figure 6-19: Flow duration curve showing difference between results using the incomplete record and complete record.

6.3 Assessment of the predictive uncertainty

The topic of predictive uncertainty is gaining much interest in the hydrological community and figures prominently into the first of the community objectives of the PUB study:

"Advance our ability to predict with confidence the fluxes of water and associated constituents from ungauged basins, evaluated with data from selected basins in different biomes or hydro-climatic regions, including quantification of the uncertainty in these predictions in a routine manner." (Sivapalan *et al.*, 2003)

In that report the authors highlight three different types of uncertainty: input data, parameter, and model structure. The combination of all these was collectively referred to as predictive uncertainty.

The input data uncertainty refers to the fact that both the initial values of the state variables and the forcing data used in the model will always have uncertainty with respect to the measurement of the values. Using the WATFLOOD hydrological model, the uncertainty in the initial state variables will be minimized as a result of the model structure. In WATFLOOD, the effect of the initial variables will not be noticeable in the simulation results after a year or so after the start of the run, thus most of the input data uncertainty in the model will be a result of the uncertainty in the forcing data.

Parameter uncertainty refers to the difficulty in obtaining the correct parameters for each land class. As discussed in Chapter 5, there are many difficulties in trying to directly measure some, if not all of the parameters used by a hydrological model.

The uncertainty in the model structure is the most difficult type to quantify as it is associated with the assumptions made about the hydrological processes that are used by the hydrological model. All semi-empirical models are simplifications of the actual complex processes that occur in the basins. Adding to the model structure uncertainty is the discretization of the basin, for instance using the GRU concept of WATFLOOD, which inherently makes assumptions about the hydrological processes of the basin. In order to properly quantify the model structure uncertainty, it would be necessary either change the assumptions about the processes in a single model or use entirely different models to create the gridded maps of the hydrological variables. As these models are very complex, it would have been very difficult and time consuming to acquire, implement, and properly calibrate a variety of different models.

Unfortunately, it is difficult to determine the proportion of each of these uncertainties when the model evaluation is based on a single objective function (Bevin, 2006). Thus, even though the concept of predictive uncertainty has been around for over a decade, there is no consensus on how it should be quantified (Gotzinger and Bardossy, 2008). Different methods have been developed such as Monte Carlo procedures, fuzzy logic, the generalized likelihood uncertainty estimator (GLUE), and Bayesian Recursive Estimation (BaRE), each with their own supporters and detractors.

Although the GLUE method is not without its critics (Theimann *et al.*, 2001; Stedinger *et al.*, 2008) it is the most popular method to quantify the uncertainty in hydrological models (Christianes and Feyen, 2002; Aronica *et al.*, 2002; Montanari, 2005). However, this method relies on performing many runs of the hydrological model and this is only feasible when the simulated area is small or the simulation is only run for a short time period.

In this study, both the size of the study area and the simulated length resulted in execution times of the model runs that would have made it impossible to complete the number of runs needed to perform a GLUE analysis. It was also beyond the scope of this study to perform an in-depth analysis of the

predictive uncertainty of the model, however a simple technique based on using the DDS algorithm was performed to partially quantify the predictive uncertainty in the simulation results examining the parameter uncertainty. The technique that was used in this study was similar to the one proposed by Tolson and Shoemaker (2008) in a study that demonstrated the computational efficiency of using a modified DDS analysis to determine uncertainty when compared to the GLUE methodology.

The results of the 100 separate runs of the DDS technique from the calibration of the WATFLOOD model were used to determine a measure of the parameter uncertainty. The technique used was similar to the GLUE method, in that it examined the results of a number of runs and from those assumed that the range of results seen in the test runs were an envelope of likely results. The difference was that instead of using a Monte Carlo technique to choose random values for the parameters, the results of the runs of the DDS technique were used. This resulted in a more efficient use of computing time, as in general the Monte Carlo technique results in a vast majority of the runs not being used. This is because in the GLUE method, only those model runs determined to be behavioural are used in the determination of the uncertainty. Behavioural runs are defined by Bevin (2006a) as those that are "acceptably consistent with the observations". Unfortunately there are no absolute rules for determining if the results of a particular simulation are behavioural and thus it will always be a subjective criterion left up to each researcher to determine.

In this study, it was assumed that each of the 100 runs of the DDS technique was behavioural. Although each of these runs resulted in a different parameter set, if the DDS technique was performing properly, then any of the parameters sets that produced the highest value of the objective function after 200 trials of DDS should have been able to be considered as behavioural.

Assuming that each of the simulated values at each time step from all of the behavioural runs were equally valid, the streamflow values for each simulation were plotted on a graph sometimes referred to as a "spaghetti" plot (Figure 6-20). However, after plotting the results of the 100 runs, it was difficult to distinguish any of the individual runs.

There is currently an on-going debate about not only how to measure uncertainty (Bevin, 2006b; Hall *et al.*, 2007; Hamilton, 2007), but even on the very definition of the term "uncertainty" (Montanari, 2007). As well, using the GLUE method to assign confidence intervals has been criticized because of the assumptions that have to made about the distribution of the uncertainty that are not necessarily true (Manovan and Todini, 2006).

Thus the range of simulation values was labeled here as an "ensemble range" in an analogous manner to what is done in the atmospheric sciences. A benefit about using this term is that it makes no assumptions about the distribution of the uncertainty. However, a deficiency of the term is precisely that it is hard to define exactly what the range actually represents. Thus there is no implication that this range represents a specific confidence interval, but rather represents the spread of

simulated values that could be expected based on the uncertainty in deriving the correct hydrological model parameters.

If a majority of the measured streamflow was not contained within the ensemble range than it would have shown that even when a wide range of parameters had been examined, the model was not able to properly simulate the streamflow. This would indicate that either there were processes that were either missing from the model or were not properly simulated as well it could have also indicated that there was a problem with the input data being used to run the model. If all of the measured streamflow was within the ensemble range it cannot be definitively said that all parts of the model were working correctly, however it would indicate that overall the model was able to properly simulate the streamflow from the basin.

In this example (Figure 6-20), most of the measured streamflow is bounded within the ensemble range. This indicates that for this basin the model was generally able to adequately simulate the streamflow. However, in the fall of 1990 the ensemble range has a secondary peak while the measured data quickly goes down, falling outside of the ensemble range. This indicates a problem with the model and as the model appears to be working during other years, this may indicate a problem with the input data and that the input data should be examined for this time period to see if there is a problem.

The ensemble range is presented for each of the calibration streamflow gauges in Appendix B. It can be seen that for some of the gauges the measured streamflow is consistently outside of the ensemble range. This indicates that either there is a chronic problem with the input data over these basins or there is some process that is not being adequately simulated by the model.

An ensemble range was also plotted for a sample flow duration curve (Figure 6-21). This type of information on the range of peak flows could be used as part of a risk assessment for the design of engineering structures such as spillways. The range in the low flows could be used to assess the viability of hydroelectric power or the impact of drought conditions on irrigation practices.

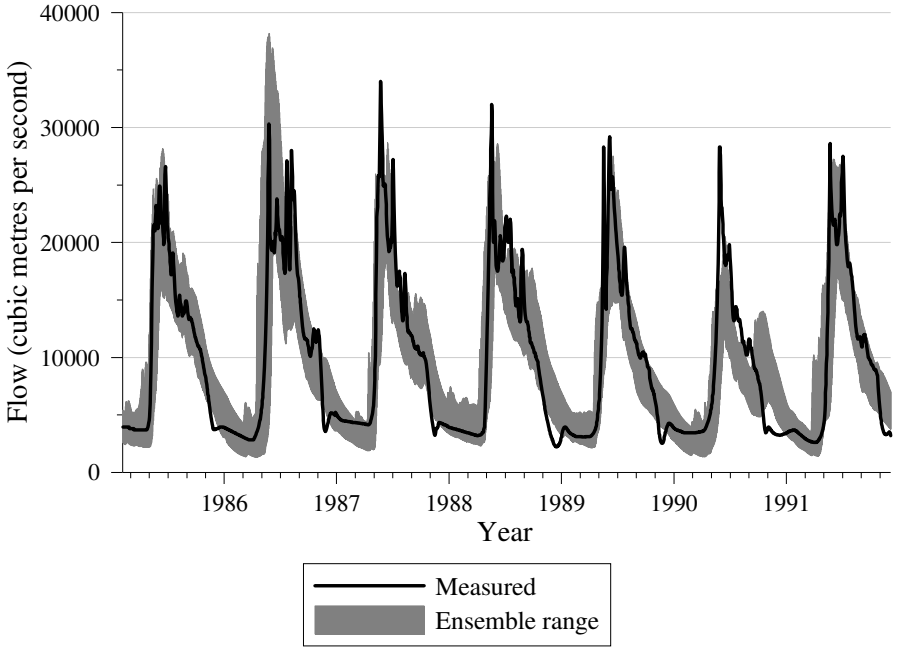

Figure 6-20: Hydrograph showing ensemble range of simulated flows when examining parameter uncertainty.

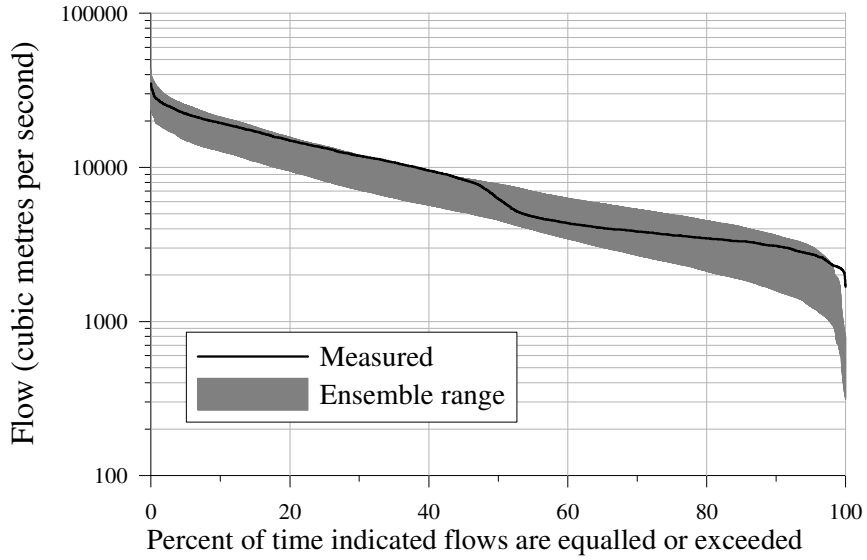

Figure 6-21: Flow duration curve showing uncertainty range.

This treatment of uncertainty also allowed ensemble ranges to be shown on the hydrological variable datasets presented in Section 6.2. Shown here is the ensemble spread of the runoff (Figure 6-22) and upper-zone storage (Figure 6-23) for the mountain and Ontario climate regions.

It is interesting that although there was a lot more runoff in the mountain climate zone, the ensemble range in the Ontario climate zone was actually larger during the spring melt period. However the range was much smaller in the Ontario climate zone during the fall and winter. For upper zone storage the range was much larger in the Ontario climate zone for all times of the year than it was for the mountain climate zone

In order to display the ensemble spread of the gridded data, the magnitude of the ensemble spread was calculated for runoff (Figure 6-24) and AET (Figure 6-25). In these figures the spread was normalized with the average value of the variable. It is interesting to note that in general the Arctic did not have a large relative ensemble range for both of these variables when compared to the rest of Canada. This was despite the fact that there were relatively few measurement stations in that part of the country.

It would be informative to determine the reasons why there are areas that have a large magnitude of the ensemble spread. If, for instance, it was found that the reason for the high magnitude of the ensemble spread was a result of poor input precipitation, then perhaps adding a measured precipitation station near that location could reduce the magnitude of the ensemble spread and thus also reduce the predictive uncertainty. Hence using these maps of uncertainty could be the first step in the determination of the locations where future measurement stations would do the most good in reducing the predictive uncertainty.

It must also be remembered that the way the ensemble range was derived it only examined the parameter uncertainty. Thus in order to get an estimate of the total uncertainty, methods have be developed that will also assess the magnitude of both the model and the input data uncertainty. It is only with this type of information that fully informed decisions can be made with the simulation results.

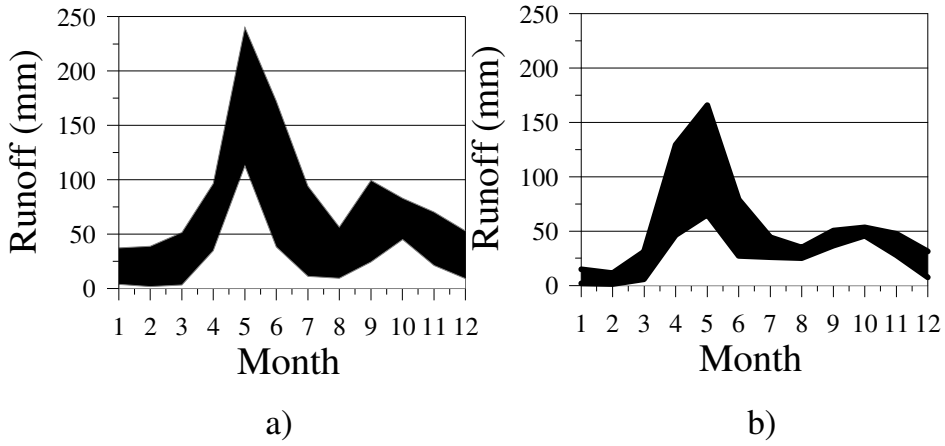

Figure 6-22: Ensemble spread of runoff in the a) mountain and b) Ontario climate zones.

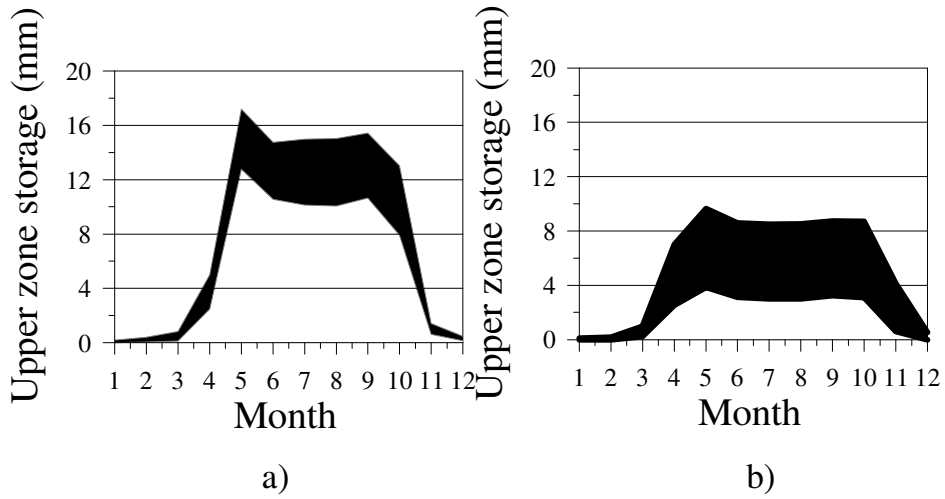

Figure 6-23: Ensemble spread of the upper-zone storage in the a) mountain and b) Ontario climate zones.

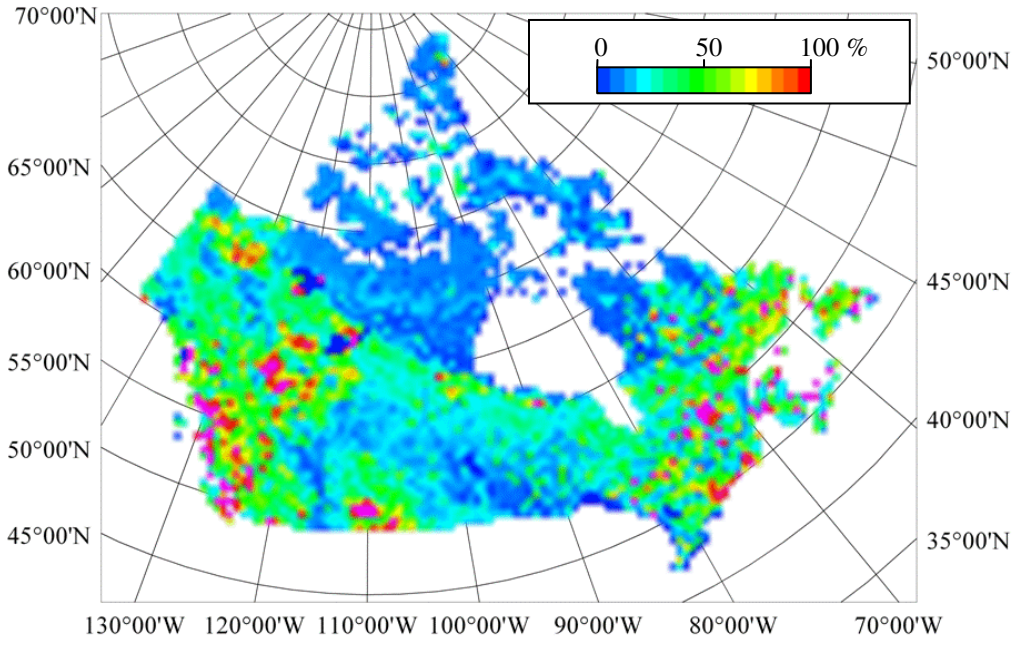

Figure 6-24: Magnitude of the ensemble spread of runoff normalized using the average value.

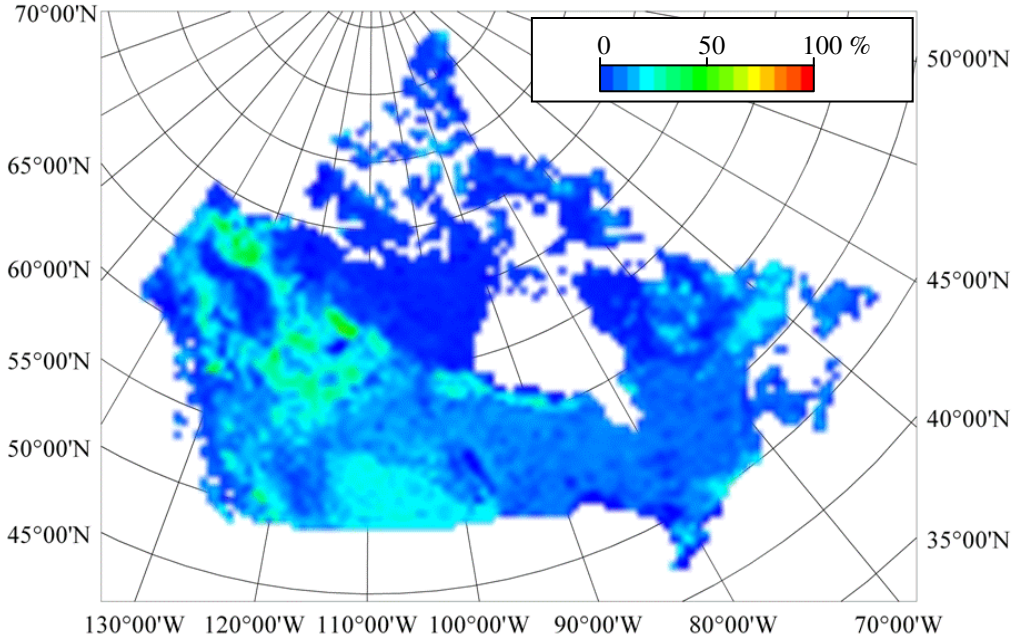

Figure 6-25: Magnitude of the ensemble spread of AET normalized using the average value.

6.4 Effects of changes in temperature and precipitation

As a first step in examining the effects of climate change, WATFLOOD runs were carried out where the precipitation was held constant and the temperature was adjusted from 2 ºC below the current climate to 8 ºC above the current climate. Similarly, a set of runs was also performed where the temperature was held constant and the precipitation was adjusted from 20% below the current climate to 20% above the current climate.

Results were examined in the same climate zones as Section 6.2. A similar relative effect was seen in all of the climate zones; thus, only the results from the mountain grid square are shown here for clarity. Presented are the relative change in the average annual values of the hydrologic variables as a result of changes in the temperature and precipitation.

In general, a rise in temperatures caused a dramatic lowering of the snow-water equivalent and a rise in the amount of upper-zone storage and AET. This rise in AET caused a lowering of the runoff, at the most extreme rise in temperature of 8 ºC the runoff was lowered by 11.7% (Figure 6-26 and Figure 6-27).

The effect of having more or less precipitation was predominantly linear with a 20% increase in precipitation resulting in a 24% rise in runoff and a 22% rise in snow-water equivalent. The AET only changed by 1.2% showing that the limit on AET was not the amount of water in the system but rather the temperature. It is not shown, but the effect of a 20% increase in precipitation on AET was slightly higher in the Arctic (5.2%) and the prairie (3.6%) climate zones.

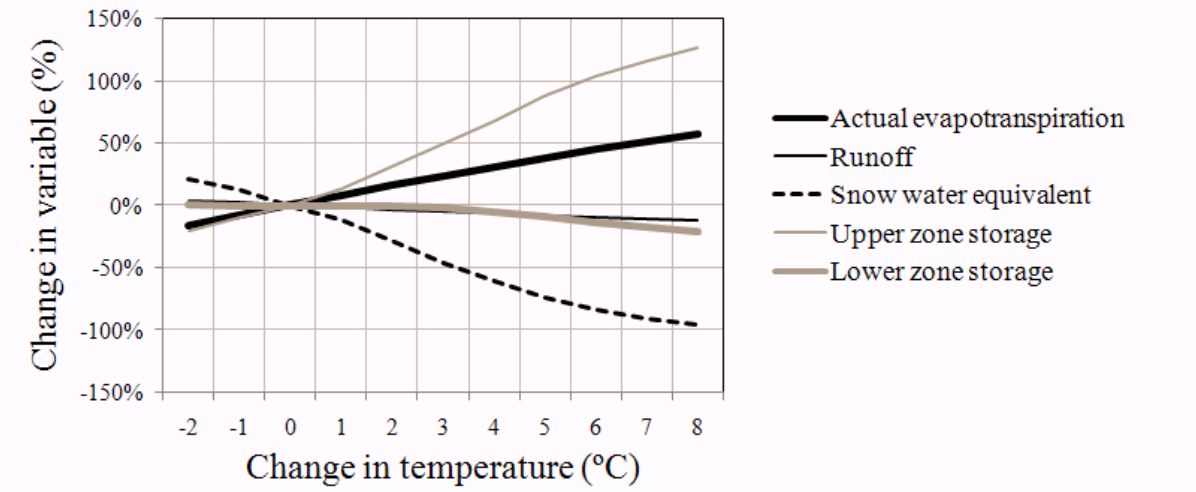

Figure 6-26: Change in hydrological variables in the west coast mountain climate zone as a result of changes in temperature.

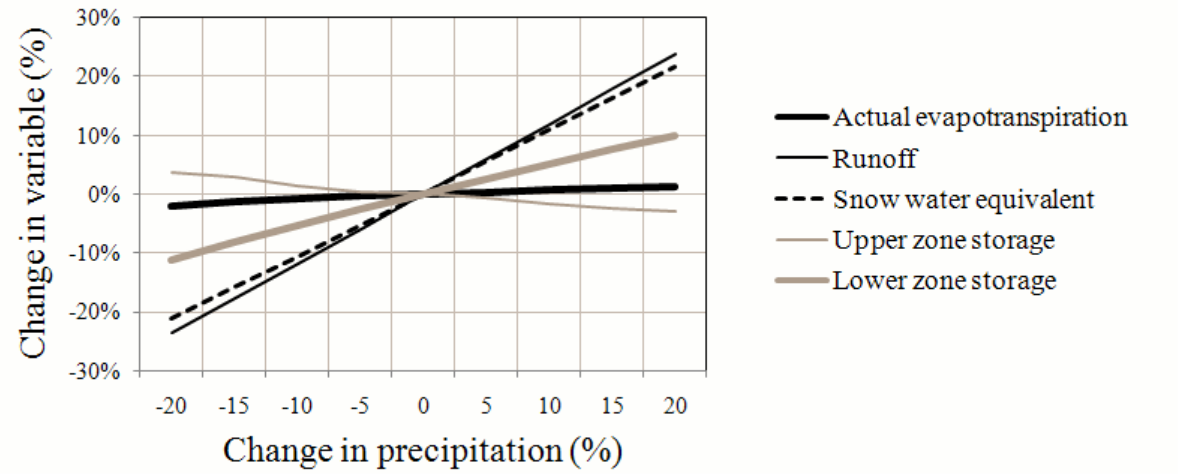

Figure 6-27: Change in hydrological variables in the west coast mountain climate zone as a result of changes in precipitation.

To further examine these effects, the monthly averages of runoff and snow water equivalent were calculated for the current climate and temperature rises of 4 ºC and 8 ºC (Figure 6-28 and Figure 6-29). The annual pattern of runoff dramatically changed under a warming climate with a lowering of the peak spring runoff and more flow in the winter months. This was a result of the reduction of the snow-water equivalent to very small values as the temperature is increased.

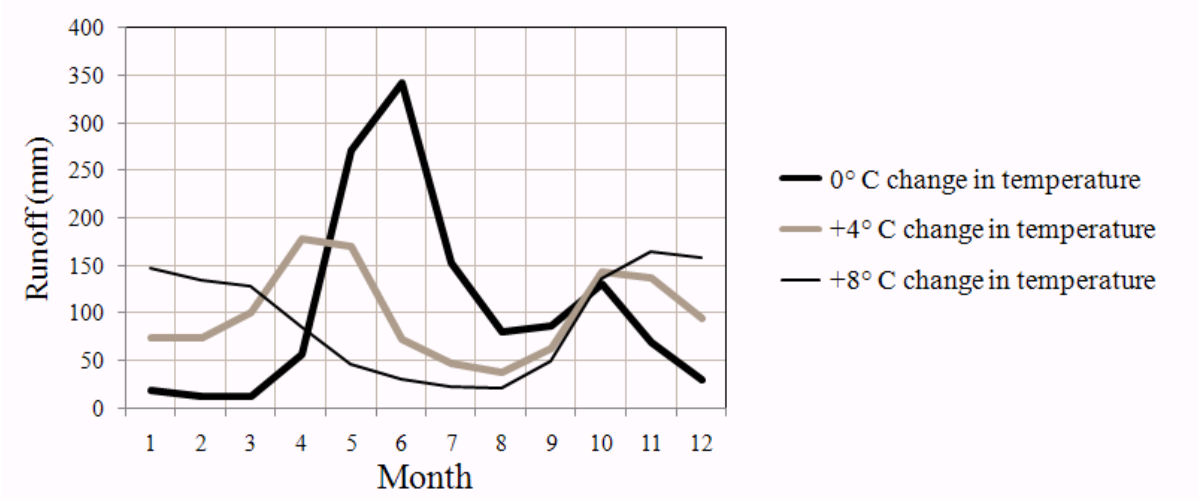

Figure 6-28: Change in monthly runoff in the west coast mountain climate zone as a result of changes in temperature.

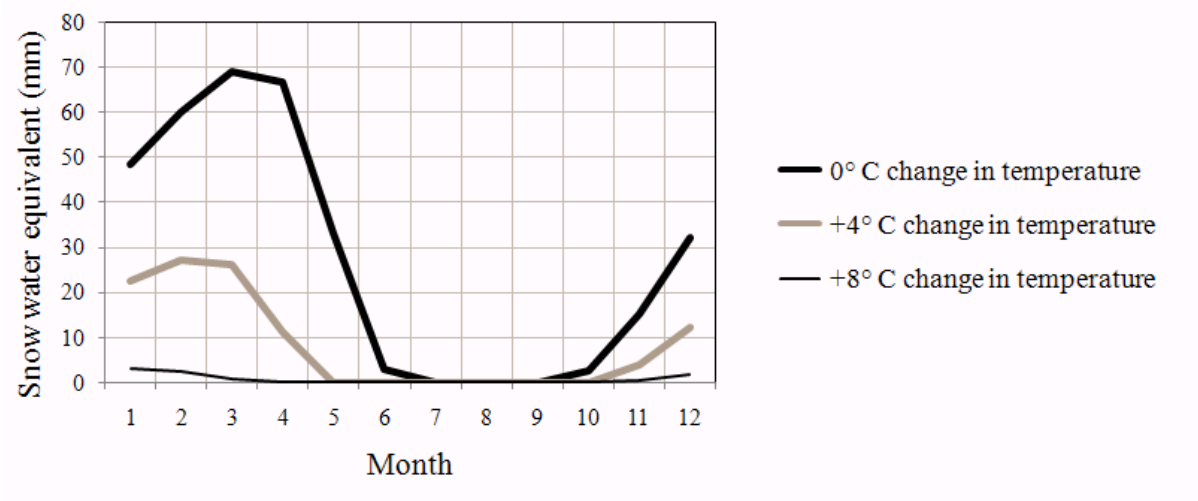

Figure 6-29: Change in monthly snow water equivalent in the west coast mountain climate zone as a result of changes in temperature.

The change in the amount of precipitation did not dramatically change the pattern of the monthly runoff (Figure 6-30). The increase or decrease in the amount of precipitation merely acted to shift in the amount of runoff up and down.

There were only small changes seen in the annual amount of AET with the variations in precipitation. The reason for this was evident when viewing the monthly values (Figure 6-31). As most of the AET only occurs in a few months in the year, even with the extra water present when the precipitation was increased by 20%, there was only a small rise in total AET during July and August and almost nothing during the other months of the year.

As even increasing the amount of precipitation this much only had small change in the AET, this indicated that the limiting factor of AET was the amount of energy input into the system and it was not limited by the amount of water. It must be remembered that the results were shown here only for the mountain climate zone; although the other climate zones had the same general behavior results with other land cover types may be different. Also important is that the results are the average values over the 40 year WATFLOOD runs and thus there may be particular years when the change in precipitation may have a greater effect on the AET.

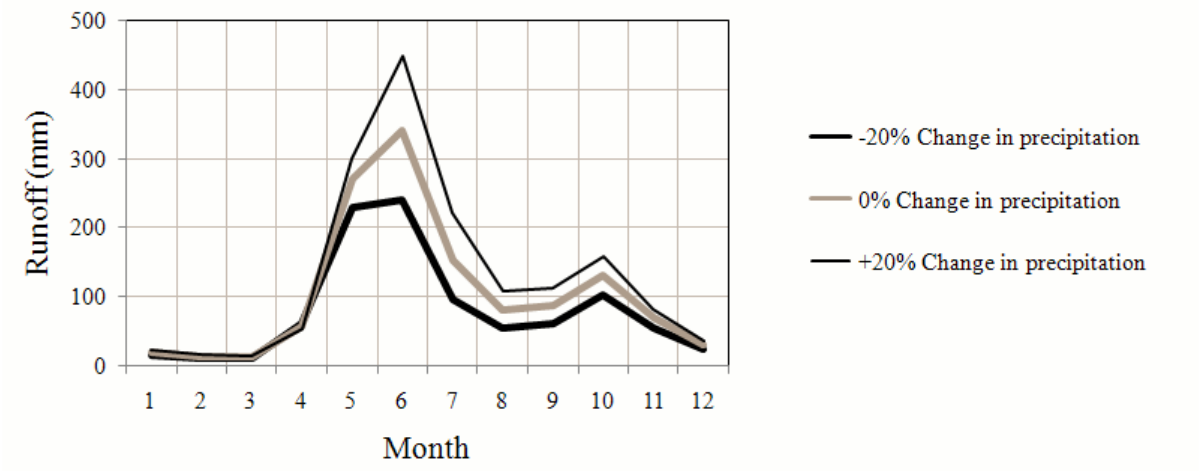

Figure 6-30: Change in monthly runoff in the west coast mountain climate zone as a result of changes in precipitation.

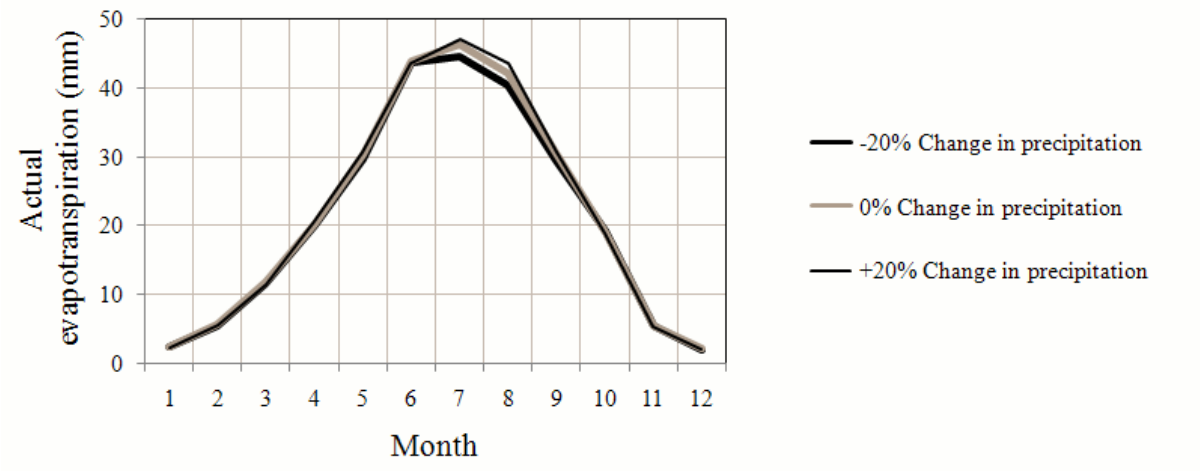

Figure 6-31: Change in monthly AET in the west coast mountain climate zone as a result of changes in precipitation.

6.5 Future climate scenarios

A future climate scenario refers to the predicted rise of carbon in the atmosphere based on such factors as world population, economic growth, adaptation of alternative energy sources, and the global distribution of new technologies. There are many different future climate scenarios based on these different factors (IPCC, 2007).

The analysis of these scenarios is further complicated by the fact that there are also many different climate models that can be used to estimate the changes in temperature and precipitation based on the different scenarios. Each one of these will produce different results even if they use the same future atmospheric carbon conditions. As a result, there are many different possible values for temperature and precipitation depending on which climate scenario and which model you choose.

It would have been impossible to produce maps of the hydrological variables for all of the different combinations of future climate scenarios and prediction models. Instead, an example is shown here of a particular future climate scenario, referred to as the A2 scenario. This scenario considers a very heterogeneous world with medium economic growth, increasing population growth, and high energy use with slow introduction of new and efficient technologies. It assumes that the level of CO_2 concentration in the atmosphere will reach 850 ppm in the year 2100 (IPCC, 2007).

This climate scenario was used as input into the second version of the Coupled Global Circulation Model (CGMC2) created by the Canadian Centre for Climate Modelling and Analysis (CCCma). The results of the model run for the time period between 2050 and 2060 were available from the Pacific Climate Impacts Consortium in Victoria, BC. Shown here are the changes in temperature (Figure 6-32) and precipitation (Figure 6-33) based on this model.

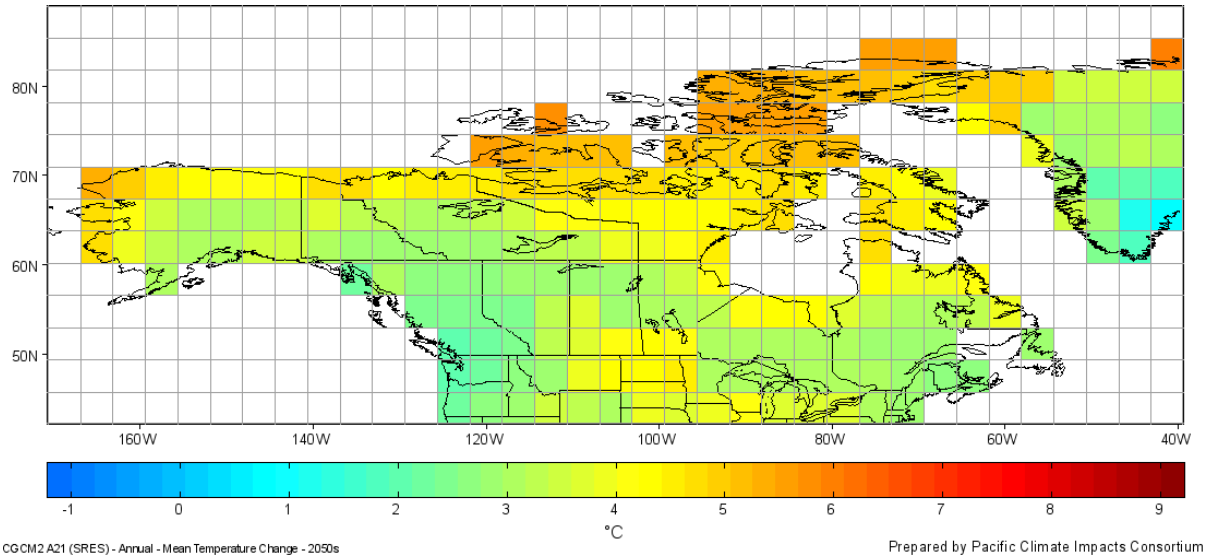

Figure 6-32: Mean annual temperature change from the A2 scenario using the CGCM2 model for 2050-2060.

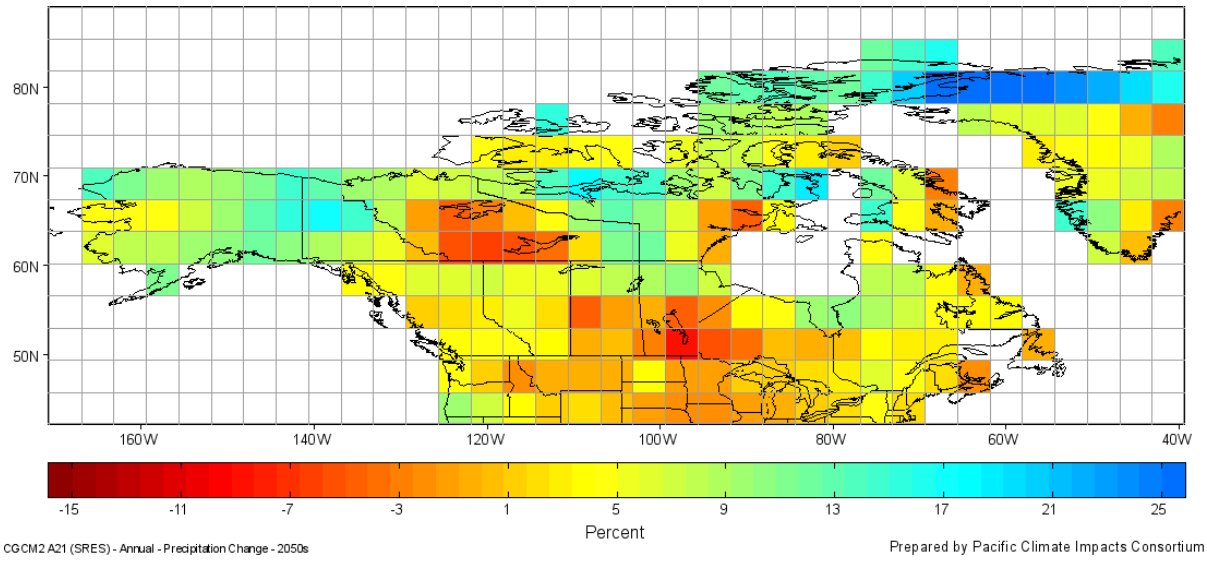

Figure 6-33: Annual precipitation change from the A2 scenario using the CGCM2 model for 2050-2060.

For this example, the effects of the future climate were examined for the streamflow station located on the Liard River at Fort Liard, this streamflow station drains a large area in northern British Columbia and northern Alberta. Examining the CGCM2 results for the A2 climate scenario in this area, the temperature shows a rise in annual mean temperature of about 3 ºC and a rise in precipitation of about 5%.

The WATFLOOD model was run adjusting the input temperature and precipitation by the amounts calculated by the CGCM2 model. The resulting hydrograph displayed a very pronounced flattening of the peak spring flow and an overall reduction in the total amount of runoff (Figure 6-34). This was reflected in the flow duration curve as a general flattening out of the curve (Figure 6-35). Such an analysis allows for an engineer to use such a curve to design structures that have a design life that will be impacted by the effects of climate change.

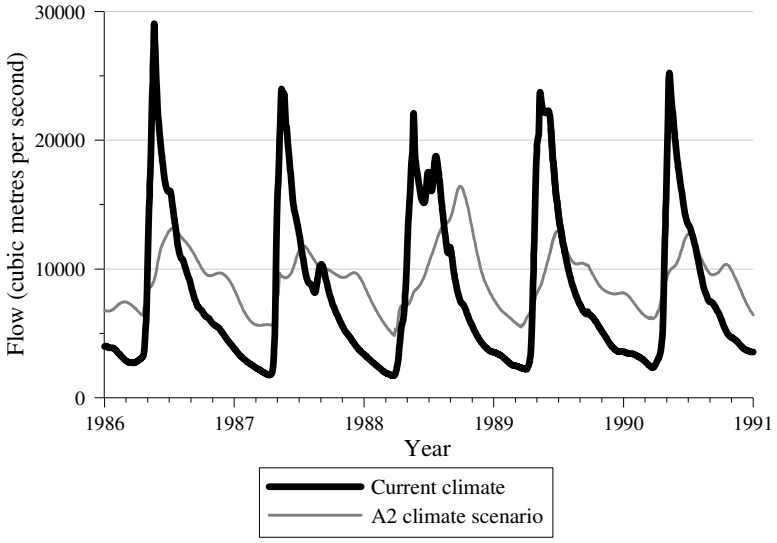

Figure 6-34: Simulated streamflow comparison between the current climate and the A2 climate scenario for the Liard River at Fort Liard gauge.

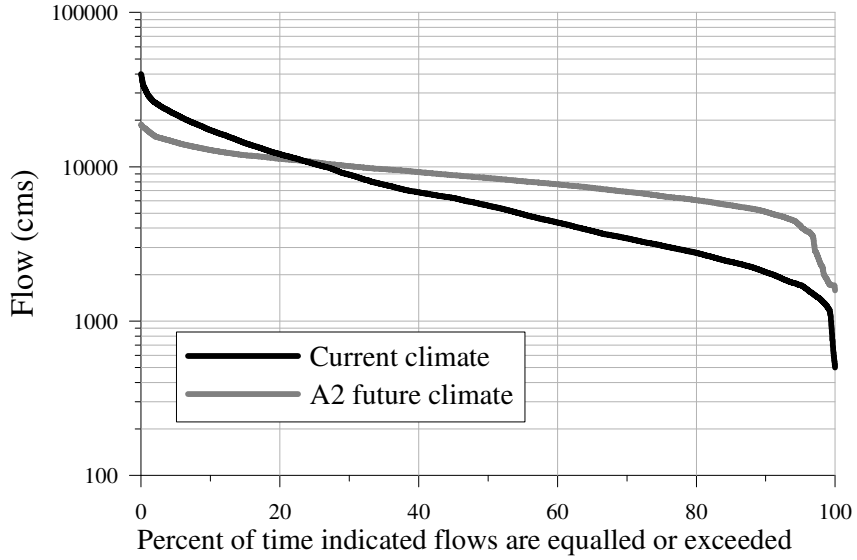

Figure 6-35: Simulated flow distribution curve comparison between the current climate and the A2 climate scenario for the Liard River at Fort Liard gauge.

6.6 Chapter discussion

In this chapter, the best estimates of a time series of gridded values for the major hydrological variables were presented. The hydrological model used was constrained by measured temperature, precipitation, and streamflow. For this reason there is confidence that the other hydrological variables are also correct. It will now be possible to use these gridded time series as comparisons for other gridded products such as the NCEP or ECMWF re-analysis products or climate simulations of the current climate. The values of these other hydrological variables were examined for the entire country as well as a detailed examination at specific points representing different climatic zones within the country.

An attempt was then made to quantify the relative contributions to the overall predictive uncertainty from the input data uncertainty and the parameter uncertainty. Finally, the general effects of future climate scenarios on the hydrological variables were examined for a uniform change in temperature and precipitation as well as the specific effects of a particular future climate scenario on a particular watershed.

The effects of a changing climate on the hydrological variables are quite dramatic. The overall effect on the runoff would suggest a lowering of peak flows and a rise in the low flows. However, it should be remembered that these future climate simulations are based on very broad adjustments to the temperature and precipitation on the monthly scale. In the near future models of future climate scenarios will become available using models that have a finer scale in both time and space. The output of these models will give a better indication if these future climate scenarios will lead to more extreme storms and periods of drought. For the moment, the analysis done in this study will serve to indicate the broad changes that can be expected in the hydrological variables under currently available climate change scenarios.

One advantage of the hydrological model used in this study is that simulated daily streamflow data are available from the model. This allowed for flow duration curves to be created from the output simulations. If the analysis had only been done on a monthly or annual basis such curves would not have been possible.

Chapter 7
Conclusions and Recommendations

7.1 Conclusions

7.1.1 Drainage database

It was shown through various tests that the WATMAP technique developed for this project, produced a better representation of the drainage characteristics of a watershed than the simple D8 technique based on the average elevation of the model grid square.

The assumption that all of the drainage from a model grid square leaves the grid square in the direction of the principal drainage direction, leads to estimates of drainage area that are further from the actual measured values than using the WATMAP technique. Using this technique, proportions of the flow from each model grid square are allowed to flow out of the model grid square in different directions.

The need to account for different types of diagonal flow was also demonstrated. Again this was done by comparing the difference between the simulated and measured drainage areas of a number of watersheds in Canada using different values of a parameter dubbed the diagonal factor. A diagonal factor of 15% was found to minimize the error in the simulation of the drainage areas.

7.1.2 Station data interpolation

It was found that the WATMAPPR technique generally performed better than an IWD technique in the interpolation of distributed measured station data. This better performance was shown by both a reduction in the root mean squared error of the interpolation as well as a reduction in the mean error. In particular, the WATMAPPR technique showed the most improvement over the IWD technique in the Arctic regions of Canada, suggesting that it does well in areas with very sparse measured data.

In order to best utilize the benefits of the WATMAPPR technique, the country had to be divided into six regions for the precipitation interpolation and into three regions for the temperature interpolation.

There were however certain regions of the country and certain time periods where the simpler IWD technique did outperform WATMAPPR. As well, the final maps of precipitation and temperature sometimes showed discontinuities between the different regions that were unrealistic.

A technique was designed to use WATMAPPR in the interpolation of daily data for precipitation. This technique used the value of the daily precipitation and the monthly precipitation patterns to produce daily precipitation fields in order that the final interpolated fields were not biased by the presence of 0 values. These daily estimates were also shown to have less error than the comparable daily interpolations using the IWD technique.

In the end, gridded time series of precipitation and temperature were created that were based on measured data; because of the techniques used to create them, they were not biased by the locations of measurement stations.

7.1.3 Model calibration

It was shown that it was best to choose which parameters to calibrate based on the objective function that is used in the calibration. When using the annual difference in the simulated and measured total runoff, the most important parameters to optimize were those related to the calculation of evapotranspiration. While using an objective function that took into account the timing of the differences in the measured and simulated flow, more parameters were now needed in the calibration. These included the parameters that control the snowmelt, flow through the soil, and river channel roughness.

It was also demonstrated that it is best to first calibrate the parameters on basins which are mostly comprised of only one or two different land classes. This initial calibration will only adjust the parameters for these individual land classes. Then the results of this calibration should be used as the starting parameter set in a calibration using all of the basins that contain all of the land classes.

The final calibration consisted of 100 separate 200-trial DDS calibration runs, and it was found that the best simulation results were obtained by averaging the simulation outputs from each of the 100 DDS calibrations.

Although the overall average objective functions were better after calibration, there were individual basins where the results were not improved and the simulated streamflow was still quite poor. This indicated that the choice of parameters was not the main reason for the poor results but rather there were probably problems with the drainage database for those basins, there are processes that are missing from the hydrological model, or there were problems with the input data.

7.1.4 Gridded products

Gridded time-series datasets were presented for the hydrological variables of evapotranspiration, snow water equivalent, soil moisture, and runoff. Along with the monthly gridded averages for the entire country, annual time series of the hydrological parameters were examined in six locations in Canada representing different climatic regions.

The areas of highest runoff, snow-water equivalent, and soil moisture coincided with the highest values seen along the west coast and western mountains, with another peak along the east coast. The Arctic showed much less evapotranspiration and a delayed runoff peak.

For runoff, the utility of using the techniques to derive flow frequency at ungauged locations was demonstrated, along with the ability to fill in missing parts of measured streamflow records and to create flow frequency diagrams.

A simple technique was presented to evaluate the magnitude of the parameter uncertainty. The technique allowed for the presentation of simulation results of both the runoff products and the gridded hydrological variables that showed an ensemble range of values as opposed to simply a single value.

The change in the hydrological variables as a result of changes in the temperature and precipitation were examined. The results showed that increases in temperature led to a sharp increase in the amount of actual evapotranspiration and a decrease in snow-water equivalent, leading to a decrease in runoff, especially in the spring and early summer. The changes seen as a result of variations in the precipitation were generally linear and did not greatly affect the monthly pattern of runoff.

7.2 Recommendations

This thesis presented the gridded hydrological variable time series that could be achieved with the current state of hydrological modelling and computer resources. Inevitably in the years to come, advances in both of these areas will lead to opportunities to push the science even further. Considering this, the following recommendations are made that would advance the science presented in this thesis.

7.2.1 Verification

Although the runoff calculated by the hydrological model used in this study was compared to measured streamflow, the internal variables of the model need to be verified with some type of independent field measurement. This will increase confidence that the model is correctly simulating all of the hydrological processes.

However, it is difficult to acquire datasets to verify the gridded datasets of the hydrological variables. Point measurements could be used, but scaling issues must be considered to ensure that the point measurements that are taken can be directly relatable to the grid average values which are calculated using the models.

One example of an available gridded dataset is the output from the Gravity Recovery and Climate Experiment (GRACE) satellites (Tapley *et al.*, 2004). These satellites measure the change of gravitational pull as they orbit the earth and it is thought that one of the factors affecting these changes is the amount of water stored in the earth. It is theorized that the change in gravitational pull from an area is related to the amount of water stored in the land surface, thus the GRACE data should be comparable to the change in storage in the hydrological model (Van der Wal *et al.*, 2008). Unfortunately, as the GRACE satellites were only operational beginning in 2002, the use of the information from these satellites could not be done for this study.

Other possibilities include the use of satellite data to verify the gridded maps of snow water equivalent or evapotranspiration. But as these are remotely sensed datasets, care must be taken to ensure that they have been properly verified as well.

7.2.2 Trends

As this study has resulted in a time series of the hydrological variables on a gridded basis for the entire country, their trends can now be examined to see if any significant trends existed in the variables. As explained in the study, there are existing techniques that have been proven to reliably detect trends in annual data.

As each grid square of the model has its own time series, instead of just examining the trends for a specific station, they could be calculated for each grid square showing the pattern of the trends across the country. This could be a valuable tool to determine if the effects of climate change have affected one area of the country more than others.

7.2.3 Predictive uncertainty

This study was only able to perform a simple examination of the predictive uncertainty on the simulated streamflow coming from the parameter uncertainty. More work needs to be done in order to evaluate the proportion of the overall predictive uncertainty that is a result of the parameter, input data, and model uncertainty.

The model uncertainty portion of the predictive uncertainty should be examined by setting up other hydrological models to simulate river flow. These different models will have different governing equations and will have different assumptions about the processes that make up the hydrological cycle. Using a combination of these models will allow for a quantitative determination of the model uncertainty.

Models such as the VIC model and the MESH model are based on the same grid structure for the drainage database as WATFLOOD and this should simplify the process of implementing these other models.

7.2.4 Regional climate models

A new generation of climate-change scenarios are currently being developed using output from Regional Climate Models (RCMs). These models are an exciting opportunity to make more detailed conclusions about the future climate. Not only do they offer better resolution in the spatial sense, but they also offer a better temporal resolution. This will allow for the determination of the effects of climate change on particular areas as well as the effects on extreme events instead of just making conclusions on monthly or annual averages.

As the RCM output contains many fields, they will be able to be used by more advanced hydrological models such as MESH hydrological model being developed by Environment Canada. MESH has a more rigorous treatment of the energy balance and of the flow of water through the soil, however as well as temperature and precipitation it also needs additional forcing data such as radiative inputs, wind speed, pressure and humidity. However, these additional forcing fields are part of the RCM output.

7.2.5 Improvement in the model implementation

In general, the RCM models discussed in the previous section are run at a finer model scale than the drainage database that was created for this study. However, the WATMAP technique developed here could be used to create the drainage database files at these smaller resolutions. Running a hydrological model at smaller resolutions would allow for regional effects of climate change to be examined as well allowing for smaller basins to be used in the model calibration.

The current version of the WATFLOOD model does not allow for the change of land-cover type during the simulation. This is not of concern during shorter model runs, but as the length of simulations have grown to decades, there is a need to be able to adjust the percentages of land cover types in each model grid square during the simulation. This will become more important in studying future climate scenarios, especially in areas that currently contain glaciers, since the glacial area has been greatly reduced in past decades. The flow characteristics of a river that currently has a significant portion of glacial flow will be drastically changed if the glacial area is reduced or eliminated. The drainage database of the hydrological model must be able to dynamically reflect these changes.

7.2.6 Other input datasets

There also exists a precipitation data set where the raw station readings have been rehabilitated by Environment Canada (Mekis and Hogg, 1999). This dataset was corrected for a variety of effects, for example Metadata records from each station were examined to determine when the type of instrument changed, when the instruments were moved, or other instruments were added. However, this dataset is currently only available on a monthly basis and, since this study needed to examine data on a daily basis, it could not be used here. However, it should be considered for future studies once the daily rehabilitated dataset is available.

7.3 Summary discussion

This work has produced what I believe is the most reliable time series of gridded hydrological parameters based on station data for all of Canada currently available. The goal was not to create a dataset that would replace other datasets that are based on modeled output from atmospheric or numerical weather models. Rather, as the datasets created in this study are based on station data, it is hoped that the data sets will be useful for future studies as a comparison to other gridded parameter sets, whether they are created from numerical weather output, hydrological models, or remote sensing.

In 1971, it was concluded by Hare and Hay (1971) that because of the limitations in the amount of data available in northern Canada, accurate seasonal water balances could not be made. It is hoped that using current technological advances in data assimilation and modelling this thesis has demonstrated that it is now possible to accurately examine various components of the water balance at monthly timescales for the entire country including the Canadian Arctic.

This thesis also demonstrated a technique that can be used to derive other hydrological variables in the study of predictions in ungauged basins, as the hydrological variables used in this study are not the only ones that could be derived using this technique. Depending on the model used, other parameters, such as soil temperature or latent heat, could theoretically be mapped for the entire country as well.

However, this type of work should not be seen as an excuse to no longer fund direct measurement of these hydrological variables. Indeed, the work done in this thesis was only possible as a result of the availability of previous direct measurements. The predictions made in ungauged basins will be made more reliable with the addition of direct measurements and unfortunately will be made less reliable with every loss of a long-term monitoring station.

This thesis is also valuable in the study of predictions in ungauged basins. First, using precipitation and temperature from measured stations, a technique was developed to interpolate these

data on a daily basis to all areas of Canada, including the vast ungauged northern portion of the country; second, using streamflow (the most reliably measured hydrologic parameter), land-class parameters were developed that could be transferred to the ungauged river basins of Canada.

The scale of the investigation done in this thesis must also be considered when examining how the processes and products can be used. For instance, the spatial scale of 51 km limits the application of this dataset to larger watersheds and would not be useful for such applications as municipal storm water management studies where the spatial scale of interest is on the order of hundreds of metres.

On a temporal scale, although an hourly time step was used for the hydrological model, the actual measured data was only available on a daily basis and the flow data were only verified on a monthly time scale. Given this, it is probably best to only consider the products from this thesis at a minimum of a monthly time scale, while the daily results should only be used if subjected to further verification.

However, the processes that were used to create the products of this thesis are generally applicable to different scales and thus could be useful in other types of studies after careful consideration. As stated in the introduction to this thesis, it is hoped that at least some (if not all) of the techniques developed here will be useful to other researchers in the future.

References

Abbott, M. B. and J. C. Refsgaard, 1996. *Distributed hydrological modelling*. Kluwer Academic, Dordrecht, pp. 323.

Adler, R.F., G.J. Huffman, A. Chang, R. Ferraro, P. Xie, J. Janowiak, B. Rudolf, U. Schneider, S. Curtis, D. Bolvin, A. Gruber, J. Susskind, P. Arkin, E. Nelkin, 2003. The Version 2 Global Precipitation Climatology Project (GPCP) Monthly Precipitation Analysis (1979-Present). *Journal of Hydrometeorolgy*, Vol 4, pp. 1147-1167.

Agnew, M. D. and J. P. Palutikof, 2000. GIS-based construction of baseline climatologies for the Mediterranean using terrain variables. *Climate Research*, Vol. 14, pp. 115-127.

Anderson, E. A. 1973. The National Weather Service river forecast system - snow accumulation and ablation model, NOAA Technical Memorandum, NWS HYDRO - 17. NOAA, Washington, DC.

Andréassian, V., J. Lerat, C. Loumagne, T. Mathevet, C. Michel, L. Oudin,C. Perrin, 2007. What is really undermining hydrologic science today? *Hydrological Process*, Vol. 21, No. 20, pp. 2819-2822.

Arnell, N. W., 1995. Grid mapping of river discharge. *Journal of Hydrology*, Vol. 167, No.1-4, pp. 39-56.

Aronica, G., P. D. Bates, and M.S.Horritt, 2002. Assessing the uncertainty in distributed model predictions using observed binary pattern information within GLUE. *Hydrological Processes*, Vol. 16, No.10, pp. 2001-2016.

Band, L. E, 1986. Topographic Partition of Watersheds with Digital Elevation Models. *Water Resources Research*, Vol. 22, No.1, pp. 15-24.

Baumgartner, A. and E. Reichel, 1975. World water balance : mean annual global, continental and maritime precipitation, evaporation and run-off. Elsevier, New York, pp. 179.

Benoit, R., N. Kouwen, W. Yu, S. Chamberland and P. Pellerin, 1999. Hydrometeorological aspects of the Real-Time Ultrafinescale Forecast Support during the Special Observing Period of the MAP. *Hydrological Earth System Sciences*, Vol. 7, No.6, pp. 877-889.

Bergström, S. and A. Forsman, 1973. Development of a conceptual deterministic rainfall–runoff model. *Nordic Hydrology*, Vol. 4, pp. 147–170.

Beven, K., 2006a. A manifesto for the equifinality thesis. *Journal of Hydrology*, Vol. 320, No.1-2, pp. 18-36.

Bevin, K., 2006b. On undermining the science? *Hydrological Processes*, Vol. 20, No. 14, pp. 3141-3146.

Bevin, K.J. and M. J. Kirkby, 1979. A physically-based variable contributing area model of basin hydrology. *Hydrological Sciences Bulletin,* Vol. 24, pp. 43–69.

Bishop, G. D. and M. R. Church, 1992. Automated approaches for regional runoff mapping in the northeastern United States. *Journal of Hydrology*, Vol. 138, No.3-4, pp. 361-383.

Burn, D. H. and M. A. Hag Elnur, 2002. Detection of hydrologic trends and variability. *Journal of Hydrology*, Vol. 255, No.1-4, pp. 107-122.

Caya, D. and R. Laprise, 1999. A Semi-Implicit Semi-Lagrangian Regional Climate Model: The Canadian RCM. *Monthly Weather Review*, Vol. 127, pp. 341-362.

Christiaens, K. and Feyen J., 2002. Constraining soil hydraulic parameter and output uncertainty of the distributed hydrological MIKE SHE model using the GLUE framework. *Hydrological Processes*, Vol. 16, No.2, pp. 373-391.

Christensen, N. S., A. W. Wood, N. Voisin, D. P. Lettenmaier and R. N. Palmer, 2004. The Effects of Climate Change on the Hydrology and Water Resources of the Colorado River Basin. *Climatic Change*, Vol. 62, No.1, pp. 337-363.

Creutin, J. D. and C. Obled, 1982. Objective Analyses and Mapping Techniques for Rainfall Fields: An Objective Comparison. *Water Resources Research*, Vol. 18, No.2, pp. 413-431.

Daly, C., R. P. Neilson and D. L. Phillips, 1994. A Statistical-Topographic Model for Mapping Climatological Precipitation over Mountainous Terrain. *Journal of Applied Meteorology*, Vol. 33, No.2, pp. 140.

Dingman, S. L, 1994. *Physical hydrology*. Prentice-Hall, London, pp. 575.

Dodson, R. and D. Marks, 1997. Daily air temperature interpolated at high spatial resolution over a large mountainous region. *Climate Research*, Vol. 8, No.1, pp. 1-20.

Doll, P. and B. Lehner, 2002. Validation of a new global 30-min drainage direction map. *Journal of Hydrology*, Vol. 258, No.1-4, pp. 214-231.

Environment Canada, 2002. HYDAT surface water and sediment data CD-ROM. Water Survey of Canada.

Fassnacht, S. R., K. A. Dressler and R. C. Bales, 2003. Snow water equivalent interpolation for the Colorado River Basin from snow telemetry (SNOTEL) data. *Water Resources Research*, Vol. 39, No.8, 1208.

Fekete, B. M., C. J. Vörösmarty and R. B. Lammers, 2001. Scaling gridded river networks for macroscale hydrology: Development, analysis, and control of error. *Water Resources Research*, Vol. 37, No.7, pp. 1955-1967.

Fekete, B. M., C. J. Vörösmarty and W. Grabs, 2002. High-resolution fields of global runoff combining observed river discharge and simulated water balances. *Global Biogeochemical Cycles*, Vol. 16, No.3, pp. 1042.

Fleming, M. D., F. S. Chapin, W. Cramer, G. L. Hufford and M. C. Serreze, 2000. Geographic patterns and dynamics of Alaskan climate interpolated from a sparse station record. *Global Change Biology*, Vol. 6, No.s1, pp. 49-58.

Garbrecht, J. and L. W. Martz, 1997. The assignment of drainage direction over flat surfaces in raster digital elevation models. *Journal of Hydrology*, Vol. 193, No.1-4, pp. 204-213.

Glazer, A., R. Benoit, and W. Yu, 2005. Numerical Wind Energy Atlas for Canada. Geophysical Research Abstracts, Vol. 7, no. 05185.

Gotzinger, J. and A. Bardossy, 2008. Generic error model for calibration and uncertainty estimation of hydrological models. *Water Resources Research*, Vol. 44.

GRDC, 1999. GRDC Station Catalog (available online at www.bafg.de/html/internat/grdc/download.html).

Hall, J., E. O'Connell, and J. Ewen, 2007. On not undermining the science: coherence, validation, and expertise. *Hydrological Processes*, Vol. 21, No. 7, pp. 985-988.

Hamilton, S., 2007. Just say NO to equifinality. *Hydrological Processes*, Vol. 21, No. 14, pp. 1979-1980.

Hamlin, L., Pietroniro, A., Prowse, T., Soulis, E.D., and N. Kouwen, 1998. Application of indexed snowmelt algorithms in a northern wetland regime. *Hydrological Processes*, Vol. 12, No.10-11, pp. 1641-1657.

Hare, F. K. and J. E. Hay, 1971. Anomalies in the large-scale annual water balance over northern North America. *Canadian Geographer*, Vol. 15, No.2, pp. 79-94.

Hartman, L. and O. Hössjer, 2008. Fast kriging of large data sets with Gaussian Markov random fields. *Computational Statistics & Data Analysis*, Vol. 52, No.5, pp. 2331-2349.

Hevesi, J. A., J. D. Istok and A. L. Flint, 1992. Precipitation Estimation in Mountainous Terrain Using Multivariate Geostatistics. Part I: Structural Analysis. *Journal of Applied Meteorology*, Vol. 31, No. 7, pp. 661-676.

Hutchinson, M. F, 1995. Interpolating mean rainfall using thin plate smoothing splines. *International Journal of Geographical Information Science*, Vol. 9, No.4, pp. 385-403.

IPCC. 2007. Climate Change 2007: The Physical Science Basis. Contribution of Working Group I to the Fourth Assessment Report of the Intergovernmental Panel on Climate Change (Solomon, S. ,

D. Qin, M. Manning, Z. Chen, M. Marquis, K.B. Averyt, M. Tignor and H.L. Miller (eds.)). Cambridge University Press, Cambridge, United Kingdom and New York, NY, USA.

Isaaks, E. H. and R. M. Srivastava, 1989. Applied geostatistics. Oxford University Press, New York, pp. 561.

Jenson, S. K. and J. O. Domingue, 1988. Extracting Topographic Structure from Digital Elevation Data for Geographic Information System Analsys. *Photogrammetric Engineering and Remote Sensing*, Vol. 54, No.11, pp. 1593-1600.

Jothityangkoon, C., M. Sivapalan and D. L. Farmer, 2001. Process controls of water balance variability in a large semi-arid catchment: downward approach to hydrological model development. *Journal of Hydrology*, Vol. 254, No.1-4, pp. 174-198.

Journel, A. and C. Huijbregts, 1978. *Mining Geostatistics*. Academic, London, pp. 600.

Kalnay, E., R. Kistler, W. Collins, S. Saha, G. White, J. Woollen, M. Chelliah, W. Ebisuzaki, M. Kanamitsu, V. Kousky, H. van den Dool, R. Jenne and M. Fiorino, 2001. The NCEP–NCAR 50–Year Reanalysis: Monthly Means CD–ROM and Documentation. *Bulletin of the American Meteorological Society*, Vol. 82, No.2, pp. 247-267.

Kite, G, 1987. Manual for the SLURP hydrological model. NHRI, Saskatoon, pp. 159.

Klemes, V, 1983. Conceptualization and scale in hydrology. *Journal of Hydrology*, Vol. 65, pp. 1-23.

Kouwen, N. and S-F. Mousavi, 2002. WATFLOOD/SPL9 Hydrological Model and Flood Forecasting System, Chapter 15 in *Mathematical Models of Large Watershed Hydrology*, edited by V.P. Singh and D.K. Frevert. Water Resources Publications, Highlands Research, Colorado. pp. 649-686.

Kouwen, N., M. Danard, A. Bingeman, W. Luo, F. Seglenieks and E. D. Soulis, 2005. Case Study: Watershed Modeling with Distributed Weather Model Data. *Journal of Hydrologic Engineering*, Vol. 10, No.1, pp. 23-38.

Kouwen, N., E. D. Soulis, A. Pietroniro, J. Donald and R. A. Harrington, 1993. Grouped Response Units for Distributed Hydrologic Modeling. *Journal of Water Resources Planning and Management*, Vol. 119, No.3, pp. 289-305.

Krahe, P. and W. Grabs, 1996. Development of a GIS-supported water balance model as a tool for the validation of climate models and hydrometeorological data sets. In Workshop on Continental Scale Hydrological Models: Charting Future. World Meteorological Organization.

Lacroix, M. P., L. W. Martz, G. W. Kite and J. Garbrecht, 2002. Using digital terrain analysis modeling techniques for the parameterization of a hydrologic model. *Environmental Modelling & Software*, Vol. 17, No.2, pp. 125-134.

Lammers, R. B., A. I. Shiklomanov, C. J. Vorosmarty, B. M. Fekete and B. J. Peterson, 2001. Assessment of contemporary Arctic river runoff based on observational discharge records . *Journal of Geophysical Research - Atmospheres*, Vol. 106, No. 4, pp. 3321-3334.

Lebel, T., G. Bastin, C. Obled and J. D. Creutin, 1987. On the Accuracy of Areal Rainfall Estimation: A Case Study. *Water Resources Research*, Vol. 23, No.11, pp. 2123-2134.

Legates, D. R. and McCabe, Jr., Gregory J, 1999. Evaluating the use of "goodness-of-fit" measures in hydrologic and hydroclimatic model validation. *Water Resources Research*, Vol. 35, No.1, pp. 233-241.

Liang, X., D. P. Lettenmaier, E. F. Wood and S. J. Burges, 1994. A simple hydrologically based model of land surface water and energy fluxes for general circulation models. *Journal of Geophysical Research*, Vol. 99, No. D7, pp. 14415-14428.

Manovan, P. and E. Todini, 2006. Hydrological forecasting uncertainty assessment: Incoherence of the GLUE methodology. *Journal of Hydrology*, Vol. 330, Vol. (1-2), pp. 368-381.

Marani, M., G. Grossi, M. Wallace, F. Napolitano, and D. Entekhabi, 1997. Forcing, intermittency, and land surface hydrological portioning. *Water Resources Research*, Vol. 33, pp. 167-175.

Martz, L. W. and j. Garbrecht, 1993. Automated extraction of drainage network and watershed data from digital elevation models. *Water Resources Bulletin*, Vol. 29, No.6, pp. 901-908.

Maurer, E.P., A.W. Wood, J.C. Adam, D.P. Lettenmaier, and B. Nijssen, 2002. A Long-Term Hydrologically-Based Data Set of Land Surface Fluxes and States for the Conterminous United States, *Journal of Climate*, Vol. 15, No. 22, pp. 3237-3251.

McCuen, R. H., Z. Knight and A. G. Cutter, 2006. Evaluation of the Nash--Sutcliffe Efficiency Index. *Journal of Hydrologic Engineering*, Vol. 11, No.6, pp. 597-602.

McKenney, D. W., M. F. Hutchinson, J. L. Kesteven and L. A. Venier, 2001. Canada's plant hardiness zones revisited using modern climate interpolation techniques. *Canadian Journal of Plant Sciences*, Vol. 81, No.1, pp. 129-143.

Mekis, E. and W. D. Hogg, 1999. Rehabilitation and Analysis of Canadian Daily Precipitation Time Series. *Atmosphere-Ocean*, Vol. 37, No.1, pp. 53-85.

Mitás L., and H. Mitásová, 1999: Spatial interpolation. *Geographical Information Systems*, P. A. Longley et al., Eds., John Wiley and Sons, pp. 481–492.

Mitchell, K. E., D. Lohmann, P. R. Houser, E. F. Wood, J. C. Schaake, A. Robock, B. A. Cosgrove, J. Sheffield, Q. Duan, L. Luo, R. W. Higgins, R. T. Pinker, J. D. Tarpley, D. P. Lettenmaier, C. H. Marshall, J. K. Entin, M. Pan, W. Shi, V. Koren, J. Meng, B. H. Ramsay, and A. A. Bailey, 2004. The multi-institution North American Land Data Assimilation System (NLDAS): Utilizing

multiple GCIP products and partners in a continental distributed hydrological modeling system, *Journal of Geophysical Reserach*, Vol. 109, D07S90.

Montanari, A, 2005. Large sample behaviors of the generalized likelihood uncertainty estimation (GLUE) in assessing the uncertainty of rainfall-runoff simulations. *Water Resources Research*, Vol. 41, No. 10, pp.1029.

Montanari, A, 2007. What do we mean by 'uncertainty'? The need for consistent working about uncertainty assessment in hydrology. *Hydrological Processes*, Vol. 21, No. 6, pp. 841-845.

Morris, D. G. and R. G. Heerdegen, 1988. Automatically derived catchment boundaries and channel networks and their hydrological applications. *Geomorphology*, Vol. 1, No.2, pp. 131-141.

Mueller, T. G., N. B. Pusuluri, K. K. Mathias, P. L. Cornelius, R. I. Barnhisel and S. A. Shearer, 2004. Map Quality for Ordinary Kriging and Inverse Distance Weighted Interpolation. *Soil Science Society of America Journal*, Vol. 68, No.6, pp. 2042-2047.

Nalder, I. A. and R. W. Wein, 1998. Spatial interpolation of climatic Normals: test of a new method in the Canadian boreal forest. *Agricultural and Forest Meteorology*, Vol. 92, No.4, pp. 211-225.

Nash, J. E. and J. V. Sutcliffe, 1970. River flow forecasting through conceptual models part I - A discussion of principles. *Journal of Hydrology*, Vol. 10, No.3, pp. 282-290.

New, M., M. Hulme, and P. Jones, 1999. Representing twentieth-century space-time climate variability. Part I: Development of a 1961-90 mean terrestrial climatology. *Journal of Climate*, Vol. 12, No. 3, pp. 829-856.

Ninyerola, M., X. Pons and J. M. Roure, 2000. A methodological approach of climatological modelling of air temperature and precipitation through GIS techniques. *International Journal of Climatology*, Vol. 20, No.14, pp. 1823-1841.

O'Callaghan, J. F. and D. M. Mark, 1984. The extraction of drainage networks from digital elevation data. *Computer Vision, Graphics, and Image Processing*, Vol. 28, No.3, pp. 323-344.

O'Donnell, G., B. Nijssen and D. P. Lettenmaier, 1999. A simple algorithm for generating streamflow networks for grid-based, macroscale hydrological models. *Hydrological Processes*, Vol. 13, No.8, pp. 1269-1275.

PCI Geomatics, 2004. Geomatica: User Manual. Version 9.1, pp. 129.

Perry, M. and D. Hollis, 2005. The development of a new set of long-term climate averages for the UK. *International Journal of Climatology*, Vol. 25, No.8, pp. 1023-1039.

Pietroniro, A., V. Fortin, N. Kouwen, C. Neal, R. Turcotte, B. Davison, D. Verseghy, E. D. Soulis, R. Caldwell, N. Evora and P. Pellerin, 2007. Development of the MESH modelling system for

hydrological ensemble forecasting of the Laurentian Great Lakes at the regional scale. *Hydrology and Earth Systems Sciences*, Vol. 11, No.4, pp. 1279-1294.

Price, D. T., D. W. McKenney, I. A. Nalder, M. F. Hutchinson and J. L. Kesteven, 2000. A comparison of two statistical methods for spatial interpolation of Canadian monthly mean climate data. *Agricultural and Forest Meteorology*, Vol. 101, No.2-3, pp. 81-94.

Prudhomme, C. and D. W. Reed, 1999. Mapping extreme rainfall in a mountainous region using geostatistical techniques: a case study in Scotland. *International Journal of Climatology*, Vol. 19, No.12, pp. 1337-1356.

Quick, M.C. and A. Pipes, 1976. A combined snowmelt and rainfall runoff model. *Canadian Journal of Civil Engineering*, Volume 3., No. 3.pp. 449–460.

Rabus, B., M. Eineder, A. Roth and R. Bamler, 2003. The shuttle radar topography mission—a new class of digital elevation models acquired by spaceborne radar. *ISPRS Journal of Photogrammetry and Remote Sensing*, Vol. 57, No.4, pp. 241-262.

Rango A. and J. Martinec, 1979. Application of a snowmelt runoff model using Landsat data, *Nordic Hydrology*, Vol. 10, pp. 225–238.

Reed, S.M., 2003. Deriving flow directions for coarse-resolution (1-4 km) gridded hydrologic modeling. *Water Resources Research*, Vol. 39, No. 9.

Refsgaard, J.C. and B. Storm, 1995. In: Singh, V.P., Editor. Computer Models of Watershed Hydrology, Water Resources Publications, Englewood, USA, pp. 809–846.

Richardson, D.S., 2000. Skill and relative economic value of the ECMWF ensemble prediction system. *Quarterly Journal of the Royal Meteorological Society*, Vol. 126, No. 563, pp. 649-667.

Rodell, M., P. R. Houser, U. Jambor, J. Gottschalck, K. Mitchell, C.-J. Meng, K. Arsenault, B. Cosgrove, J. Radakovich, M. Bosilovich, J. K. Entin, J. P. Walker, D. Lohmann, and D. Toll, 2004. The Global Land Data Assimilation System, *Bulletin of the American Meteorological Society*, Vol. 85, No. 3, pp. 3813-94.

Seglenieks, F., E.D. Soulis, and M. MacKay, 2004. Producing the Drianage Layer Database for North America (WATGRID). AGU-CGU Joint Assembly, May 17-21, Montreal, Canada. Eos Trans. AGU, 85 (17), Jt. Assem. Suppl., Abstract H43C-06.

Shaw, D.A, L.W. Martz, and A. Pietroniro, 2005. A methodology for preserving channel flow networks and connectivity patterns in large-scale distributed hydrological models. *Hydrological Processes*, Vol. 19, No.1, pp. 149-168.

Sheffield J, G. Goteti G, and E.F. Wood, 2006. Development of a 50-year high-resolution global dataset of meteorological forcings for land surface modeling. Journal of Climate, Vol. 19, pp. 3088–3111.

Shen, S. S. P., P. Dzikowski, G. Li and D. Griffith, 2001. Interpolation of 1961–97 Daily Temperature and Precipitation Data onto Alberta Polygons of Ecodistrict and Soil Landscapes of Canada. *Journal of Applied Meteorology*, Vol. 40, No.12, pp. 2162-2177.

Shepard, D, 1968. A two-dimensional interpolation function for irregularly-spaced data. Proceedings of the 23rd National Conference of American Computing Machinery, Princton, NJ, pp. 517-524.

Singh, V. P, 1995. *Computer models of watershed hydrology*. Water Resources Publications, Highlands Ranch,CO, pp. 1130.

Singh, V. P. and D. K. Frevert, 2002. *Mathematical models of small watershed hydrology and applications*. Water Resources Publications, Highlands Ranch,CO , pp. 950.

Sivapalan, M., K. Takeuchi, S. W. Franks, V. K. Gupta, H. Karambiri, V. Lakshmi, X. Liang, J. J. McDonnell, E. M. Mendiondo, P. E. O'Connell, T. Oki, J. W. Pomeroy, D. Schertzer, S. Uhlenbrook and E. Zehe, 2003. IAHS Decade on Predictions in Ungauged Basins (PUB), 2003–2012: Shaping an exciting future for the hydrological sciences. *Hydrological Sciences*, Vol. 48, No.6, pp. 857-880.

Soille, P., J. Vogt and R. Colombo, 2003. Carving and adaptive drainage enforcement of grid digital elevation models. *Water Resources Research*, Vol. 39, No.12.

Solomon, S. I., J. P. Denouvilliez, E. J. Chart, J. A. Woolley and C. Cadou, 1968. The Use of a Square Grid System for Computer Estimation of Precipitation, Temperature, and Runoff. *Water Resources Research*, Vol. 4, No.5, pp. 919-929.

Soulis, E. D., S. I. Solomon, M. Lee and N. Kouwen, 1994. Changes to the Distribution of Monthly and Annual Runoff in the Mackenzie Basin Under Climate Change using a Modified Square Grid Approach. Mackenzie Basin Impact Study, Interim Report No. 2, Environment Canada, North York, ON, pp. 197-2002.

Soulis, E.D., and F. Seglenieks, 2007. The MAGS Integrated Modeling System. Cold Regions Atmospheric and Hydrologic Studies: the Mackenzie GEWEX Experience. Vol. II: Hydrologic Processes, Ed. M.K. Woo, Springer-Verlag. 445-474.

Stedinger, J. R., R. M. Vogel, S. U. Lee and R. Batchelder, 2008. Appraisal of the generalized likelihood uncertainty estimation (GLUE) method. *Water Resources Research*, Vol. 44.

Tapley, B. D., S. Bettadpur, J. C. Ries, P. F. Thompson and M. M. Watkins, 2004. GRACE Measurements of Mass Variability in the Earth System. *Science*, Vol. 305, No.5683, pp. 503-505.

Tarboton, D. G, 1997. A new method for the determination of flow directions and upslope areas in grid digital elevation models. *Water Resources Research*, Vol. 33, No.2, pp. 309-319.

Thiemann, M., M. Trosset, H. Gupta and S. Sorooshian, 2001. Bayesian Recursive Parameter Estimation For Hydrologic Models. *Water Resources Research*, Vol. 37, No.10, pp. 2521-2535.

Thornton, P. E., S. W. Running and M. A. White, 1997. Generating surfaces of daily meteorological variables over large regions of complex terrain. *Journal of Hydrology*, Vol. 190, No.3-4, pp. 214-251.

Todini, E, 1988. Rainfall-runoff modeling - Past, present and future. *Journal of Hydrology*, Vol. 100, No.1-3, pp. 341-352.

Tolson, B. A. and C. A. Shoemaker, 2007. Dynamically dimensioned search algorithm for computationally efficient watershed model calibration. *Water Resources Research*, Vol. 43.

Tolson, B. A. and C. A. Shoemaker, 2008. Efficient prediction uncertainty approximation in the calibration of environmental simulation models. *Water Resources Research*, Vol. 44.

Tribe, A, 1992. Automated recognition of valley lines and drainage networks from grid digital elevation models: a review and a new method. *Journal of Hydrology*, Vol. 139, No.1-4, pp. 263-293.

UNESCO, 1978. World Water Balance and Water Resources of the Earth. Unesco Press, Leningrad, USSR, pp. 663.

Uppala, S.M., P. W. KÅllberg, A. J. Simmons, U. Andrae, V. Da Costa Bechtold, M. Fiorino, J. K. Gibson, J. Haseler, A. Hernandez, G. A. Kelly, X. Li, K. Onogi, S. Saarinen, N. Sokka, R. P. Allan, E. Andersson, K. Arpe, M. A. Balmaseda, A. C. M. Beljaars, L. Van De Berg, J. Bidlot, N. Bormann, S. Caires, F. Chevallier, A. Dethof, M. Dragosavac, M. Fisher, M. Fuentes, S. Hagemann, E. Hólm, B. J. Hoskins, L. Isaksen, P. A. E. M. Janssen, R. Jenne, A. P. Mcnally, J.-F. Mahfouf, J.-J. Morcrette, N. A. Rayner, R. W. Saunders, P. Simon, A. Sterl, K. E. Trenberth, A. Untch, D. Vasiljevic, P. Viterbo, and J.Woollen, 2005. The ERA-40 re-analysis. *Quarterly Journal of the Royal Meteorological Society*, Vol. 131, No.612, pp. 2961-3012.

U.S. Geological Survey, 1997. GTOPO30 Global 30 Arc Second Elevation Data Set, available at http://edc.usgs.gov/products/elevation/gtopo30/gtopo30.html.

U.S. Geological Survey, 2006. HydroSHEDS: Global River Network Derived from SRTM Elevation Data, available at http://hydrosheds.cr.usgs.gov/.

Van der Wal, W., P. Wu, M. G. Sideris and C. K. Shum, 2008. Use of GRACE determined secular gravity rates for glacial isostatic adjustment studies in North-America. *Journal of Geodynamics*, Vol. 46, No.3-5, pp. 144-154.

Venier, L. A., D. W. McKenney, Y. Wang and J. McKee, 1999. Models of large-scale breeding-bird distribution as a function of macro-climate in Ontario, Canada. *Journal of Biogeography*, Vol. 26, No.2, pp. 315-328.

Verseghy, D.L., 1991. Class - A Canadian land surface scheme for GCMS. I. Soil model. *International Journal of Climatology*, Vol. 11, No.2, pp. 111-133.

Vieux, B. E, 2004. Distributed Hydrologic Modeling Using GIS. Kluwer Academic Publishers, Dordrecht, The Netherlands, pp. 176.

Vorosmarty, C. J., B. M. Fekete, M. Meybeck and R. B. Lammers, 2000. Global system of rivers: its role in organizing continental land mass and defining land-to-ocean linkages. *Global Biogeochemical Cycles*, Vol. 14, No.2, pp. 599-621.

Willmott, C.J. and S. Robeson, 1995. Climatologically aided interpolation (CAI) of terrestrial air temperature. *International Journal of Climatology*, Vol. 15, No.2, pp. 221-229.

Wood, A.W., 2008. The University of Washington Surface Water Monitor: an experimental platform for national hydrologic assessment and prediction. Presented at the 22nd Conference on Hydrology, part of the 88th annual meeting of the AMS, January 20-24, 2008.

Wurbs, R, 1998. Dissemination of generalized water resources models in the United States. *Water International*, Vol. 23, No.3, pp. 190-198.

Yapo, P.O., H.V. Gupta, and S. Sorooshian, 1998. Multi-objective global optimization for hydrologic models. *Journal of Hydrology*, Vol. 24, pp. 83-97.

Appendix A
Monthly gridded precipitation and temperature

A.1 Introduction to WATFLOOD

The hydrological model used in this study was the Waterloo Flood Forecasting (WATFLOOD) developed at the University of Waterloo; WATFLOOD is a physically based semi-empirical distributed hydrologic model (Kouwen and Mousavi, 2002). In WATFLOOD, the basin to be modeled is divided into grid squares, typically with a grid size between 1 km and 50 km, which are allowed to have different temperatures and amounts of precipitation.

Each of these grid squares is divided into a number of Grouped Response Units (GRUs). These GRUs can be based on any criteria: slope, soil type, elevation, and (most typically) land class. The most important concept of the GRU is that the actual physical location of the elements of the GRU need not be specified. Instead, all of the instances of the land class are grouped, and it is the response of that grouping to the meteorological forcings that is used in the model. It is assumed that this GRU is located an average distance from the stream channels running through the grid, even though in reality some elements of the GRU are closer and some are further away.

The GRU concept allows a heterogeneous landscape to be efficiently modeled in WATFLOOD. Consider a satellite image of a typical landscape (Figure A-1). It would be impossible to simulate the flow of water through each different element of this landscape. Even if we classify the image in six major groupings, it would still be very difficult to consider the individual locations of each instance of each land class (Figure A-2). With the GRU concept, the proportions of the different land classes within each grid square are conceptualized as occurring together (Figure A-3). This greatly simplifies the necessary calculations of flow while still retaining the different characteristics of flow in each land class.

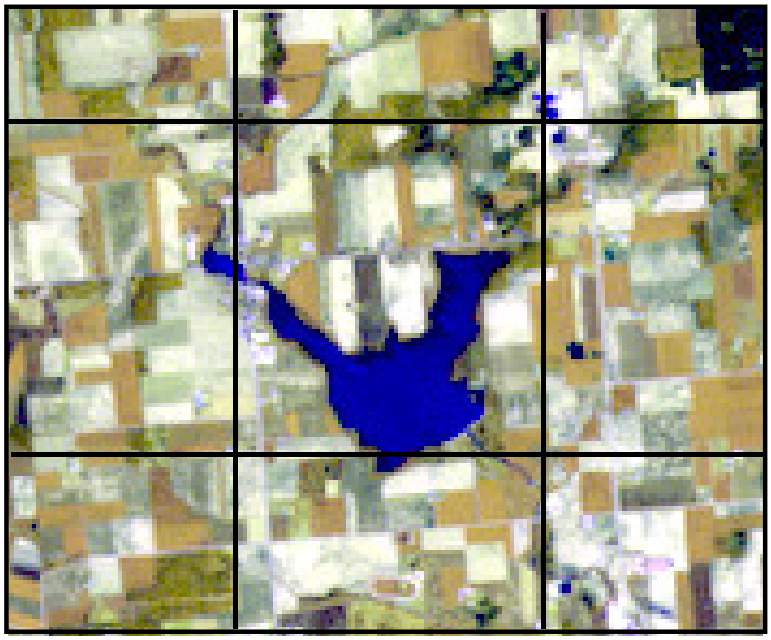

Figure A-1: LANDSAT satellite image of typical heterogeneous landscape.

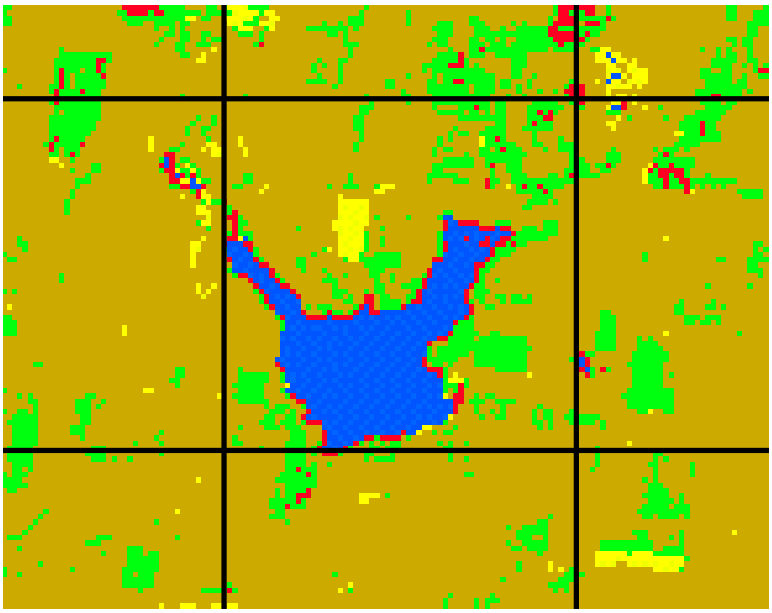

Figure A-2: Classified image of typical heterogeneous landscape (blue=water, green=forest, yellow=low vegetation, red=wetland, and brown=agricultural).

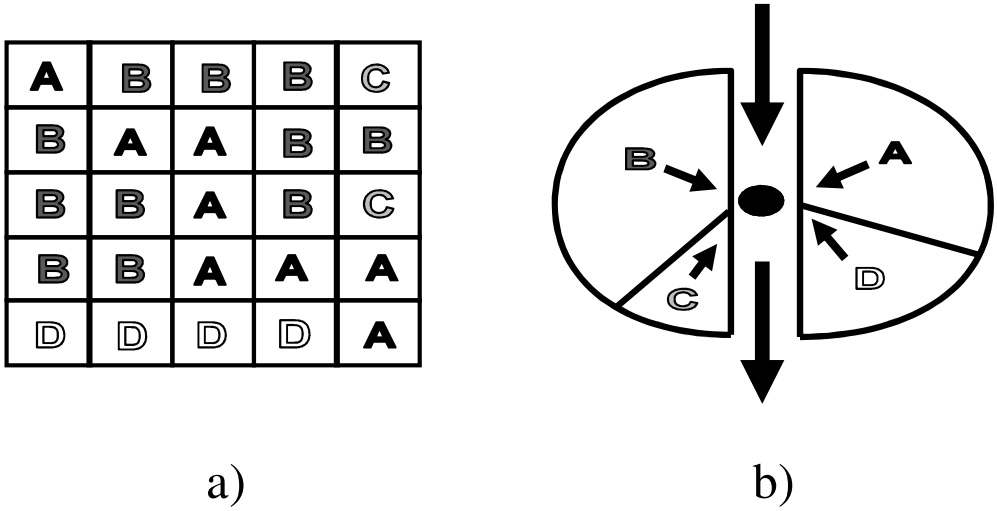

Figure A-3: Comparison of a) actual physical locations of landscape units and b) grouped response unit conceptualization of landscape units.

The contribution to streamflow from each of the GRUs is summed and added to the streamflow contribution upstream of the grid square. The flows from each of the grid squares are routed down the river network and used to calculate streamflow at the basin outlet.

A.2 WATFLOOD processes

The different processes that are considered by the WATFLOOD model are shown in Figure A-4. The detailed calculation of each of the processes will be presented in this section.

A.2.1 Interception

The amount of interception storage and the amount of interception evapotranspiration is based on the technique presented by Linsley et al. (1949).

The calculation of the amount of water in interception storage is done using the formula:

$$V = F \cdot X2$$

Where V is the interception storage (mm), F is the interception fraction, and X2 is the sum of the maximum storage and the interception evapotranspiration (IET) (mm).

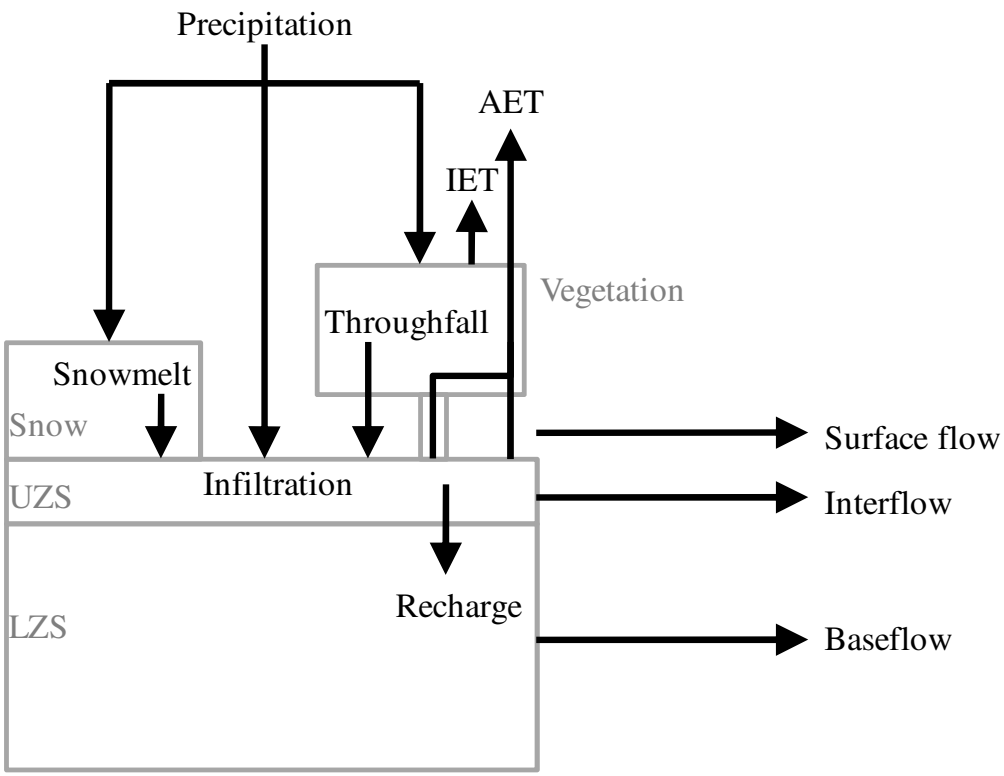

Figure A-4: Schematic representation of the major flow processes modelled by WATFLOOD.

The interception fraction decays exponentially from the beginning of a storm as more water is intercepted:

$$F = e^{\frac{-P_i}{X2}}$$

Where F is the interception fraction, P_i is the total precipitation since the beginning of the storm (mm), and X2 is the sum of the maximum storage and IET (mm).

The value of X2 depends on the relative magnitudes of the potential ET and the amount of maximum storage:

$$X2 = h + FIET \cdot PET, \quad if\ PET \leq h \quad and$$

$$X2 = h + FIET \cdot h, \quad if\ PET > h$$

Where h is the maximum canopy storage (mm), FIET is an adjustment factor for the ET, and PET is the potential ET (mm). The maximum canopy storage is a calibrated parameter that is generally reduced during the dormant season to reflect the loss of storage capacity. The value of FIET is set at

1.0 during a storm event and is gradually increased to 3.0 after the event until no more water is available in the interception storage.

Finally, the throughfall can be calculated based on the amount of precipitation and interception storage:

$$TF = P - (V_2 - V_1)$$

Where TF is the throughfall (mm), V is the interception storage (mm), and the subscripts 1 or 2 refer to the previous (1) and current (2) time step.

A.2.2 Infiltration and surface flow

Infiltration is estimated using the Philip formula (Philip, 1954) which is a modification of the solution of the Richard's equation (Richards, 1931). This formula has a ponded water surface and assumes a homogeneous soil with uniform antecedent water conditions.

Example of Philip formula:

$$\frac{dF}{dt} = K\left[1 + \frac{(m - m_0)(Pot + D1)}{F}\right]$$

Where F is the total depth of infiltrated water (mm), t is the time step, K is the hydraulic conductivity (mm/hour), m is the average moisture content of the soil to the depth of the wetting front (mm), m_o is the initial soil moisture content (mm), Pot is the capillary potential at the wetting front (mm), and D1 is the depth of water on the soil surface (mm).

The value of K is an optimized parameter that generally has values that are lower than would be expected for an individual land type. This is because in the real world water does not infiltrate over an entire area, but rather flows to areas of low elevation where they infiltrate from ponded water. Thus the K parameter is lower than expected to reflect the large areas of the watershed that generally do not contribute to the infiltration.

When the wetting front is at a shallow depth below the ground surface it causes a large pressure gradient that results in high infiltration. As the wetting front gets deeper this pressure gradient is reduced along with the infiltration rate. Philip (1954) also presented a relationship between the capillary potential at the wetting front and permeability:

$$Pot = 250\ \log(K) + 100$$

Where Pot is the capillary potential at the wetting front (mm) and K is the hydraulic conductivity (mm/hour).

The initial water that arrives at the water surface fills the depression storage and is not available for surface runoff. The amount of depression storage is calculated using the formula from Linsley et al. (1982):

$$D_S = S_d\ (1 - e^{-K\ P_e})$$

Where D_s is the depression storage (mm), P_e is the accumulated rainfall excess (mm), K is a constanct (mm-1), and S_d is the maximum value of the depression storage (mm). The value of S_d depends on the land class and is usually must be determined using calibration. A higher value for S_d would allow for more water to be stored in the depression storage.

The remaining water is available for surface runoff that is calculated using a modification of the Manning's equations:

$$Q_{surf} = \frac{1}{R3 * (D_1 - D_S) * 1.7 * S * 0.5 * A}$$

Where Q_{surf} is the surface runoff that makes it to the river channel (m3/s), D_1 is the water depth ponding on the surface (mm), D_s is the depression storage (mm), S is the average overland slope of the grid, and A is the area of the basin element (m2). R3 is a parameter that incorporates the roughness of the land surface, the drainage density, the shape of the contributing area, and units of conversion. Thus it is obvious that this parameter cannot be measured and must be calibrated, smaller values would indicate a smoother surface allowing for more surface runoff.

A.3.1 Subsurface flow

When water is infiltrated from the ground surface it first enters into the Upper Zone Storage (UZS). Water is removed from the UZS in three different ways: evapotranspiration, interflow, and transfer to Lower Zone Storage (LZS). Separate calculations are made for both bare ground and snow covered ground and pro-rated based on the amount of snow covered of the GRU.

A.3.1.1 Evapotranspiration

As only temperature and precipitation are available for the WATFLOOD model, the ET calculated by WATFLOOD cannot be calculated using a full energy balance. The first step is to calculate the maximum possible potential evapotranspiration rate, this is then modified based on soil temperature and vegetation. The potential evapotranspiration is then compared to the amount of available water to calculate the actual evapotranspiration.

The original empirical Hargreeves formula (Hargreaves, 1982) to calculate the maximum amount of PET is:

$$PET_m = 0.0075 * Rz * Ct * \partial t * T$$

Where PET_m is the maximum potential evapotranspiration rate in (mm per time step), Rz is the total incoming solar radiation (mm), Ct is a temperature reduction coefficient based on relative humidity, δt is the difference between the mean monthly maximum temperature and the mean monthly minimum temperature (°C), and T is the temperature during the time step (°C).

A calculation of Ra by Duffie and Beckman (1980) only requires the current temperature, the latitude (lat), the solar declination (SD), the sunset hour angle (SH) and the Julian day (JD) instead of the incoming solar radiation:

$$Ra = 15.392\, Dr\, (SH * \sin(lat)\, \sin(SD)\, \cos(lat)\, \cos(SD)\, \sin(SH))$$

Dr is the relative distance between the earth and the sun which can be calculated with the forumula:

$$Dr = 1 + 0.033\, \cos(\frac{2\,\pi\, JD}{365})$$

SD is calculated with the formula:

$$SD = 0.4093\, \sin(\frac{2\,\pi\, JD}{365} - 1.405)$$

The sunset hour angle is calculated using:

$$SH = \cos^{-1}(-\tan(lat)\tan(SD))$$

The maximum PET is then reduced based on two factors: FPET – the soil temperature coefficient and FTALL – the forest vegetation coefficient. FPET is designed to compensate for the differences in soil temperature at different times of the year. FTALL is used as a result of studies showing that ET can be significantly less than maximum PET for tall vegetation.

The final PET is simply the maximum PET multiplied by the reduction factors:

$$PET = PET_m \cdot FPET \cdot FTALL$$

Where PET is potential evapotranspiration (mm), PET_m is the maximum potential evapotranspiration (mm), FPET is the soil temperature coefficient and FTALL is the forest vegetation coefficient.

The amount of PET is then compared to the amount of water available in the UZS. If the amount of water in the UZS is less than the PET then the amount of AET is set as the amount of the UZS (ie.

there is not enough water available to satisfy the PET). If the UZS is greater than PET then the amount of AET is the same as PET and the leftover amount is kept in the UZS.

A.3.1.2 Interflow

The remaining water in the UZS is then available to be added to the river channel as interflow. The amount of interflow is calculated using the following formula:

$$Q_{int} = REC\ (\ UZS - RETN)\ S$$

Where Qint is the interflow (mm), REC is a coefficient that is obtained through calibration, RETN is the specific retention of the soil, and S is the average overland slope of the grid. RETN can be thought of as similar to the field capacity of the soil, but again this cannot be directly measured and the parameter can only be determined using calibration.

A.3.1.3 Transfer to lower zone storage

Any remaining water in the UZS is now available to be drained into the LZS:

$$Recharge = AK2\ (\ UZS - RETN\ )$$

Where recharge is the amount of water transferred between the UZS and LZS (mm), RETN is as above (mm), and AK2 is the intermediate zone resistance parameter. As before AK2 must be found using calibration.

A.3.2 Baseflow

Water can only be removed from the LZS as baseflow (Qbase) calculated using the formula:

$$Q_{base} = LZF * LZS^2$$

Where Q_{base} is the baseflow (mm) and LZF is the lower zone drainage function. Note that LZS is not calculated separately for each GRU, thus all GRUs contribute to the same LZS. Obviously the value of LZF can only be obtained using calibration.

The initial value of LZS is determined by pro-rating the initial streamflow sequentially from measured streamflow locations upstream to the drainage divides. Thus WATFLOOD assumes that

the initial measured flows represent the baseflow of the basin and the model should not be started during an event.

The total runoff from the grid square is the addition of the runoff from each GRU.

A.3.3 Snowmelt

In WATFLOOD, meltwater is only able to leave the bottom of the snowpack when the snowpack has become "ripe", this means that the temperature of the entire snowpack has been reduced to zero degrees. The cumulative amount of heat in the snowpack is referred to as to as the heat deficit in the units of mm of water equivalent. Thus meltwater only leaves the snowpack when the heat deficit has been reduced to zero.

When the air temperature is less than 0°C, the change in heat deficit is calculated using the formula:

$$\Delta H_S = NMF\ (\ ATI\ -\ T_a\ ) - \frac{S_f T_a}{160}$$

Where ΔH_s is the change in heat deficit (mm), NMF is the negative melt factor representing the rate of change of heat deficit for each degree of air temperature above zero per unit time (mm °C /day), ATI is the antecedent temperature index, T_a is the air temperature, and S_f is the amount of snow fallen per unit time represented as snow water equivalent (mm).

ATI is calculated based on the transient heat flow equation for semi-infinite solids:

$$T(x,t) = T_o + \text{erf}\left(\frac{x}{2\sqrt{\frac{\kappa t}{c}}}\right)(T_i - T_o)$$

Where T(x,t) is the temperature at depth "x" at time "t" (°C), To is the altered surface temperature (°C), Ti is the original surface temperature (°C), κ is the thermal conductivity (W/m^2°C), and c is the specific heat of snow (KJ/kg/°C).

The erf function accounts for the changes in temperature as a result of the different energy fluxes acting on the snowpack. Although this function varies with the snowpack density, in WATFLOOD the function is represented by the parameter TIPM and is held constant so simplify the calculation of the heat deficit.

The ATI is adjusted using a formula that is analogous to the one used to calculate snowmelt:

$$ATI_2 = ATI_1 + TIPM\ (T_a - ATI_1\ )$$

Where ATI is the antecedent temperature index, the subscripts 1 or 2 refer to the previous (1) and current (2) time step.

When the air temperature is greater than 0°C, then the heat deficit is reduced by the amount of snowmelt. The amount of snowmelt in WATFLOOD is calculated using a modification of the National Weather Service River Flow Forecast system originally created by Anderson (1973):

$$M = MF\ (T_a - T_{base}\ )$$

Where M is the daily snowmelt depth (mm), MF is the melt factor representing the mm of melt per degree of unit time (mm/°C/h), T_a is the air temperature (°C), and T_{base} is the base temperature when the snow begins to melt (°C).

The heat deficit is reduced until it reaches zero, at this time any additional melt is assumed to be runoff and the volume of the snowpack is reduced by the amount of runoff until no more snow remains.

A.4 Routing

The routing method used by WATFLOOD is based on the storage routing technique, the technique was chosen as it needs a minimal amount of river cross-section and profile data. As well it has been shown to comparable results to more sophisticated routing schemes, especially for larger watersheds (Ponce, 1990).

The storage routing technique is based on the continuity equation:

$$\frac{I_1 + I_2}{2} - \frac{O_1 + O_2}{2} = \frac{S_2 - S_1}{\Delta t}$$

Where I is the inflow to the reach (this is the combination of overland flow, interflow, baseflow, and the flow from the upstream reach) (m^3/s), O is the outflow from the reach (m^3/s), S is the storage in the reach (m^3), and Δt is the time step (s). The subscripts refer to the beginning (1) and the end (2) of the time step.

Flow is related to the storage using a modification of the Manning formula:

$$O = \frac{1}{R2}\ (A)^{1.33} {S_o}^{0.5}$$

Where O is the flow (m^3/s), R2 is the channel roughness parameter, A is the channel cross-section area, S_o is the channel slope. Thus R2 incorporates the channel shape, the width to depth ration, and Manning's n and as such its value is generally obtained through calibration.

A.5 Final thoughts

All of these processes are controlled by parameters that can be different for each GRU. Some of these parameters are based on specific physical processes while others are effective parameters. Although the physical parameters should be measureable, scaling issues sometimes make it difficult to take a measured value at a specific point and relate it to a value that is valid over the entire grid square. For this reason, it is sometime more reliable to use calibration to determine their most appropriate values. As the effective parameters have no physical basis, by definition they cannot be directly measured, leaving only the option of calibration to determine their values.

The WATFLOOD model has been successfully implemented in various watersheds throughout Canada (Hamlin *et al.*, 1998; Kouwen *et al.*, 2005; Soulis and Seglenieks, 2007) and the world (Benoit *et al.*, 2004).

Appendix B
Monthly gridded precipitation and temperature

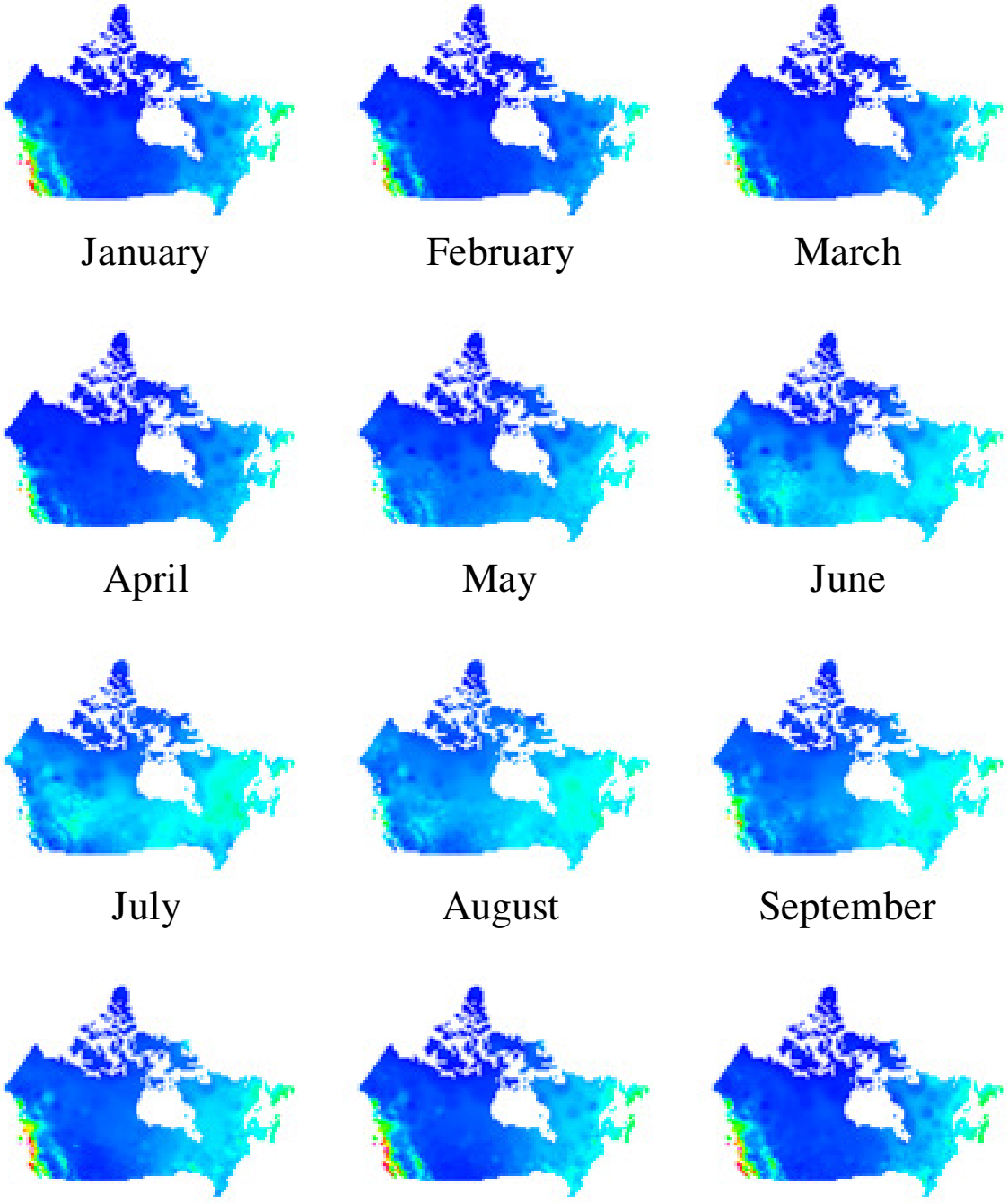

IWD interpolation of monthly precipitation

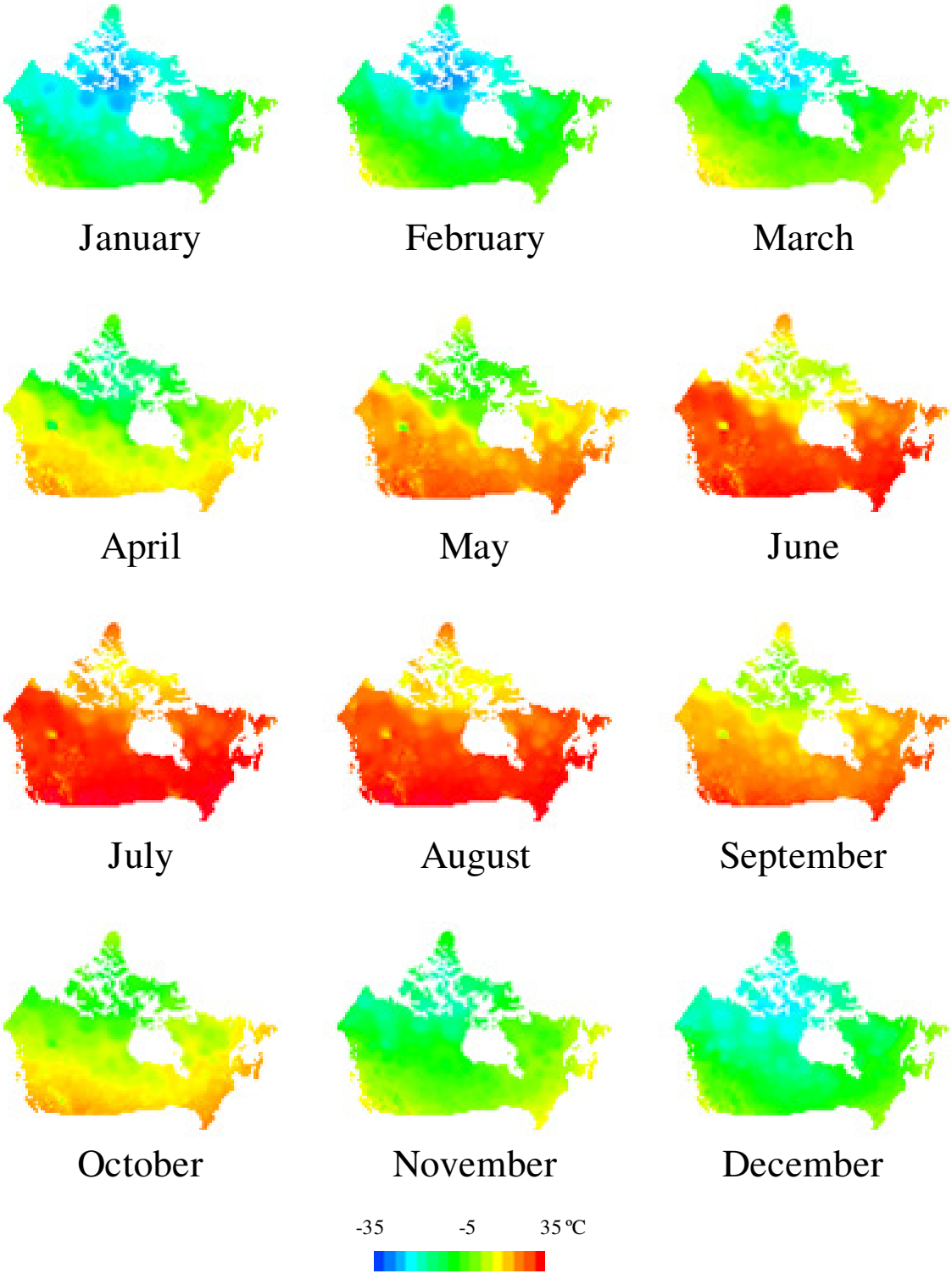

IWD interpolation of monthly average maximum temperature

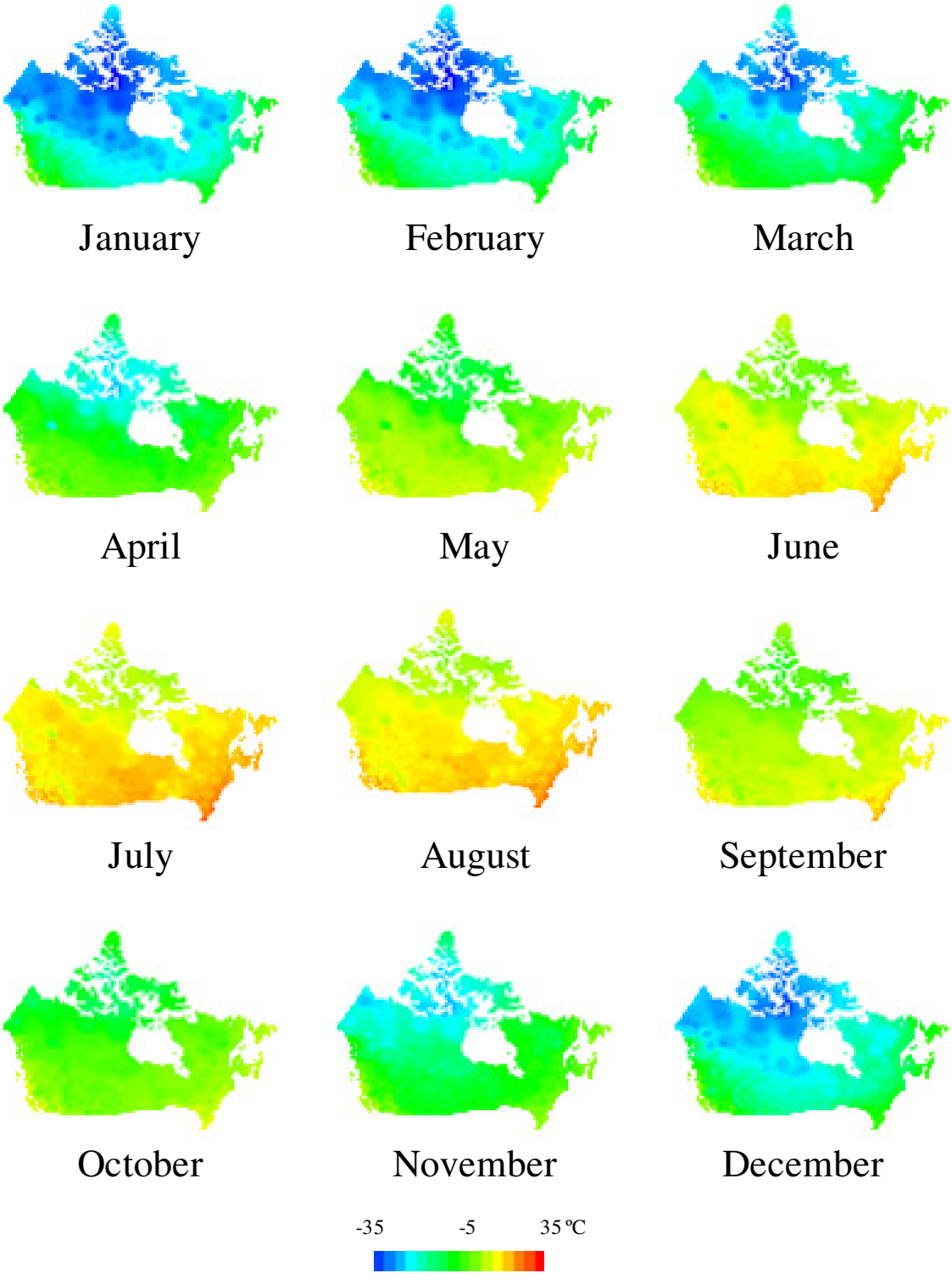

IWD interpolation of monthly average minimum temperature

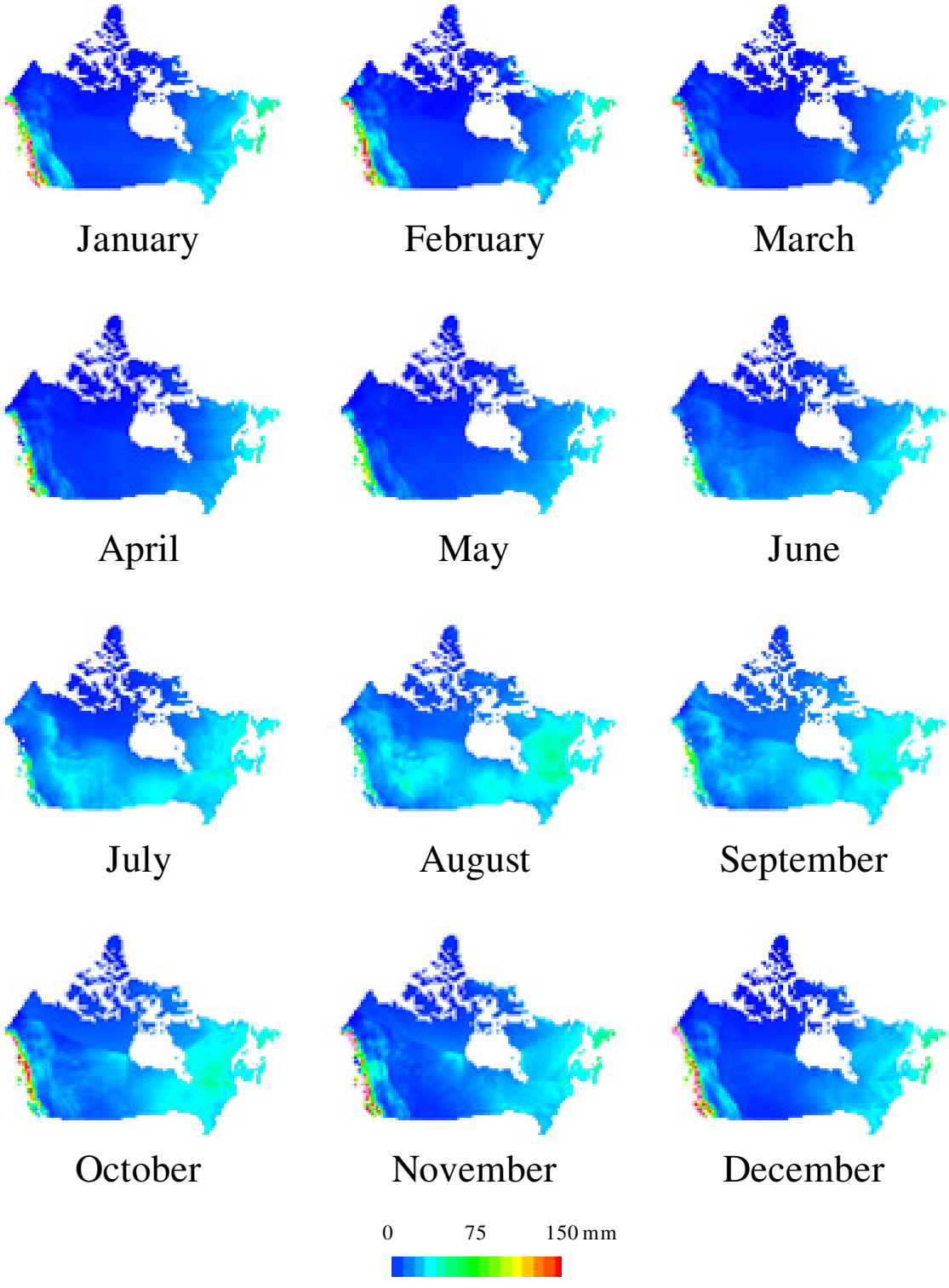

WATMAPPR interpolation of monthly precipitation

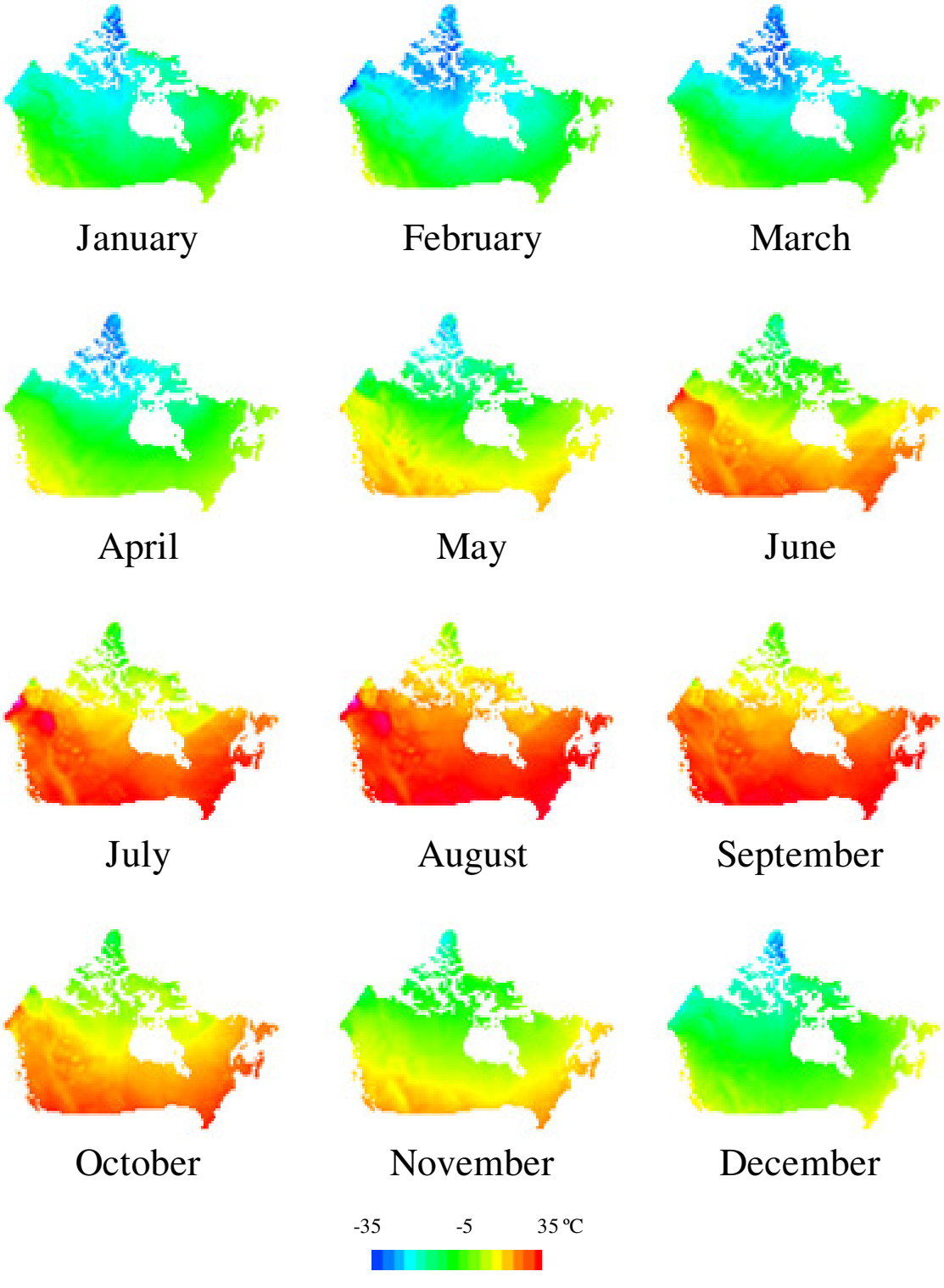

WATMAPPR interpolation of monthly average maximum temperature

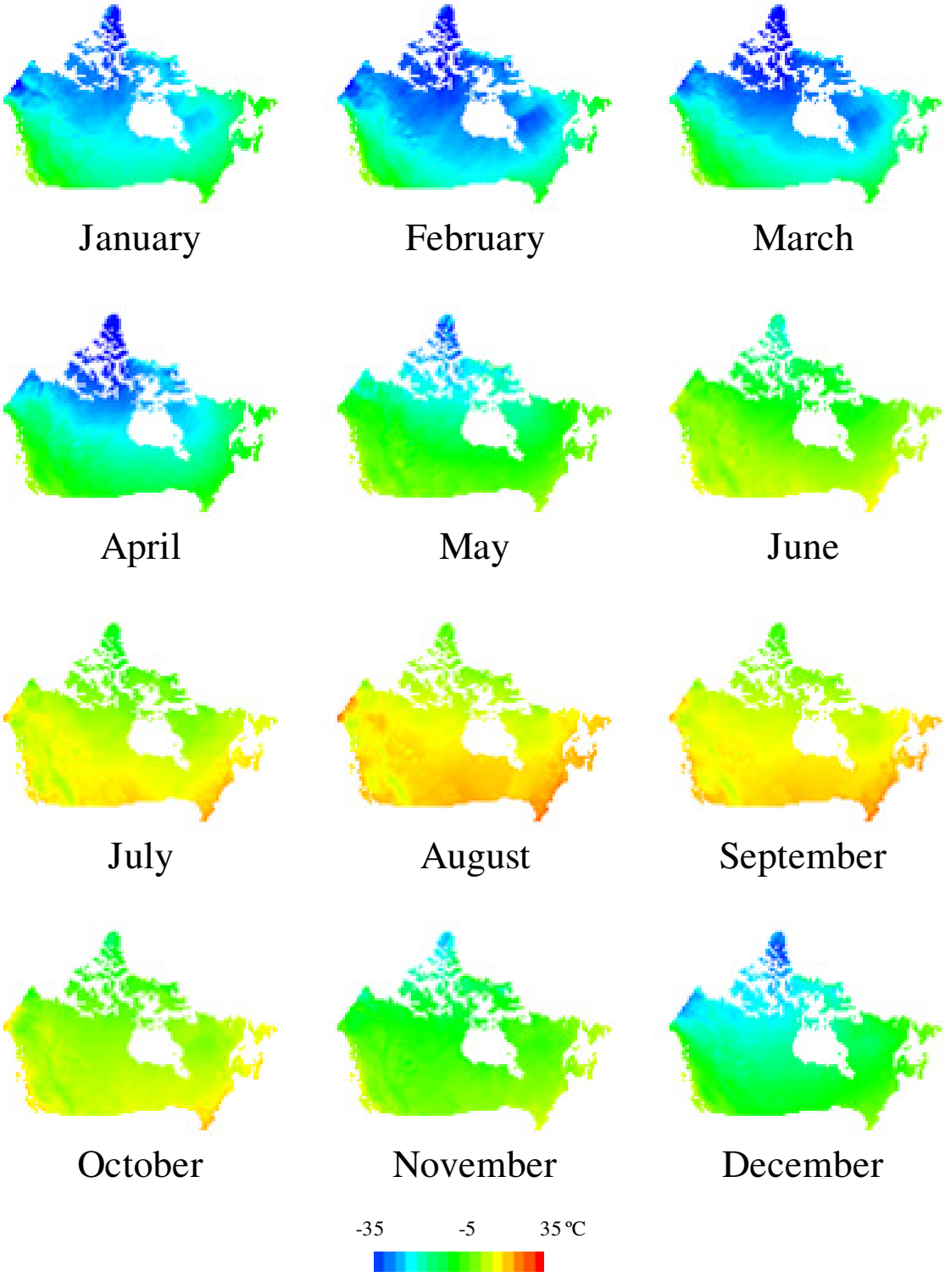

WATMAPPR interpolation of monthly average minimum temperature

Appendix C

Hydrographs of all calibration stations showing ensemble spread

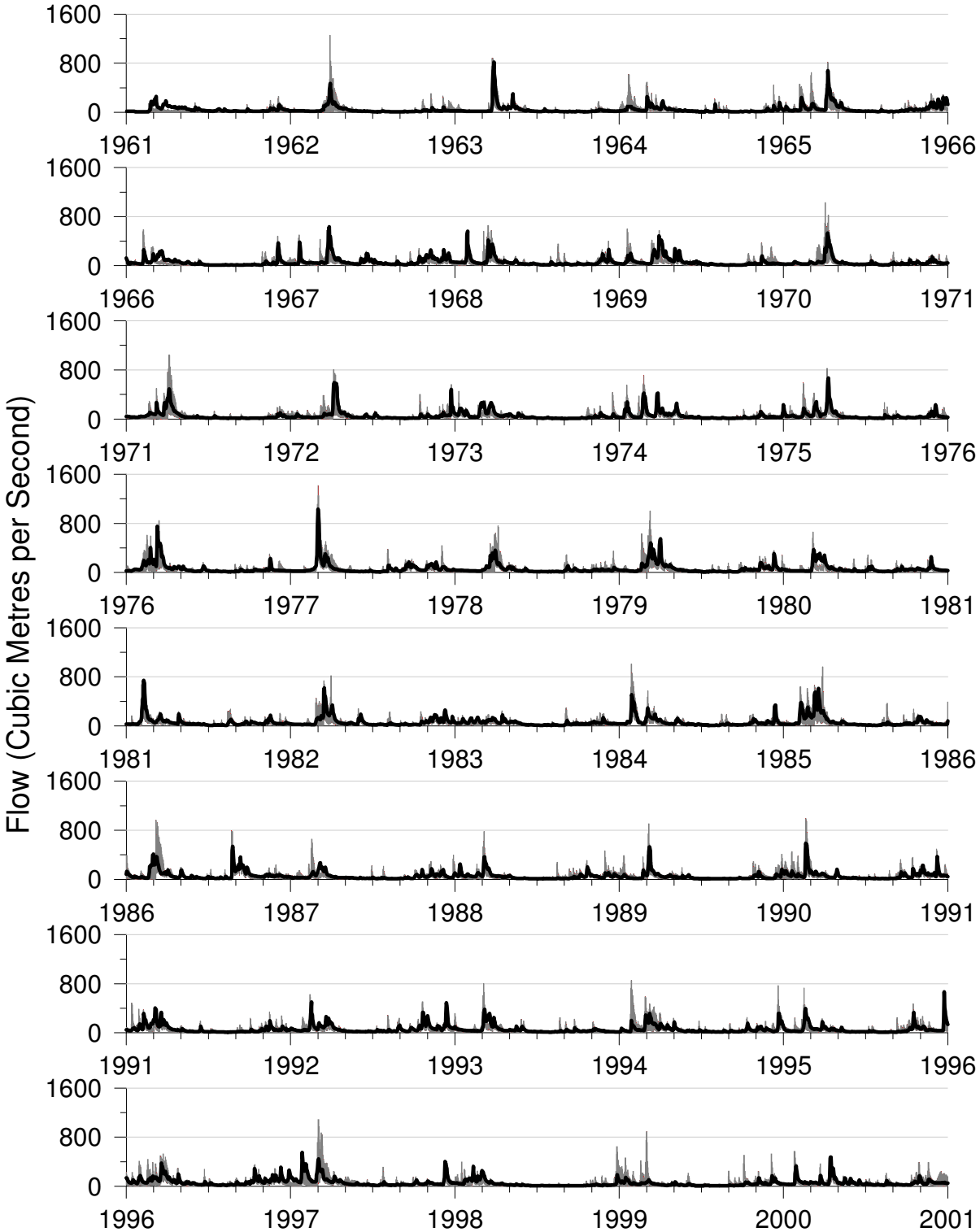
Flow (Cubic Metres per Second)
1600
800
0
1961
1962
1963
1964
1965
1966
1971
1972
1973
1974
1975
1976
1981
1982
1983
1984
1985
1986
1991
1992
1993
1994
1995
1996
2000
2001
Saugeen River near Port Elgin
(black - measured, gray - ensemble spread)

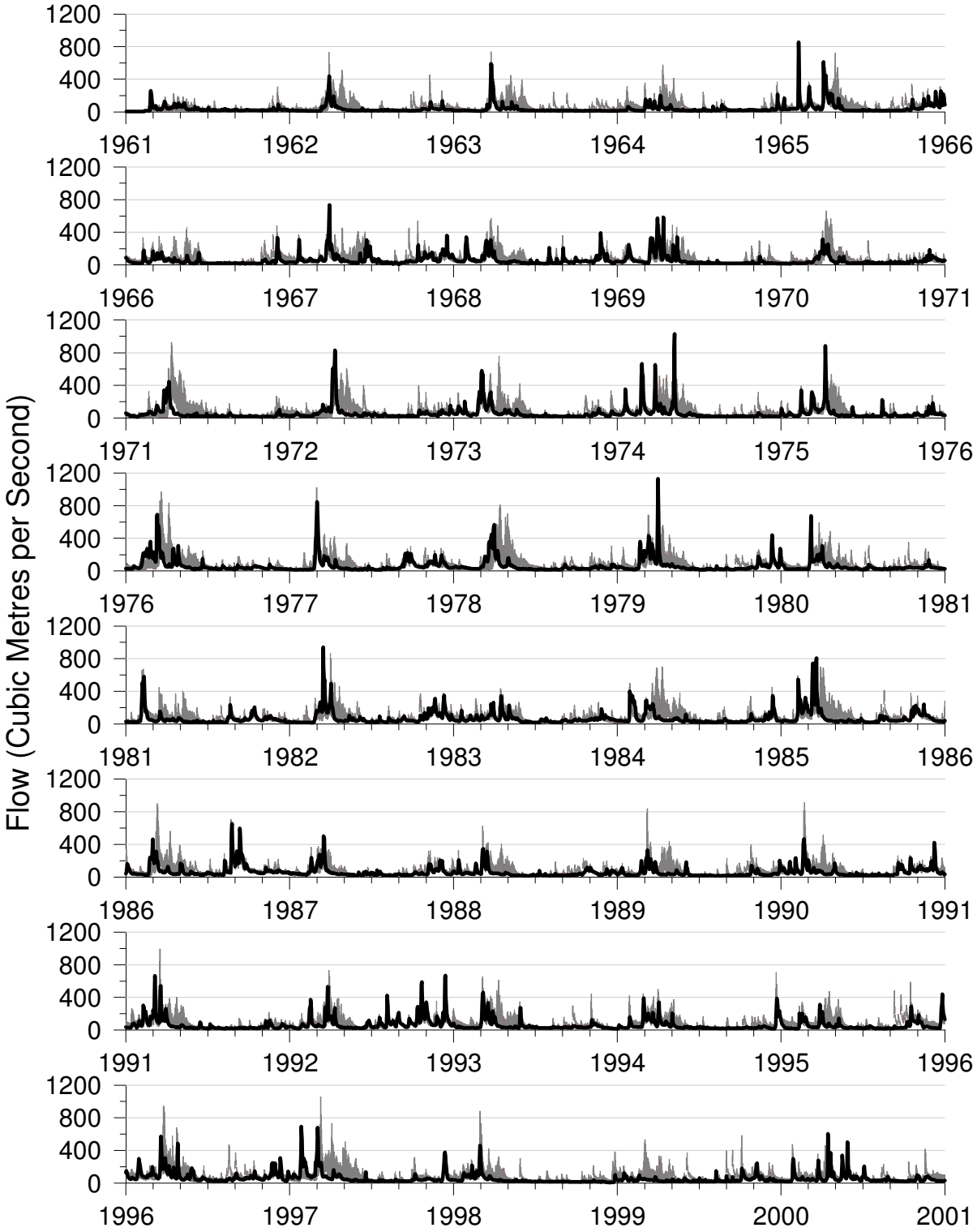
Flow (Cubic Metres per Second)
1200
800
400
0
1961
1962
1963
1964
1965
1966
1967
1968
1969
1970
1971
1972
1973
1974
1975
1976
1977
1978
1979
1980
1981
1982
1983
1984
1985
1986
1987
1988
1989
1990
1991
1992
1993
1994
1995
1996
1997
1998
1999
2000
2001
Grand River at Brantford
(black - measured, gray - ensemble spread)

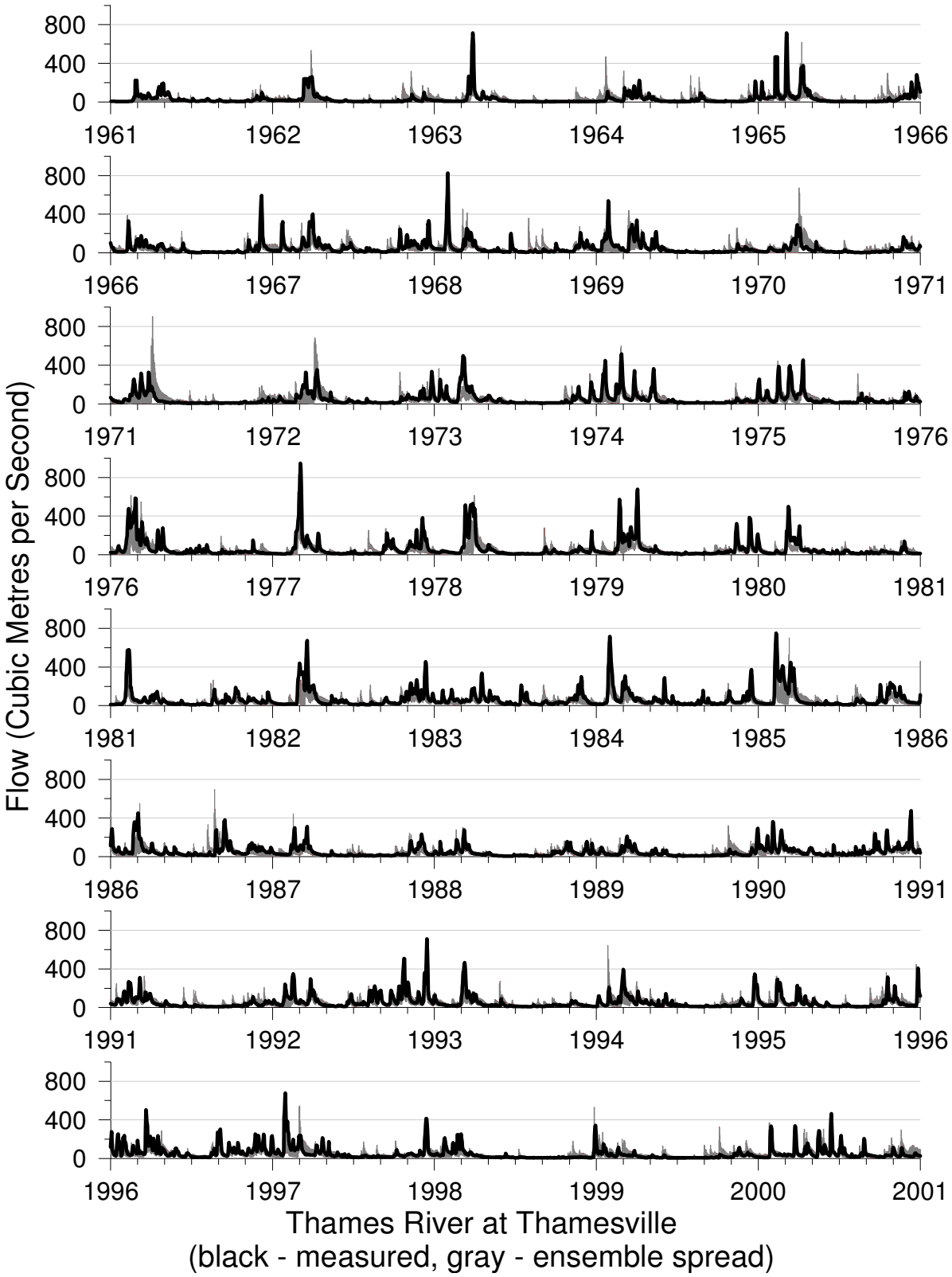
Flow (Cubic Metres per Second)
800
400
0
1961
1962
1963
1964
1965
1966
1971
1976
1981
1986
1991
1996
2000
2001
Thames River at Thamesville
(black - measured, gray - ensemble spread)

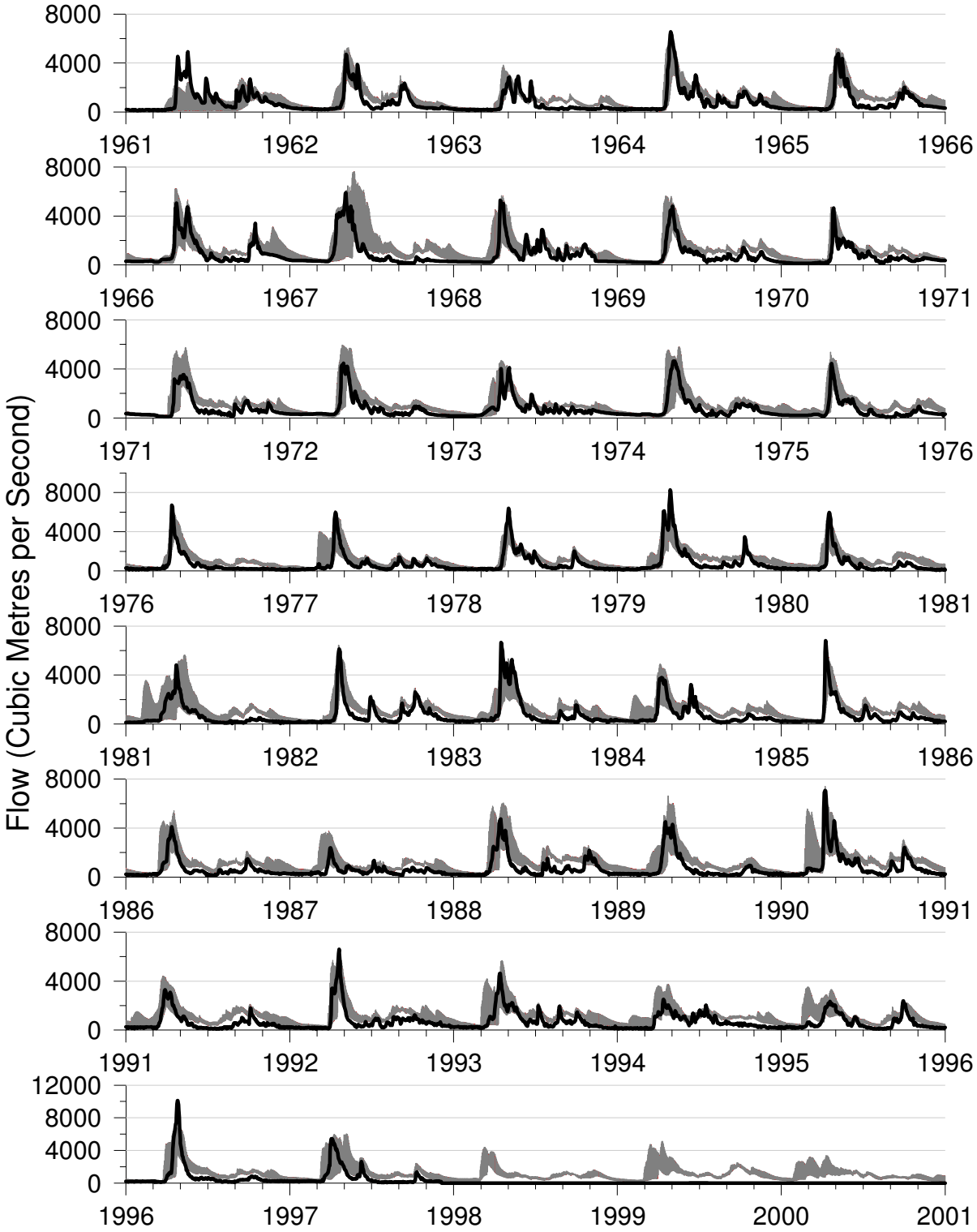
Flow (Cubic Metres per Second)
8000
4000
0
1961
1962
1963
1964
1965
1966
1966
1967
1968
1969
1970
1971
1971
1972
1973
1974
1975
1976
1976
1977
1978
1979
1980
1981
1981
1982
1983
1984
1985
1986
1986
1987
1988
1989
1990
1991
1991
1992
1993
1994
1995
1996
12000
1996
1997
1998
1999
2000
2001
Moose River at Moose River
(black - measured, gray - ensemble spread)

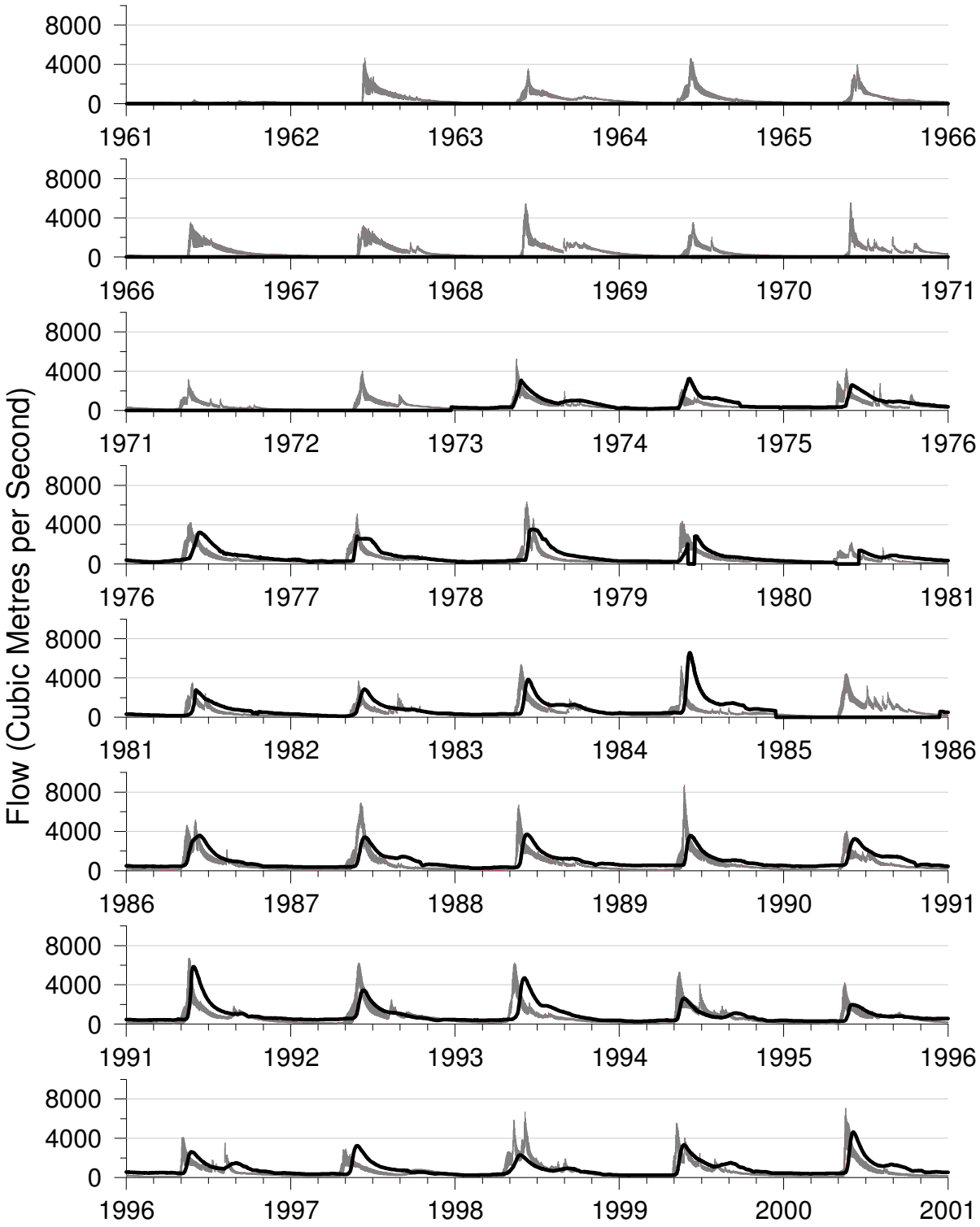
8000
4000
0
1961
1962
1963
1964
1965
1966
1966
1967
1968
1969
1970
1971
1971
1972
1973
1974
1975
1976
1976
1977
1978
1979
1980
1981
1981
1982
1983
1984
1985
1986
1986
1987
1988
1989
1990
1991
1991
1992
1993
1994
1995
1996
1996
1997
1998
1999
2000
2001
Flow (Cubic Metres per Second)
Thelon River above Baker Lake
(black - measured, gray - ensemble spread)

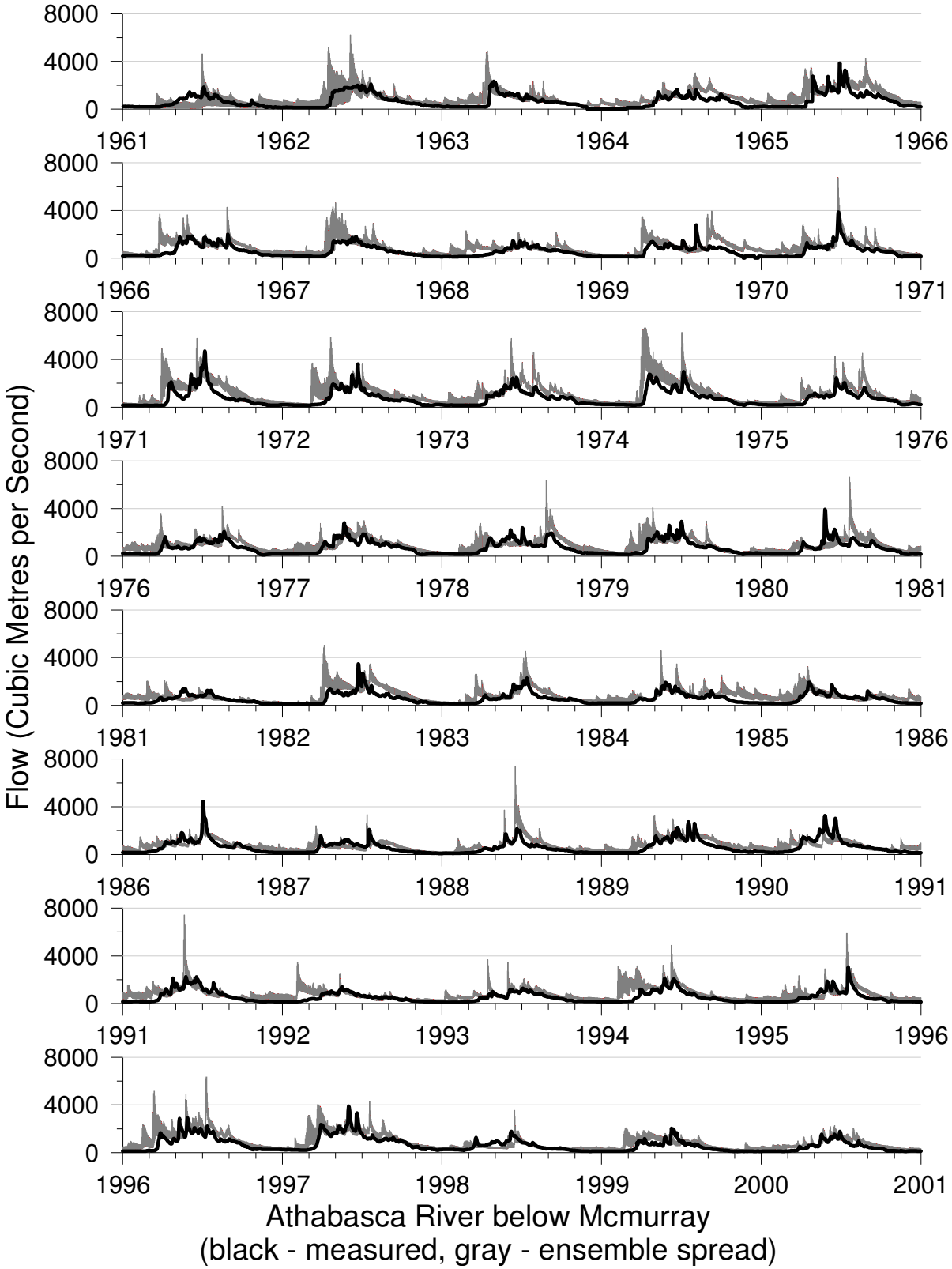
Flow (Cubic Metres per Second)
8000
4000
0
1961
1962
1963
1964
1965
1966
1966
1967
1968
1969
1970
1971
1971
1972
1973
1974
1975
1976
1976
1977
1978
1979
1980
1981
1981
1982
1983
1984
1985
1986
1986
1987
1988
1989
1990
1991
1991
1992
1993
1994
1995
1996
1996
1997
1998
1999
2000
2001
Athabasca River below Mcmurray
(black - measured, gray - ensemble spread)

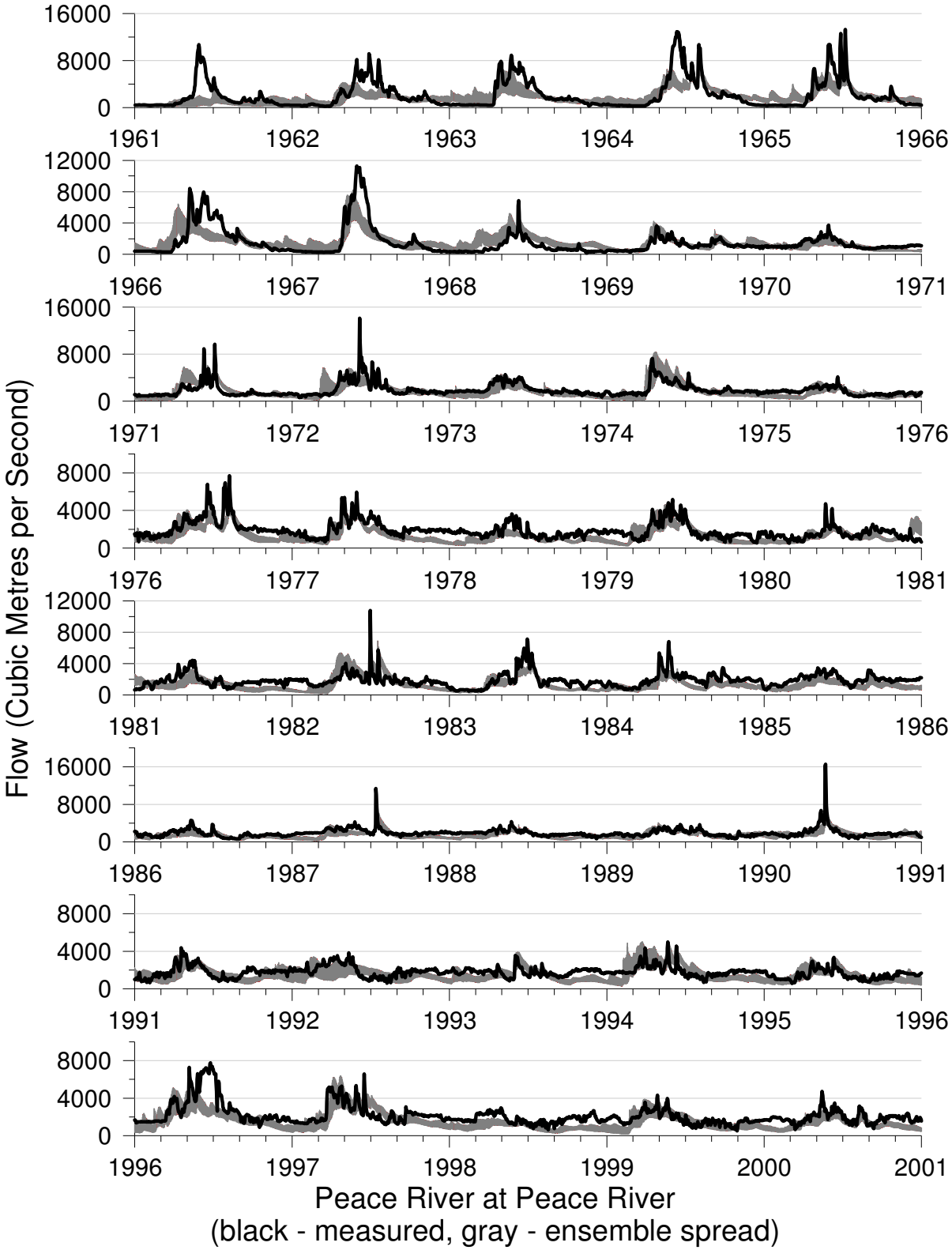
Flow (Cubic Metres per Second)
16000
8000
0
1961
1962
1963
1964
1965
1966
12000
8000
4000
0
1966
1967
1968
1969
1970
1971
16000
8000
0
1971
1972
1973
1974
1975
1976
8000
4000
0
1976
1977
1978
1979
1980
1981
12000
8000
4000
0
1981
1982
1983
1984
1985
1986
16000
8000
0
1986
1987
1988
1989
1990
1991
8000
4000
0
1991
1992
1993
1994
1995
1996
8000
4000
0
1996
1997
1998
1999
2000
2001
Peace River at Peace River
(black - measured, gray - ensemble spread)

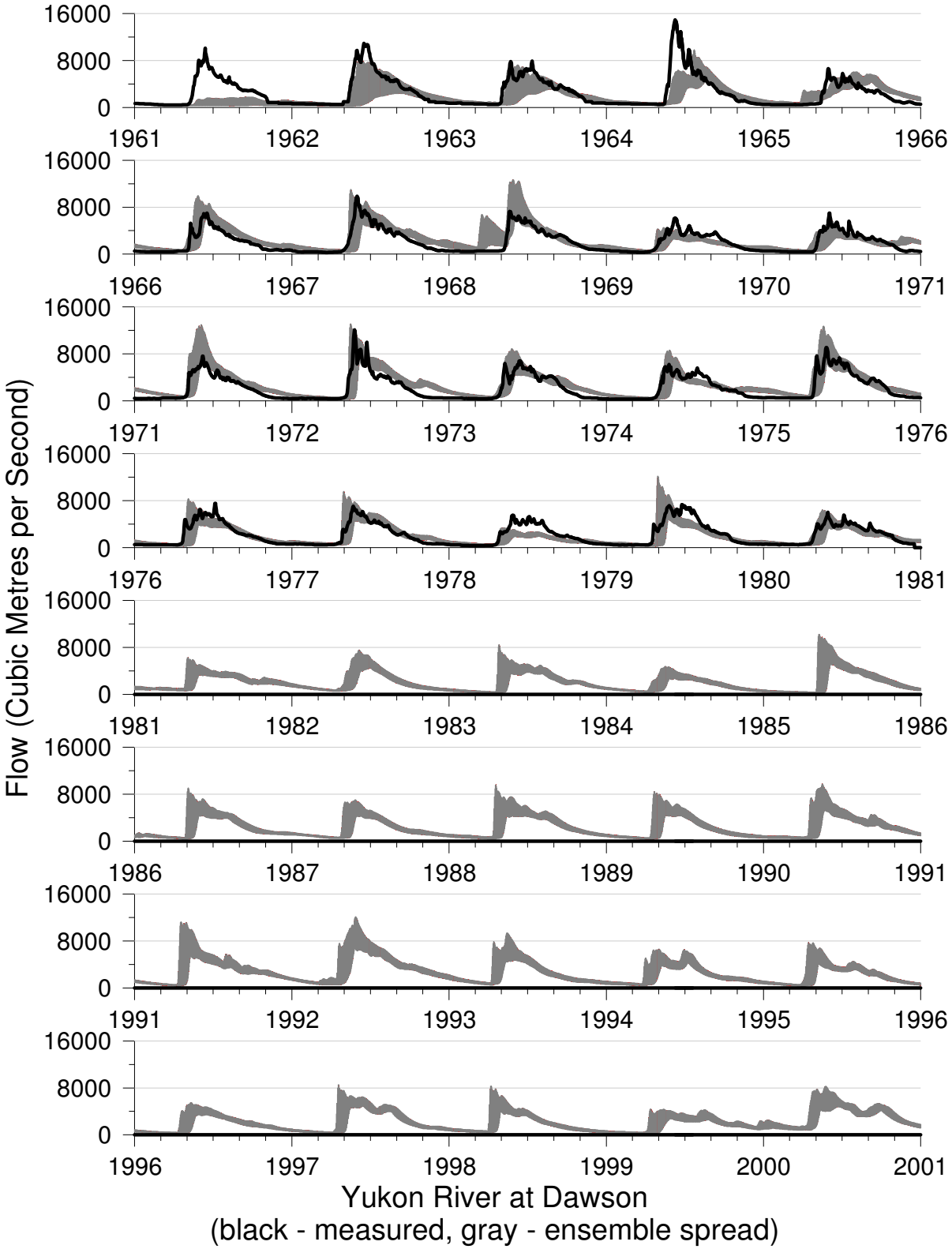
Flow (Cubic Metres per Second)
16000
8000
0
1961
1962
1963
1964
1965
1966
1967
1968
1969
1970
1971
1972
1973
1974
1975
1976
1977
1978
1979
1980
1981
1982
1983
1984
1985
1986
1987
1988
1989
1990
1991
1992
1993
1994
1995
1996
1997
1998
1999
2000
2001
Yukon River at Dawson
(black - measured, gray - ensemble spread)

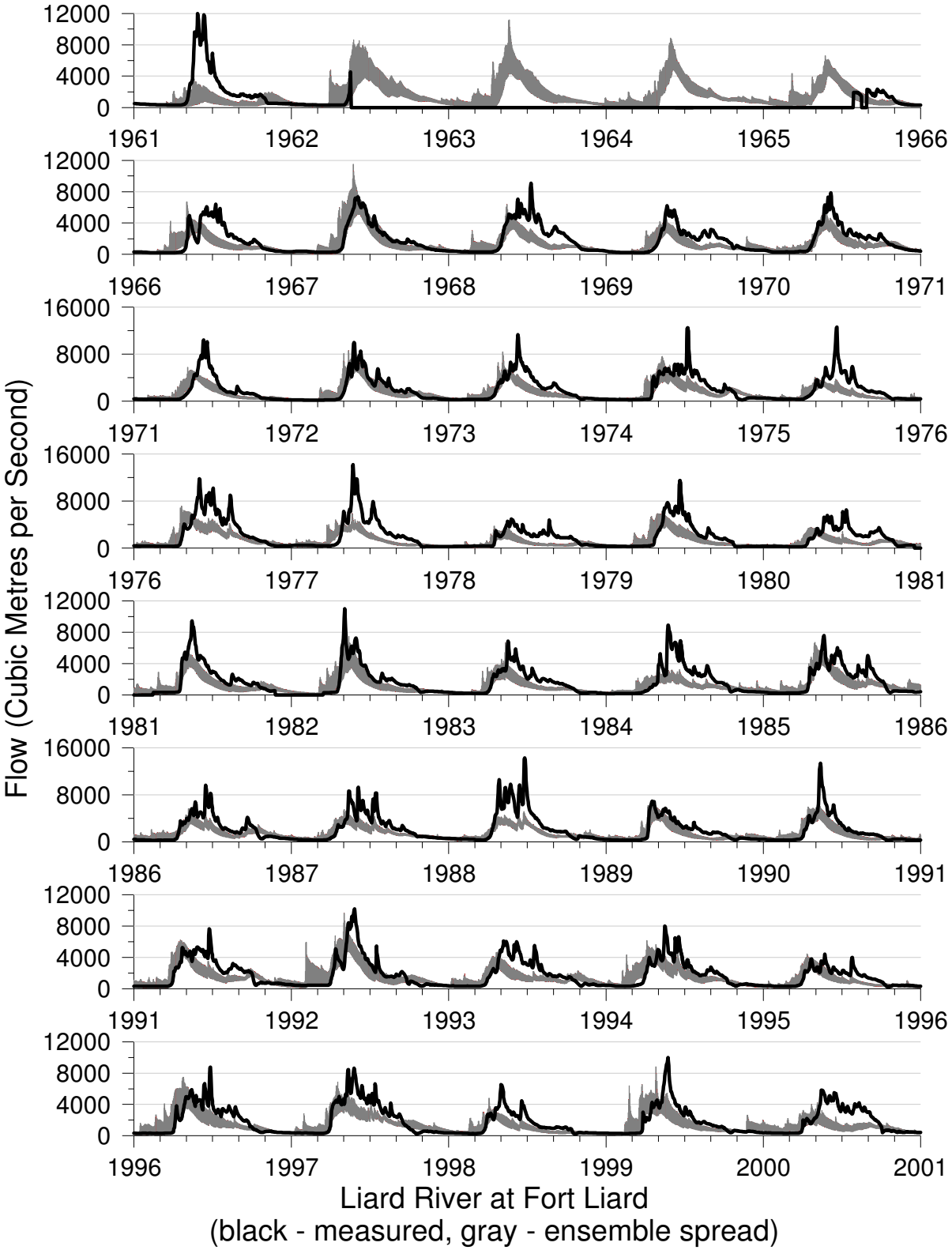
Flow (Cubic Metres per Second)
12000
8000
4000
0
1961
1962
1963
1964
1965
1966
1967
1968
1969
1970
1971
16000
1972
1973
1974
1975
1976
1977
1978
1979
1980
1981
1982
1983
1984
1985
1986
1987
1988
1989
1990
1991
1992
1993
1994
1995
1996
1997
1998
1999
2000
2001
Liard River at Fort Liard
(black - measured, gray - ensemble spread)

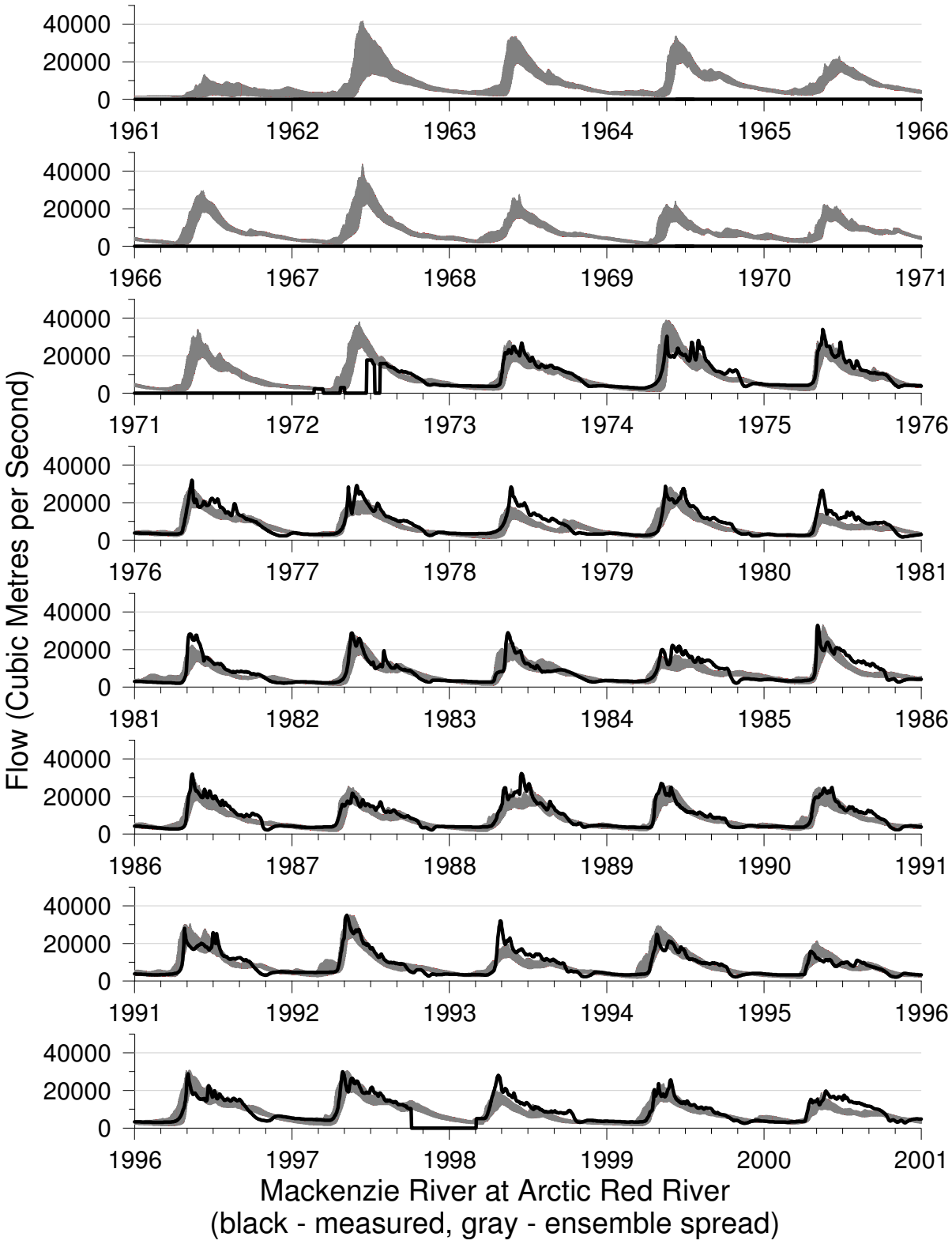
Flow (Cubic Metres per Second)
40000
20000
0
1961
1962
1963
1964
1965
1966
1966
1967
1968
1969
1970
1971
1971
1972
1973
1974
1975
1976
1976
1977
1978
1979
1980
1981
1981
1982
1983
1984
1985
1986
1986
1987
1988
1989
1990
1991
1991
1992
1993
1994
1995
1996
1996
1997
1998
1999
2000
2001
Mackenzie River at Arctic Red River
(black - measured, gray - ensemble spread)

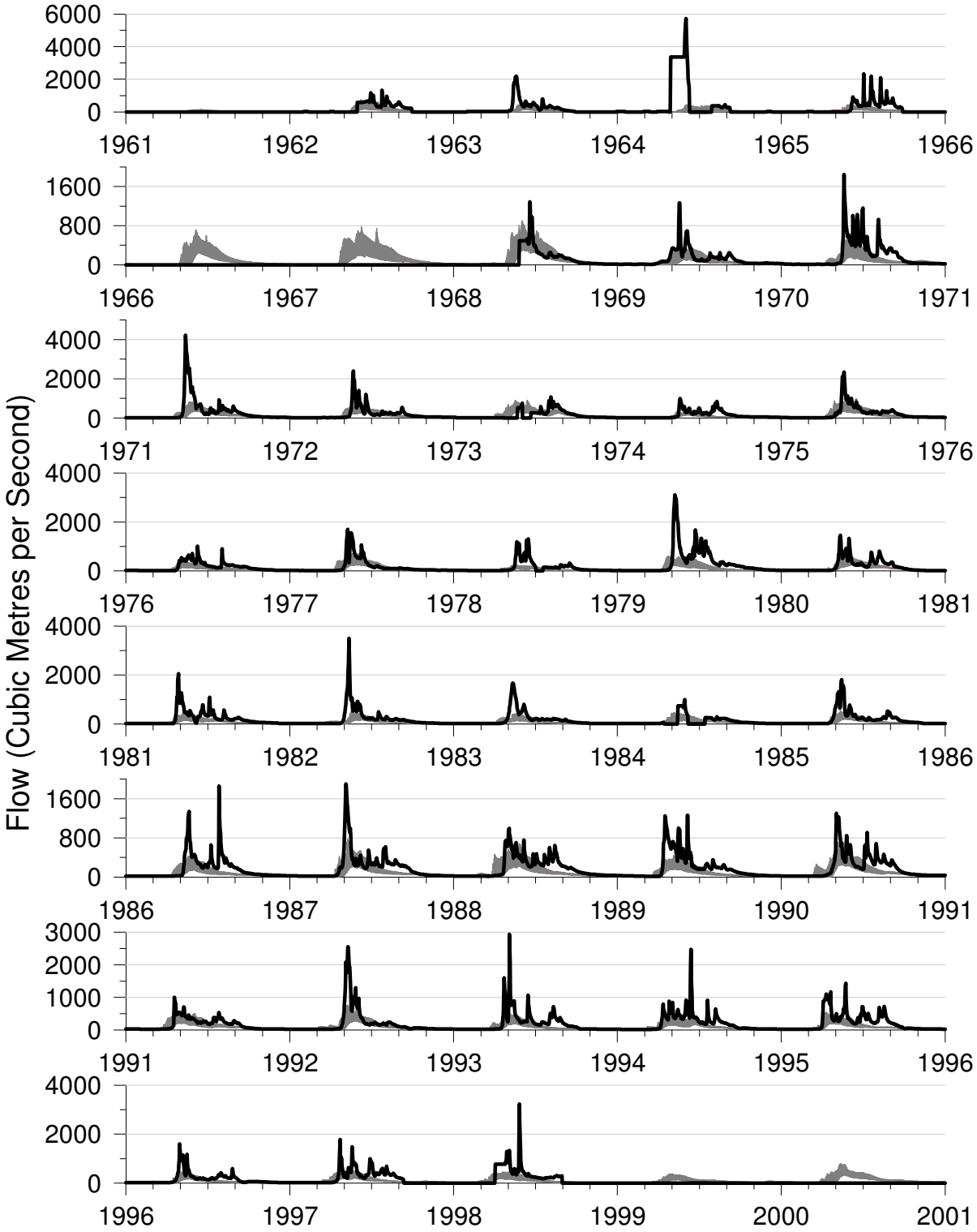
Flow (Cubic Metres per Second)
6000
4000
2000
0
1961
1962
1963
1964
1965
1966
1600
800
0
1966
1967
1968
1969
1970
1971
4000
2000
0
1971
1972
1973
1974
1975
1976
4000
2000
0
1976
1977
1978
1979
1980
1981
4000
2000
0
1981
1982
1983
1984
1985
1986
1600
800
0
1986
1987
1988
1989
1990
1991
3000
2000
1000
0
1991
1992
1993
1994
1995
1996
4000
2000
0
1996
1997
1998
1999
2000
2001
Peel River above Canyon Creek
(black - measured, gray - ensemble spread)

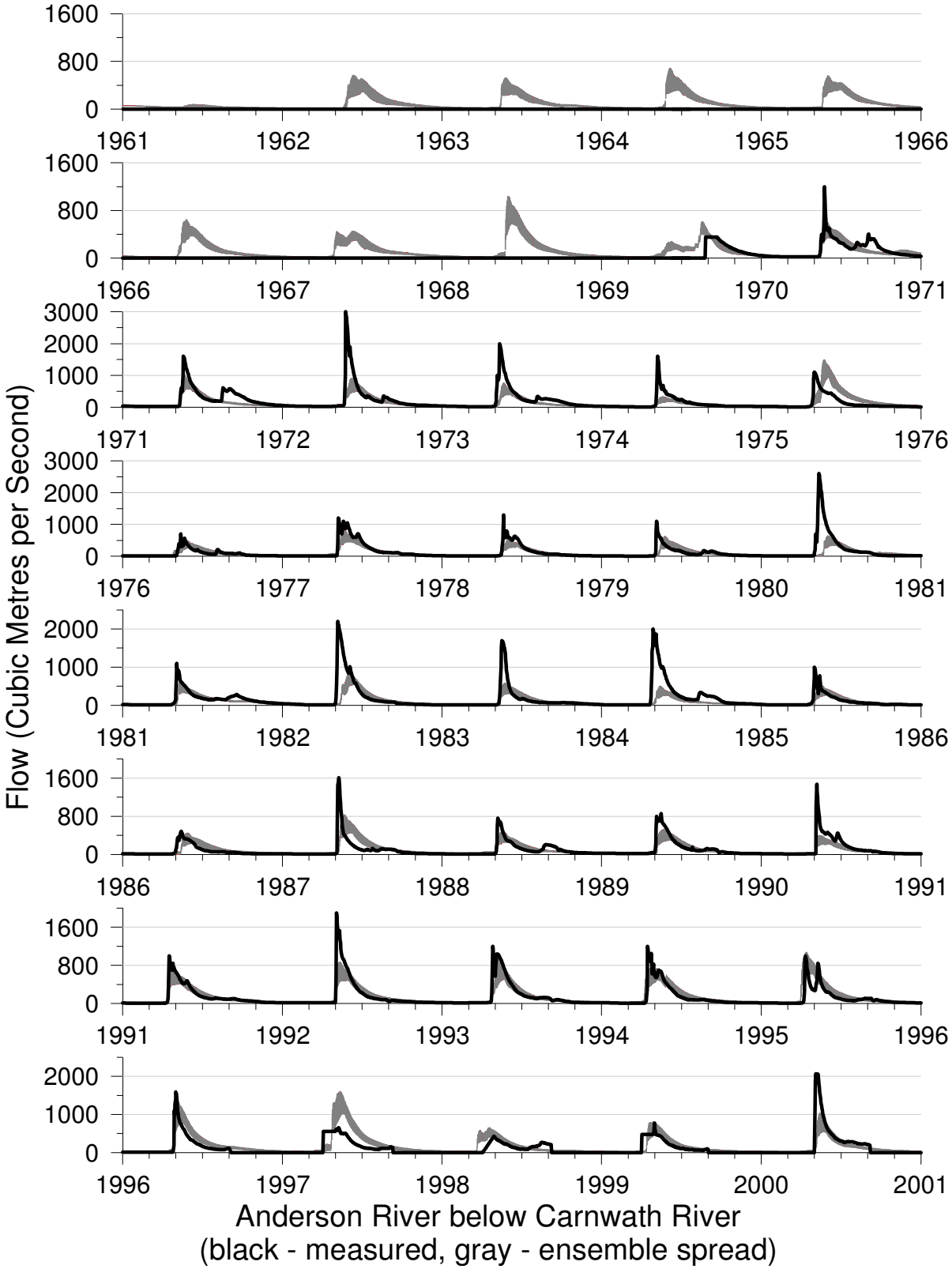
Flow (Cubic Metres per Second)
1600
800
0
1961
1962
1963
1964
1965
1966
1600
800
0
1966
1967
1968
1969
1970
1971
3000
2000
1000
0
1971
1972
1973
1974
1975
1976
3000
2000
1000
0
1976
1977
1978
1979
1980
1981
2000
1000
0
1981
1982
1983
1984
1985
1986
1600
800
0
1986
1987
1988
1989
1990
1991
1600
800
0
1991
1992
1993
1994
1995
1996
2000
1000
0
1996
1997
1998
1999
2000
2001
Anderson River below Carnwath River
(black - measured, gray - ensemble spread)

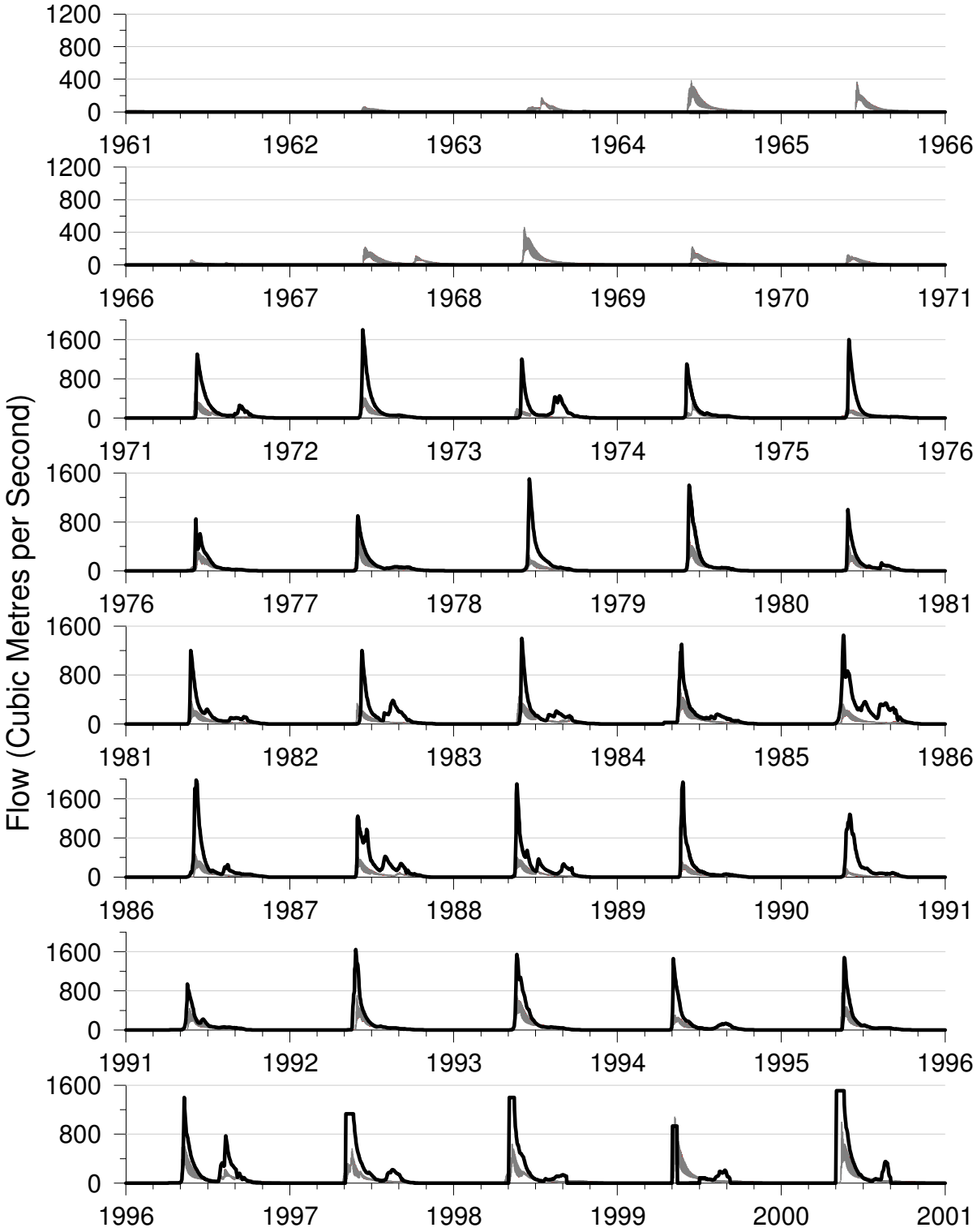
Flow (Cubic Metres per Second)
1200
800
400
0
1961
1962
1963
1964
1965
1966
1200
800
400
0
1966
1967
1968
1969
1970
1971
1600
800
0
1971
1972
1973
1974
1975
1976
1600
800
0
1976
1977
1978
1979
1980
1981
1600
800
0
1981
1982
1983
1984
1985
1986
1600
800
0
1986
1987
1988
1989
1990
1991
1600
800
0
1991
1992
1993
1994
1995
1996
1600
800
0
1996
1997
1998
1999
2000
2001
Ellice River near the mouth
(black - measured, gray - ensemble spread)

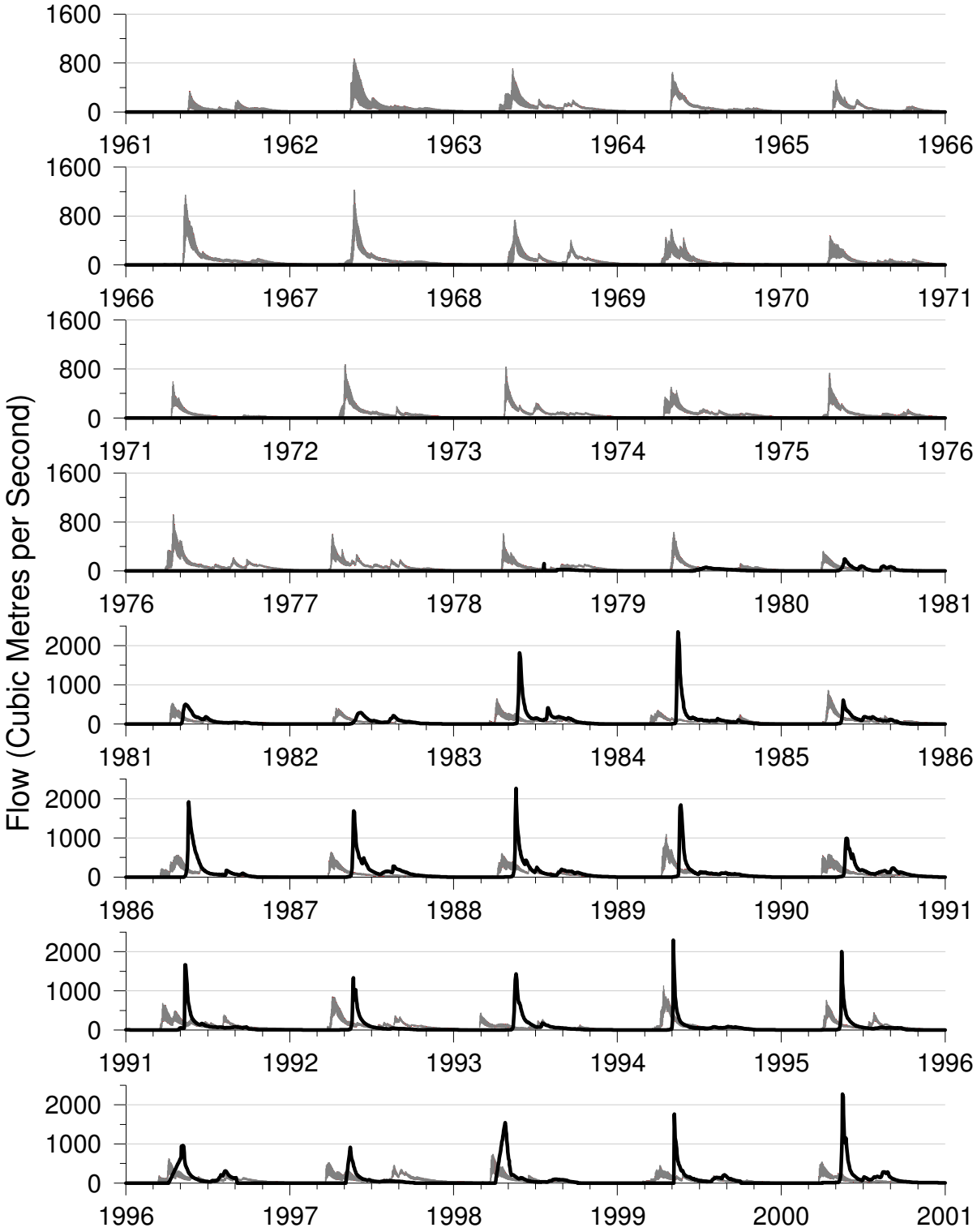
Flow (Cubic Metres per Second)
1600
800
0
1961
1962
1963
1964
1965
1966
1600
800
0
1966
1967
1968
1969
1970
1971
1600
800
0
1971
1972
1973
1974
1975
1976
1600
800
0
1976
1977
1978
1979
1980
1981
2000
1000
0
1981
1982
1983
1984
1985
1986
2000
1000
0
1986
1987
1988
1989
1990
1991
2000
1000
0
1991
1992
1993
1994
1995
1996
2000
1000
0
1996
1997
1998
1999
2000
2001
Baillie River near the mouth
(black - measured, gray - ensemble spread)

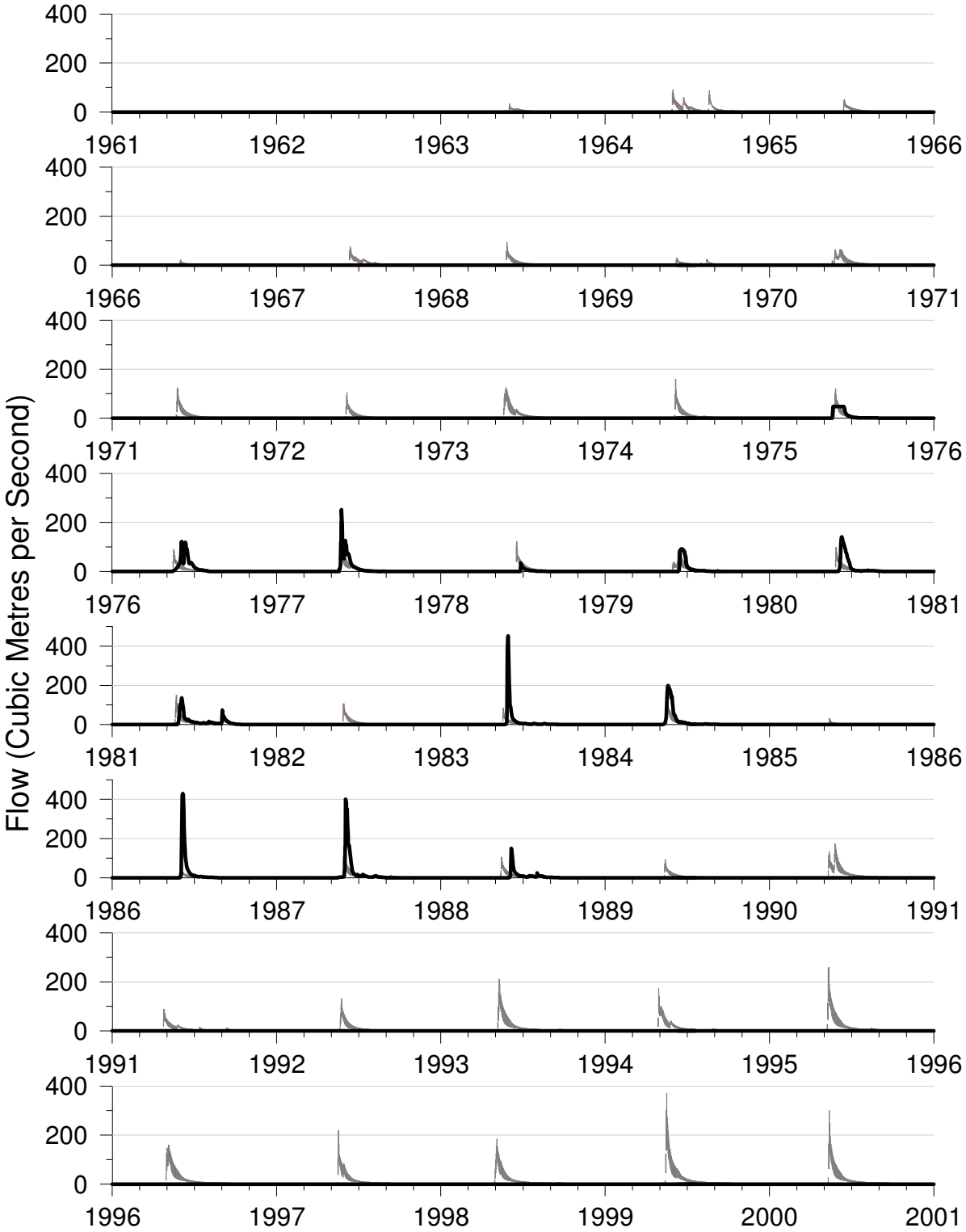
Flow (Cubic Metres per Second)
400
200
0
1961
1962
1963
1964
1965
1966
1971
1972
1973
1974
1975
1976
1981
1982
1983
1984
1985
1986
1991
1992
1993
1994
1995
1996
2000
2001
Big River above Egg River
(black - measured, gray - ensemble spread)

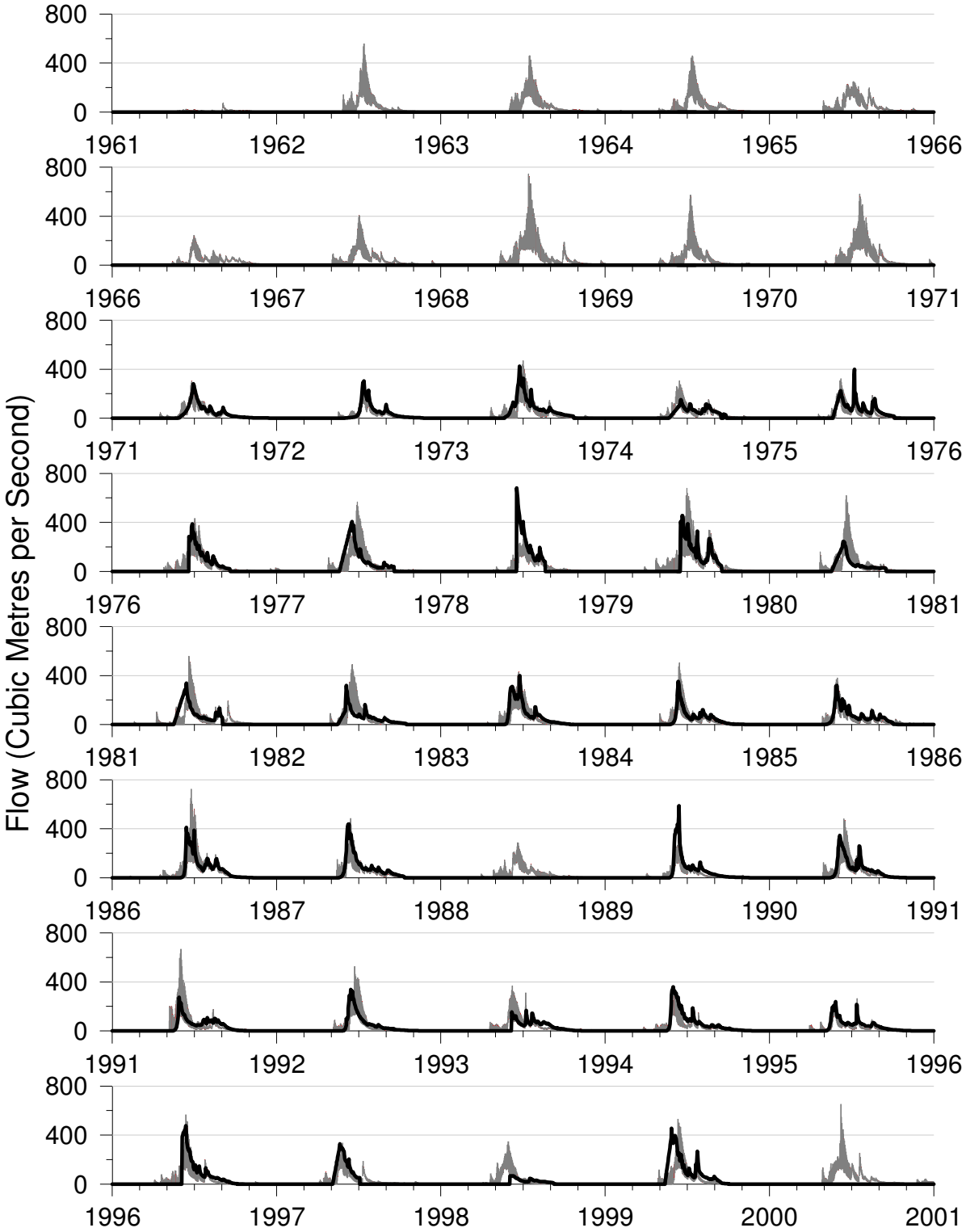
Flow (Cubic Metres per Second)
800
400
0
1961
1962
1963
1964
1965
1966
1967
1968
1969
1970
1971
1972
1973
1974
1975
1976
1977
1978
1979
1980
1981
1982
1983
1984
1985
1986
1987
1988
1989
1990
1991
1992
1993
1994
1995
1996
1997
1998
1999
2000
2001
Sylvia Grinnell River near Iqaluit
(black - measured, gray - ensemble spread)

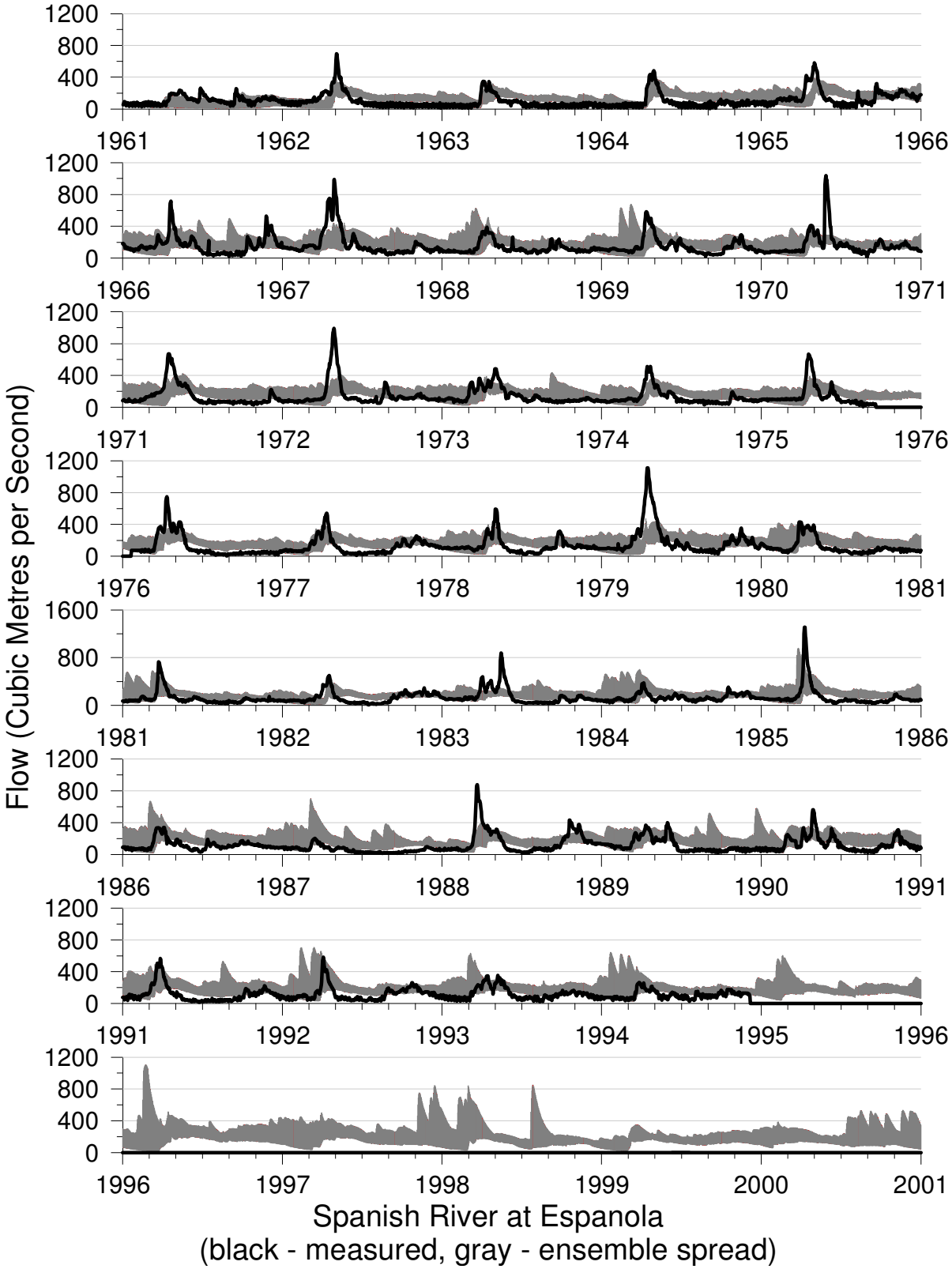
Flow (Cubic Metres per Second)
1200
800
400
0
1961
1962
1963
1964
1965
1966
1971
1972
1973
1974
1975
1976
1981
1982
1983
1984
1985
1986
1991
1992
1993
1994
1995
1996
2000
2001
1600
Spanish River at Espanola
(black - measured, gray - ensemble spread)